ISTANBUL TECHNICAL UNIVERSITY ★ GRADUATE SCHOOL OF SCIENCE ENGINEERING AND TECHNOLOGY

ROLLOVER CRASHWORTHINESS OF A MULTIPURPOSE COACH

M.Sc. THESIS

Özgün KÜÇÜK

Department of Mechanical Engineering

Solid Mechanics Programme

JANUARY 2015

ISTANBUL TECHNICAL UNIVERSITY ★ GRADUATE SCHOOL OF SCIENCE ENGINEERING AND TECHNOLOGY

ROLLOVER CRASHWORTHINESS OF A MULTIPURPOSE COACH

M.Sc. THESIS

Özgün KÜÇÜK
(503111509)

Department of Mechanical Engineering

Solid Mechanics Programme

Thesis Advisor: Dr. S. Ergün BOZDAĞ

JANUARY 2015

İSTANBUL TEKNİK ÜNİVERSİTESİ ★ FEN BİLİMLERİ ENSTİTÜSÜ

ÇOK AMAÇLI BİR OTOBÜSÜN DEVRİLME GÜVENLİĞİNİN İNCELENMESİ

YÜKSEK LİSANS TEZİ

Özgün KÜÇÜK
(503111509)

Makina Mühendisliği Anabilim Dalı

Katı Cisimlerin Mekaniği Programı

Tez Danışmanı: Dr. S. Ergün BOZDAĞ

OCAK 2015

Özgün KÜÇÜK, a M.Sc. student of ITU Graduate School of Science Engineering and Technology student ID 503111509, successfully defended the thesis entitled "**ROLLOVER CRASHWORTHINESS OF A MULTIPURPUSE COACH**", which he prepared after fulfilling the requirements specified in the associated legislations, before the jury whose signatures are below.

Thesis Advisor :	**Dr. S. Ergün BOZDAĞ** İstanbul Technical University	.....
Jury Members :	**Dr. Emin SÜNBÜLOĞLU** İstanbul Technical University	.....
	Assos. Prof. Dr. Cüneyt FETVACI İstanbul University	.....

Date of Submission : 15 December 2014
Date of Defense : 20 January 2015

To my mother,

FOREWORD

I would like to thank to Dr. S. Ergün BOZDAĞ and Dr. Emin SÜNBÜLOĞLU at Istanbul Technical University for their help and guidance throughout the thesis and my postgraduate studies.

I would like to extent my great appreciation to HEXAGON STUDIO and KARSAN for giving permission to use their resources and giving opportunity to make a contribution for passenger safety researches of their vehicle.

I would also like to thank Mertcan KAPTANOĞLU for continuous support and useful comments. I also wish to thank Mustafa SAYIN for his very helpful assistance.

I would like to express my sincere gratefulness to my mother Özlem KÜÇÜK who have always believe in my visions and have supported me unconditionally in every aspect of my education and my life. I especially thank Elis TUNABOYLU for her kind support and motivation.

January 2015

Özgün KÜÇÜK
(Mechanical Engineer)

TABLE OF CONTENTS

Page

FOREWORD ..... **ix**
TABLE OF CONTENTS ..... **xi**
ABBREVIATIONS ..... **xv**
LIST OF TABLES ..... **xvii**
LIST OF FIGURES ..... **xix**
SUMMARY ..... **xxiii**
ÖZET ..... **xxv**
1. INTRODUCTION **1**
1.1 Purpose of Thesis 1
1.2 Bus Classification 1
1.3 Bus and Coach Rollover Incidents 2
1.4 Severe Rollover Crashes 3
1.5 Statistics about Bus Rollover Accidents 5
1.6 Severity of Different Types of Rollover Accidents 8
1.7 Literature Review 15
1.8 Hypothesis 20
1.9 Discussion 20
2. ROLLOVER SAFETY OF BUSES **23**
2.1 Introduction 23
2.2 International Safety Regulations 23
2.2.1 Principle of passive safety 23
2.2.2 Standard accidents 23
2.2.3 Risk of the passengers 24
2.2.4 Life danger 24
2.2.5 Survival possibility 24
2.2.6 Test and analysis methods 25
2.3 ECE Safety Regulations 25
2.4 ECE 66-02 Regulation 25
2.4.1 Introduction 25
2.4.2 General specifications and requirements 26
2.4.3 Equivalent approval methods 29
2.4.4 Background 29
2.4.5 Quasi-static calculation method 29
2.4.6 Computer simulation method 31
3. SUPERSTRUCTURES OF BUSES **33**
3.1 Plastic Hinges 33
3.2 The Plastic Hinge Concept 33
3.3 Definition of Plastic Hinges 34
3.3.1 Elementary hinge 35
3.3.2 Combined hinge 35

3.4 Types of Plastic Hinges 37
3.4.1 Linear plastic hinge 37
3.4.2 Rotational plastic hinge 40
3.4.3 Combination of elementary plastic hinge 41
3.4.4 Mixed plastic hinge 41
3.4.5 The type of the plastic hinge 41
3.5 Plastic Hinge Characteristics 44
3.5.1 General hinge characteristic 44
3.5.2 Deviations from the general form 46
3.5.3 Mathematical equation 47
3.5.4 Probability approach 47
3.5.5 Dynamic characteristics 48
3.5.6 Repeated loading of a hinge 49
3.6 Some Constructional View Points of Forming Plastic Hinges 49
3.6.1 Testing elementary hinges 49
3.6.2 Testing combined hinges 52
3.6.3 Testing safety rings and bays 54
4. NUMERICAL METHODOLOGIES FOR CRASHWORTHINESS DESIGN AND ANALYSIS 59
4.1 Introduction 59
4.2 Structural Impact 60
4.3 FE Technology in Crashworthiness Analysis 62
4.4 Direct Time Integration 64
4.4.1 Newmark's method 64
4.4.2 The central difference algorithm 65
4.4.3 Numerical procedure 66
4.5 Explicit Solution Strategy 68
4.6 Conclusion 69
5. VALIDATION AND VERIFICATION OF THE COMPUTATIONAL CALCULATION 71
5.1 Introduction 71
5.2 Fundamentals of Validation 72
5.3 Characteristics of Validation Experiments 73
5.4 Validation Metrics 76
5.5 Accuracy of Validation 78
5.6 Validation in Computational Solid Mechanics Models 80
5.6.1 Description 80
5.6.2 Researches 81
5.6.3 Bending test of knots 83
5.6.4 Finite element models of knots 85
5.6.5 Results 90
5.6.6 Convergence between test and simulation results 96
5.6.6.1 Mesh convergence 96
5.6.6.2 Solution accuracy 96
5.6.6.3 CPU time requirement 97
5.6.6.4 Convergence study 97
5.6.7 Conclusion 107
6. NUMERICAL MODEL FOR COACH ROLLOVER ANALYSIS 109
6.1 Actual Structure of the Vehicle 109
6.2 Center of Gravity Measurement of the Vehicle 110

6.3 FE Modeling of the Components of the Vehicle 116
6.3.1 General definition 116
6.3.2 0D elements 123
6.3.3 1D elements 123
6.3.4 2D elements 125
6.3.5 Element integration 125
6.3.6 Computation of thickness change 129
6.3.7 Elastic-plastic stress calculation 130
6.4 Residual Space Modeling 132
6.5 Material Modeling 134
6.5.1 Mechanical properties of materials used in the vehicle 134
6.5.2 Plastic tabulated piecewise linear material model 137
6.5.3 Failure model 138
6.6 Contact Modeling 141
6.6.1 Introduction 141
6.6.2 Equations of equilibrium 142
6.6.3 Principle of virtual power 143
6.6.4 Penalty method 144
6.6.5 Contact interface 145
6.7 Kinematic Conditions of the Rollover Event 149
6.7.1 Boundary condition 149
6.7.1.1 Fixed rigid wall 149
6.7.1.2 Slave node penetration 150
6.7.1.3 Rigid wall impact force 151
6.7.1.4 Rigid wall modeling according to the ECE 66-02 regulation 151
6.7.2 Initial conditions 153
6.7.2.1 Gravity load 153
6.7.2.2 Initial angular velocity 153
6.8 Time Step 157
6.8.1 Element time step control 158
6.8.2 Nodal time step control 159
6.9 Parallel Computation 159
7. RESULTS 161
8. CONCLUSION 177
REFERENCES 179
APPENDICES 185
APPENDIX A 186
APPENDIX B 189
APPENDIX C 190
CURRICULUM VITAE 193

ABBREVIATIONS

AIS	**:** Abbreviated Injury Score
A.P.T.	**:** American Public Transit Association
CAE	**:** Computer Aided Engineering
CG	**:** Center of Gravity
CIC	**:** Cranfield Impact Centre
CPU	**:** Central Processing Unit
DD	**:** Double Decker
EC	**:** European Parliament and of the Council
ECBOS	**:** Enhanced Coach and Bus Occupant Safety
ECE	**:** Economic Commission for Europe
EEC	**:** European Economic Community
EU	**:** European Union
FE	**:** Finite Element
FEA	**:** Finite Element Analysis
FEM	**:** Finite Element Method
FMVSS	**:** Federal Motor Vehicle Safety Standards and Regulations
FRP	**:** Fiber-Reinforced Plastic
GB	**:** Gigabyte
GHz	**:** Gigahertz
GRSA	**:** Group of Rapporteurs on the Safety of Buses and Coaches
HD	**:** High Decker
ITU	**:** Istanbul Technical University
KSI	**:** Killed or Seriously Injured
MB	**:** Multibody
NHTSA	**:** National Highway Traffic Safety Administration
PH	**:** Plastic Hinge
QEPH	**:** Quadrilateral Elasto Plastic Physical Hourglass Control
RAM	**:** Random Access Memory
R&D	**:** Research and Development
SMP	**:** Shared Memory Processors
OECD	**:** Organization for Economic Co-operation and Development
UK	**:** United Kingdom
UN	**:** United Nations
V&V	**:** Verification and Validation

LIST OF TABLES

Page

Table 1.1 : Statistics about types of rollover accidents in different countries [13-17]. 6
Table 1.2 : Summary of statistics (APPENDIX A). 7
Table 1.3 : Occupant injury severity in 21 severe intercity bus collisions in Canada [18].....9
Table 1.4 : Ejection status by collision type in 21 severe intercity bus collisions in Canada [18]. 9
Table 1.5 : Statistics about construction of coaches having rollover accidents (APPENDIX A).....10
Table 1.6 : Statistics about different types of rollover accidents (APPENDIX A). ..10
Table 1.7 : Statistics about injury levels in accidents belonging to ”turn on side” and “rollover from the road” (APPENDIX A). 10
Table 1.8 : Statistics about construction of coaches having rollover accidents (APPENDIX A).....15
Table 5.1 : Relative error between breast knot’s tests and finite element simulation results with respect to maximum loads (full welding).....91
Table 5.2 : Relative error between breast knot’s tests and finite element simulation results with respect to maximum loads (half welding). 92
Table 5.3 : Relative error between roof edge knot’s tests and finite element simulation results with respect to maximum loads (full welding).....94
Table 5.4 : Relative error between roof edge knot’s tests and finite element simulation results with respect to maximum loads (half welding). 95
Table 5.5 : Relative error between breast knot’s test and mesh convergence results with respect to maximum loads (full welding).....99
Table 5.6 : Relative error between breast knot’s test and mesh convergence results with respect to maximum loads (half welding). 100
Table 5.7 : Relative error between roof edge knot’s test and mesh convergence results with respect to maximum loads (full welding).....101
Table 5.8 : Relative error between roof edge knot’s test and mesh convergence results with respect to maximum loads (half welding). 102
Table 6.1 : Location of the CG of the coach at unladen kerb mass. 116
Table 6.2 : Total occupant mass distribution.....123
Table 6.3 : Location of the CG of the coach at total effective mass.....123
Table 7.1 : Maximum relative displacement between edge of residual space and pillars of the vehicle with respect to factor of correlation [mm].....167
Table A.1: Bus rollover accidents statistics. 186

LIST OF FIGURES

Page

Figure 1.1 : Turn on side, where the rotation is stopped by a tree [17]. 11
Figure 1.2 : Turn on side in a snowy ditch - 1 [17]. 11
Figure 1.3 : Turn on side in a ditch - 2 [19]. 12
Figure 1.4 : The results of real rollover accidents with weak superstructure [23]. .13
Figure 1.5 : Rollover accident with reinforced superstructure [17].....13
Figure 1.6 : Strong superstructure assures the survival space [24].....14
Figure 2.1 : Rollover test setup according to ECE 66-02 [1]. 27
Figure 2.2 : Residual space in bus cross-section in ECE 66-02 [1].....28
Figure 2.3 : Characteristics measured in static and dynamic bay section tests [40]. 31
Figure 2.4 : Output results of simulation as an example [40]. 32
Figure 3.1 : Plastic hinge concept [41]. 33
Figure 3.2 : Plastic hinge constitutive relationship [42]. 34
Figure 3.3 : Bus superstructure after rollover [17]. 35
Figure 3.4 : Combined plastic hinge [44].....36
Figure 3.5 : Linear PH's on real bus structures: (a)Unlimited displacement. (b)Limited displacement. [44]. 38
Figure 3.6 : Plastic hinges on "T" joint [45]. 38
Figure 3.7 : Different types of "T" joint [45]. 39
Figure 3.8 : Different window columns [45].....39
Figure 3.9 : Compression test of underframe structure [44]. 40
Figure 3.10 : Different types of plastic hinges: (a)Linear hinge. (b)Rotational hinge. (c)Combination of hinges. [45].....41
Figure 3.11 : Combined PH on front wall frame [44]. 42
Figure 3.12 : Probability of forming folding type plastic hinge [46]. 43
Figure 3.13 : General form of plastic hinge characteristic [46]. 43
Figure 3.14 : Deviation from the general characteristic: (a)Hardening. (b)Fracture. (c)Fluction. (d)Combined. [46].....46
Figure 3.15 : Fractures on safety rings of bus frame [40].....46
Figure 3.16 : Static and dynamic pendulum bay section tests [40]. 49
Figure 3.17 : Effect on tube length on the hinge characteristic [46]. 50
Figure 3.18 : Rotational PH characteristics: (a)Different joints. (b)Different tubes. [46]. 51
Figure 3.19 : Repeated bending of PH [46]. 52
Figure 3.20 : Geometrical effects on PH characteristics of "T" joints [45].....52
Figure 3.21 : Laboratory test of front wall waistrail [44]. 53
Figure 3.22 : Test results of front wall waistrails [44].....54
Figure 3.23 : PH characteristic of combined linear hinges [45].....54
Figure 3.24 : Different safety rings after pendulum impact [40]. 56
Figure 3.25 : Deformed safety ring in the rear wall [40]. 57

Figure 4.1 : Numerical procedure of time integration. 67
Figure 4.2 : Simplified explicit solution strategy flow chart. 69
Figure 5.1 : Validation process [54]. 72
Figure 5.2 : Interaction of various experimental and computational activities [55]. 75
Figure 5.3 : Increasing quality of validation metrics: (a) Deterministic. (b) Experimental uncertainty [55]. 77
Figure 5.4 : Relationship between validation, calibration and prediction [58]. 79
Figure 5.5 : Selected plastic hinges for validation process. 81
Figure 5.6 : Moment vs. angle schematic characteristics for plastic hinge [59]. 82
Figure 5.7 : Moment vs. angle characteristics for plastic hinge (PH) in thin walled tube [1]. 83
Figure 5.8 : Four point bending approach for breast knot. 83
Figure 5.9 : Four point bending test setups for breast knots. 84
Figure 5.10 : Optical displacement measurement system used in bending tests. 84
Figure 5.11 : Force measurement system (loadcell) used in bending tests. 85
Figure 5.12 : Finite element model and boundary conditions of breast knot simulation. 86
Figure 5.13 : Finite element model and boundary conditions of roof edge knot simulation. 87
Figure 5.14 : True stress – strain curves of S420MC and S355JR steels. 88
Figure 5.15 : Weld connection modeling with rigid elements (RBODY): (a)Breast knot (full welding). (b)Breast knot (half welding). (c)Roof edge knot (full welding). (d)Roof edge knot (half welding). 89
Figure 5.16 : Similarity between test setup and finite element model of breast knot. 90
Figure 5.17 : Similarity between test result and finite element analysis result visuals of breast knot. 90
Figure 5.18 : Load – displacement curves of breast knot's tests and finite element simulation results (full welding). 91
Figure 5.19 : Load – displacement curves of breast knot's tests and finite element simulation results (half welding). 92
Figure 5.20 : Similarity between test setup and finite element model of roof edge knot. 93
Figure 5.21 : Similarity between test result and finite element analysis result visuals of roof edge knot. 93
Figure 5.22 : Load – displacement curves of roof edge knot's tests and finite element simulation results (full welding). 94
Figure 5.23 : Load – displacement curves of roof edge knot's tests and finite element simulation results (half welding). 95
Figure 5.24 : Mesh convergence study according to load – displacement curves of breast knot's test and finite element simulation results (full welding). 99
Figure 5.25 : Mesh convergence study according to load – displacement curves of breast knot's test and finite element simulation results (half welding). 100
Figure 5.26 : Mesh convergence study according to load – displacement curves of roof edge knot's test and finite element simulation results (full welding). 101

Figure 5.27 : Mesh convergence study according to load – displacement curves of roof edge knot's test and finite element simulation results (half welding).....102
Figure 5.28 : Local buckling deformation of breast knot in the FE models: (a)Fine mesh. (b)Medium mesh. (c)Coarse mesh. (d)Experiment.....103
Figure 5.29 : Nonlinearity convergence study according to load – displacement curves of breast knot's test and finite element simulation results (full welding).....105
Figure 5.30 : Nonlinearity convergence study according to load – displacement curves of breast knot's test and finite element simulation results (half welding).....105
Figure 5.31 : Nonlinearity convergence study according to load – displacement curves of roof edge knot's test and finite element simulation results (full welding).....106
Figure 5.32 : Nonlinearity convergence study according to load – displacement curves of roof edge knot's test and finite element simulation results (half welding).....106
Figure 6.1 : The coach chosen for rollover simulation (KARSAN STAR).....110
Figure 6.2 : Longitudinal position of the centre of gravity [1].....112
Figure 6.3 : Transverse position of centre of gravity [1].....113
Figure 6.4 : Determination of height of centre of gravity [1].....114
Figure 6.5 : The center of gravity measurement test of the coach.....115
Figure 6.6 : Finite element model of the vehicle.....117
Figure 6.7 : Mesh details of the finite element model.....118
Figure 6.8 : Non-structural components of the finite element model for mass and inertia compliance.....119
Figure 6.9 : Simplified finite element model of powertrain components.....120
Figure 6.10 : Simplified finite element model of rear axle components.....120
Figure 6.11 : Simplified finite element model of front axle components.....121
Figure 6.12 : Simplified finite element model of human masses.....122
Figure 6.13 : Dimensions for anthropomorphic ballast [1].....122
Figure 6.14 : Hourglass modes at translational modes of shell [60].....127
Figure 6.15 : Material curves for plastic stress calculation [60].....130
Figure 6.16 : Specification of residual space [1].....132
Figure 6.17 : Finite element model of the vehicle and residual space.....133
Figure 6.18 : Residual space connection to the base of the vehicle.....134
Figure 6.19 : Test specimen for tensile strength tests.....135
Figure 6.20 : Picture of tensile strength test system.....135
Figure 6.21 : The specimens for tensile strength tests. (a) During test. (b) After Test. 136
Figure 6.22 : True stress - strain curves of S420MC and S355JR steels.....137
Figure 6.23 : Stress – strain curve for damage affected material [60].....140
Figure 6.24 : Cloumb friction [60].....147
Figure 6.25 : Friction on type 7 interface [60].....148
Figure 6.26 : Self-contact surfaces in FE model of the vehicle 149
Figure 6.27 : Fixed rigid wall definition [60].....150
Figure 6.28 : Slave node penetration [60].....150
Figure 6.29 : Rigid wall modeling according to the ECE 66-02 regulation - 1. 152
Figure 6.30 : Rigid wall modeling according to the ECE 66-02 regulation - 2. 152

Figure 6.31 : Rotation of the vehicle to the point of first contact with the ground - 1 [1]..... 155
Figure 6.32 : Geometry of the tilting bench [1]..... 156
Figure 6.33 : Rotation of the vehicle to the point of first contact with the ground - 2 [1]..... 156
Figure 6.34 : Architecture of shared memory [60]..... 160
Figure 7.1 : Sequential pictures showing behavior of deformation of the vehicle through the time steps..... 162
Figure 7.2 : Bay sections of the coach structure..... 163
Figure 7.3 : Maximum deformation at Section B at 0.1375 second..... 164
Figure 7.4 : Maximum deformation at Section C at 0.1425 second..... 164
Figure 7.5 : Maximum deformation at Section D at 0.125 second..... 165
Figure 7.6 : Maximum deformation at Section E at 0.1175 second..... 165
Figure 7.7 : Maximum deformation at Section F at 0.12 second..... 166
Figure 7.8 : Maximum deformation at Section G at 0.1 second..... 166
Figure 7.9 : Maximum deformation at Section H at 0.1025 second..... 167
Figure 7.10 : Distance between upper edge of the residual space and pillars of the vehicle..... 168
Figure 7.11 : Distance between lower edge of the residual space and pillars of the vehicle..... 169
Figure 7.12 : Contours of von Mises stress distribution for maximum stress value from front view of the vehicle..... 170
Figure 7.13 : Contours of von Mises stress distribution for maximum stress value from rear view of the vehicle..... 171
Figure 7.14 : Contours of von Mises stress distribution for maximum stress value from general view of the vehicle..... 171
Figure 7.15 : Contours of plastic strain distribution at the end of the simulation from front view of the vehicle..... 172
Figure 7.16 : Contours of plastic strain distribution at the end of the simulation from rear view of the vehicle..... 173
Figure 7.17 : Contours of plastic strain distribution at the end of the simulation from general view of the vehicle..... 174
Figure 7.18 : Energy distribution of the simulation versus time..... 175
Figure 7.19 : Comparison of the internal and kinetic energy distribution of the simulation versus time..... 176
Figure A.1 : Technical drawing of breast knot..... 189
Figure A.2 : Technical drawing of roof edge knot..... 189
Figure A.3 : Geometrical sketch of KARSAN STAR..... 190
Figure A.4 : Seat layout of the KARSAN STAR..... 191

ROLLOVER CRASHWORTHINESS OF A MULTIPURPOSE COACH

SUMMARY

Buses are widely used mode of transport in worldwide. With growth in economy, the numbers of buses have increased tremendously both in rural and urban areas. With increased number of buses, the issue of safety of passengers and the crew assumes special importance. A large number of bus accidents involve rollovers and falling into ditches or downhill sides.

Bus rollover is one of the most serious types of accident as compared to other modes of bus accidents. In the past years, it was observed after the accidents that the deforming body structure seriously threatens the lives of the passengers and thus, the rollover strength has become an important issue for bus and coach manufacturers. In the European countries, the certification of sufficient deformation strength when overturning is compulsory for the approval of a coach according to the ECE 66-02 regulation. According to the said regulation, the certification can be gained either by full-scale vehicle testing, or by calculation techniques based on advanced numerical methods (i.e. non-linear explicit dynamic finite element analysis). The quantity of interest at the end is the bending deformation enabling engineers to investigate whether there is any intrusion in the passenger survival space (residual space) along the entire vehicle. The simulation specifies either overturning of the vehicle structure from tilting platform or the impact of a plate on the coach structure as it would correspond to the crash of the structure when falling onto the ground.

According to the ECE 66-02 regulation, a passenger's survival space is defined in the coach model to check whether there is any intrusion into the survival space during the rollover. This ensures that the coach structure has sufficient strength to avoid intrusions into the survival space. The effect of passenger and luggage weights on energy absorbed by the coach structure during rollover will be also discussed.

Rollover test on a complete vehicle is the basic testing method, the expensive cost and time-consuming nature make it difficult to be implemented during the process of

product research and development (R&D). The high cost of real tests and difficulties in collecting data has resulted in an increasing interest in the analytical and computational methods of evaluation. The advancement of computer simulation technology enables the quick assessment of coach rollover crashworthiness even at the initial design phase. Simulation-based rollover analysis can assist, even replace the experimental testing, if properly performed. With the advancement in computer simulations, full finite element validated vehicle models are being analyzed crashworthiness characteristic and occupant safety of vehicle.

In this thesis, the rollover analysis of the coach structure will be performed nonlinear explicit dynamic FEM code RADIOSS software as a solver because of the time integration, large displacements, local bucklings and plastic deformations. FE model of the rollover analysis will be generated with HyperMesh and HyperCrash pre-processor softwares. The results of the explicit dynamic rollover analysis results and the strength of the vehicle will be assessed with respect to the requirements of the official regulation with using HyperView post-processor software.

ÇOK AMAÇLI BİR OTOBÜSÜN DEVRİLME GÜVENLİĞİNİN İNCELENMESİ

ÖZET

Otobüsler dünya çapında geniş bir şekilde kullanılan toplu taşıma araçlarıdır. Ekonominin gelişmesiyle, otobüslerin sayısı hem kırsal hem şehirsel alanlarda hızla artmaktadır. Otobüs sayının artmasıyla, yolcuların ve otobüs personelinin güvenliğinin önemi daha da anlaşılmıştır. Otobüs kazalarının büyük çoğunluğu; devrilme, çukura veya şarampole yuvarlanma kazalarıdır. Devrilme kazaları sonucunda otobüs gövdesindeki aşırı deformasyon da yaralanmalara sebep olmaktadır. Deforme olan parçalar ile yolcu vücudu arasında darbe nedeniyle oluşan yüksek temas kuvvetleri ciddi yaralanmalara sebep olmaktadır. Otobüs gövdesinin yaşam hacmine girişimini minimize ederek bu tarz yaralanmalar azaltılabilinir. Araştırmalar göstermektedir ki, devrilme sırasında yaşam hacmine bir girişim yaşanmadığında, otobüs devrilme kazalarında görülen ağır yaralanma ve ölüm oranlarında önemli bir düşüş tespit edilmiştir.

Otobüsün devrilmesi sırasında, otobüs yolcuları otomobil yolcularına kıyasla daha geniş bir dönme merkezinden devrildikleri için daha yüksek bir enerjiye maruz kalırlar. Bu nedenle, ECE 66-02 regülasyonu devrilme kazalarındaki katostrofik/feci sonuçları önleyecek ve otobüs yolcularının güvenliği sağlayacak yaptırımları içerir. ECE 66-02 regülasyonunda, bir otobüsün devrilme güvenliğini değerlendirmek için bir temel ve dört muadil metot tanımlanmıştır. Temel metotta, bütün bir araç gerçek şartlarda devrilme testine maruz bırakılır. Muadil metotlardan biri ise devrilme testini bilgisayar simülasyonu ile yapmaktır. ECE 66-02 regülasyonu, uygulanabilir testlerle sonlu elemanlar modelinin doğrulanması şartıyla, bilgisayar destekli mekanik hesaplamalarını otobüslerin güvenlik değerlendirmesinde kullanılmasını kabul eder. Araştırmalar gösteriyor ki; sonlu elemanlar yöntemini kullanan programlar kullanılarak simüle edilen otobüs devrilme analiz sonuçları ile gerçek devrilme test sonuçları arasında iyi bir uyuşum olduğu görülmüştür.

Otobüs devrilme kazaları, önden ve yandan çarpma kazalarına nazaran diğer kaza türlerine göre en önemli kaza tipidir. Geçen yıllar göstermiş ki, devrilme kazası ile deforme olan otobüs gövdesi yolcuların hayatını büyük ölçüde tehdit etmiştir. Bu nedenle, otobüs üreticileri için otobüslerin devrilme dayanımı çok önemli bir güvenlik maddesi haline gelmiştir. Avrupa ülkelerinde, otobüslerin devrilme durumundaki deformasyon dayanımını sağlamaları ECE 66-02 regülasyonu ile zorunlu hale getirilmiştir. Regülasyonun belirttiği üzere, sertifikasyon hem araç bazında gerçek bir devrilme testiyle hem de ileri nümerik metotlara dayanan hesaplama teknikleri ile alınabilir (örn., doğrusal olmayan eksplisit dinamik sonlu elemanlar yöntemi). Testin veya bilgisayar analizlerinin sonunda eğilme deformasyonunu miktarını inceleyen mühendisler, regülasyonda tanımlanan yaşam hacmine herhangi bir girişim olmaması ile ilgilenir. Devrilme simülasyonu, gerek otobüs gövdesinin devrilme platformundan devrilmesini, gerekse otobüs gövdesinin yere çarpmasını inceler.

ECE 66-02 regülasyonu gereğince, yolcuların yaşam hacmi otobüsün gövdesine göre tanımlanmıştır ve bu bölgeye devrilme kazası sırasında herhangi bir girişim olmamalıdır. Bu regülasyon, yaşam hacmine girişimleri engellemek için otobüs gövdesinin yeterli dayanıma sahip olmasını sağlamaktadır. Yolcularının ve bagajların ağırlığının devrilme enerjisine etkisi ayrıca incelemelidir.

Bir otobüsün araştırma geliştirme (ARGE) sürecinde, bütün bir araca gerçek devrilme testi uygulamak yüksek maliyeti ve oldukça zaman alan süreci nedeniyle oldukça zahmetlidir. Gerçek testlerin yüksek maliyeti ve test sırasında veri toplama zorlukları nedeniyle, analitik veya bilgisayar destekli hesaplama metotlarına olan ilgi arttırmıştır. Bilgisayar destekli simülasyon teknolojisinin avantajları, başlangıç tasarım safhasında bile mühendislere otobüs yapının devrilme güvenliğinin hızlıca belirlenmesine olanak sağlar. Eğer doğru yapılırsa, simülasyon tabanlı devrilme analizi gerçek devrilme testlerinin yerine geçebilmektedir. Bilgisayar simülasyonlarının gelişmesi ile birlikte, sonlu elemanlar metodu kullanılarak doğrulanmış araç modelleri ile aracın çarpışma karakteristiğinin ve çarpışma sırasında yolcuların güvenliğinin analizi yapılabilinir.

Simülasyon tabanlı devrilme analizi korelasyonu için gerekli olan bilgisayar destekli katı mekaniği modellerinin validasyon çalışması; sonlu elemanlar yöntemiyle

oluşturulan matematik modellerin yapılacak fiili testler ile doğruluğunu karşılaştırmak ve yapılan varsayımları teyit etmek amacıyla yapılacaktır. Bu çalışma ile elde edilecek bilgi birikimi araç seviyesindeki devrilme analizi modeline aktarılacak olması tez çalışmasının ARGE niteliklerinden biridir.

Bu tez çalışmasında, otobüs gövdesinin devrilme analizinde zaman integrasyonu, yüksek deformasyonlar, lokal burkulmalar ve plastik deformasyonlar nedeniyle doğrusal olmayan eksplisit dinamik sonlu elemanlar çözücü kodu olarak RADIOSS programı kullanılacaktır. Devrilme analizinde kullanılacak olan sonlu elemanlar modeli HyperMesh ve HyperCrash programları kullanılarak oluşturulacaktır. Devrilme analizinin sonuçları ve regülasyona göre araç dayanımın değerlendirilmesi HyperView programı kullanılarak yapılacaktır.

1. INTRODUCTION

1.1 Purpose of Thesis

The aim of the thesis is minimized severity of rollover crashes to identify and describe a pattern in bus and coach related incidents leading to injuries and fatalities, with special attention to injury causation and injury mechanisms, and to strengthen superstructure for the improvement of bus and coach safety, especially with respect to passive safety regulation ECE 66-02 [1].

The purpose of the ECE 66-02 regulation is to ensure that the superstructure of the vehicles, which belonging to Categories M2 or M3, Classes II or III or Class B having more than 16 passengers, have the sufficient strength that the residual space during and after the rollover is unharmed.

The target of this study is using the advancement of computer simulation technology to make quick assessment of coach rollover crashworthiness even at the initial design phase. Simulation-based rollover analysis can assist, even replace the experimental testing, if properly performed. With the advancement in computer simulations, full finite element validated vehicle models are being analyzed crashworthiness characteristic and occupant safety of vehicle.

1.2 Bus Classification

There is no universal definition of buses and coaches. Generally, buses are defined and named after purpose and use. In Europe, the term bus is used to describe a city bus used for short-term transportation of people on urban streets, carrying standing and seated passengers. Local buses and transit buses are other examples of this category. Inter-city bus describes another type that mainly has seated passengers, but is allowed to transport standing passengers and is used on both urban and rural roads. Coach is yet another type, which generally means vehicles transporting seated

passengers long distances on rural roads. They are also called tourist/touring coaches or long-distance coaches.

Within the EU, the M-definition was constructed and used, in order to include all road vehicles under a common classification (Directive, 1970/156/EEC, 1970), classifying vehicles after seating capacity, usage and weight. M1 are vehicles with no more than eight passenger seats. M2 are vehicles with more than eight passenger seats and a mass not exceeding 5 tones, while M3 are M2 vehicles but exceeding 5 tones. The M-definitions are further divided into classes (I – III) depending on field of application [2].

The concept bus translated into the M-classification means M2 or M3 vehicles class I, with areas for standing passengers to allow for their frequent movements. Coach means M2 or M3 vehicles class II and III, where class II are vehicles principally for carriage of seated passengers and designed to allow standing passengers while class III are vehicles designed for seated passengers, exclusively.

1.3 Bus and Coach Rollover Incidents

In order to identify and describe a pattern in bus and coach incident related injuries and fatalities, and to suggest possible future measures for improvement of bus and coach safety, a literature analysis was performed. Of all traffic fatalities in Europe, bus and coach fatalities represented 0.3–0.5%. In the OECD countries, the risk of being killed or seriously injured was found to be seven to nine times lower for bus and coach occupants as compared to those of car occupants. Despite the fact that fatalities were more frequent on rural roads, a vast majority of all bus and coach casualties occurred on urban roads and in dry weather conditions. Boarding and alighting caused about one-third of all injury cases. Collisions were a major injury contributing factor. Buses and coaches most frequently collided with cars, but unprotected road users were hit in about one-third of all cases of a collision, the point of impact on the bus or the coach being typically frontal or side. Rollovers occurred in almost all cases of severe coach crashes. In this type of crash projection, total ejection, partial ejection, intrusion and smoke inhalation were the main injury mechanisms and among those, ejection being the most dangerous.

The traffic in general continues to increase in Europe (European Commission, 2001) [3]. Unlike the trend for cars, however, deaths and injuries involving buses and coaches have been stable over recent years in the European Union (EU) (European Commission, 2002) [4]. For example, in the eight countries covered by the Enhanced Coach and Bus Occupant Safety (ECBOS) project approximately 20 000 buses and coaches with a kerb weight >5000 kg, were involved in crashes, the consequences being approximately 35 000 people injured and 150 killed, annually [5]. In fact, in France, the Netherlands, Spain and Sweden the casualties in buses and coaches have increased during the years 1994–1998 [5].

Based on a investigation study about and coach transport, with respect to travel habits, crashes, injury data and restraint systems, possible future preventive measures could hopefully be suggested, in order to contribute to improved safety in buses and coaches. The measures to reduce harm can either be to decrease the probability of a crash (active safety) or minimize the consequences, (passive safety), and in case of an injury-related incident, enhancement of rescue and medical treatment [6].

In the EU, a new bus-directive “Directive, 2001/85/EC” of the European Parliament and of the Council, (Directive, 2001/85/EC, 2002) has recently been implemented, which prescribes mandatory seatbelts in all new buses or coaches for seated passengers, exclusively [7].

1.4 Severe Rollover Crashes

Based on 47 real-world coach crashes with at least one “severe injury or passenger fatality”, Botto et al. (1994) found that rollovers and tipovers occurred in 42% of the cases. The study outlined five main injury mechanisms in severe coach crashes [8].

1) Projection: occupant interaction with other occupants and the interior of the coach. Projection was the most frequent injury mechanism, but on average the lowest injury severity. Due to the uncontrolled movement of the occupants inside the bus, their impacts the structural parts of the passenger compartment.
2) Total ejection: the occupant being ejected or thrown out of the vehicle. During the rollover process, the occupants could be ejected through the broken or fallen windows and crushed by rolling bus.

3) Partial ejection: part of the occupant's body was thrown out of the compartment. During the rollover process, parts of the passenger's body come contact with outside surface and can be strongly scratched or parts of the body (head, arms and chest) get under window column or waistrail and are pressed by it.
4) Intrusion: the occupant being injured inside the vehicle, due to structural deformation or intrusion of an object. Due to large scale structural deformations and the loss of the residual space, structural elements intrude the body of the occupants or crash them.
5) Inhalation of smoke following a fire.

There are five important injury mechanisms, which should be considered enhancing the passenger safety in rollover. The most dangerous one is the intrusion, when due to the large scale structural deformation structural parts intrude into the passenger, or compress them (lack of the strength of superstructure).

Injury mechanisms in rollover coach crashes were further analyzed in Botto and Got (1996) [9]. Two separate sources were used, 16 real-world crashes and 3 experimental crash tests using road ready vehicles. In the real-world crashes, 19% of the occupants were killed. The highest proportions were found in rollovers over a fixed barrier, yielding a 30% rate of KSI (killed or seriously injured). In rollovers without a fixed barrier, the KSI rate decreased to 14%. If the coach had an upper and a lower compartment then more than 80% of KSI were located in the upper section of the coach. The most severe injuries occurred during sliding over the outside ground after the rollover.

From the Great Britain's part of the ECBOS project, it was reported that rollovers were the cause for 1% of all casualties, but representing only 0.2% of all vehicles involved in crashes [5]. Spanish data from 1995–1999 showed a rollover frequency of 4% of all coach "accidents" on roads and highways, and the risk for fatalities in a rollover was five times higher than in any other coach "accident" type [10].

Rasenack et al. (1996) analyzed 48 touring coach crashes in Germany of which eight were rollover/overturn crashes. These eight crashes accounted for 50% of all severe injuries and 90% of all fatalities [11].

1.5 Statistics about Bus Rollover Accidents

After a very serious rollover accident (happened in 1973), the problem of the required strength of bus superstructures in the case of rollover accidents is discussed in ECE Geneva. The born of an international regulation needed 12 years. The major problem was to find an appropriate standard rollover test, which is easy to perform, repeatable, which can separate the strong superstructure from the weak one, which leads to a higher level of passenger safety. [12]. In the mid of ’70-s there was no experience and knowledge about the bus rollover accidents, therefore the first step was to collect some statistical data. One of the first rollover statistics came from Hungary [13] collecting 19 rollover accidents from 1973-76. The main categories of these rollover accidents can be seen in Table 1.1. These accidents “produced” altogether 10 fatalities, 37 serious and 55 light injuries. However, it has to be mentioned that there was no injury data available about five accidents and in five buses, there were only two or three people, together with the driven. Another interesting information that the speed of the bus was less than 10 km/h in five cases, no speed information in three cases and there were only four accidents where the speed exceeded the 40 km/h when the rollover process started. All of these buses were large (11 m long) vehicles, the superstructure collapsed totally in 8 accidents, strongly damaged in 3 accidents, no information about the damage in 3 cases.

Another collection was presented in UK [14] containing the description of 8 rollover accidents from 1976-77 (see also in Table 1). Four superstructures completely collapsed, two of them seriously damaged. 50 persons were killed in these accidents and many of them injured. They reported four accidents in which passengers were ejected from the bus and then rolled on (killed) by the vehicle (altogether 8 fatalities on that way). Two buses belonged to the midi category (7-8 m long).

Table 1.1 : Statistics about types of rollover accidents in different countries [13-17].

Type of rollover	Hungary [13]	U.K. [14]	GRSA [15]	Hungary [16,17]
On flat road, turn on side (1/4 rotation)	6	2	11	6
On flat road rolled on the roof (1/2 rotation)	2	3	6	5
Rolling down on a slope (3/4 – 1,5 rotation)	9	2	17	6
Rolling around falling down from overbridge	2	1	-	-
Severe or combined rollover accident	-	-	-	2
Altogether	19	8	33	19

On the basis of these accident statistics GRSA (the international working group in Geneva, which worked out the ECE Regulation 66) started to work and continued to collect accident statistics. During the period, 1980-1988 altogether 33 rollover bus accidents have been reported in GRSA involving eight countries as the scene of the accidents. [15] The distribution of the type of these accidents is also shown in Table 1.1. Their result was 93 fatalities and 206 injuries. This was the first statistics in which the high decker coaches appeared as victims of rollover: six high decker coaches were reported turning on their side.

The brief results of another Hungarian rollover statistics [16,17] is given in Table 1.1, too. These accidents are resulted 13 fatalities, 205 injuries in Table 1.2 and there were no data about fatalities/injuries at five accidents.

Table 1.2 : Summary of statistics (APPENDIX A).

Summary of rollover statistics	Statistics I. 1990-1999	Statistics II 01.01.2000 01.03.2001	Statistics III 01.03.2001 31.07.2002	Statistics IV 01.08.2002 31.12.2002	Sum of I - IV
The number of accidents	23	23	51	20	117
The number of countries involved[(1)]	min.15	min.15	min.26	min.14	min.40
Total number of fatalities	238	254	519	170	1181
- serious injuries	103	107	94	56	360
- light injuries	122	123	170	47	462
- injuries without classification	197	122	189	160	668
- reported “many injuries”	2 times	1 time	6 times	1 time	10 times
Type of rollover accident (severity)					
- turned on side	4	2	5	5	15
- rollover from the road[(2)]	13	12	18	7	50
- serious rollover [(3)]	3	6	9	3	21
- combined accident with rollover[(4)]	3	3	19	5	30
Category of the bus rolled over					
- Category I. (city, suburban)	2	2	2	-	6
- Category II (intercity, local)	-	2	2	-	6
- Category III (tourist, long-distance)	18	10	20	9	57
- Small bus	-	2	9	8	19
- Double decker	2	2	1	-	5
- School bus	-	1	2	-	3
- Other (worker, pilgrim, etc.)	-	1	4	-	5
- unknown	1	3	9	3	16
Deformation of the superstructure					
- serious deformation[(5)]	4	5	6	9	24
- slight deformation[(6)]	5	5	11	7	28
- no information	14	13	34	4	65

(1) Countries may be involved as manufacturer, approval authority, operator or the scene of the accident.

(2) Not too severe accident, but more than turning on side (1/4 rotation) roll down into a ditch, down on a slope (not more than two rotation) turned down from an overbridge of a highway.

(3) More than two rotations, more than 8 m level difference in the rollover or falling dawn.

(4) The combined accident means e.g. rollover after a serious frontal collision, rollover with fire, falling into water after rollover, etc.

(5) Serious deformation means the damage of the survival space (the collapse of the superstructure obviously belongs to this category).

(6) Slight deformation means that the survival space very likely did not damage in the rollover accident.

1.6 Severity of Different Types of Rollover Accidents

Serious bus crashes, particularly those involving school buses and intercity buses are investigating by Transport Canada's multidisciplinary collision investigation teams. In an attempted to better understand the injury circumstances in bus collisions in Canada, data were extracted by Transport Canada on 21 collisions involving intercity buses, which occurred between 1990-2001 and were investigated by the teams [18]. These collisions came to the attention because of their high level of severity or their high profile in the media. Although this is a biased sample, the data are useful in considering the circumstances of fatal and serious injuries and ways in which they may be prevented. A summary of the known occupancy and injury severity levels is given in Table 1.3.

Table 1.3 : Occupant injury severity in 21 severe intercity bus collisions in Canada [18].

	Injury Level (AIS)								Number of total people	Number of known ejections
	0	1	2	3	4	5	6	9		
Rollover										
Driver	0	3	0	1	0	0	2	1	7	1
Passenger	26	110	12	5	9	1	50	4	212	22
Total	26	113	12	6	9	1	52	5	219	23
Non-Rollover										
Driver	6	2	0	1	1	0	3	1	14	0
Passenger	173	90	30	15	9	1	14	0	332	11
Total	179	98	30	16	10	1	17	1	346	11

Of the 21 selected collisions, there were seven (33%) rollover events, which accounted for the majority of severe and fatal injuries (Table 1.4). There were a total of 64 passenger fatalities and 5 driver fatalities. Two-thirds of the fatalities occurred in one collision in which the driver and 43 passengers were killed when the bus fell down a ravine. Of the remaining 25 fatalities, 16 (64%) occurred in rollover collisions. There were 31 occupants ejected, 16 (51.6%) of whom were fatally injured. Rollover collisions accounted for 23 (74.2%) of the 31 ejections. A summary of the ejections by collision was not always known, percentages are not included.

Table 1.4 : Ejection status by collision type in 21 severe intercity bus collisions in Canada [18].

	Ejected		Not Ejected	
	Fatal	Non-Fatal	Fatal	Non-Fatal
Rollover	7	16	45	156
Non-Rollover	11	0	6	341
Total	18	16	51	497

The severity of the accident is an essential issue when determining the standard approval test, this expresses the demand of the public opinion: in which kind of accident situations should be the passengers protected, the survival possibility assured. It seems to be acceptable to say that the first two accident type, the “turn on

side" and, "rollover from the road" accident categories (protected accidents) should be covered by the standard rollover test. 65 accidents (55% of the total) belong to these two categories.

Table 1.5 : Statistics about construction of coaches having rollover accidents (APPENDIX A).

Construction of coaches having rollover accident	Number	Percentage (%)
Traditional (total height 3-3,2 m)	17	27,5
Probably traditional	5	8,0
HD (total height more than 3,4 m)	17	27,5
DD (double decker coach)	5	8,0
No information about construction	18	29,0
Total	62	100

Table 1.6 : Statistics about different types of rollover accidents (APPENDIX A).

	Turned on side	Rollover from the road	Combined rollover	Serious rollover	Total
Hungary	9 (26%)	21 (60%)	5 (14%)	-	35 (100%)
Europe (excl. Hungary)	6 (15%)	15 (37%)	10 (25%)	9 (29%)	40 (100%)
Other than Europe	1 (3%)	14 (33%)	15 (36%)	12 (28%)	42 (100%)
Total	16	50	30	21	117

Table 1.7 : Statistics about injury levels in accidents belonging to "turn on side" and "rollover from the road" (APPENDIX A).

Injury levels in accidents belonging to "turn on side" and "rollover from the road" (totally 63 accidents)	Number of persons	% of the total, given in Table 1.2	Number per accident
Fatalities	351	30%	5,7
Serious injuries	218	60%	3,5
Light injuries	310	67%	5,0
Injuries without classification	297	44%	4,8
Statement "more fatalities and injuries"	5 times	50%	-

Some words about the virtual severity of the accident type, "Turn on side" accident seems to be the less severe rollover accident. Two comments to this statement:



Figure 1.1 : Turn on side, where the rotation is stopped by a tree [17].

What accident situation will result “turn on side” rollover accident? It depends mainly on the circumstances and not on the construction of the vehicle. Many rollover accident start on the following way: the bus slips on the road, the one side wheels are stopped (blocked) by the soft, deep soil of the roadside (or by the curbstone) and the lateral accelerations rotates the bus around the blocked wheels. The further motion depends on the circumstances. Figure 1.1 shows a situation, when a tree or another example: the shape of the ditch and the soft deep snow (Figure 1.2) prevented the further rotation.



Figure 1.2 : Turn on side in a snowy ditch - 1 [17].



Figure 1.3 : Turn on side in a ditch - 2 [19].

Very typical “turn on side” accident may be ended by a very severe situation. Three similar accidents were analyzed, which started on the same way: driving with high speed, after a sudden steering the bus turned on its side crosswise on the road and slipped away.

- Slipped into a ditch and the superstructure collapsed, 20 fatalities [20].
- Slipped away and rolled down on the slope of the elevated road and the superstructure collapsed, 46 fatalities [21].
- Slipped away and hit the steel side rail of the road, which cut and pressed the superstructure, 20 fatalities [22].

It is difficult to control whether the decided and used standard approval test is adequate to separate the strong superstructure from the weak one, to meet the demand of the public, to assure the required safety for the passenger. A slow feedback can be found from the accident statistics, from the analysis of rollover accidents. Figure 1.4 shows the result of rollover accident, rolled over on a flat road. It is obvious that the superstructure is weak, cannot assure a survival space for the passengers. Different kind of standard rollover tests showed the same result [12]. After reinforcing the superstructure, all the different standard rollover tests gave positive result. Figure 1.5 shows the final position of a reinforced bus in a rollover accident, Figure 1.6 gives another example with an approved vehicle rolled down on the same slope of the road which destroyed the weak superstructure.



Figure 1.4 : The results of real rollover accidents with weak superstructure [23].

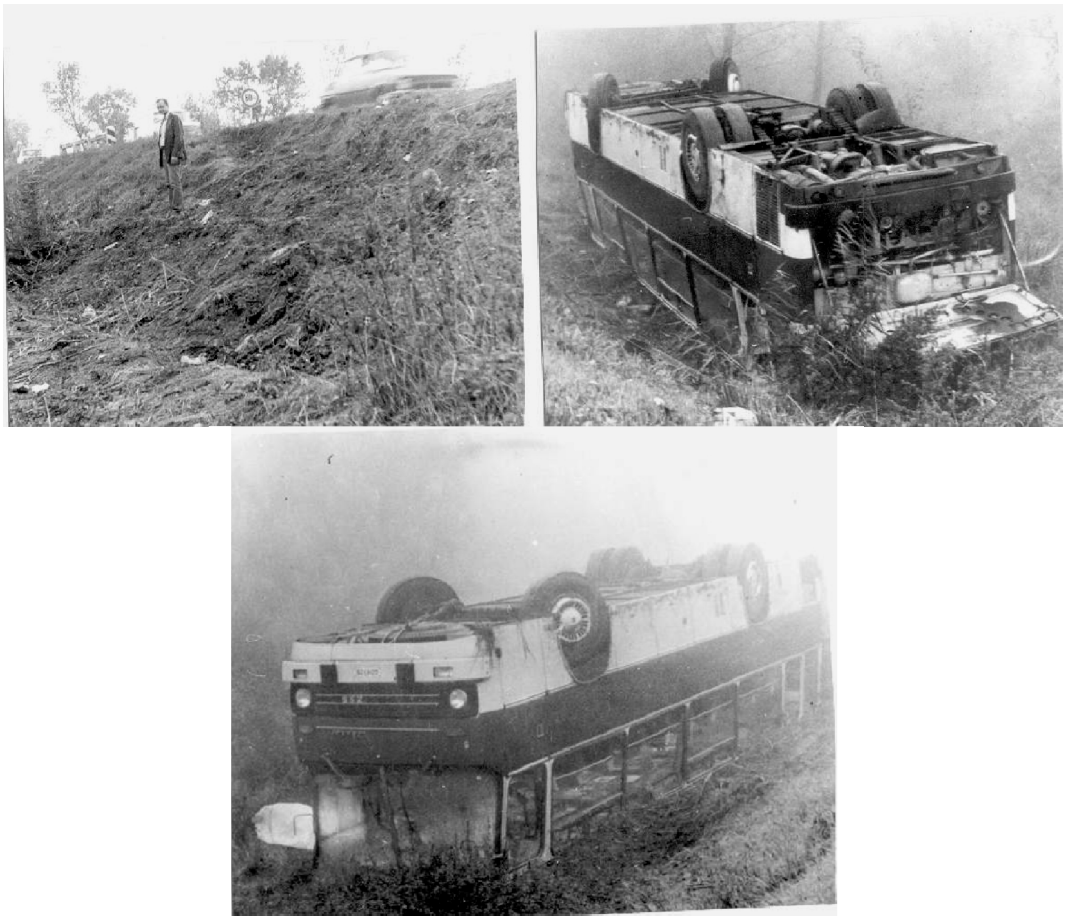


Figure 1.5 : Rollover accident with reinforced superstructure [17].



Figure 1.6 : Strong superstructure assures the survival space [24].

This new rollover statistics does not give direct information about the approval of the buses regarding ECE 66-02 [1]. However, indirectly, Table 1.8 gives an interesting comparison. As it was defined above, “protected rollover accident” covers those accidents in which the passengers should be protected, the survival space shall be maintained. Among the 117 rollover accidents, there are 49 in which we have information about the behavior of the superstructure: 26 accidents did not cause damage in the survival space and in 23 accidents the survival space was harmed, including the total collapse, too. The casualties belonging to these two groups are significantly different. The fatality rate is 16 times, the serious injury rate 3 times higher when the survival space was damaged. From this recognition, it comes the clear goal of the international regulation: in the protected accidents, the survival space shall be maintained. It is interesting to mention on the basis of Table 1.8, that the numbers of the light injuries are not closely related to the type or category of the accident. It may be assumed that this type of injuries are caused mainly by the inside collision of the passengers when they are leaving their seats, seating position during the rollover process. The main tool to reduce this kind of injuries could be the use of seat belts (It has to be emphasized that the seat belt can reduce the number of fatalities and serious injuries, too.)

Table 1.8 : Statistics about construction of coaches having rollover accidents (APPENDIX A).

Considered accidents	Number of events	Casualty per accident			
		Fatality	Serious injury	Light injury	Injury without classification
All rollover accidents	117	10,1	3,0	3,9	5,7
Protected rollover accidents	65	5,7	3,5	5,0	4,8
Survival space unharmed	26	0,8	18	4,8	1,7
Survival space damaged	23	13,2	5,6	4,9	7,6

Introducing a new method of collecting statistics about bus rollover accidents, on the basis of 117 accidents some interesting information, evidences and tendencies could be recognized:

- The high vehicles (HD and DD coaches) are over represented in the rollover statistics, compared to their rate in the bus population (they need special attention in respect of lateral stability and strength of superstructure)
- The severity of an accident type depends on the circumstances of the individual accidents, the “turn on side” accident could be more severe than another accident type having higher virtual severity.
- The small buses, minibuses are also endangered by the rollover accident. Until now they were out of interest, therefore further investigation is needed to study the strength of their superstructure.
- The public demand may be formulated: the buses and coaches have to assure the survival space in the case of “turn on side” and “rollover from the road” type accidents. This two accident types covers around 70% of the total number of rollover accidents.
- If the survival space is assured in a rollover accident, the rate of fatality is reduced by 90-95% and the rate of serious injury by 60-65%.

1.7 Literature Review

ECE 66 [1] is one of the first international documents allowing for substitution of full scale tests with the computational analysis for vehicle approval. This type of decision definitely leads to broader usage of FE analysis in the bus industry. The

evidence of such tendency can be noticed from published in the last two decades research outcomes where FE simulations were used for bus safety assessment.

One of the first publications where computational analysis of the bus structure was presented at Subic et al. [25]. The bus superstructure (elements contributing to the bus strength) was modeled here using 260 beam elements in Pro/MECHANICA FE code for the structural optimization. The model validation process was not present in the report and only modal analysis was performed there. Based on findings from the research the recommendations were addressed aiming to reduce weight, increase structural damping and reduce the height of the CG location.

The study described in Borkowski et al. (2006) concerned a public transportation city bus. The model of the superstructure was developed together with the model of the representative bus section [26]. The response of the segment and the whole bus structure was compared with respect to the maximum deformation. The difference between these both cases was below 10%. In this case, no information was provided regarding the experimental testing and validation efforts for the FE model.

Another research on bus segment rollover performance was presented in Belingardi et al. [27]. This time the authors used MADYMO software to study the influence of passengers and different restraint types on deformation extent in the rollover test. FE modeling was coupled with the so called multibody (MB) simulations to obtain nonlinear characteristics of seat structure elements. The MB model was then validated against laboratory results and then multiple load cases were simulated. In addition, dummy MB models were included in the model to provide prediction data about injury level of the bus passengers. This study seems to be one of higher reliability among others found in the literature. However, the tests and simulations were performed on the bay level only.

In Elitok et al. (2006) researchers developed the detailed FE LS-DYNA model of an intercity coach bus [28]. Validation tests on connection of the main vertical beams of the superstructure to the horizontal beam at the waistrail level of the bus were conducted. The connection was quasi-statically bent and good correlation was found in the LS-DYNA simulations. A similar test was repeated for connection between roof bows and wall horizontal beams at the cantrail level. The model was reflecting

the superstructure of the bus since ECE 66 [1] allows for such simplification. The skin part was not modeled in LS-DYNA making the results more conservative and easier to predict. The main objective of the research was to check the influence of the seat structure to the overall bus strength. It turned out that the seat structure reduces about 20% of the deformation if included in the FE model.

Overall mass-transit bus FE detailed model development process was a part of the work described in Deshmukh (2006) [29]. It is probably the broadest report about the numerical study on the bus published so far. The authors used LS-DYNA FE code to assess bus strength according to the ECE 66 [1]. They built a shell element based FE model that included the superstructure as well as the skin and some elements of the interior of the bus. The model was partially validated for a roof crush test. It was only checked if the deflection of the roof under the 1.5 bus load is smaller than the limit value of 152 mm (6 in) resulting from A.P.T. (1997) [30]. No validation tests were done on low and intermediate levels of the bus assembly hierarchy.

Researchers in Spain, Castejon et al. (2006) were developed a FE model of a bus to test usefulness of designed by them energy absorbers for rollover type accidents [31]. The numerical model was validated through the rollover test on the bus segment. When good correlation was found, the model of the full bus was developed. It was shown that the energy absorbers could take up to 30% of the energy from the impact. The same authors in Castejon et al. (2006) used FE simulations of rollover test for early study of the strength of their prototype composite bus [32]. After numerical studies on the bus strength, a new design of lightweight bus structure was built and tested experimentally.

Tata Technologies (part of Tata Motors, India) is a research institute performing among others full scale rollover tests on their coach buses. The ECE 66 [1] procedure was also ratified in India and the institute utilizes both experimental and numerical approaches to the approval process. The FE models of buses are analyzed in the LS-DYNA program. Tata Technologies used simplified method based on the beam elements and assumptions that primary deformations occur in the steel structure of the bus body [33]. The rollover event was also simplified and the bus structure is loaded by impactor instead of the impact caused by rotational movement of the bus falling into the flooring. The joints between members were assigned the bending

characteristics (bending moment vs. angle change) from the experimental tests. Such way of representation, the complex system like a bus body structure significantly reduces the computational time. However, the failure mode of the system is predetermined by the model developer and no behavior like local buckling of the tubes can be accounted for in the simulation.

A lot of practical value concerning bus rollover testing can be attributed to the ongoing research at Cranfield Impact Centre (CIC), UK [34]. CIC performs many full scale tests and FE simulations on small busses (called in Europe M2 category of buses) and intercity coaches (M3 category) for numerous bus producers in the Europe. The simplified FE models of the bus bays are built usually by the combination of the shell and beam elements or detailed models from shell elements depending on the complexity of the problem and the used software (from the simplest for PAMCRASH through the more intricate for MSC) DYTRAN and ANSYS programs [5]. The models are validated through the integral (full scale) validation using the ECE 66-02 [1] rollover procedure for the bus bay. The FE dummies' response is also a merit of the research in both experiment and FE programs (MADYMO and LS-DYNA) [5,35]. The studies confirmed the necessity of having at least 2-point seatbelts in the buses to prevent majority of injuries caused during a rollover accident. The mass of belted passengers should be then considered during the simulation of the test. The research proposes inclusion of the M2 vehicles into the scope of the ECE 66 [1].

In Pavlata et al. (2005), researchers presented results from advanced study on the virtual bus rollover testing. FE models of several bus superstructures were developed and analyzed according to the ECE 66-02 [1] for the approval purposes [36]. PAM-Crash software was utilized. Rollover tests according to the equivalent ECE 66 [1] approval procedure on the segments were performed to validate the FE models. In addition, the dynamic bending of structural tubes was performed to calibrate the strain rate parameters in the steel material. However, the most important part of the structure connections was not tested and again was simplified in all models. There was no physical representation of welds and bolts.

FE simulations became indispensable tools supporting the design process in many engineering fields including metal forming, automotive crash simulations, vehicle

occupant protection, building blast resistance, structures' progressive collapse and many others. Recent developments in FE explicit codes and huge increase in computational power allow for modeling complex systems with detailed reflection of their mechanical behavior, exact contact impact description and their representation in hundreds of thousands of elements. FE simulations even started to be advocated by government agencies like the National Science Foundation [37,38] as approval techniques for new designs whose full scale testing is difficult, if possible at all, or is not cost effective. Decisions are made based on the results from numerical simulations. At the same time, parallel development of GUI for FE explicit codes made it easy to create FE models, run advanced numerical simulations and post-process results by very inexperienced researchers. Results are often generated without a thorough Verification and Validation process (V&V) of the FE model or this process is just insufficient for the application regime of the model. In such an environment, the outcome of calculations may be way off of reality and wrong conclusions can be drawn. Due to increased trust given to the FE simulations the efforts, need to be strengthened to ensure an appropriate level of credibility assigned to the obtained numerical results.

The numerical approach to the rollover crashworthiness of buses is relatively new and not fully explored research area. Although, the ECE 66 [1] allows for the bus approval based on the validated models and the numerical simulations, yet few can prove that their models can be used for that purpose with the high confidence. In fact, even in the ECE 66 [1] only general guidelines are stated how to build the numerical model and perform rollover test simulations. The last appendix of ECE 66 [1] sets these requirements. As indicate referenced publications, most of the rollover simulations are used rather for the comparative study and introduction of the modifications in the existing designs. The verification of the model is usually not even mentioned and the validation tests are only selective. In the FE models, the most relevant bus structure parts for the rollover response – connections are overly simplified in the published analyses and rarely tested. The research in numerical rollover testing area should focus now on standardization of the methods for verification and validation, that ultimately would lead to trustworthy, numerical approvals of the buses [1]. One of goals of this dissertation is to present a modest plan, which would lead to development of such a trust.

1.8 Hypothesis

The scope of this study was expanded to cover other rollover scenarios it is likely that roof intrusion would play a greater role in occupant injury, the most obvious injury mechanism being crush of the roof structures and intrusion into the passenger survival space. During this study, the most common crash mechanism for serious injury when the coach is involved in a single crash were investigated to analyze the potential injury reduction for the passengers on the assumption that all have used a proper seat belt system, either 2-point or 3-point belt. This was done by registering all occupants, their seat position and the sustained injuries.

The survival space concept and the belonging existing requirements are very effective. Statistical data prove that the all casualty rate is 3 – 4 times lower, the fatality rate is lower with one order (10 times) when the survival space remains intact.

The strength of a structure changes during collapse, which may be very important in a rollover accident since the deformed roof should support the vehicle weight. This variation is controlled by the hinge behavior. It is convenient to discuss the hinge strength in terms of a moment that it can develop at a particular stage of deformation.

- Rollover is the crash mode, which caused most of the fatal and serious injury to bus occupants.
- There are several injury mechanisms, which should be considered enhancing the passenger safety in rollover. The most dangerous one is the intrusion, when due to the large scale structural deformation structural parts intrude into the passenger, or compress them (lack of the strength of superstructure).
- The fixes proposed in regulations consisted of improving the bus structure to ensure that no infringement of the occupant space occurred.
- Various type approval methods in the ECE 66 Regulation have been using for testing of bus superstructure with bus manufacturers.

1.9 Discussion

Non-collision incidents are an important cause for injuries in buses and coaches and in some countries, they constitute a major part of all casualties. Obviously, they are

not as spectacular as a rollover and, therefore, do not become the newspaper headlines, but are an important issue when addressing the total injury problem in buses and coaches. In non-collisions, emergency braking, boarding and alighting seem to be crucial parts and, hence, constitute a major cause for these injuries.

Rollovers seemed to be rare events but when they occur, they may cause a number of severe injuries. If the bus or coach had two levels, an upper and a lower section, it seemed that the vast part of the severe injuries was located in the upper section. In case of a rollover, passengers run the risk for being exposed to ejection, partial ejection or intrusion and thus exposed to a high-fatality risk [18].

The difference for a bus or coach passenger, with respect to biomechanics and space, as compared to those of lighter vehicle passenger becomes obvious in a rollover crash. During a bus or coach rollover, the occupant will have a larger distance from the centre of rotation as compared to that of a car occupant. Due to this fact, an unbelted bus or coach occupant will have a larger velocity when projected or ejected, than a car occupant.

2. ROLLOVER SAFETY OF BUSES

2.1 Introduction

The passive safety problems of buses, has been arisen - in the early 70's - on international level. The GRSA (expert group of bus safety, ECE WP29 in Geneva) started to work on two main subjects: the rollover of buses (required strength of the superstructure) and the frontal impact (strength of seats and their anchorage, the retention of passengers). The goal of this work was to produce international regulations for bus type approvals. In the same time, there was another international forum - the Meeting of Bus and Coach Experts, organized in every 3rd year in Budapest, which provided a good opportunity for the researches, bus manufacturers and other experts to discuss the whole subject (accident statistics, test methods, test results, computer simulation, etc.) on a technical-scientific level. This thesis tries to give a survey about the most important subjects belonging to the passive safety of buses, mostly based on the Hungarian experiences, test results and research works.

2.2 International Safety Regulations

2.2.1 Principle of passive safety

The goal of the passive safety developments and regulations is to reduce the injury risk of the passengers down to an acceptable limit in a measurable way, to ensure their survival possibility in a certain accident situation. To understand this general statement, some ideas have to be discussed and cleared.

2.2.2 Standard accidents

It is clear that every safety development (and regulation) is connected to a certain type of accident, but every type of accident has very large number of variations in respect to the severity and the way of process. For example; a bus overturn is when it turns down to its side with a speed closing to zero, and another overturn is when the

bus rolls down into a precipice having a depth of 20 m. It is obvious that in the first case, the passengers must be protected. In the second case, this is almost impossible. Talking about injury risk and its reduction a standard accident has to be defined on the basis of the followings. It must be based on statistical evidences, technically well defined, producible repeatable and agreed by the society in respect of its severity.

2.2.3 Risk of the passengers

This means the injury probability in a given accident situation, including the degree of injury severity (e.g. light, serious injury, fatality) The acceptable risk means the implicit agreement of the society about the tolerable injury probability in a certain standard accident. It is not the goal of the safety developments to reduce the risk down to zero in every case. Not because the risk depends not only on the standard accident but also on the individual health condition of the passengers and on a lot of accidental things.

2.2.4 Life danger

The life danger is a special kind of risk, which can be caused by the following major effects:

a) Losing the required survival space (when structural elements, even sharp, broken edges penetrate into this space, into the passenger).
b) The deceleration creates undesirable motion of the passengers in passenger compartment impacting different structural parts and these inner impact forces can cause fatality.

The individual capability of the passengers, their tolerance limits against different kind of impacts appears in the accident statistics, in the number of fatalities, but it cannot be involved into the international regulations. These figures are replaced by the average biomechanical parameters of the human being.

2.2.5 Survival possibility

It means the main components of circumstances, which give a chance to the passengers for survive. The survival possibility and the injury risk may be determined by detailed analysis of real accidents, standard accidents (tests) and the biomechanical behaviors of the human being.

2.2.6 Test and analysis methods

It is very important to have reproducible test methods - mainly the standard accident or equivalent tests, which can prove that the vehicle is acceptable in respect to the injury risk or survival possibility.

2.3 ECE Safety Regulations

One of the most important international safety regulations is belonging to the ECE Geneva Agreement (Another very important group of the safety requirements are the EEC Directives, but from the technical side they are almost the same as the ECE Regulations). Among these regulations, there are some regulations dealing with the passive safety of buses. These are:

- Regulation 36 : Some safety issues like emergency exits, interior arrangement, etc. regarding to large buses
- Regulation 52 : The same for mini and midi buses
- Regulation 66 : Roof-strength in case of rollover
- Regulation 80 : Strength of seats and seat anchorage

Comparing the subject of the existing regulations and the passive safety subjects, it can be seen that many of very important problems (like driver's protection, safety bumper, integrity of important structural element, side impact of low floor buses, general use of safety belts, etc.) is not regulated yet.

2.4 ECE 66-02 Regulation

2.4.1 Introduction

Bus rollover is one of the most serious types of accident as compared to other modes of bus accidents. Strengthening bus frames to maintain residual space (occupant space) and minimizing occupant injury are necessary. In the European countries, the certification of sufficient deformation strength when overturning is compulsory for the approval of a coach according to the ECE 66-02 [1] regulation. The certification is granted after positive results from computer simulations with full bus structure. The ECE 66-02 [1] regulation defines a survival space for the passengers, which must remain intact after the accident. The simulation specifies either overturning of

the vehicle structure from tilting platform or the impact of a plate on the coach structure as it would correspond to the crash of the structure when falling onto the ground. Since such tests with real structure are costly and computer efficiency, on the other hand, is becoming increasingly better and cheaper, rollover simulations have been playing a more important role for the approval. The verification of calculation is a compulsory requirement of the regulation, as it is the technical service's responsibility to verify the assumptions used in the finite element analysis.

Many researchers point out that such quasi-static tests with symmetric loading poorly represent the sequential dynamic load (in particular it's varying value, direction, and intensity) observed during actual bus rollovers. However, they provide greater repeatability of results than foreign dynamic test procedures like that introduced in the European Union (EU) directives and the United Nations (UN) regulations. Nonetheless, currently efforts are made by NHTSA to provide comparative study of bus structure rollover resistance tested according to FMVSS 220 [39] and ECE 66 [1]. Two bracket buses in respect of their strength will be chosen based on engineering judgment and tested according to both regulations. The comparison is supposed to show discrepancies between dynamic and static methods of testing and indicate a more conservative standard. This strategy is in agreement with the international tendency of unification rollover protection standards that led so far to ratification of ECE 66 by 44 countries worldwide [1].

2.4.2 General specifications and requirements

ECE 66-02 [1] refers to integrity of a bus roof and is based on a rollover test, Figure 2.1. The purpose of the ECE 66-02 [1] is to ensure a superstructure of sufficient strength so that the residual space, as defined in Figure 2.2, stays intact both during and after the dynamic rollover test. It stipulates that the entire vehicle resting on the tilt table is quasi-statically rotated on one of its sides. When the center of gravity reaches its highest, critical point, the bus begins falling due to gravity. The concrete surface of the ditch is placed 800 mm beneath the table's horizontal position. The angular velocity of table tilt shall not exceed 5 degrees per second. The test procedure is shown schematically in Figure 2.1.

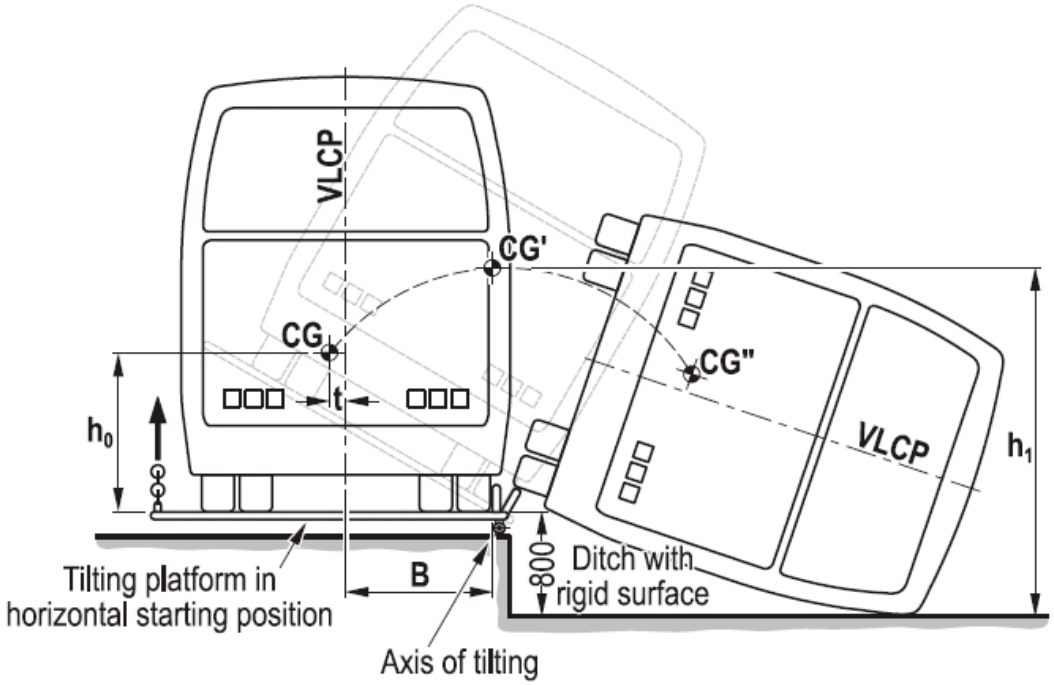


Figure 2.1 : Rollover test setup according to ECE 66-02 [1].

The rollover test shall be carried out on that side of the vehicle, which is more dangerous with respect to the residual space. The decision is made by the competent technical service on the basis of the manufacturer's proposal.

The lateral eccentricity of the centre of gravity and its effect on the potential energy in the unstable, starting position of the vehicle; the asymmetry of the residual space; the different, asymmetrical constructional features of the two sides of the vehicle; which side is stronger, better supported by partitions or inner boxes (e.g. wardrobe, toilet, kitchenette). The side with the lesser support shall be chosen as the direction of the rollover test.

The envelope of the vehicle’s residual space is defined by creating a vertical transverse plane within the vehicle, which has the periphery described in Figure 2.2, and moving this plane through the length of the vehicle.

The superstructure of the vehicle shall have the sufficient strength to ensure that the residual space during and after the rollover test on complete vehicle is unharmed. No part of the vehicle, which is outside the residual space at the start of the test (e.g. pillars, safety rings, luggage racks) shall intrude into the residual space during the test. Any structural parts, which are originally in the residual space (e.g. vertical

handholds, partitions, kitchenettes, toilets) shall be ignored when evaluating the intrusion into the residual space.

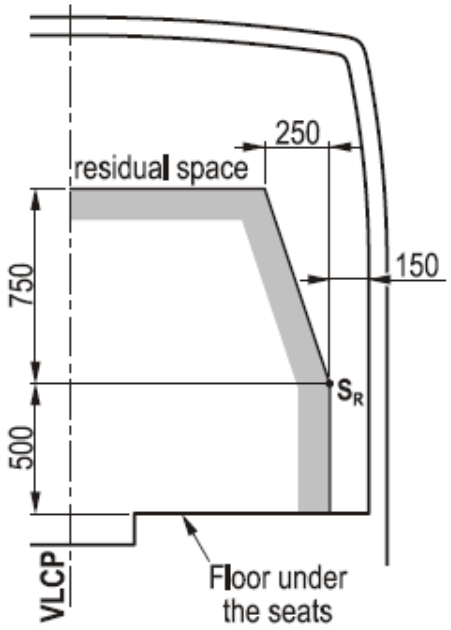


Figure 2.2 : Residual space in bus cross-section in ECE 66-02 [1].

ECE 66-02 [1] lists one basic and four equivalent methods for the bus crashworthiness assessment. A rollover test on a complete vehicle is performed as the basic approval method. From equivalent methods the one also adopted in proposed by authors procedure is a computer simulation of a rollover test on a complete vehicle. ECE 66-02 [1] recognizes computational mechanics and validated FE models as viable tools for crash and safety assessment of buses. As mentioned, ECE 66-02 [1] approval methods are listed below.

1) A rollover test on a complete vehicle. The vehicle is placed on a horizontal platform and then tilted (without dynamic effects) until it rolls over. The angular of tilting movement shall not exceed 5 degrees per second (0.087 rad/s).
2) A rollover test a body section or section.
3) Quasi-static loading test of a body section or section.
4) A verification of strength of superstructure by calculation.
5) Computer simulation of rollover test on complete vehicle.

2.4.3 Equivalent approval methods

2.4.4 Background

The theoretical background of these four methods is the "principle of equivalence". Although it is not written in the ECE 66-02 [1], the "principle of equivalence" means the following: the basic test method is the full scale rollover test with complete bus and it is assumed that the other three methods give the same results, produce equivalent deformations of the superstructure (Bigger deformation is acceptable from the point of view of safety).

- The angle of impact is artificial and not related to the bus being tested.
- The change of the impact angle during the pendulum test differs from that in a rollover test.
- The ground effect (secondary impact in the waistrail) is absolutely neglected.
- The mass effect of the body section, the height of its centre of gravity does not play any role during the pendulum test.
- The anchorage of the body bay for pendulum test can completely change the whole deformation and energy absorption process.

The reason, why the pendulum test has been accepted in ECE 66 [1] regulation is historical. It was the first test in mind when GRSA (Working Group of Experts) started to work in that subject. The main argument for it was that it is a simple and cheap test comparing to the full scale rollover test, at that time which was rather complicated and not agreed (Hungarian method, U.K. methods, etc.). When agreeing in the full scale rollover test method described in ECE 66 [1], another simple and cheap method came into the picture: the rollover test of full scale body sections, bays. Nevertheless, the pendulum test remained in force.

2.4.5 Quasi-static calculation method

The calculation method (Annex 8) is not well clarified in ECE 66-02 [1]. Some requirements are fixed, but these are not enough to repeat a calculation, these do not describe unambiguously a calculation process. Therefore, this method is not repeatable by others. The basis of the calculation as an equivalent method was the assumption that it is simple and cheap and it could be the method of the small bus manufacturers, body builders. But these kind of calculation are sophisticated enough

to need computer, and it raises the question of the program as well as the mechanical model. To be familiar with this kind of calculation needs special knowledge in mechanics (theory of large scale plastic deformations, theory of modeling) and in computation (software problems, generation of input data). The Annex 8 of ECE 66-02 [1] gives some requirements of the calculation method. These requirements are summarized and commented below:

a) The calculation may be carried out on the complete body or on its segments. This means that the whole process, which is simulated by calculation is not well dermed, the initial conditions are not unambiguously described. In other words, this extends the "principle of equivalence" to an unacceptable measure, the substitutional method is (can be) replaced by another substitutional method. However, this replacement (trough the mechanical model and the computer program) brings unacceptable simplifications into the calculation. It would be very important and necessary to state in the regulation that the calculation must simulate the basic test method, the full scale rollover test of complete buses.
b) Annex 8 deals with the problem of plastic deformation in more paragraphs. The important requirements are the followings:

i. The whole rollover process should be analyzed in the range of large plastic deformations.
ii. The calculation has to point out the structural elements, in which the stress exceeds the yield strength, where the plastic hinges will be formed.
iii. The characteristics of plastic hinges should be determined by physical tests.

c) If the calculation does not involve the fracture process of the structural elements, it must be proved by tests that the fracture will not occur in the range of the plastic deformation. It is a very important requirement and - while the mechanical models and calculation methods are not, and will not be able to prove that in the near future - these physical tests should be generally required in any case.

To analyze the stresses and deformations of complete bus body (or even a segment of it) generally the FEM technique is used. This arises two question: first, that the calculated stress strongly depends on the mechanical model, and second that it is not sure that plastic hinges are forming on that (and only on that) structural elements where the stress exceeds the yield strength in the very early stage of the calculation.

Annex 8 refers to that possibility but it contradicts the automatic indication of plastic hinges by FEM analysis to determine the location of the plastic hinges by engineering analysis of the structure.

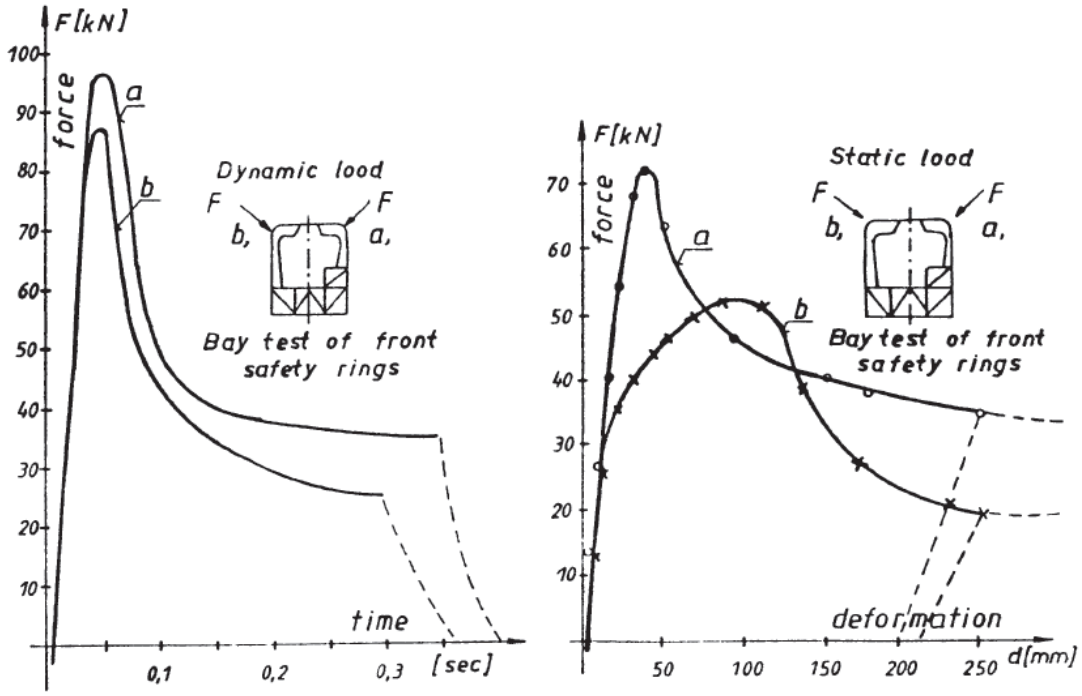


Figure 2.3 : Characteristics measured in static and dynamic bay section tests [40].

2.4.6 Computer simulation method

The basic question is the simulation of the rollover process, more exactly the simulation of the full scale rollover test of the complete bus. The structure and the capability of the computer program determine the mechanical model of the superstructure. The process simulation should start when the cantrail of the roof just touches the ground, this is the starting time t=0. In this moment, the longitudinal symmetry plane of the bus has an angle φ_0 related to the horizontal ground, and the bus has a kinetic energy E_0 angle of velocity ω_0. Along the contrail a supporting force F is built up, which causes a certain angular deceleration e and all characteristics of the program should be the following:

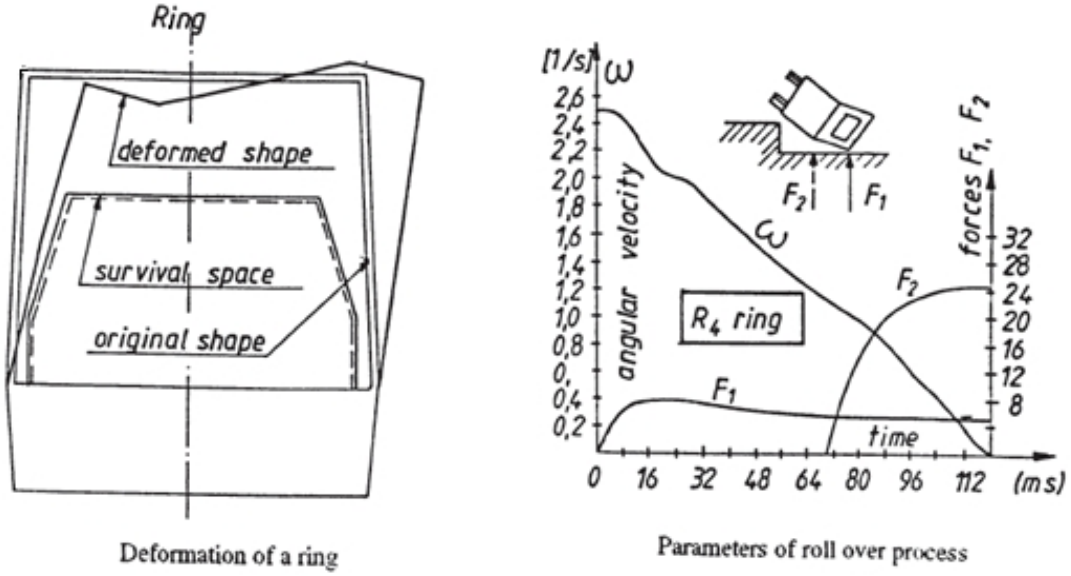
- The position of the plastic hinges should be determined by engineering analysis, engineering decision. They can be placed on the so called rings, which are part of the body.
- The rings, representing the whole superstructure of the bus are not independent from each other, their motion and deformation are linked through the rigid

chassis and the in-plane rigid roof and side wall structures which have only elastic deformations in their planes. The consequence of the above said is that the rings produce a certain amount of torque to each other promoting or hindering the neighbors deformation.

- The simulation (computation) process starts with the moment $t = 0$, when the cantrail touches the ground and it goes step by step with a time interval Δt.

The output of the simulation has to prove and show at least the followings:

- The intact survival space at all of the rings like it is shown on Figure 2.4. If it is needed, between two rings linear interpolation may be done.
- The energy absorption of the individual rings and balance the energy of the whole bus.
- Representative parameters of the rollover process as the function of time Δt_0. Figure 2.4 shows (as an example) the supporting forces F_1 and F_2 and the angular velocity ω for the ring.



Deformation of a ring

Parameters of roll over process

Figure 2.4 : Output results of simulation as an example [40].

3. SUPERSTRUCTURES OF BUSES

3.1 Plastic Hinges

Studying the damaged bus frame structures after a collision, it can be established that the deformations are not evenly distributed; some structural elements are deformed and others are not and also in one individual element, there are locally strongly deformed sections and large rigid undeformed parts.

3.2 The Plastic Hinge Concept

In many impact situations, the individual structural members are overloaded, principally in bending giving rise to plastic deformations in highly localized regions, called plastic hinges. These deformations, called hinges develop at points where maximum bending moments occur, or at load application points and at joints and locally weak areas. Therefore, for most practical situations, their location can be predicted well in advance. The plastic hinge concept has been previously developed by utilizing generalized spring elements to represent constitutive characteristics of localized plastic deformation of beams and kinematic joints to control de kinematics of the deformation. The bending plastic deformation at an attachment node is modeled by revolute joints, as shown in Figure 3.1.

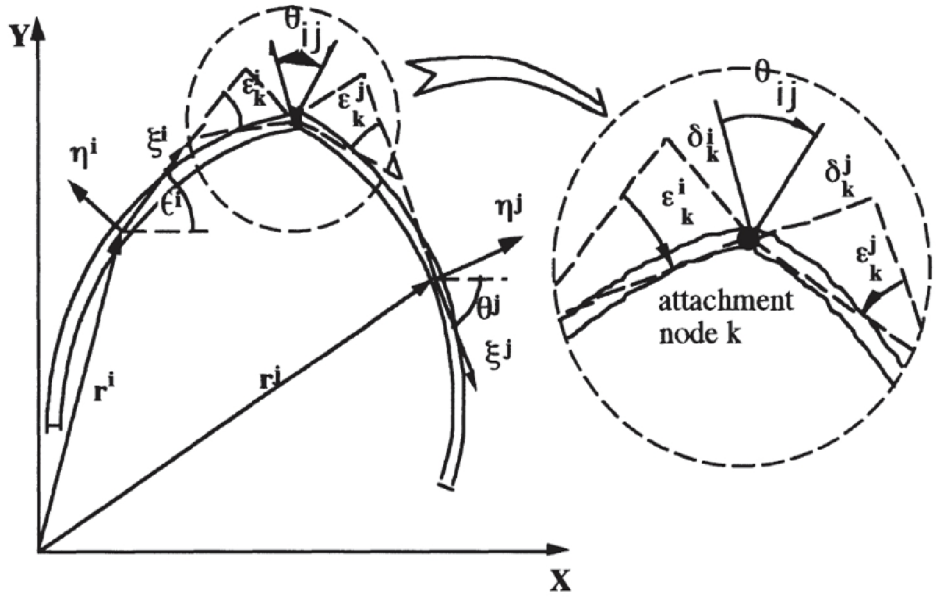


Figure 3.1 : Plastic hinge concept [41].

The revolute joint must be simultaneously perpendicular to the neutral axis of the beam and to the plastic hinge bending plane. From Figure 3.1 the following relationship can be written:

$$\theta^{ij} = \theta^{i} + \varepsilon_k{}^{i} - \theta^{j} - \varepsilon_k{}^{j} \qquad \textbf{(3.1)}$$

which shows the dependency of the plastic hinge angle on the rigid bodies relative rotation and on the elastic rotations of body *i* and body *j* at the attachment node k. The angle values are directly obtained as relative coordinates from the integration process and correspond to the relative degree of freedom, θ^{ij}, of the revolute joint under consideration.

A typical torque - angle constitutive relationship illustrated in Figure 3.2, was obtained in an earlier work for the case of a steel tubular cross section based on a kinematic folding model [42,43]. This model was modified to take into account elastic plastic material properties including strain hardening.

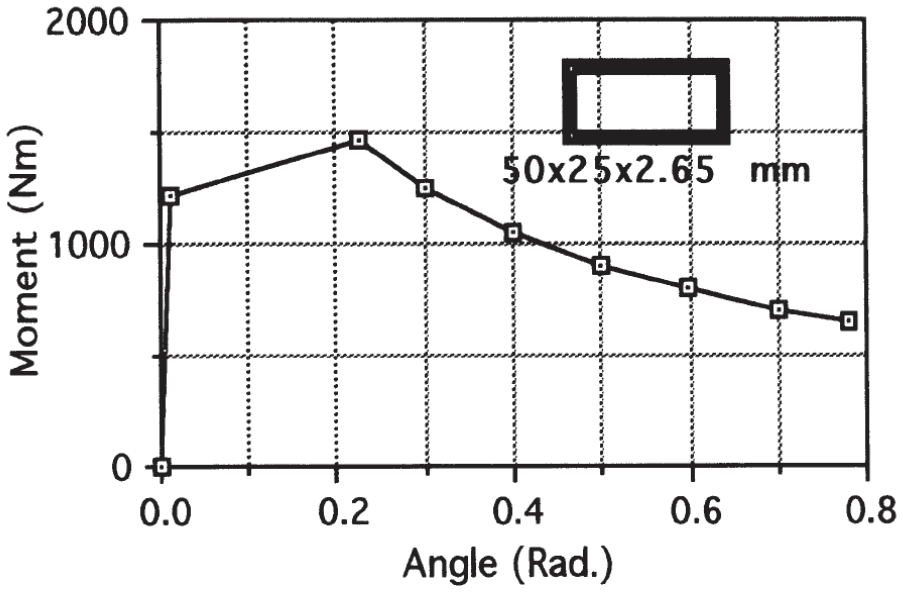


Figure 3.2 : Plastic hinge constitutive relationship [42].

3.3 Definition of Plastic Hinges

The concept of "plastic hinge" (PH) is widely used in the technical publications, even when there is no exact, internationally accepted definition of it. In this thesis, the following definitions will be used for PH:

3.3.1 Elementary hinge

On rod-like elements including the thin-walled tubes (where the length of the element is much bigger than the two other dimensions) that relative small section is called as PH where:

a) The local buckling results in the loss of stability.
b) The plastic deformation is concentrated being larger than the other parts of the rod.
c) The original cross section of the rod is essentially distorted.
d) The length of which is bigger than the rod cross section, where it is formed.

Figure 3.3 shows elementary PH formed on a bus superstructure. It should be emphasized that the local, high scale plastic deformations of PH results in large scale rotation, displacement, shortening, etc. of the rigid undeformed part(s) of the rod, on which the hinge is formed.

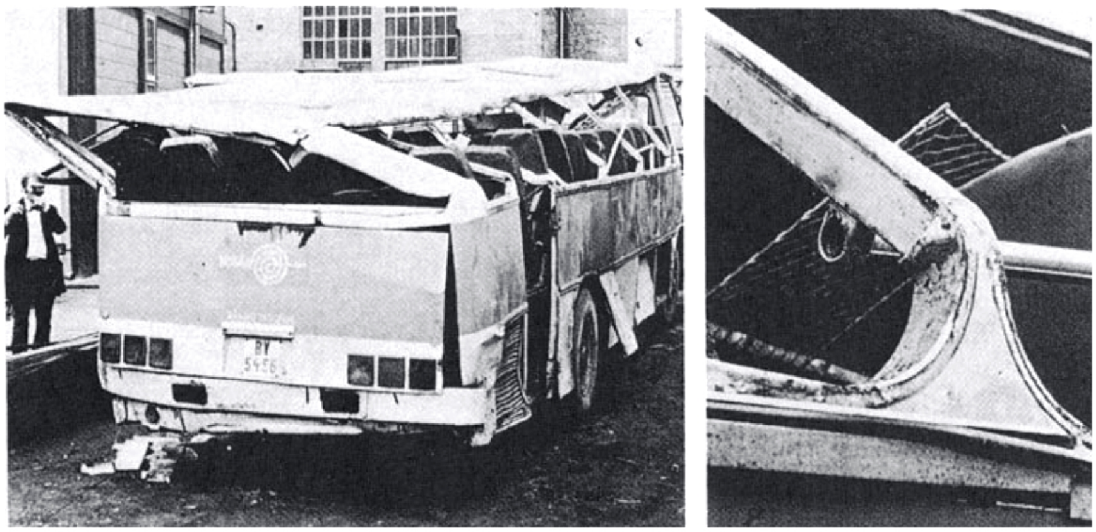


Figure 3.3 : Bus superstructure after rollover [17].

3.3.2 Combined hinge

This is developed on special safety structural elements (e.g., safety rings for rollover, safety platform in the driver's cab, or safety bumper system, etc.). These special structural elements generally are not rod-like type; they contain more tubes and connecting plates. Therefore, the basic assumption that their length is much bigger than the two other dimensions is not valid anymore. Trying to generalize the PH definition given above, we have to comment the four conditions:

a) More than one local buckling take place and the loss of stability is the collective result of them. It means, for example that the first (and second) local buckling does not cause the loss of stability yet.
b) The high scale plastic deformations are connected to the narrow surroundings of the individual local bucklings.
c) While the special elements are not rod-like type, the distortion cannot be common to all of the neighboring local bucklings.
d) Generally, it is meaningless to talk about the length of the plastic hinge.

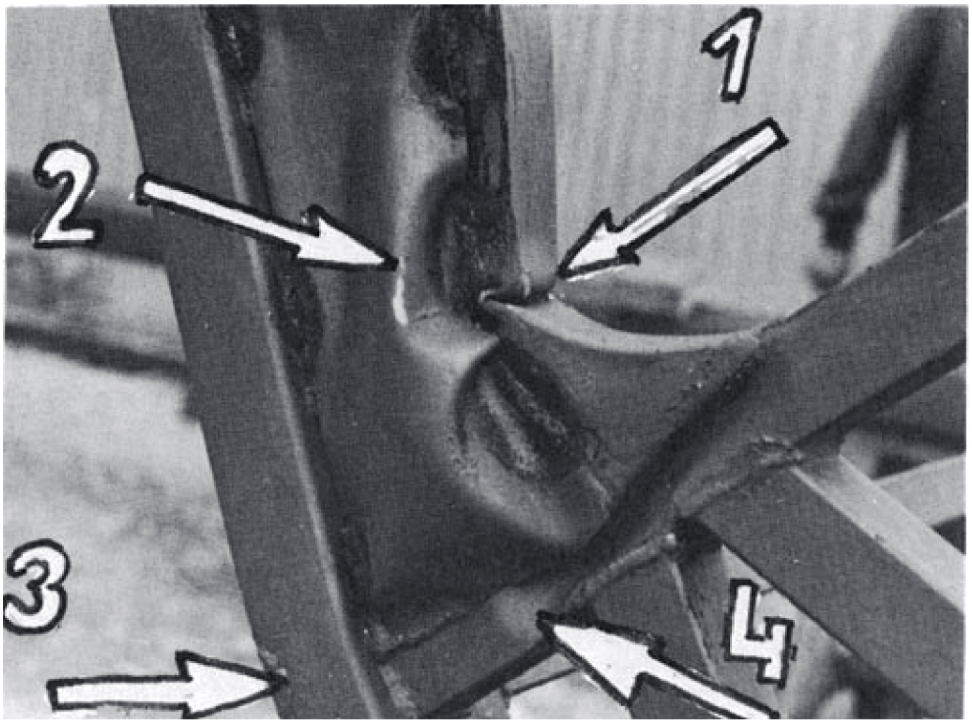


Figure 3.4 : Combined plastic hinge [44].

The reason, why we can call this sophisticated phenomenon as PH is the fact that the other parts of the special structural elements are undeformed (rigid) while they endure large scale rotation, displacement, shortening, etc. because of the intensive plastic deformations of the hinge region. Figure 3.4 shows an example for the combined PH formed on a bus safety ring, which is connected to the cross member of the underframe structure. The first local buckling formed on the inner column of the plated safety ring (No.1) after that the plate was strongly deformed in the neighborhood of the first buckling and influenced by the weldings. (No.2) Local buckling can be observed on the side wall column, too (No.3). Finally the upper horizontal rail of the cross member was deformed (No.4). The final result of these

local buckling and deformations produced a rotation of the safety ring compared to the cross member. The other parts of the safety ring and the cross member remained underformed.

3.4 Types of Plastic Hinges

There are many possibilities to categorize PH's; the basis of our categorization is their motion capability.

3.4.1 Linear plastic hinge

When a compressive force, acting parallel to the longitudinal axis of the rod creates the PH and its deformation results a compressive displacement, the original longitudinal axis of the rod does not change, there is no angular distortion. Figure 3.5 shows two examples from real bus structures. "a" is a folding type PH, while "b" is a buckling type one. The buckling type linear PH, formed on "T" joint of thin-walled tubes, can be seen on Figure 3.6, where the tube dimensions are 40 x 40 x l,5 mm. It is interesting to mention that depending on the tube thickness different kind of buckling mechanisms can be observed. Figure 3.7 shows the same "T" joints with different thickness (40 x 40 x 3 mm) and with different buckling mechanism. Figure 3.8 gives a new variation with "T" joint; if the joint is rounded (like in the case of bus window columns), the PH is formed in the transition range and its shape, depending on the technology differs from the two others discussed above. There are two kinds of linear PH (see Figure 3.5);

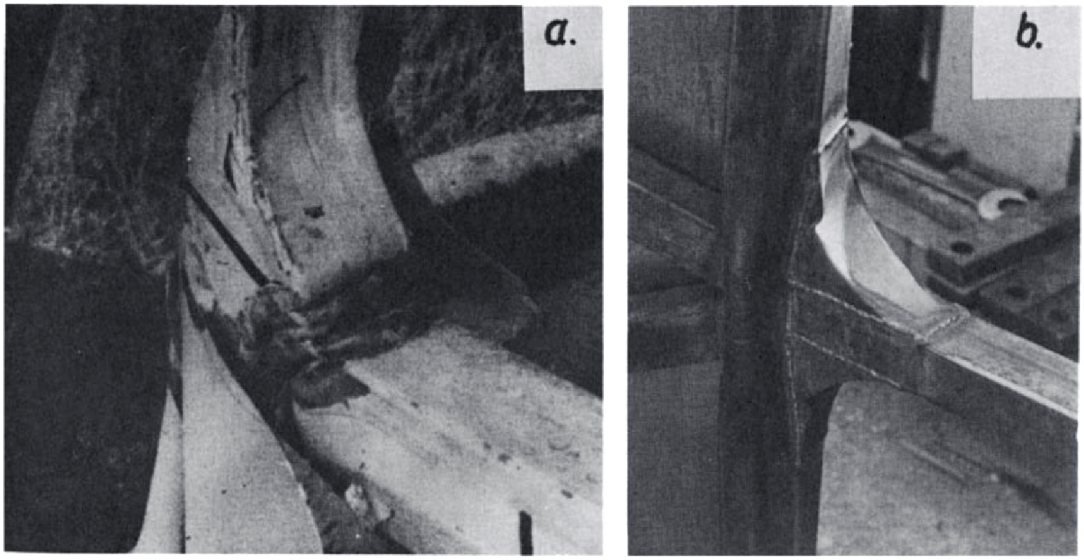


Figure 3.5 : Linear PH's on real bus structures: (a)Unlimited displacement. (b)Limited displacement. [44].

a) Linear hinge with unlimited displacement. In the needed working range of the hinge (during the considered deformation). There is no limitation.
b) Linear hinge with limited displacement. The working range of the hinge is clearly limited by geometrical reasons.

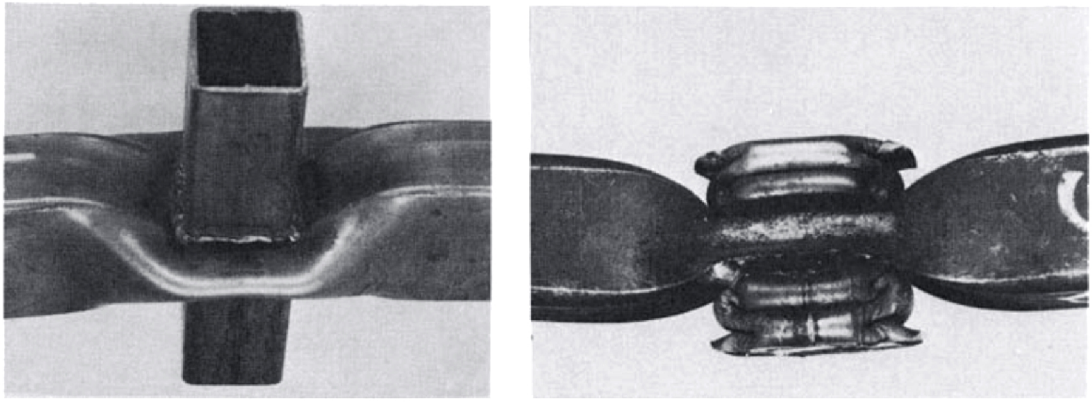


Figure 3.6 : Plastic hinges on "T" joint [45].

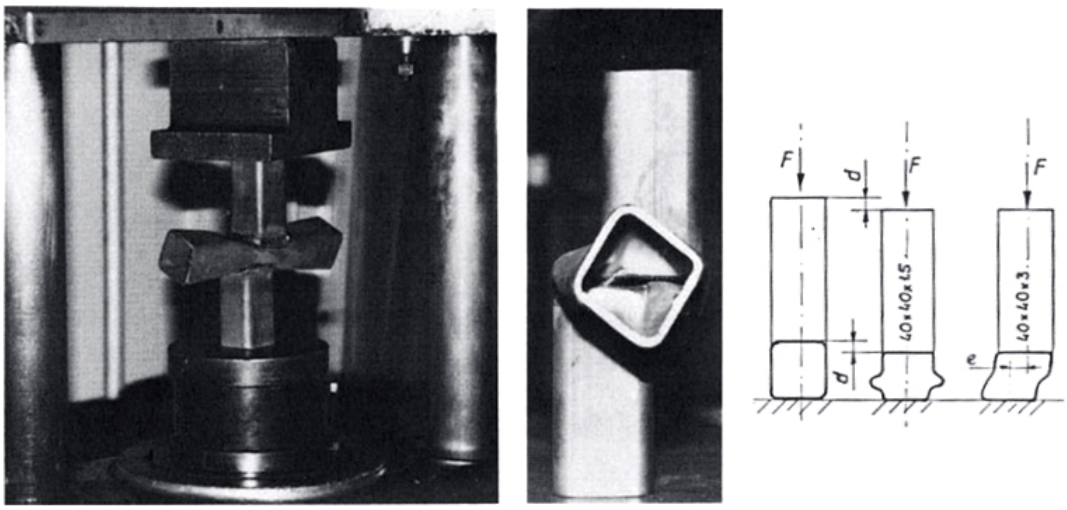


Figure 3.7 : Different types of “T” joint [45].

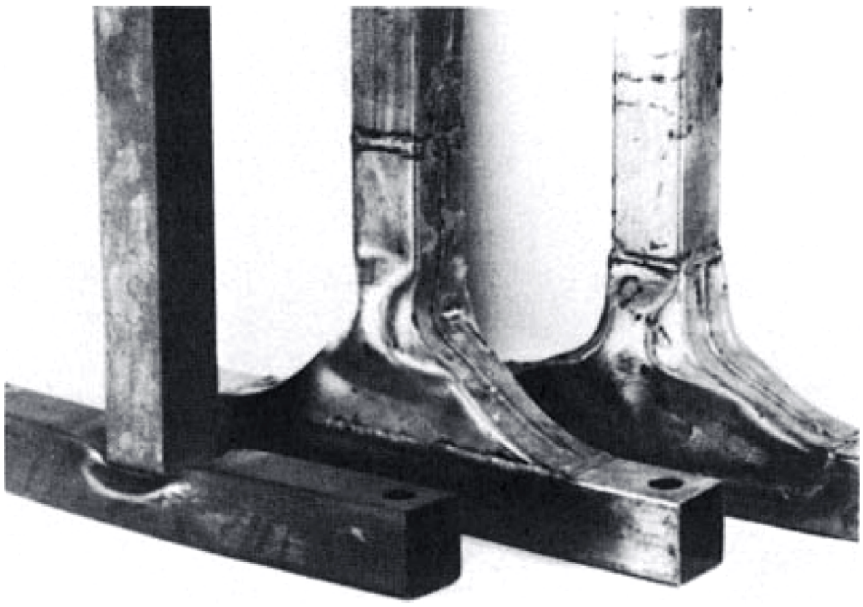


Figure 3.8 : Different window columns [45].

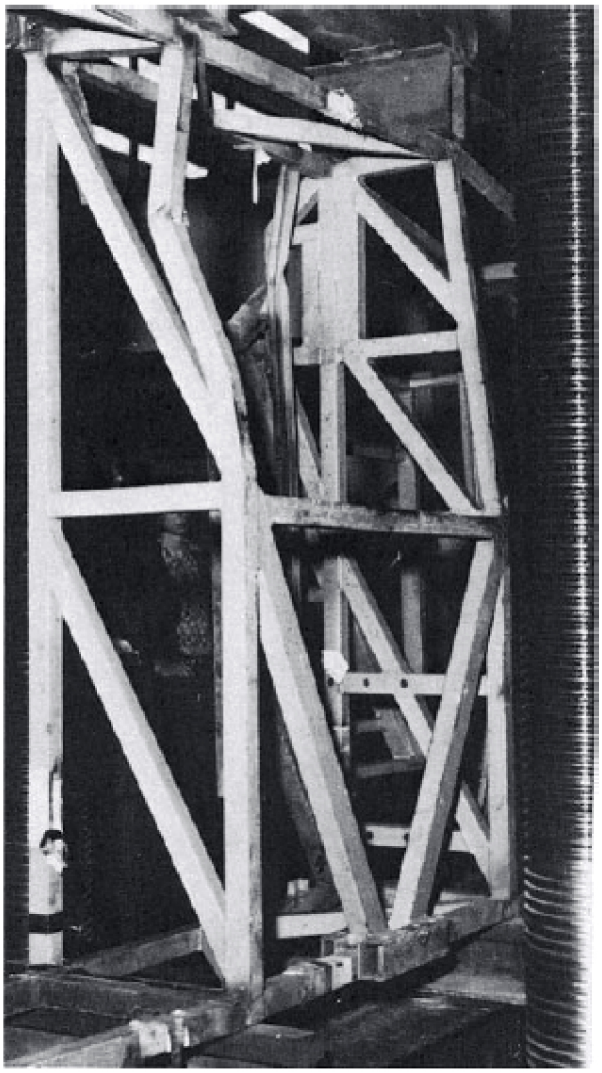


Figure 3.9 : Compression test of underframe structure [44].

3.4.2 Rotational plastic hinge

When a bending moment creates the PH and it has an angular deformation or rotation, or in other words, the original longitudinal axis of the rod is broken and there is an angular distortion. This kind of hinges can be observed not only on window and door columns (see Figure 3.3) but for example on a lattice type underframe structure when tested against front impact forces (Figure 3.9). There are two kinds of rotational PH's (see Figure 3.10):

a) Rotational hinge with unlimited angular displacement.
b) Rotational hinge with limited angular displacement. The limitation is given by the geometry or by fracture.

3.4.3 Combination of elementary plastic hinge

There are hinges, which start to work as linear hinges and after that they get rotational displacement and change into a rotational hinge (see Figure 3.9). Examples are given on Figure 3.11 showing the front wall - side wall connection of a full scale specimen after a pendulum impact test, simulating a front impact accident. The white arrows show combinations of elementary PH's. Figure 3.6 shows a combination of two linear, one folding and one buckling type PH working after each other.

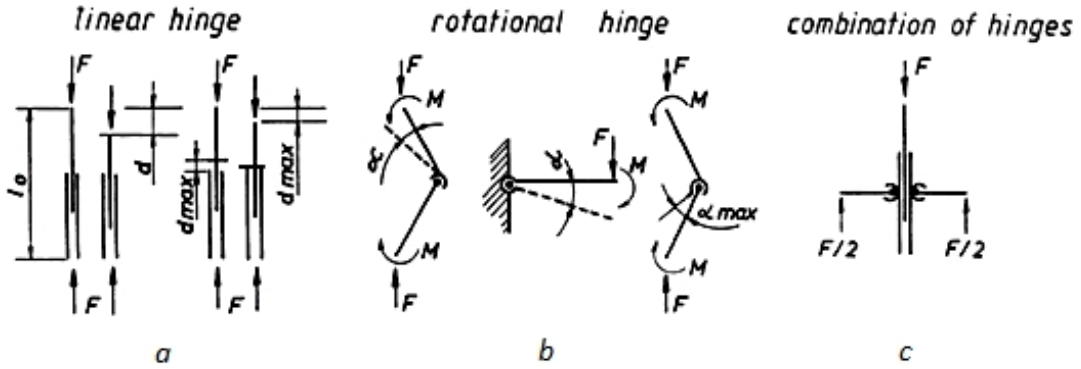


Figure 3.10 : Different types of plastic hinges: (a)Linear hinge. (b)Rotational hinge. (c)Combination of hinges. [45].

3.4.4 Mixed plastic hinge

In the case of combined hinges, more local buckling result a mixed type of deformation. Sometimes the linear behavior dominates, once the rotational one results in the same manner.

3.4.5 The type of the plastic hinge

On the same rectangular tube under the same compressive force (acting parallel to the longitudinal axis of the tube) can be either linear or rotational depending on the length of the tube. A test series was made with tubes (40 x 40 x 2 mm) having fourteen different length in the range of 50-900 mm. In every length category, ten tubes were tested. On the short tubes, linear plastic hinge was formed and on the long ones rotational hinges occurred. In the middle length-range, a certain ratio of the tubes with a given length showed rotational and the others linear plastic hinges. Figure 3.12 (upper line) gives the probability of forming linear PH on the tube, when the two ends of the tube are free:

- If the length of the tube is less than the critical value of I_{c1} = 200 mm, the probability of forming linear hinge is 100%.
- If the length is more than another critical value of l_{c2} = 700 mm, the probability of forming linear hinge is 0% or in other words, rotational hinge is formed.
- Between the two critical values, the formation of linear hinge has a decreasing probability.

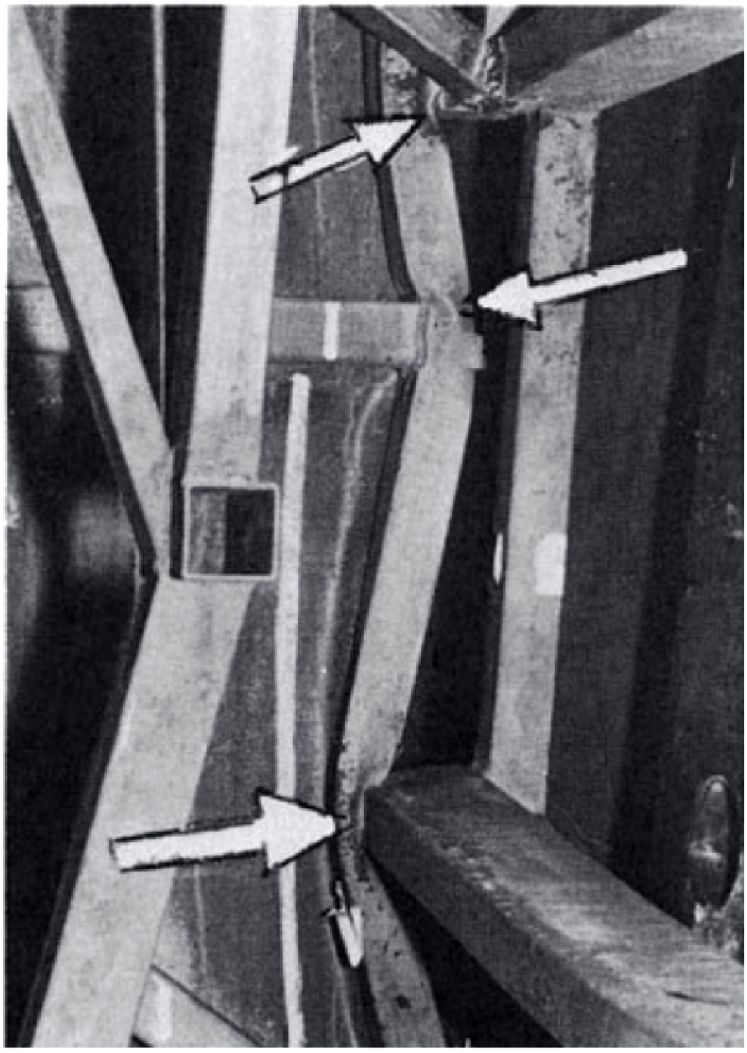


Figure 3.11 : Combined PH on front wall frame [44].

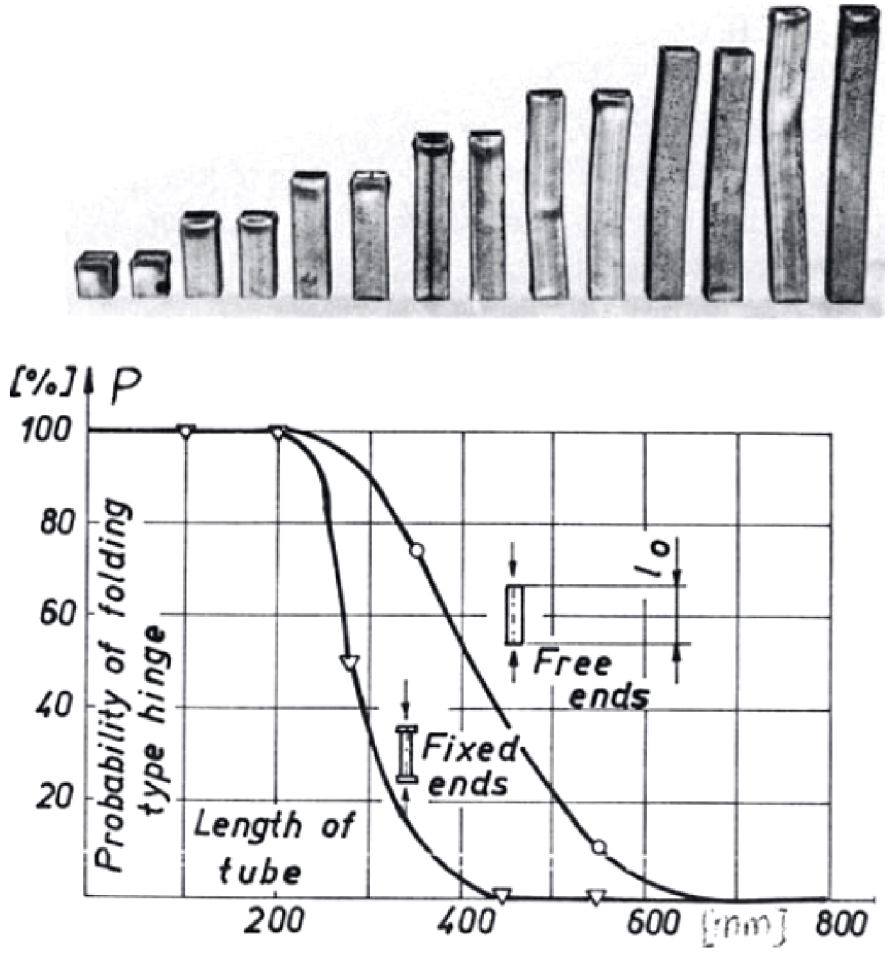


Figure 3.12 : Probability of forming folding type plastic hinge [46].

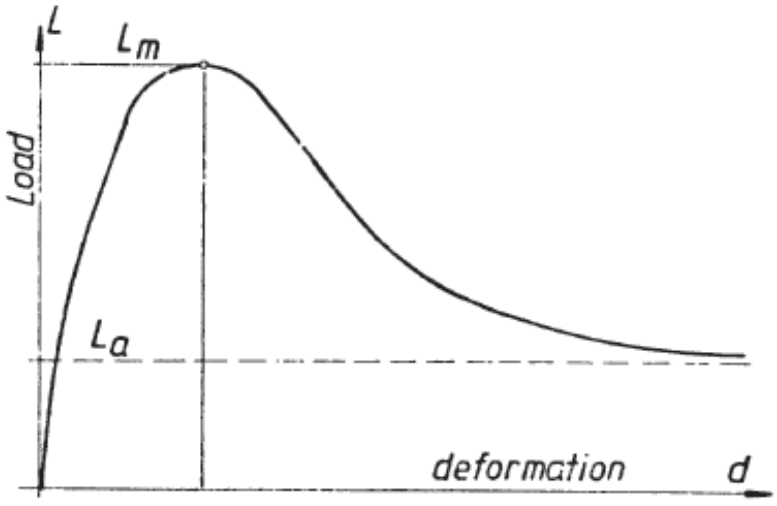


Figure 3.13 : General form of plastic hinge characteristic [46].

The lower line on Figure 3.12 gives the same kind of results of a parallel test series using tubes with fixed ends (welded plates are fixed the cross sections at the two ends). These kinds of tubes have a shorter transient length range (l_{c2} - l_{c1}). The explanation of this phenomenon can be given by the geometrical imperfections of the tubes coming from the manufacturing process.

The longer tube provides a higher probability of a significant bending moment when acting a parallel compressive force, and this moment creates a rotational PH.

3.5 Plastic Hinge Characteristics

3.5.1 General hinge characteristic

Every PH can be characterized by a function between the load (L) and the corresponding deformation (d). On the basis of many tests, Figure 3.13 shows the general form of the plastic hinge characteristic. When generally speaking about PH's, it is useful to use the concept of the generalized deformation:

$$x = \frac{d}{d_m} \tag{3.2}$$

where d_m is the deformation belonging to the maximum load (L_m) of the hinge characteristic. The main features of the L(x) function are the followings:

- if $L = 0$ then $x = 0$
- in the range of the small deformations (x_s) the function is nearly linear, it can be linearized. The gradient of the function in the range of these small deformations:

$$\left.\frac{d\,L}{d\,x}\right|_{x=0} = v \tag{3.3}$$

relates to the starting stiffness of the hinge. It is interesting to note that the energy absorption in this range is negligible **(3.3)**.

- the load has a maximum value (L_m) and the corresponding deformation (x = l)

$$\left.\frac{d\,L}{d\,x}\right|_{x=1} = 0 \tag{3.4}$$

gives the starting point of loss of stability. The load maximum is an important value showing the loadability of the hinge. It founded that it is proportional to the yield strength (R_y) of the material, the function of the thickness (t) and a cross section parameter (K),

$$L_m = C_m \cdot K \cdot R_y \cdot t \tag{3.5}$$

where C_m is a constant, depending on some other geometrical ratios ($C_m < 1$). For example in the case of a linear PH, the K parameter could be the area of the cross section, while in a rotational hinge the bending coefficient.

- In the deformation range of $x_s < x \leq 1$, there is a significant plastic deformation, non-linear behavior of the hinge.
- If the deformation exceeds the critical value ($x > 1$) belonging to the loss of stability, the loadability of the hinge decreases. In case of a constant load reaching the maximum value, this is an unstable working range of the PH
- In the range of the large deformations ($x >> 1$), the load tends to an asymptotic value (L_a). The ratio:

$$\mu = \frac{L_a}{L_m} = c_a \cdot \frac{t}{b} \tag{3.6}$$

can be related to the distortion of the cross section at the plastic hinge and it is proportional to the relative thickness (t / b), while c_a is a constant

- the energy absorbed by the hinge, until a certain deformation (x) is

$$W(x) = \int_0^x L(x)\, dx \tag{3.7}$$

The average energy density of the hinge is the relative absorbed energy:

$$\overline{W} = \frac{W(x)}{x} = \frac{1}{x}\int_0^x L(x)\, dx \tag{3.8}$$

which is a good characteristic when comparing different PH's from the point of view of energy absorption.

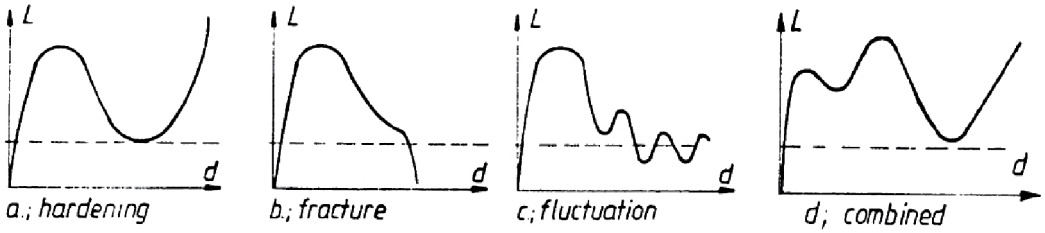


Figure 3.14 : Deviation from the general characteristic: (a)Hardening. (b)Fracture. (c)Fluction. (d)Combined. [46].

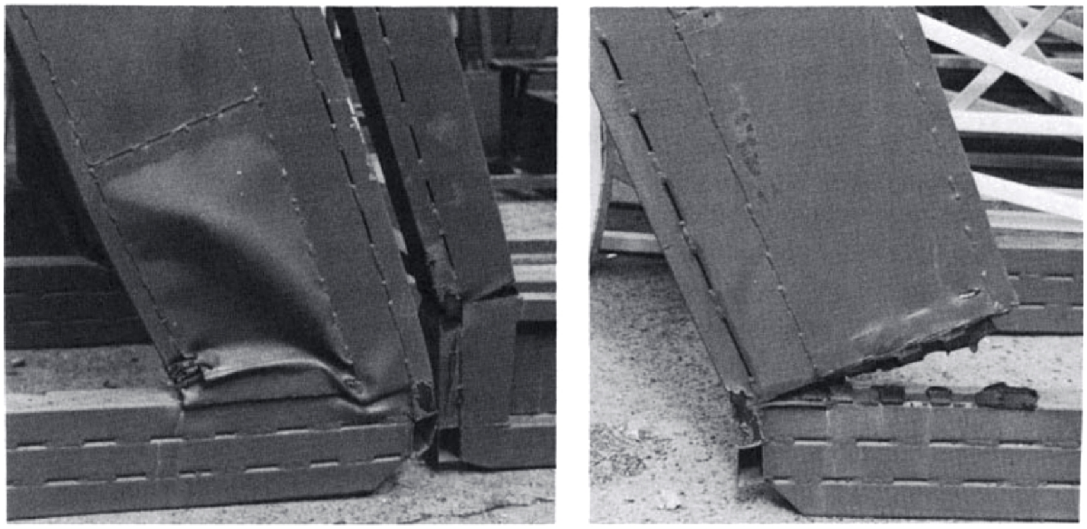


Figure 3.15 : Fractures on safety rings of bus frame [40].

3.5.2 Deviations from the general form

There are at least four kinds of major deviations:

a) In the case of limited deformation, a hardening process takes place, when the deformation capability is exhausted, the deformation-load curve starts to increase very rapidly and the gradient can reach or exceed the starting stiffness *v* (see Figure 3.14/a).
b) If a fracture takes place in a plastic hinge, the hinge loses its loading capability; the deformation-load curve quickly decreases and can reach the zero, see on Figure 3.14/b. The fracture starts on the tension part of the hinge, as Figure 3.15 shows.
c) In the case of folding type hinges, waves are superimposed on the general deformation- load curve. This fluctuation is related to the individual folds following each other. It can be seen on Figure 3.14/c.

d) In the case of a combined hinge, when different local bucklings follow each other (see Figure 3.4) dominating in different way the PH characteristic, (see on Figure 3.14/d.) Although the individual local buckling ("sub-hinge") can be described by Eq. (3.9), the final formula generally cannot be given in a simple, explicit form **(3.9)**.

3.5.3 Mathematical equation

In practice, it could be useful to find mathematical formula to describe the hinge characteristic shown on Figure 3.13. The formula has to fulfill the conditions mentioned in the earlier paragraph. The equations used in several publications (according to the several types of plastic hinges and test methods) are different. They generally are based on an exponential type function. The following five parametric empirical equations can satisfy fairly well the conditions discussed above:

$$L(x) = L_a(1 - e^{-\nu x})(1 + \beta x^{a} e^{-\gamma x}) \qquad \textbf{(3.9)}$$

where α, β, γ are constants, depending on the geometrical and material properties of the rod, on which the plastic hinge takes place, while v is the starting stiffness defined in Eq. **(3.3)**. Unfortunately; α, β and γ are not independent from each other. There are very complicated relations among them. This are proved either by test results or by Eq. (3.9) from which it comes **(3.9)**:

$$\beta = \frac{w\,(u - u\mu + 1)}{\mu\,(u-1)} \qquad \gamma = \frac{v}{(u-1)(1-\mu+\frac{\mu}{u})} + 1 \qquad \textbf{(3.10)}$$

where $u = e^{v}$ and $w = e^{\gamma}$. Eq.(3.9) involves the formula used by Tidbury (1975) [47]: if $\alpha = 0$, $\beta = 1$ and $x > 1$ **(3.9)**. This approach is based on the assumption that the initial part of hinge characteristic is linearly elastic and $x < 1$ negligible small. In the range of small deformations, where the effect of the horizontal asymptote can be neglected, the unit in the second bracket is negligible compared to the product, and if $v \to \infty$, $\beta = 1$, we can get the equation suggested by Voith (1976) [48].

3.5.4 Probability approach

The local buckling and the loss of stability are influenced by a lot of accidental effects, like the geometrical, technological and material defects, and imperfections. When loading more, nominally identical rods and tubes in the same way, the main

parameters of the hinge characteristic have a significant scatter. The deformation process can be considered as a random process and the main parameters (like the maximum load, asymptotic load, etc.) should be described by probability functions. On the basis of test results the Gaussian normal distribution can be proposed for this purpose. From this fact, it follows that the absorbed energy, also the other technical features of the vehicles depending on these essential PH parameters (impact forces, decelerations, deformations around the survival space, injuries, etc.) have a certain occurrence probability. It is very important to know when designing and calculating a required safety level that it can be done only with a well defined probability value, so the absolute safety does not exists theoretically; practically it is very expensive.

3.5.5 Dynamic characteristics

The plastic hinge characteristic (see Eq. 3.9) is based on the results of static or quasi-static tests; but in the real accidents the deformation process is quick and the impact is a dynamic process **(3.9)**. The comparison of dynamic and static test results [45] has shown that strain rate has an influence on the PH characteristic, especially on the maximum load (L_m) and on the average energy density **(3.8)**. When the strain rate is discussed, it is important to emphasize, there is only a very weak correlation between the impact speed of the vehicle and the strain rate in the PH deformation. The real impact speed can be modified by two ways:

- The structural stiffness between the impact surface and the PH can have a strong influence; the softer structure leads to higher reduction in the strain rate.
- The buckling and folding mechanism is the other essential effect on the strain rate.

The shape and the general form of the dynamic hinge characteristic is similar to the static one; the ratio between the two parameters mentioned above, can be expressed as follows:

$$\frac{L_m}{L_{md}} = a_1 E^{c_1} \qquad \text{and} \qquad \frac{\overline{W}}{\overline{W_d}} = a_2 E^{c_2} \qquad \textbf{(3.11)}$$

where L_{md} is the maximum dynamic load, $\overline{W_d}$ is the dynamic energy density and E is the strain rate, while a_1, a_2 c_1 and c_2 are constants, depending on the structural geometry and material properties as well as on the mass ratio between the impacting

and impacted parts. Figure 3.16 shows static and dynamic (pendulum) bay tests; the location and the shape of the PH are similar.

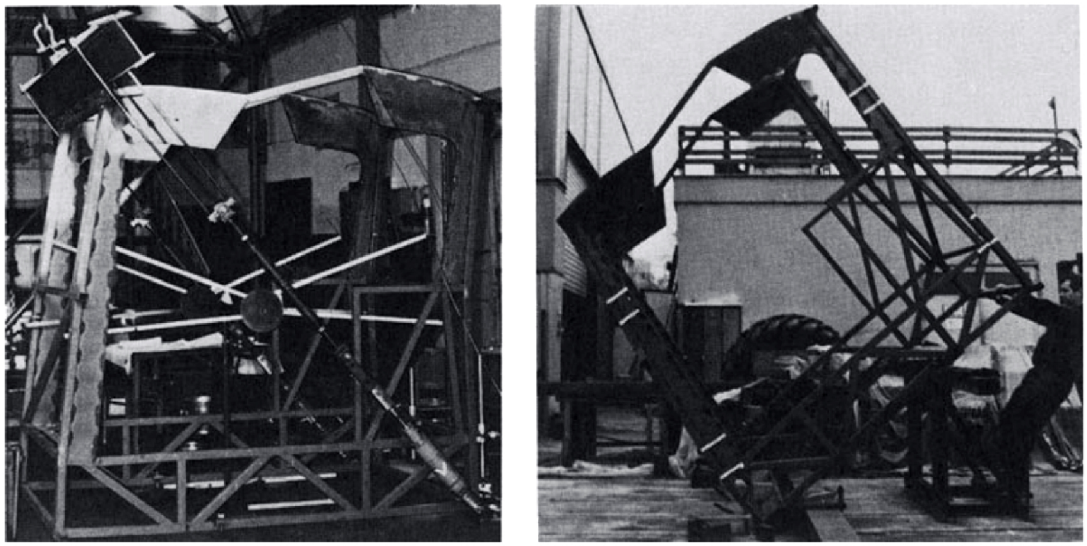


Figure 3.16 : Static and dynamic pendulum bay section tests [40].

3.5.6 Repeated loading of a hinge

When a complete bus rolls over, when it makes a rotation at least a degree of 270°, or in other words the roof of structure hits the ground on both cantrails, following each other. The PH formed for example on a window pillar first gets a bending moment from right side causing a certain deformation (rotation) and after that a bending moment from left side when the earlier deformed PH has to deform "backwards". It is interesting to emphasize that Eq. 3.9 can describe both hinge characteristics, but the "backward" curve has lower load values (L_m and L_a) and different parameters **(3.9)**. It has an "elongated" shape on the same deformation scale.

3.6 Some Constructional View Points of Forming Plastic Hinges

3.6.1 Testing elementary hinges

Figure 3.17 gives the results of a test series with compressed rectangular tubes of different lengths. Two types of PH can be observed on this figure: the linear (folding type) hinge and the rotational one. The short tubes produced a hardening type characteristic, when the folding capabilities of the tube were exhausted.

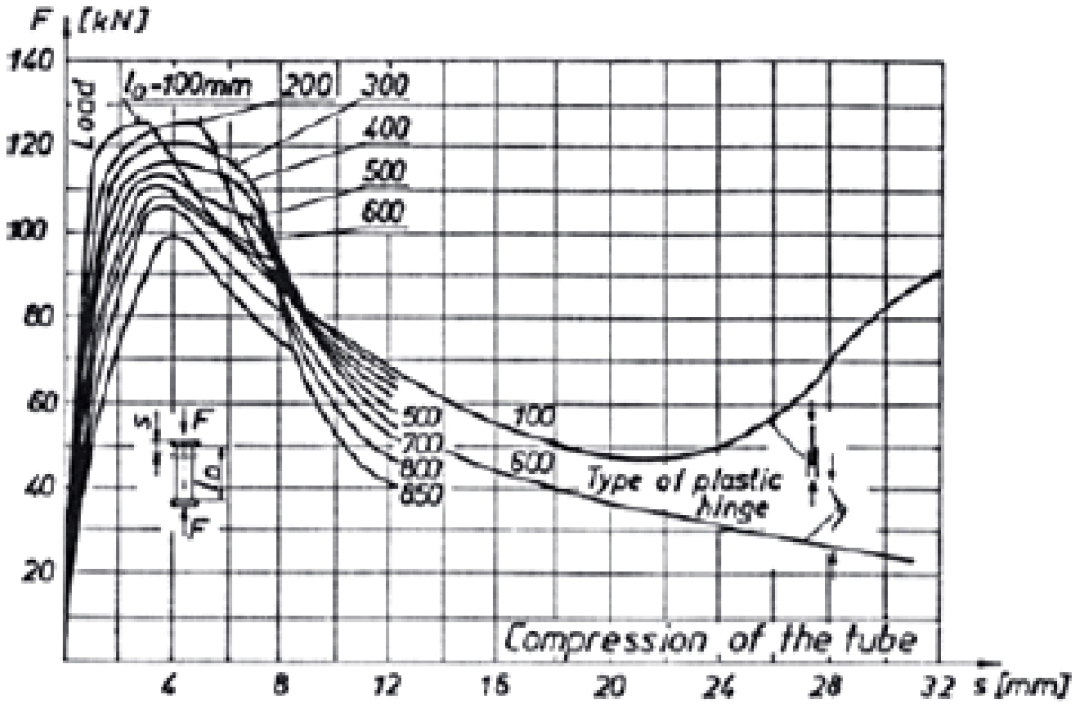


Figure 3.17 : Effect on tube length on the hinge characteristic [46].

Figure 3.18 gives the characteristic of rotational PH. The bending moment is plotted against of the angle of rotation. On figure, "a" the specimens have modeled two kinds of bus window column: a rectangular joint and a rounded one. The figure "b" shows the effect of different tube geometry. Figure 3.19 demonstrates the phenomenon of repeated bending of a rotational hinge. The results of another test series with "T" joints are given on Figure 3.20 with different geometrical configurations.

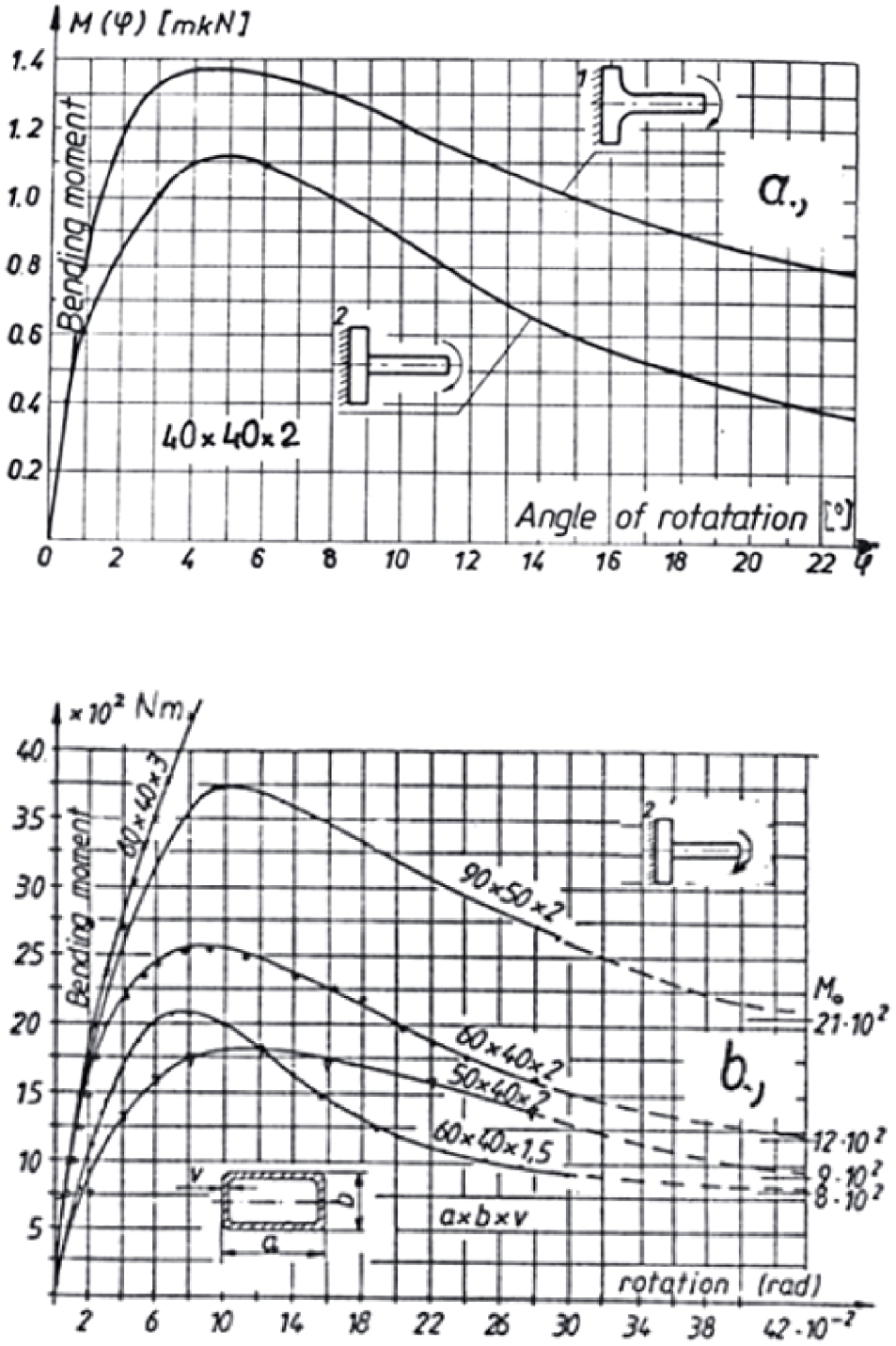


Figure 3.18 : Rotational PH characteristics: (a)Different joints. (b)Different tubes. [46].

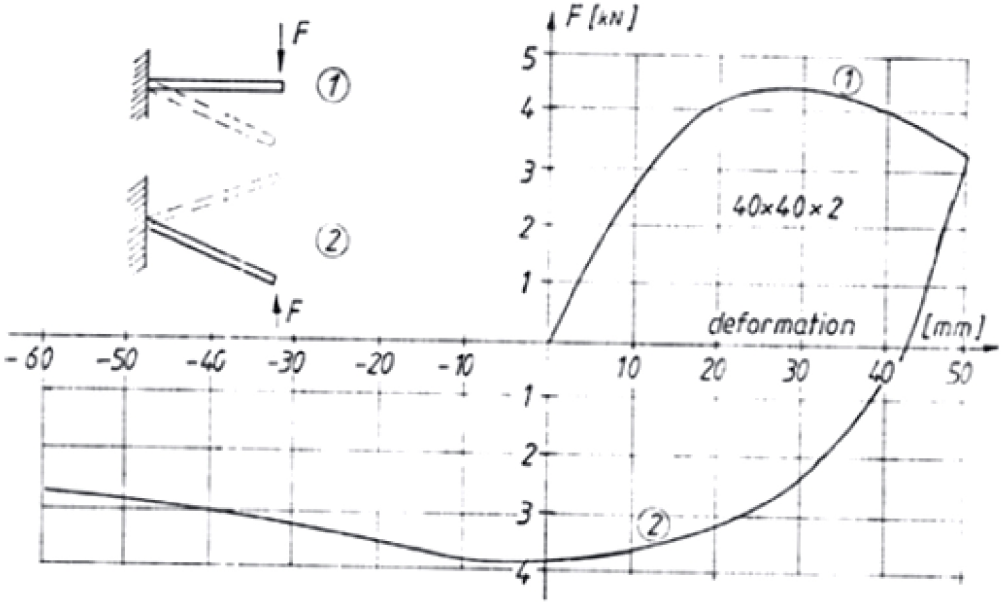


Figure 3.19 : Repeated bending of PH [46].

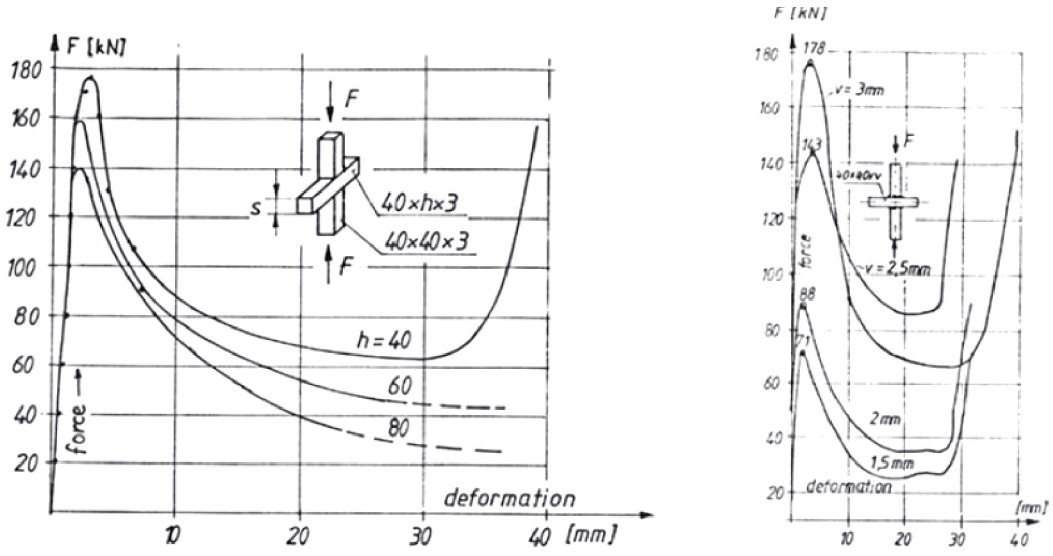


Figure 3.20 : Geometrical effects on PH characteristics of “T” joints [45].

3.6.2 Testing combined hinges

Figure 3.21 gives the test arrangement of a front wall waistrail (see Figure 3.11) which produced the combination of different types of hinges. The tested beam was built up from two tubes of 40 x 40 x 2 mm and 80 x 40 x 2 mm. This tube combination is one possible construction of the waistrail in the front wall of a bus. The characteristic of this combined PH is shown on Figure 3.22 together with results

of the other waistrail test. These curves follow the general behavior showed on Figure 3.14/d. Figure 3.23 shows the characteristic of another hinge combination: the compressed "T" joint mentioned above produces the combination of two linear hinges. The first one is the buckling of the cross tube (there are two kind of buckling mechanisms, see Figure 3.7) and the second one is the folding of the vertical tube, with the wave type hinge characteristic.

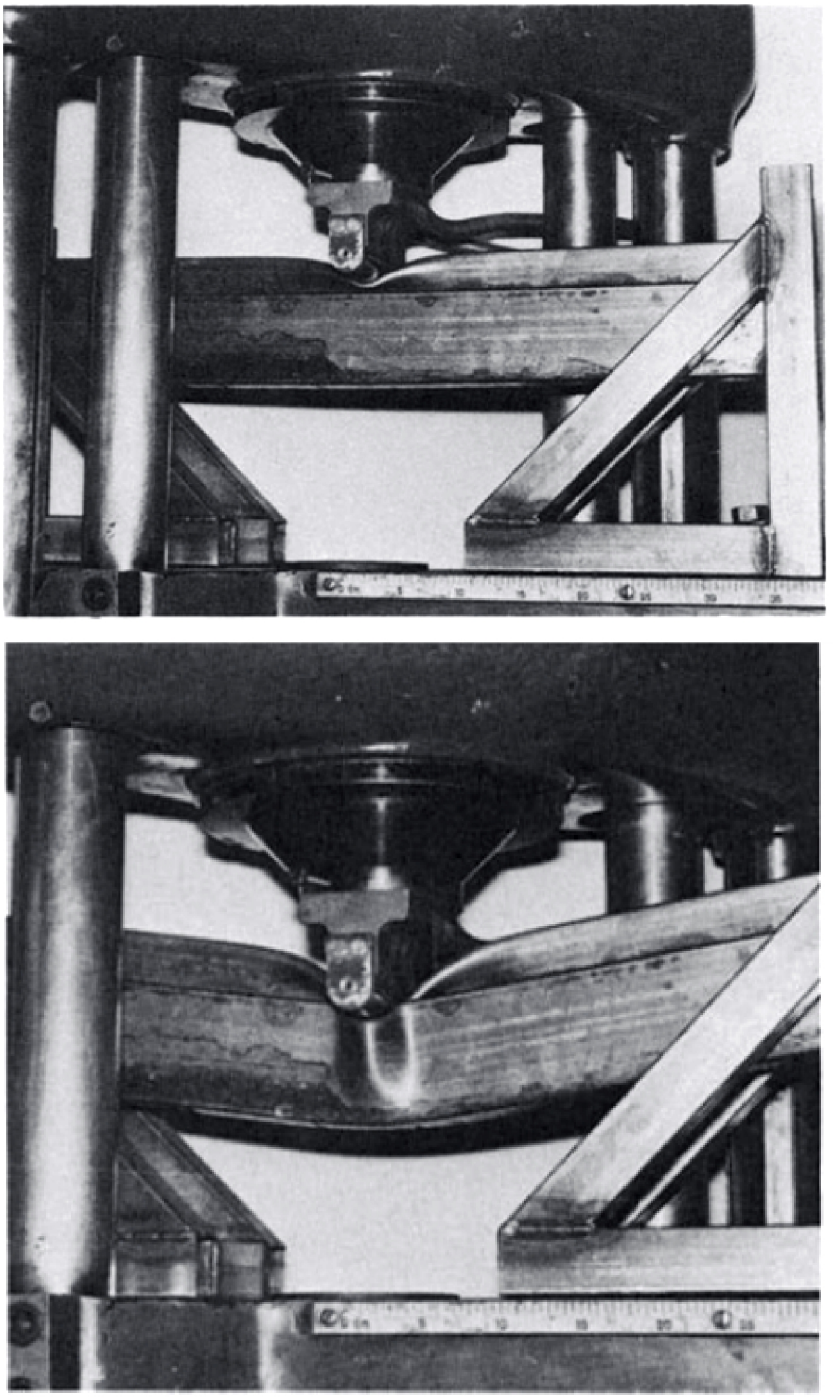


Figure 3.21 : Laboratory test of front wall waistrail [44].

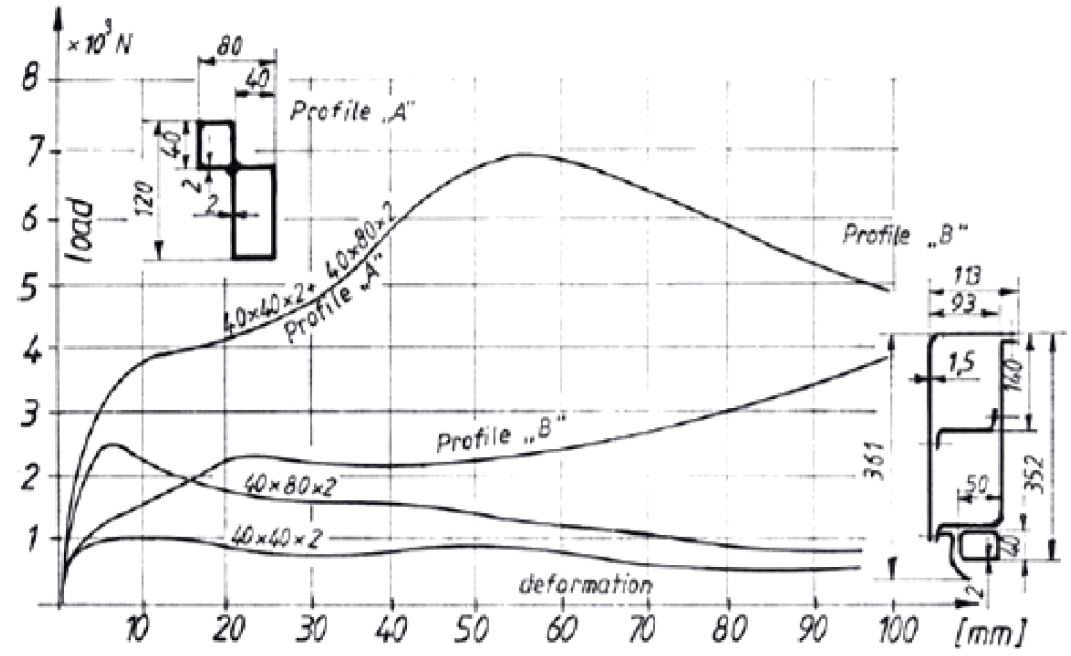


Figure 3.22 : Test results of front wall waistrails [44].

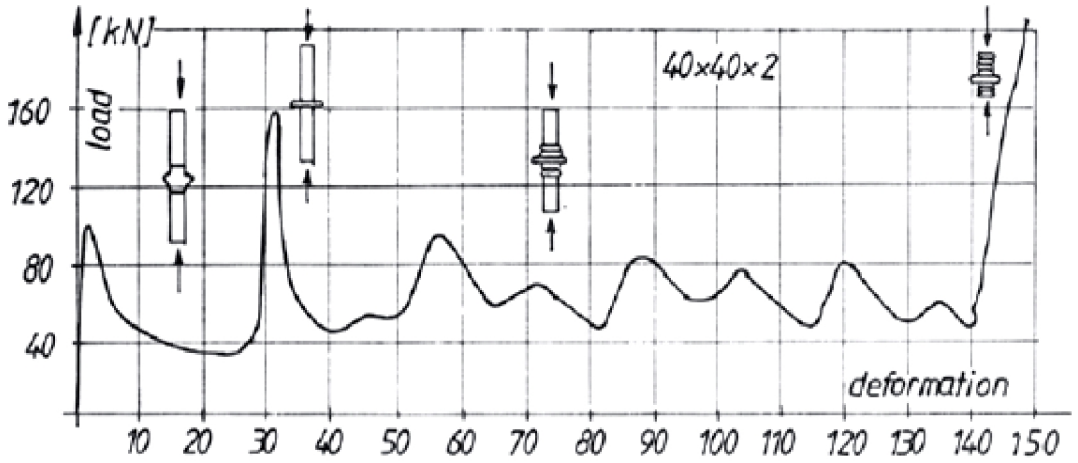


Figure 3.23 : PH characteristic of combined linear hinges [45].

3.6.3 Testing safety rings and bays

When designing a bus frame against rollover accident, generally safety rings are used, on which more (four or six) plastic hinges are planned and calculated. These hinges work together assuring the required energy absorption, residual strength and controlled deformations, and the required survival space for the passengers. Figure 2.4 compares the summarized deformations of body bays built up from two similar safety rings loaded by static and dynamic forces. The test of these bays, the deformations and the plastic hinges can be seen on Figure 3.16. The two curves on

each figure belong to two different load directions. The safety rings are not symmetrical; that is the reason for the different curves. The static load curves are plotted as the function of the deformation while the dynamic curves as the function of time. These test results show two things: the shapes of the static and dynamic curves are similar and the dynamic forces are higher.

Having the same outside contour and same loading direction but different construction of bus safety rings, the location and the form of the PH can be very different. Figure 3.17 compares three different kinds of safety rings from bus superstructures:

a) Simple ring containing an underframe cross member, two side walls with a window pillar and a cross rod of the roof. Acting a cantrail load, four PH's formed similarly to Figure 3.3. Two rotational hinges at the upper cantrail and two on the window column, just above the lower rail of the window.
b) Having a strongly reinforced safety ring, the location and the form of the hinges drastically changed: two combined hinges at the floor level, one on the roof cross member and a broken one at the right cantrail.
c) In the case of a smaller reinforcement and simulating the supporting effect of seats and partitions connected to the side walls, the PH formed on the roof cross member and at the lower rails. Figure 3.16 also gives very good evidences about these, because the tested bays had asymmetric safety ring.

If the safety ring is too wide (deep), the fracture in the tension part has a high probability. Figure 3.15 gives good examples: having a 320 mm wide safety ring the combined PH on the compression side worked well but on the other side the tension caused fracture. It should not be forgot that the broken PH is exhausted, no further energy absorption and no more loading capability. This phenomenon calls the attention to a very important fact: in this case "the stronger the better" is not valid. Figure 3.25 shows a lot of interesting details. The position of the PH formed on the rear wall column is different from that one being on the window column in front of the rear wall. The rear wall hinge is doubled: one is at the lower window rail and the other at the upper rail of the rear wall cross member. Two interesting PH's can be seen on the figure and a torsional hinge was formed on the diagonal of the rear wall cross member.



Figure 3.24 : Different safety rings after pendulum impact [40].

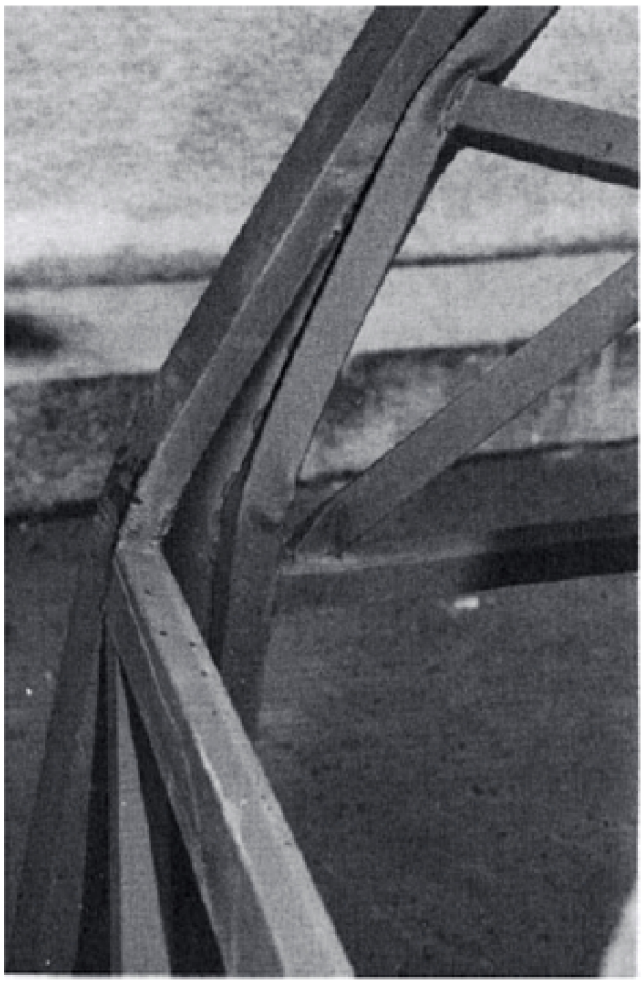


Figure 3.25 : Deformed safety ring in the rear wall [40].

Localized plastic deformations are represented by plastic hinges, which in turn are modeled by revolute joints and revolute actuators with appropriate constitutive relationships depending on the cross sections of the crushed members. Extended capabilities are achieved with the introduction of crushable elements. Both the crush behavior of plastic hinges and other structural subassemblies can be obtained experimentally or using refined finite element representations of such components with commercially available codes. Though, they lead to numerically efficient codes the location of plastic hinges needs to be known beforehand.

4. NUMERICAL METHODOLOGIES FOR CRASHWORTHINESS DESIGN AND ANALYSIS

4.1 Introduction

From an industrial point of view, the crashworthiness of land, air and water transportation systems is achieved by a combination of testing and simulations using various numerical techniques. The later have evolved to be an integral part of the design process of structural components and occupant restraint systems where many iterations are necessary to meet the product objectives. Crashworthiness aims at maintaining the vehicle structural integrity while reducing occupant harm to the extent possible in survivable crash environments. Numerical simulations evolved from one-dimensional lumped parameter spring-mass systems with few degrees of freedom, developed in the late 1960's, to current three-dimensional models with over 500,000 degrees of freedom. Models of full-scale vehicles, occupants, dummies, restraint systems or structural components are being used on a broad basis under different crash scenarios. Integrated models using biomechanical models of the occupants with and without restraint systems are now appearing as standard practice. The finite element method, multibody dynamics, macro-elements, and hybrid methodologies are the numerical tool in use today. The maximization of the vehicle performance in terms of crashworthiness requires the use of the most appropriate numerical procedure during the different design and analysis phases, according to the amount of information available.

The finite element method is today the most suitable numerical procedure for crashworthiness analysis of metallic structures where the geometry and material properties are known, due to the flexibility and possible detail of the models. However, few, as yet unsolved issues, limit the effectiveness and timeliness of the technology. Among which are: the model build time, especially for complex vehicle structures; modeling of nonmetallic soft materials such as rubbers, plastics, polyurethane foams or human tissues; strain rate effects in different materials. At the

moment, the use of strain rate effects appears to be arbitrary where it is used in component simulations and rarely in full vehicle simulations.

The use of numerical simulation in worldwide safety regulations is an issue that certainly will arise in the near future. The development of reliable simulation techniques should harmonize various safety standards and regulations and move certification techniques towards a balanced combination of experimental and numerical modeling. For example, advanced human body models are expected to be used in simulation replacing dummy models provided that the actual problems on their modeling are solved. However, a substantial effort is required to standardize the international requirements and to establish widely accepted numerical simulation techniques.

4.2 Structural Impact

The topic of structural impact is concerned with the response of structures subjected to dynamic loadings producing large inelastic strains and permanent deformations. This is relevant to safety calculations and energy absorption estimates for structural crashworthiness studies. The rigid-plastic method of analysis is introduced and used to examine the dynamic plastic response of a fully clamped beam struck by a rigid mass travelling with an initial impact velocity. This theoretical solution is used to assess the accuracy and range of validity of a quasi-static method of analysis, which is often employed to simplify impact problems in the structural crashworthiness field. The dynamic axial crushing behavior and energy absorbing capacity of a thin-walled tube is examined briefly. Also reported are the results of some recent studies on the influence of axial length on the response modes of various thin walled sections subjected to axial impact loads.

Structural crashworthiness is concerned with the design of vehicles containing structural members and systems, which are required to absorb the dynamic energies and loads arising during a collision or impact event, but in a controlled manner which minimizes injury to any occupants. The studies associated with the development of human injury criteria and the fundamental research into the dynamic response of structural members under large impact loads might be used for structural crashworthiness problems in a wide range of industries.

Most of the problems in structural impact are common in the field of crashworthiness of cars, buses, trains or airplanes. Many of the specialists in crashworthiness use, in a broad basis, what can be defined as quasi-static methods of analysis without fully understanding the range of validity of these methods. However, these techniques provide a good understanding of the physics of the problems, they are efficient for design, cheap to use and credible. These methods have a very high potential and can be improved in order to describe properly the transition between different modes and to overcome their shortcomings. In particular, this understanding and insight is indispensable for the efficient use and interpretation of numerical codes, which play an increasingly important role in engineering design.

The sophistication of the finite element method has progressed well beyond the accuracy of the input data that can be provided to those codes. Some of the points where this is visible are:

- Material properties, particularly for large strains
- Structural failure criteria
- Strain rate conditions, particularly for large strains
- Residual stresses
- Manufacturing imperfections
- Loading characteristics
- Scaling

There is a large amount of information that is not defined clearly enough as the input for finite element codes and for some simulation codes based on other formulations. This class of very large codes, which require complete information of the problem, are very good for checking the final design. Though, they do give a good physical understanding of the problems during the preliminary design they are more difficult to master. It might be that finite element programs are relatively simple to operate, but they are notoriously difficult be used properly in the sense that they incorporate the interaction between many nonlinear phenomena, some of which that are not well understood. Integrated environments for analysis and design are necessary such as those produced already by some of the larger manufacturers of automobiles and aircraft. In addition, the problem of cooperation between different communities is fundamental in order to integrate these tools to make them truly flexible.

4.3 FE Technology in Crashworthiness Analysis

Crashworthiness analysis of transportation vehicles in general and of ground vehicles in particular is among the most challenging nonlinear problems in structural mechanics. Vehicle structures are typically manufactured from many stamped thin shell parts and subsequently assembled together by various welding and fastening techniques. The structure may contain steel, aluminum and/or plastic materials. During the crash incident, the structure is subjected to high impact loads, which produce localized plastic hinges and buckling which ultimately may lead into large deformations and rotations with contact and stacking among the various components. The deformations initially involve wave effects, associated with high stresses. Once these stresses exceed the yield strength of the material and/or its critical buckling load, localized structural deformations occur during a few wave transits in the structure. This is followed by inertial effects, which dominate the subsequent transient response. Of particular interest here are structural integrity and associated kinematics and stacking of components, forces transmitted through the various members, stresses, strains, and energy absorption. In addition the rollover crash event may be considered as a low to medium speed dynamic event (2-3 rad/s) persisting for a short duration of 100-300 ms. Closed form analytical solutions for this class of problems in structural mechanics present insurmountable challenge to the analyst. Numerical techniques are the only practical option, at this time.

The FE method of structural dynamics solves numerically a set of nonlinear partial differential equations of motion in the space-time domain, coupled with material stress-strain relations along with definition of appropriate initial and boundary conditions. The solution, first, discretizes the equations in space by formulating the problem in a weak variational form and assuming an admissible displacement field. This yields a set of second order differential equations in time. Next, the systems of equations are solved by discretization in the time domain. The discretization is accomplished by the classical Newmark-Beta method [49]. The technique is labeled implicit if the selected integration parameters render the equations coupled; and in this case the solution is unconditionally stable. If the integration parameters are selected to decouple the equations, then the solution is labeled explicit; and it is conditionally stable. Earlier developments in nonlinear FE technology used primarily

implicit solutions [50]. FE simulations for structural crashworthiness by explicit solvers appear to be first introduced by Belytschko [51]. Later, Hughes et al. [52] discussed the developments of mixed explicit-implicit solutions.

The explicit FE technique solves a set of hyperbolic wave equations in the zone of influence of the wave front, and accordingly does not require coupling of large numbers of equations. On the other hand, the unconditionally stable implicit solvers provide a solution for all coupled equations of motion, which require assembly of a global stiffness matrix. The time step for implicit solvers is about 2-3 orders of magnitude of the explicit time step. For crash simulations involving extensive use of contact, multiple material models and a combination of nontraditional elements, it turned out that explicit solvers are more robust and computationally more efficient than implicit solvers. The discretized equations of motion for explicit FE formulation can be written as:

$$\underline{M}\,\underline{\ddot{x}} + \underline{C}\,\underline{\dot{x}} + \underline{K}\,\underline{x} = \underline{f}^{(ext)} \tag{4.1}$$

$$\underline{C}\,\underline{\dot{x}} + \underline{K}\,\underline{x} = \underline{f}^{(int)} \tag{4.2}$$

$$\underline{M}\,\underline{\ddot{x}} = \underline{f}^{(ext)} - \underline{f}^{(int)} \tag{4.3}$$

where; $\underline{M}$ is a diagonal inertia matrix of the structure, $\underline{\ddot{x}}$ is the nodal acceleration vector, $f^{(ext)}$ is the external force vector and $f^{(int)}$ is the internal nodal force vector.

Time integration of equations is obtained by a central difference technique **(4.3)**:

$$\underline{\ddot{x}}^{(n)} = \underline{M}^{-1}\left(\underline{f}^{(ext)^{(n)}} - \underline{f}^{(int)^{(n)}}\right)$$

$$\underline{\dot{x}}^{(n+1)} = \underline{x}^{(n)} + \underline{\dot{x}}^{(n+1)/2}\,\Delta t^{(n+1)/2} \tag{4.4}$$

$$\underline{x}^{(n+1)} = \underline{x}^{(n)} + \underline{\dot{x}}^{(n+1)/2}\,\Delta t^{(n+1)/2}$$

4.4 Direct Time Integration

In direct integration, the equations of motion are directly integrated using a numerical step by step procedure. In this method, no transformation of the equations into another basis is carried out. The dynamic equilibrium equation written at discrete time points includes the effect of inertia and damping forces. The variation of displacements, velocities and accelerations is assumed with each time interval Δt. As the solution is obtained by a step by step procedure, the diverse system nonlinearities as geometric, material, contact and large deformation nonlinearity are taken into account in a natural way even if the resolution in each step remains linear.

In transient dynamic analysis, the direct integration method is usually chosen. A few commonly used integration methods exist in the literature [55]. The method used in RADIOSS is derived from Newmark time integration scheme with central difference technique.

4.4.1 Newmark's method

Newmark's method is a one step integration method. The state of the system at a given time $t_{n+1} = t_n + h$ is computed using Taylor's formula:

$$f\ (t_n + h) = f(t_n) + hf'(t_n) + \frac{h^2}{2} f^{(2)}(t_n) + \cdots + \frac{h^s}{s!} f^{(s)}(t_n) + R_s \qquad \textbf{(4. 5)}$$

$$R_s = \frac{1}{s!} \int_{t_n}^{t_n+h} f^{(s+1)}(\tau)[t_n + h - \tau]^s \, d\tau \qquad \textbf{(4.6)}$$

The preceding formula allows the computation of displacements and velocities of the system at time $t_n + 1$:

$$\dot{u}_{n+1} = \dot{u}_n + \int_{t_n}^{t_{n+1}} \ddot{u}\,(\tau) d\tau \qquad \textbf{(4.7)}$$

$$u_{n+1} = u_n + h\dot{u}_n + \int_{t_n}^{t_{n+1}} (t_{n+1} - \tau)\, \ddot{u}(\tau) d\tau \qquad \textbf{(4.8)}$$

The approximation consists in computing the integrals for acceleration in Eq. (4.7) and in Eq. (4.6) by numerical quadrature **(4.7) (4.8)**:

$$\int_{t_n}^{t_{n+1}} \ddot{u}\,(\tau) d\tau = (1 - \gamma) h\ddot{u}_n + \gamma h\ddot{u}_{n+1} + r_n \qquad \textbf{(4.9)}$$

$$\int_{t_n}^{t_{n+1}}(t_{n+1}-\tau)\ddot{u}\,(\tau) = \left(\frac{1}{2}-\beta\right)h^2\ddot{u}_n + \beta h^2\ddot{u}_{n+1} + r_n' \qquad \textbf{(4.10)}$$

In replacing Eq. (4.7) and (4.8), one has **(4.7) (4.8)**:

$$\dot{u}_{n+1} = \dot{u}_n + (1-\gamma)h\ddot{u}_n + \gamma h\ddot{u}_{n+1} \qquad \textbf{(4.11)}$$

$$u_{n+1} = u_n + h\dot{u}_n + \left(\frac{1}{2}-\beta\right)h^2\ddot{u}_n + \beta h^2\ddot{u}_{n+1} + r_n' \qquad \textbf{(4.12)}$$

According to the values of γ and β, different algorithms can e derived:

- γ = 0, β = 0: pure explicit algorithm. It can be shown that it is always unstable. An integration scheme is stable if a critical time step exists so that, for a value of the time step lower or equal to this critical value, a finite perturbation at a given time does not lead to a growing modification at future time steps.
- γ = 1/2, β = 0: central difference algorithm.
- γ = 1/2, β = 1/2: Fox & Goodwin algorithm.
- γ = 1/2, β = 1/6: linear acceleration.
- γ = 1/2, β = 1/4: mean acceleration.

4.4.2 The central difference algorithm

The central difference algorithm corresponds to Newmark algorithm with γ = 1/2 and β = 0, so that Eq. (4.11) and (4.12) become **(4.7) (4.8)**:

$$\dot{u}_{n+1} = \dot{u}_n + \frac{1}{2}h_{n+1}(\ddot{u}_n + \ddot{u}_{n+1}) \qquad \textbf{(4.13)}$$

$$u_{n+1} = u_n + h_{n+1}\dot{u}_n + \frac{1}{2}h_{n+1}^2 + \ddot{u}_n \qquad \textbf{(4.14)}$$

with h_{n+1} the time step between t_n and t_{n+1}.

The central difference algorithm can be changed to an equivalent form with 3 time steps:

$$\ddot{u}_n = (u_{n+1} - 2u_n + u_{n-1})/2 \qquad \textbf{(4.15)}$$

if the time step is constant.

From the algorithm point of view, it is, however, more efficient to use velocities at half of the time step:

$$\dot{u}_{n+\frac{1}{2}} = \dot{u}\left(t_{n+\frac{1}{2}}\right) = \frac{1}{h_{n+1}}(u_{n+1} - u_n) \qquad \textbf{(4.16)}$$

so that:

$$\ddot{u}_n = \frac{1}{h_{n+\frac{1}{2}}}\left(\dot{u}_{n+\frac{1}{2}} - \dot{u}_{n-\frac{1}{2}}\right) \qquad \textbf{(4.17)}$$

$$h_{n+\frac{1}{2}} = (h_n + h_{n+1})/2 \qquad \textbf{(4.18)}$$

Time integration is explicit, in that if acceleration $\ddot{u}_n$ is known, the futere vlocities and displacements are calculated from past (known) values in time:

$$\dot{u}_{n+\frac{1}{2}} = \dot{u}_{n-\frac{1}{2}} + h_{n+\frac{1}{2}}\,\ddot{u}_n \qquad \textbf{(4.19)}$$

The same formulation is used for rotational velocities.

$$u_{n+1} = u_n + h_{n+1}\,\dot{u}_{n+\frac{1}{2}} \qquad \textbf{(4.20)}$$

The accuracy of the scheme is of h^2 order, i.e. if the time step is halved, the amount of error in the calculation is one quarter of the original. The time step h may be variable from one cycle to another. It is recalculated after internal forces have been computed.

4.4.3 Numerical procedure

At time t = 0, the displacement u and velocity $\dot{u}_0$ are known from initial conditions. The acceleration $\ddot{u}_0$ and time step h_1 are found from solving the equations of motion. The initial time step, h_0, is set to zero:

$$h_0 = 0; \qquad h_{\frac{1}{2}} = \frac{h_1}{2} \qquad \textbf{(4.21)}$$

$$\dot{u}_{\frac{1}{2}} = \dot{u}_0 \qquad \textbf{(4.22)}$$

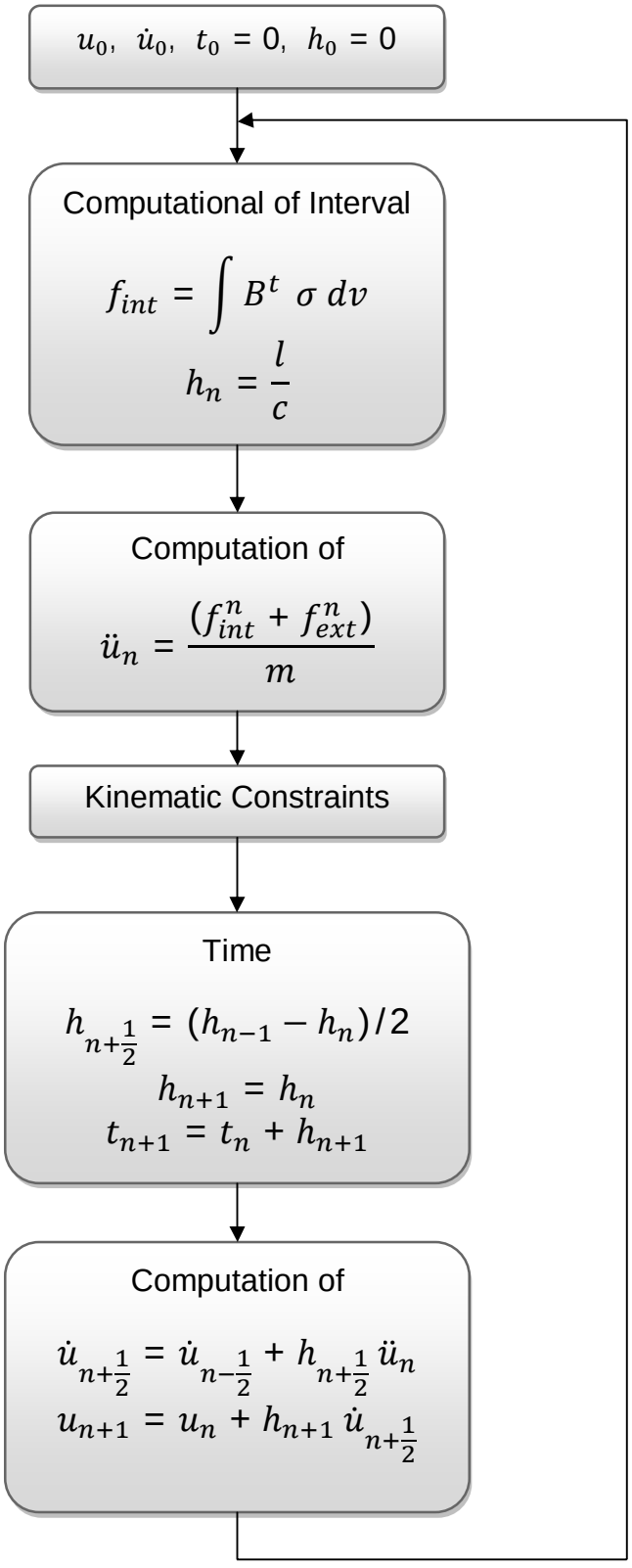


Figure 4.1 : Numerical procedure of time integration.

$$\dot{u}_{\frac{1}{2}} = \dot{u}_0 + h_{\frac{1}{2}}\,\ddot{u}_0 \qquad \textbf{(4.23)}$$

The flow chart of the central difference algorithm can be summarized as in Figure 4.1. It is pointed out that the solution of the linear system to compute accelerations is immediate if the mass matrix is diagonal.

4.5 Explicit Solution Strategy

Explicit numerical solvers can be summarized by the flow chart in Figure 4.2 below. For each time step in a particular analysis, the algorithm used to compute results is:

1) Solution starts with a mesh having assigned material properties, loads, contacts, constraints, boundary and initial conditions.
2) External nodal forces are computed from loads, contacts, constraints, boundary and initial conditions. The external force vector is constructed and applied.
3) Integration in time, produce motion at the mesh nodes. Time integration procedure is discussed at Figure 4.1.

a. With all forces known, nodal accelerations are calculated using the mass matrix and the external and internal force vectors:

$$\dot{v}_i = M^{-1}(f_{ext_i} - f_{int_i}) \qquad \textbf{(4.24)}$$

b. Time integration of velocity is performed from nodal accelerations.
c. Time integration of displacement is performed from nodal velocities.

4) Motion of nodes produces deformation of elements. Element deformation results in change in volume and density of the material in each element. Deformation rate is used to derive strain rate. The strain rate is calculated:

$$\dot{\varepsilon}_{ij} = \left(\frac{\partial \Phi_I}{\partial x_j}\right)\dot{x} = \frac{1}{2}\left(\frac{\partial v_i}{\partial x_j} + \frac{\partial v_j}{\partial x_i}\right) \qquad \textbf{(4.25)}$$

5) The stress rate is calculated:

$$\dot{\sigma}_{ij} = f(\dot{\varepsilon}, material - law) \qquad \textbf{(4.26)}$$

6) Constitutive laws derive Cauchy stresses from the stress rate using explicit time integration:

$$\sigma(t + \Delta t) = \sigma(t) + \dot{\sigma}\,\Delta t \qquad \textbf{(4.27)}$$

7) The internal and hourglass force vectors are computed. After the internal and hourglass forces are calculated for each element, the algorithm proceeds by

computing the contact forces between any interfaces. The next time step size is computed, using element or nodal time step methods. This turns the calculation back to step 2 and makes a cycle. The solution process (cycle) is repeated until the calculation end time is reached unless energy or mass error is occurred.

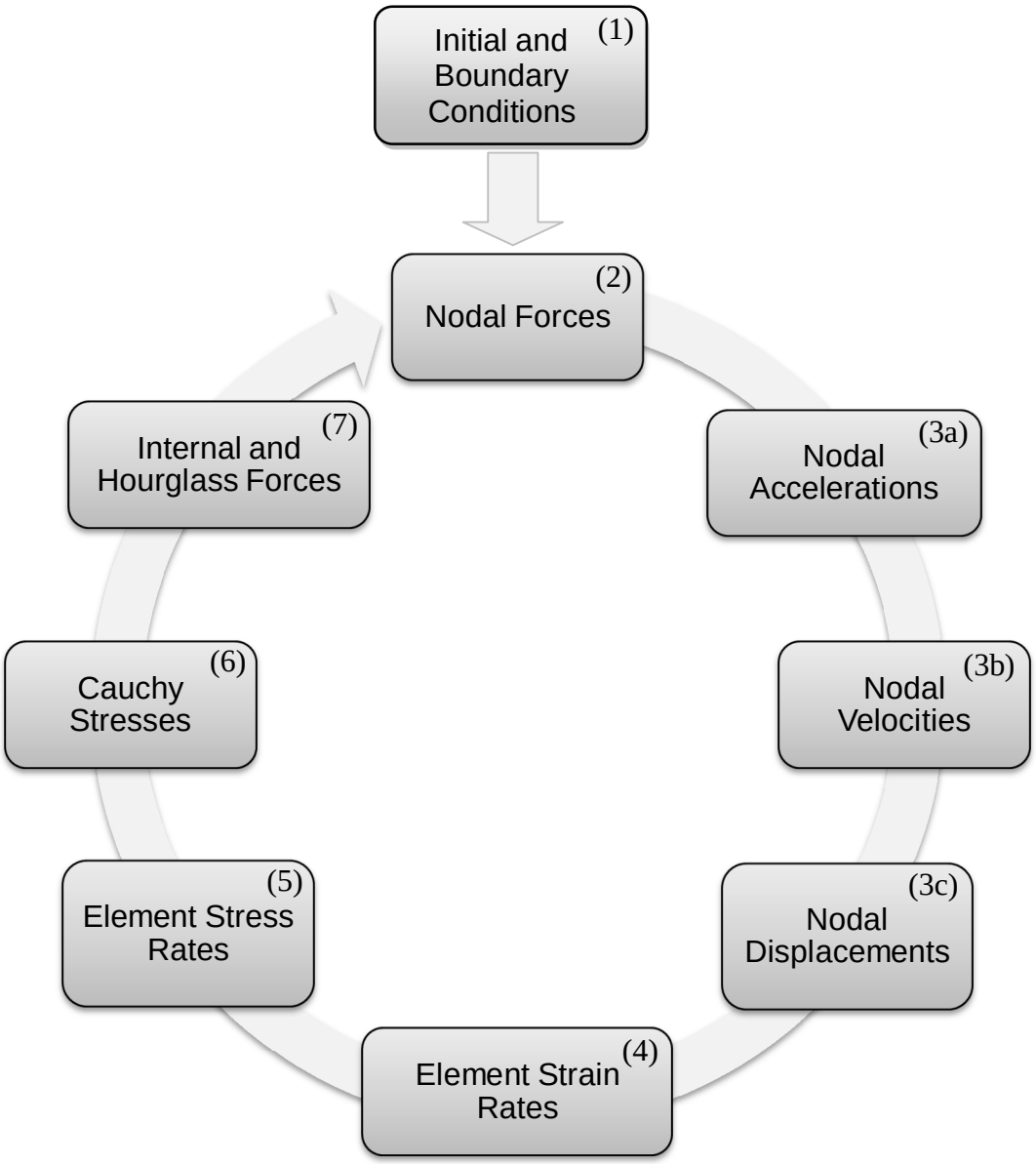


Figure 4.2 : Simplified explicit solution strategy flow chart.

4.6 Conclusion

Noteworthy advances in crashworthiness have been achieved in the past years due to improvements in the vehicle structural response, compliance of the vehicle interior

and exterior and restraint systems to control the occupant kinematics. Statistical data shows that the concurrent use of different protection systems leads to the increase of their efficiency, for instance the simultaneous use of seat belts and airbags, with the consequent minimization of injury. Integrated methodologies of analysis based on finite elements, multibody dynamics, simplified elements and experimental testing are now possible for both structural impact and occupant kinematics. From the design phases of new systems until their complete analysis, different tools of increasing complexity can be used as more information on the final design becomes available.

5. VALIDATION AND VERIFICATION OF THE COMPUTATIONAL CALCULATION

5.1 Introduction

Developers of computer codes, analysts who use the codes and decision makers who rely on the results of the analyses face a critical question: How should confidence in modeling and simulation be critically assessed? Verification and validation of computational simulations are the primary methods for building and quantifying this confidence. Briefly, verification is the assessment of the accuracy of the solution to a computational model. Validation is the assessment of the accuracy of a computational simulation by comparison with experimental data. In verification, the relationship of the simulation to the real world is not an issue. In validation, the relationship between computation and the real world, i.e., experimental data is the issue.

During the last three or four decades, computer simulations of physical processes have been increasingly used in scientific research and in the analysis and design of engineered systems. The systems of interest have been existing or proposed systems that operate, for example, at design conditions, off-design conditions, and failure-mode conditions in accident scenarios. The systems of interest have also been natural systems, for example, computer simulations for rollover impact, as in the analysis of crashworthiness of buses and the risk assessment of human injuries. These kinds of predictions are beneficial in the development of government policy, the preparation of safety procedures, and the determination of legal liability. Thus, because of the impact that modeling and simulation predictions can have, the credibility of the computational results is of great concern to engineering designers and managers, government officials, and those who are affected by the decisions that are based on these predictions.

5.2 Fundamentals of Validation

Validation : The process of determining the degree to which a model is an accurate representation of the real world from the perspective of the intended uses of the model.

The fundamental strategy of validation involves identifying and quantifying the error and uncertainty in the conceptual and computational models, quantifying the numerical error in the computational solution, estimating the experimental uncertainty, and then comparing the computational results with the experimental data. This strategy does not assume that the experimental measurements are more accurate than the computational results. The strategy only asserts that experimental measurements are the most faithful reflections of reality for the purposes of validation. Validation requires that the estimation process for error and uncertainty must occur on both sides of the coin: mathematical physics and experiment. Figure 5.1 depicts the validation process of comparing the computational results of the modeling and simulation process with experimental data from various sources [54].

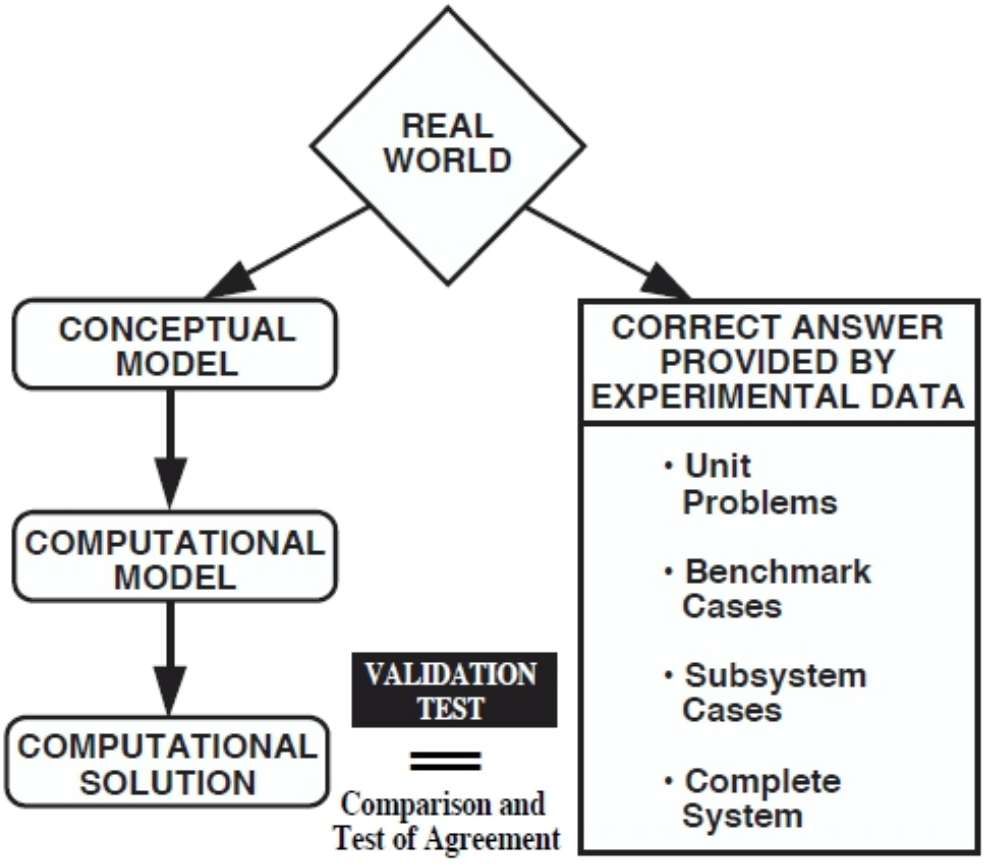


Figure 5.1 : Validation process [54].

This task must be accomplished by quantitatively comparing code calculations with experimental data, important requirements are placed on validation experiments to create the greatest opportunities for performing these comparisons. It is critically important to design and execute validation experiments that allow precise and conclusive comparisons of calculations with experimental data for the purpose of assessing model fidelity and credibility.

The experimental, computational, and comparison activities should expedite the quantitative assessment of computational models for system applications that are within the application domain. It is important to attempt to quantify the boundary separating the region of acceptability of the model from the region where the model is not acceptable for the application. Designing experiments that test a model in regions where the model is believed to be insufficiently accurate for the intended application helps locate this boundary and provides a means for quantitatively assessing the degree of the expected inaccuracy. Because such experiments are performed purposefully rather than accidentally, these experiments also further test our grasp of the conceptual models underlying the code that are probed by the validation experiments. Obviously, this goal only makes sense when experiments that probe model inaccuracy lie close enough to the boundary of applicability to be relevant. It is desirable to have experimental validation tasks that have the explicit goal of defining those application domains where use of the model is questionably adequate to better quantify the boundary of applicability of the model. To perform these validation tasks in a conscious and scientifically directed manner is not necessarily any easier than to achieve desirable levels of confidence in other application domains.

5.3 Characteristics of Validation Experiments

Validation experiments constitute a new type of experiment. A validation experiment is conducted for the primary purpose of determining the validity, or predictive accuracy, of a computational modeling and simulation capability. In other words, a validation experiment is designed, executed, and analyzed for the purpose of quantitatively determining the ability of a mathematical model and its embodiment in a computer code to simulate a well characterized physical process. Thus, in a validation experiment ‘‘the code is the customer’’ or, if you like, ‘‘the computational

analyst is the customer.'' Only during the last 10 to 20 years has computational simulation matured to the point where it could even be considered as a customer. As modern technology increasingly moves toward engineering systems that are designed, and possibly even fielded, based on modeling and simulation, then modeling and simulation itself will increasingly become the customer of experiments.

There are three aspects that should be used to optimize the effectiveness and value of validation experiments. The first aspect is to define the expected results of the experimental validation activity using the code itself. The second aspect is to design specific validation experiments by using the code in a predictive sense. The third aspect is to develop a well-thought-out plan for analyzing the computational and experimental results. These aspects emphasize tight coupling of the subject code to the experimental activity and ensure we are in the best position to learn from the comparison of computational and experimental results, regardless of whether these comparisons are good or bad.

One way of designing a validation experiment is to use the code calculations as specific guidance on where to locate the instrumentation and what kind of data to acquire for assessing the anticipated sensitivity. In the proposed validation experiments, ''design'' means specifying to the greatest degree possible the initial and boundary conditions, material properties, diagnostic locations and characteristics (strain gauge, accelerometer, high speed camera, etc.), and data fidelity. In most cases, the success of a validation experiment will often be determined by the degree to which the experiment matches these specifications. Deviations can be acceptable; but if the intent of the experiment was to measure x at location y for material z and geometry g and in all cases the experiment is significantly different from most or all of these factors, it is unlikely that the experiment would be a successful validation experiment.

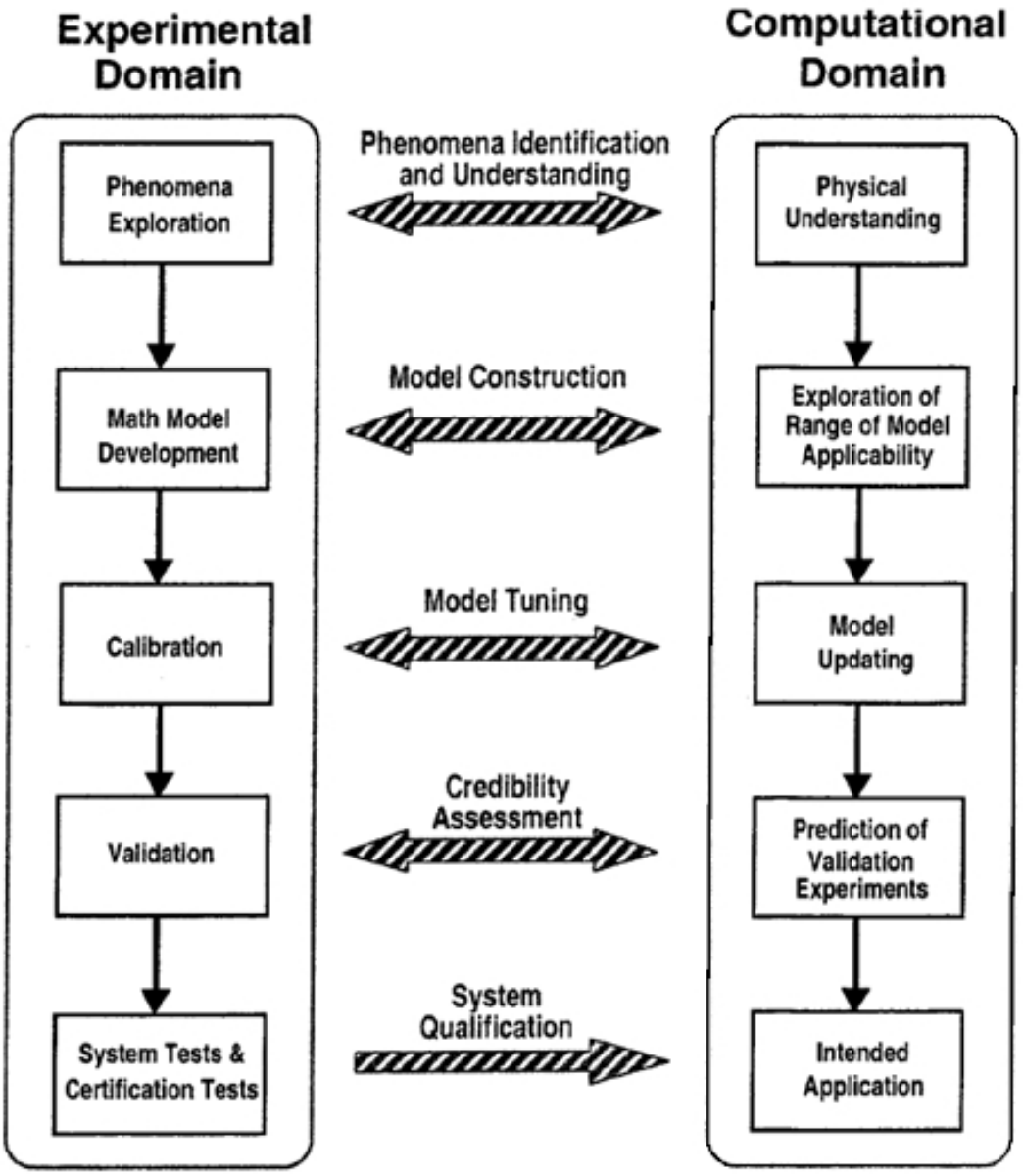


Figure 5.2 : Interaction of various experimental and computational activities [55].

Each element in the experimental domain directly interacts with an element in the computational domain. The motivating concepts generating these computational elements are suggested by the arrows in the middle of the figure that depict the flow of experimental information directly to the computational domain and vice versa. We have simplistically characterized the computational domain through the types of activities expected to be most associated with the directly correlated experimental element. We believe that our depiction in Figure 5.2 highlights the right connections between the experimental and computational domains if the experimental domain is not restricted only to validation experiments as they are defined in this report. In particular, the ultimate goal of both experimental and computational activities is to

provide a basis of confidence and decision making for the intended application of the code. We have highlighted the great weight that system tests and certification tests evoke by emphasizing a more unidirectional flow of information between the experimental and computational domains at this level. The technical weakness to their genuine physical reality, if the system can be tested, is that the test is only one physical realization of a complex, nondeterministic system.

5.4 Validation Metrics

Validation metrics are used to quantitatively compare the results of code calculations with the results of validation experiments. The straightforward interpretation of this word is that a ‘‘metric’’ is simply a ‘‘measure.’’ Thus, the choice of one or more metrics defines the means used to measure the differences between computational results and experimental data. Because we emphasize that, the overarching goal of validation experiments is to develop sufficient confidence so that the code can be used for its intended application.

Not only tests themselves but also model outputs (measures) need to be carefully selected for validation purposes. Obtained metric ideally should quantify both errors and uncertainties in the comparison of computational results and experimental data [44]. They are present in material data, loading and boundary conditions as well as representation of the geometry. Not always such advancement in results' outcome is possible to produce. Thus, the following increase in the quality of the validation metrics is used in this thesis [56]:

a) Deterministic – at most two curves of an experimental response and numerical prediction are compared.

b) Experimental uncertainty – like previous but error quantification for experimental data is provided.

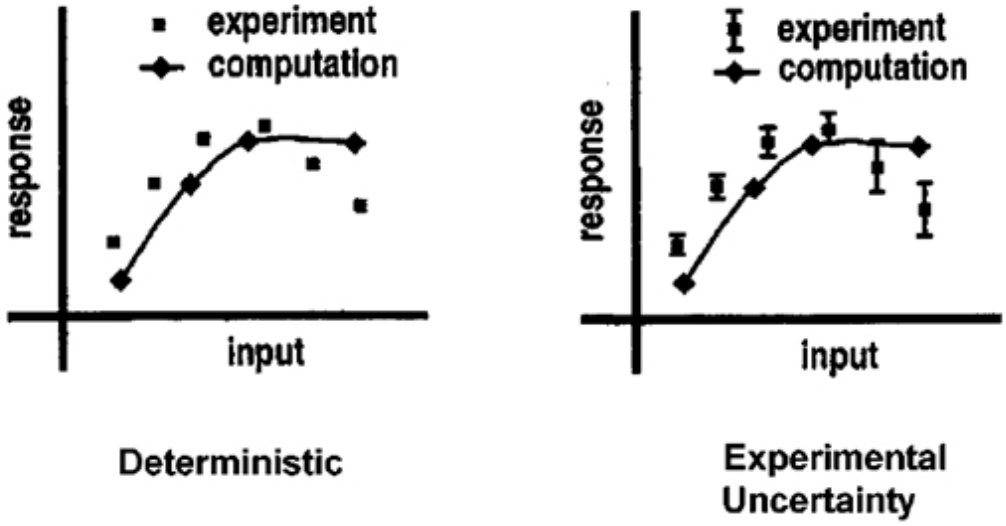


Figure 5.3 : Increasing quality of validation metrics: (a) Deterministic. (b) Experimental uncertainty [55].

The plot in Figure 5.3a portrays the most common type of comparison between computational results and experimental data. Generic axis labels of system ‘‘input’’ and ‘‘response’’ are shown, although both axes can also be system response quantities over a range of an input quantity. While discrete experimental and computational points are shown in this plot, the concept also encompasses curve overlays without any points shown. The key problem with metrics implemented at the level of Figure 5.3a is that there is no recognition of uncertainty in the comparison. Conclusions drawn from this type of comparison are really only qualitative, such as ‘‘fair agreement’’ or ‘‘generally good agreement.’’

Figure 5.3b suggests that the next step for improving the method of comparison is to place qualitatively estimated error bars around the experimental data. By ‘‘qualitatively estimated error bars’’ we mean the common practice of the experimentalist either quoting the manufacturer’s stated accuracy of the diagnostic sensor, making a statement such as ‘‘Essentially all of the experimental data fell within the error bars shown,’’ or ignoring experimental uncertainty in the input, or control, quantity. At this stage of comparison, a validation metric could be constructed that accounts for two characteristics: the difference between the computation and experiment integrated over the range of the input parameter, and some estimate of the experimental uncertainty.

It is critically important to estimate numerical errors in the computational simulation that are compared with the experimental results. Otherwise, in computational-experimental comparisons, the numerical errors can be indistinguishable from the modeling uncertainties. It is also important to properly represent the uncertainty observed in the experiment. For example, observed experimental variations can be propagated through ensembles of calculations using techniques for propagating uncertainty, and the computational results can then be analyzed to provide statistical data about the resulting computational uncertainty.

Comparing an ensemble of calculations with an ensemble of experimental data is a statistical problem of quantifying uncertainty. Statistical analysis of the differences between computational and experimental results must play a key role in the analysis and presentation of metric data. A fundamental goal of a validation metric is, then, to present at least the impact of the uncertainty of the experimental data upon the inferences that are drawn from the validation exercise. It is important to recognize that uncertainty in the experimental data (and of the computations) affects the credibility of the results of a validation metric. This fact, in turn, will impact the confidence in the proposed application domain of the code.

5.5 Accuracy of Validation

Well planned and performed V&V tasks do not always assure that problem can be %100 accurately computed afterwards. The degree of precision with which some tasks can be solved varies and is an intrinsic property of a physical problem. The factor characterizing the ability of the model to closely mimic the real event is computability of the problem [46]. The issue that often is omitted by researchers. In the research reports only matching results are shown, barriers to computability and problems with uncertainties in the input data are tacitly omitted.

The difficulty of a problem, which is the inverse of its computability, is influenced by six factors assigned to them (as proposed in Belytschko (2001) [57]):

- Smoothness of the data and the response (for example presence of material failures, contact-impact effects, sliding interfaces etc.)
- Geometric stability (for example sensitivity to imperfections)

- Material stability (for example softening of the material)
- Effectiveness of constitutive equations
- Variability in data
- Mesh resolution requirements

The accuracy of a theoretical method can be assessed in relative or absolute terms. Relatively speaking, the theory of hinge behavior presented in this thesis is acceptable because it produces reasonable agreement with experiments and because a better theory does not seem to be currently available.

The accuracy required in absolute terms depends on various circumstances regarding the structure whose collapse characteristics are being investigated. The accuracy of the method presented should be considered allowing for:

- Production tolerances regarding material properties;
- Tolerances regarding the manufacturing process of the structure itself;
- Level to which the structure is idealized by the finite element model;
- Reserve of strength and energy absorbing capacity required.

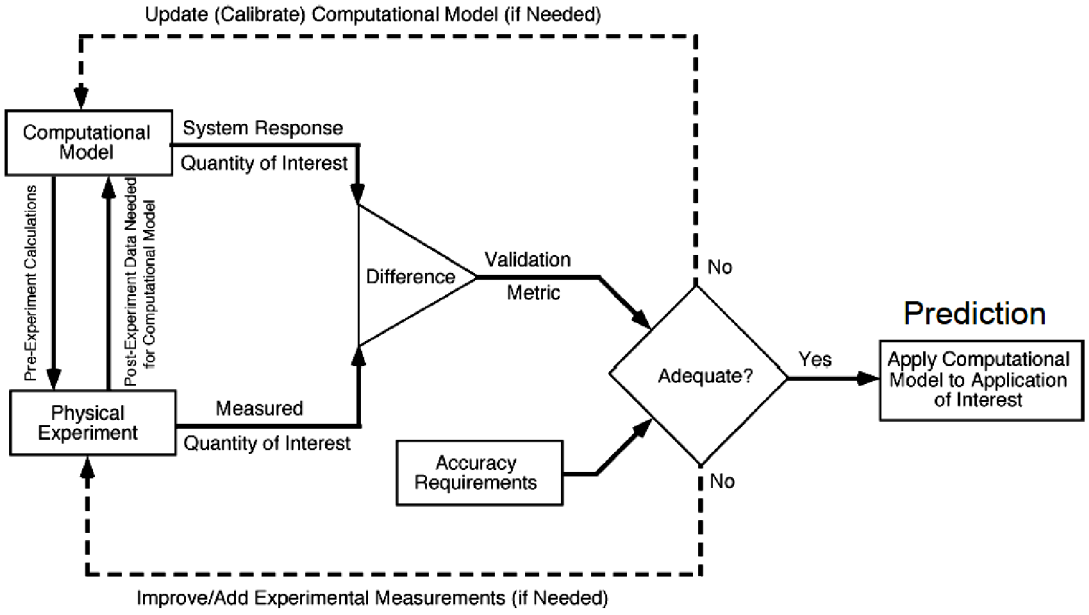


Figure 5.4 : Relationship between validation, calibration and prediction [58].

Structures are generally manufactured by putting components together and the strength of joints becomes therefore a very significant factor affecting the collapse performance. Bearing in mind the possible variations in properties of most man-made vehicle structures, it is important to design joints which would be stronger than the beams they are connecting under any circumstances.

Welding at joints may produce annealed zones near the weld with a lower yield stress than the surrounding material. If the structure is subject to large deflections, the strain concentration in these areas may cause an early material separation followed by an abrupt drop in the hinge strength.

5.6 Validation in Computational Solid Mechanics Models

5.6.1 Description

Verification and validation process is based on multi scale laboratory testing including: material characterization, wall panel and connection tests, and testing of the actual parts of bus. Validated FE models are subsequently used to provide a comprehensive safety assessment of the entire vehicle. The validation has the goal of assessing the predictive capability of the model for a given simulated event. It is performed by comparison of predicted results from FE simulations to experimental results from the same physical test. It is essential to select validation tests that are closely related to the event for which model is intended. That is why, plastic hinges, are selected for validation tests, which are showed maximum rotational deformation at bus rollover event (see Figure 5.5).

The technical service requires tests to be carried out on the actual vehicle structure to prove the validity of the mathematical model and to verify the assumptions made in the model. Load – displacement curves both for the experiments and the simulations should be compared and it should be seen that there is a consistent correlation between the experiments and the simulations results.

The model shall be capable of describing the real physical behavior of the bending tests. The mathematical model shall be constructed, and assumptions prescribed, in such a way that the calculation gives conservative results.

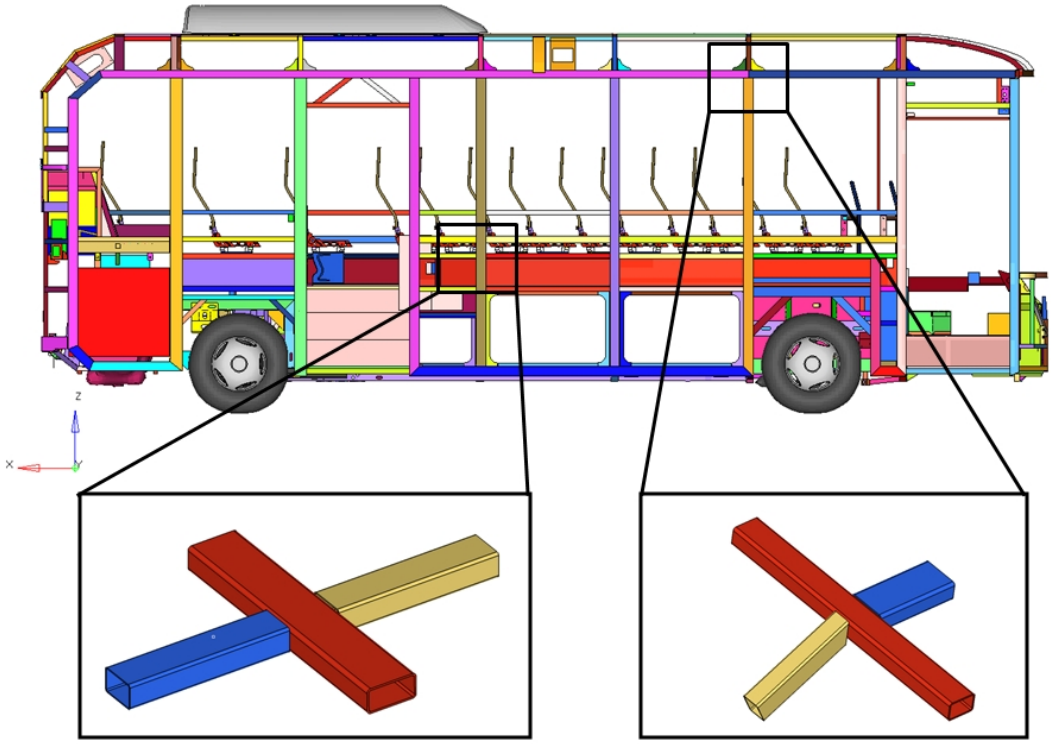


Figure 5.5 : Selected plastic hinges for validation process.

5.6.2 Researches

When the minimum number of PH is created in the structure to form one of such mechanisms, further load distribution does not progress. After this point, the final deformation of the bus structure depends largely on energy absorption capabilities of hypothetical plastic hinges. These places need to be carefully designed to allow for reaching the highest possible connection strength. Three general ways of reaching maximum strength in the connection can be expected [43,59] (see Figure 5.6):

a) The case is about the constant bending strength. The connection reaches its maximum strength by development of the plastic hinge and it is maintained throughout rest of the bending. It can occur in solid cross sections with ductile materials.
b) This is for thin walled sections that buckle locally; triggering global failure either before or after the maximum strength of material is reached. Most structural components fall into this category, which will be further. Point 1 on the plots denotes the beginning of plastic deformations. Point 2 denotes maximum strength of the PH.

c) Describes behavior of the hinge where material separation occurs (or weld/bolt failure) and sudden loss of strength may happen before maximum strength resulting from material properties is reached [34].

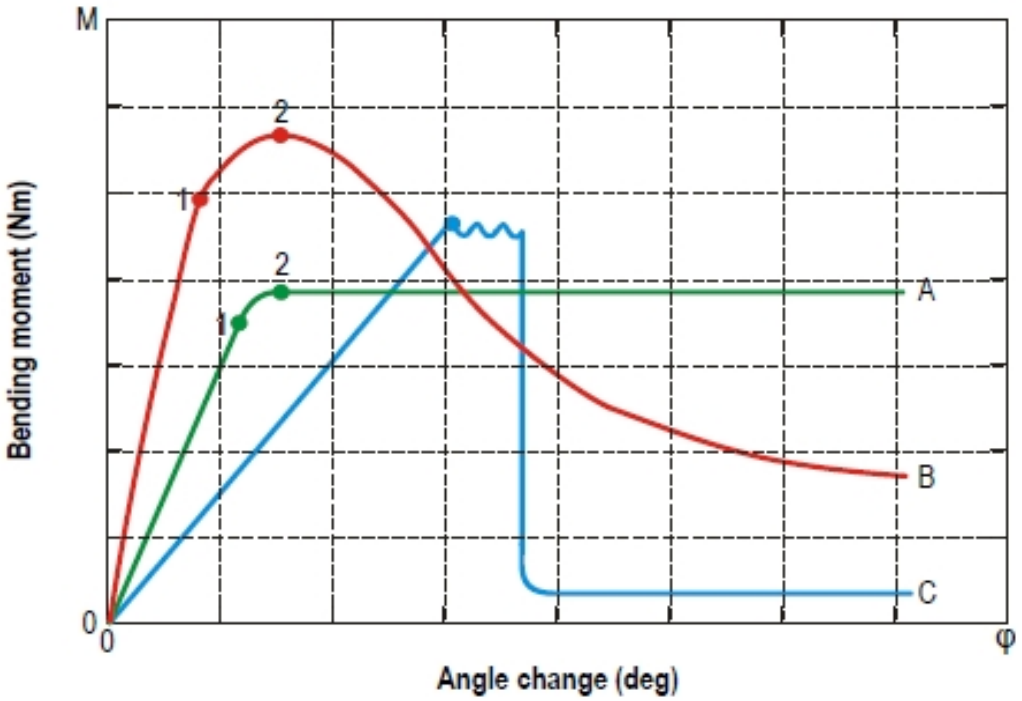


Figure 5.6 : Moment vs. angle schematic characteristics for plastic hinge [59].

Figure 5.6 shows possible shapes of moment vs. angle curve from connection bending. Curves A and B are also possible for bending of pure beams. The character of the curve after the maximum moment is reached depends on the cross section geometric properties (slenderness of the flanges and the web). Figure 5.6 shows moment – angle change characteristics for thin walled beam with main stages of the response. It is a more detailed description of the curve B from Figure 5.5. At the beginning, the curve is in linear range until local buckling of walls occurs. An inelastic transition range starts before or after that moment depending on cross section slenderness. The maximum bending moment does not result from yielding in the whole critical cross section in the case of thin walled shapes. Deep collapse process occurs due to sudden drop of the cross-section strength. The more slender the shape, the steeper the curve will be in the post buckling range. For compact cross sections in the bending, the whole critical cross section steel is yielding. It reaches the maximum strength and a plastic hinge is developed. The strength usually stays at the same level after that point and no post buckling strength reduction occurs.

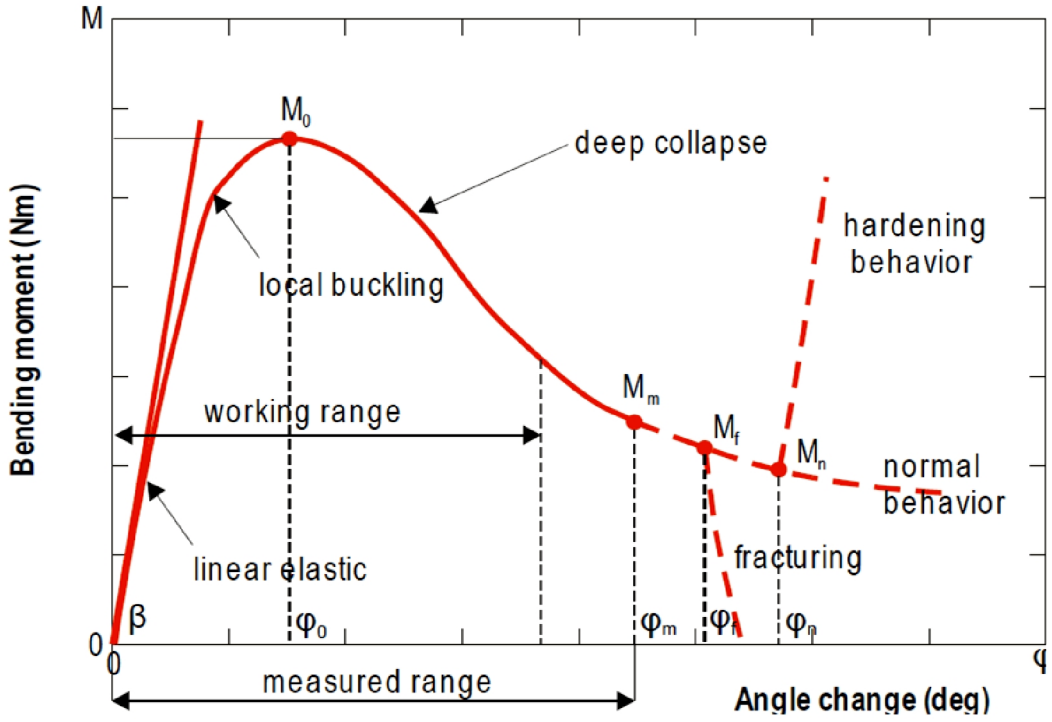


Figure 5.7 : Moment vs. angle characteristics for plastic hinge (PH) in thin walled tube [1].

5.6.3 Bending test of knots

Two different knot specimens (Breast Knot and Roof Edge Knot) were used for the bending tests. Two different welding types (Full Welding and Half Welding) were used for each bending tests specimens. At bending tests; four point bending test was performed to Breast Knot and three point bending test was performed to Roof Edge Knot. The specimens were subjected to certain boundary conditions and quasi-static loads at ITU Faculty of Mechanical Engineering; Laboratory of Strength of Materials and Biomechanics.

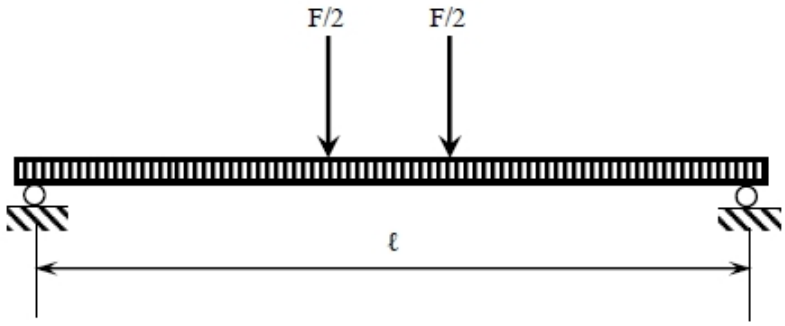


Figure 5.8 : Four point bending approach for breast knot.

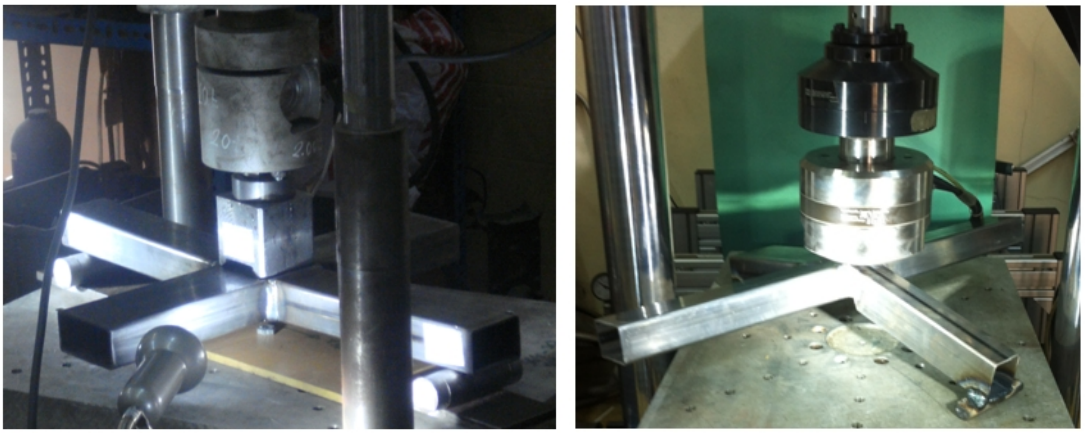


Figure 5.9 : Four point bending test setups for breast knots.

Displacements were measured with optical displacement measurement devices at bending tests. This measurement method is accepted as the most precise method for displacement measurement without touching specimens.

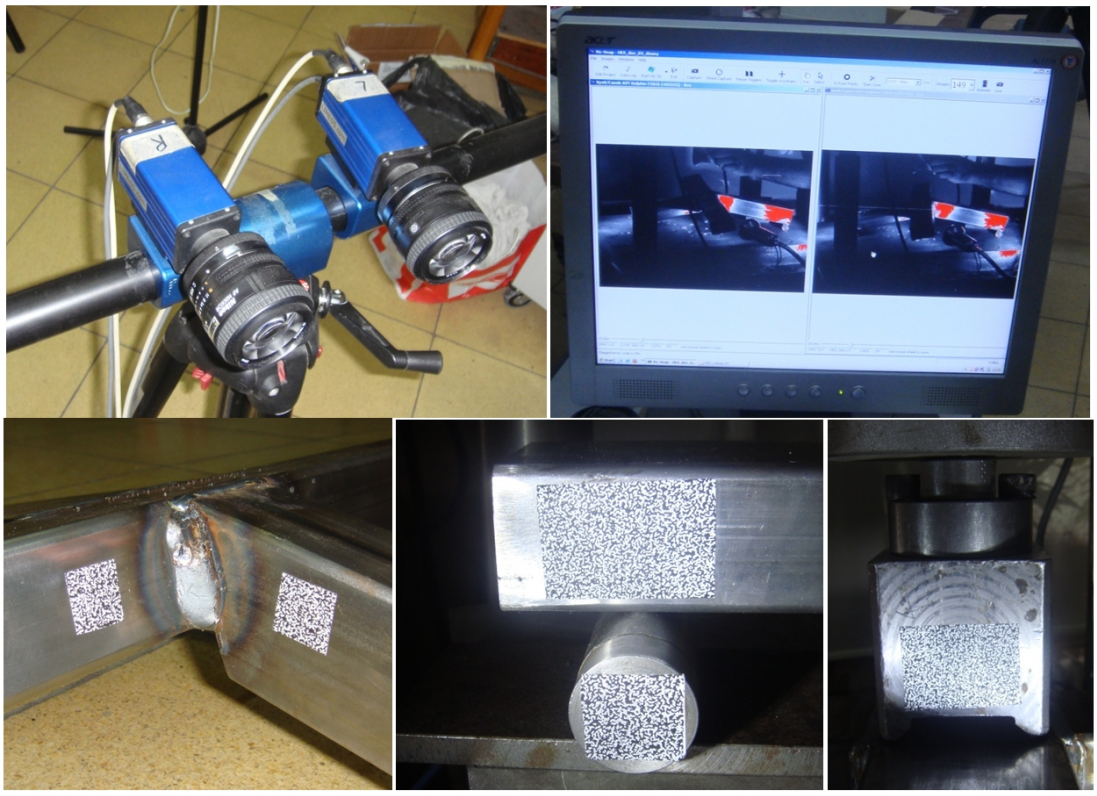


Figure 5.10 : Optical displacement measurement system used in bending tests.

In these tests, fast and accurate in-plane displacement distribution measurement method is operated that uses a digital camera and arbitrary repeated patterns based on the moiré methodology. The key aspect of this method is the use of phase information of both the fundamental frequency and the high-order frequency

components of the moiré fringe before and after deformations. Compared with conventional displacement methods and sensors, the main advantages of the method developed herein are its high resolution, accuracy, speed, low cost, and easy implementation.



Figure 5.11 : Force measurement system (loadcell) used in bending tests.

Loads were measured with ESIT SC 10 t V C4 loadcell, which has 10 t capacity. The SC shear beam loadcell has been developed for use in high capacity, compression type electronic weight and force measurement applications in industrial environments. The precise and rugged SC loadcell offers high resistance to side forces and overload conditions.

5.6.4 Finite element models of knots

The specimens were subjected to certain boundary conditions and quasi-static loads at ITU Faculty of Mechanical Engineering; Laboratory of Strength of Materials and Biomechanics. The same test scenarios were simulated by using RADIOSS explicit finite element method solver. Load – displacement curves both for the experiments and the simulations were compared. It was seen that there is a consistent correlation between the experiments and the simulations results.

The same FE parameters in the full body rollover analysis are used for the all validation analyses. The FE parameters will be discussed with details in next chapter. However, summary of the FE parameters in validation analysis are mentioned below as simplified.

The tubes were resting on two rigid cylinders. It allows for sliding elements with respect to prescribed friction. A constant upward displacement was applied to the cylinders. The explicit code was used here although the test nature is quasi-static. Since the kinetic energy in the process was low in comparison to the internal energy the density of materials was artificially increased to increase the time step in the simulation. The supports, impactor and walls were modeled with rigid elements, because their stiffnesses are too great than knots.

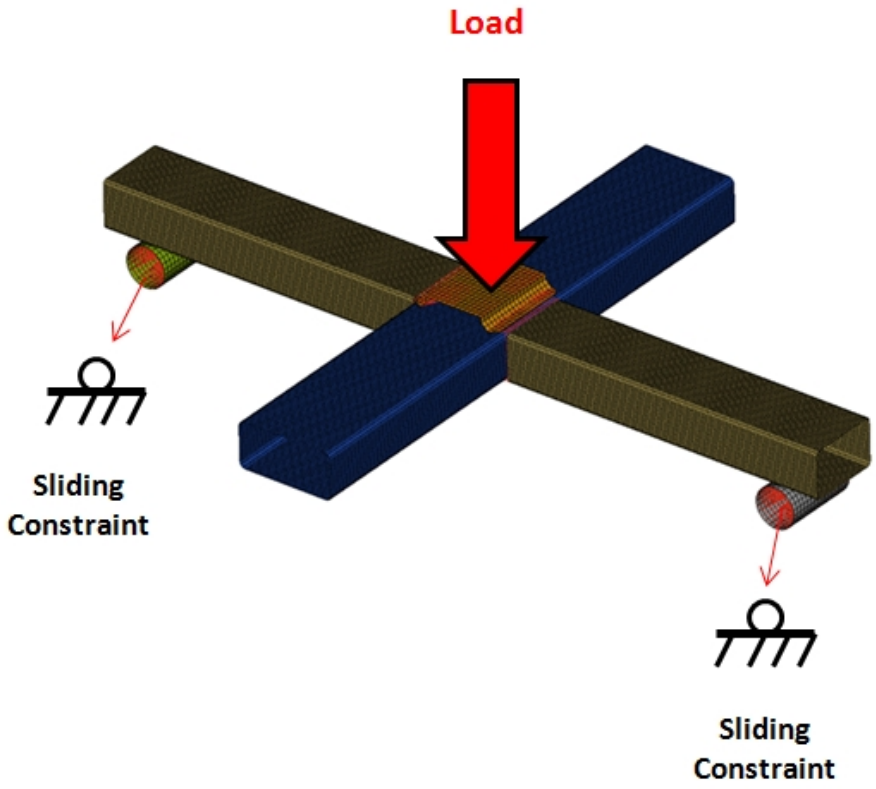


Figure 5.12 : Finite element model and boundary conditions of breast knot simulation.

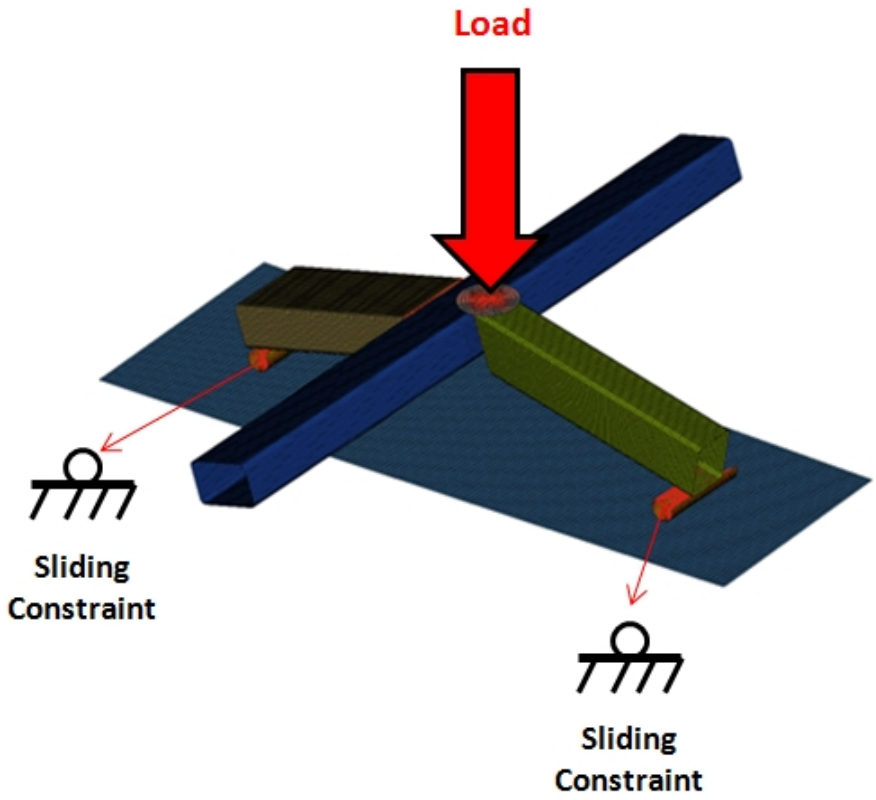


Figure 5.13 : Finite element model and boundary conditions of roof edge knot simulation.

For obtaining the material data, tensile strength tests were applied on several specimens at ITU Faculty of Mechanical Engineering; Laboratory of Strength of Materials and Biomechanics. Material tests and results will be mentioned in next chapter. The True Stress – Plastic Strain curve was imposed in RADIOSS accordingly. The material model for the deformable structure in RADIOSS is called "Elastic Plastic Piecewise Linear Material (Law 36)". This is an elasto-plastic material model which uses the Young's modulus if stresses are below the yield strength and the measured stress-strain curve if the stresses are above the yield strength. Moreover, failure criteria was defined at material model based on the tensile strength tests. Thus, elements were deleted if von Mises stresses are above the ultimate tensile strength.

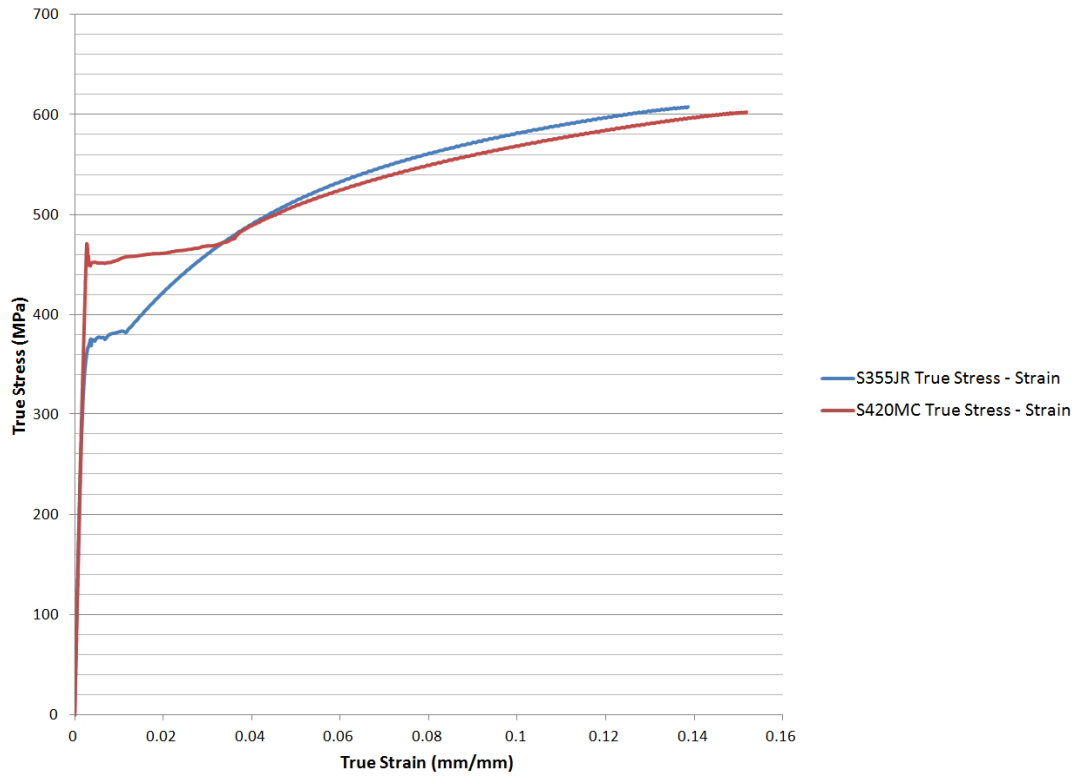


Figure 5.14 : True stress – strain curves of S420MC and S355JR steels.

The finite element modeling of breast knot and roof edge knot were performed by the specialized pre-processor software HyperMesh. Knot parts were modeled with the quad QEPH (Formulation with physical hourglass stabilization for general use) elements with five integration points through the shell thickness. The QEPH formulation provides a good precision/cost ratio. QEPH elements do not cause the hourglass energy. QEPH shells will give better results if the mesh is fine enough. QEPH formulation is recommended for isotropic materials because the stabilization forces are computed based on isotropic assumptions. During the simulation, geometric nonlinearities and thickness change at the shell elements was taken into account for membrane strain calculation. Plasticity calculation was proceeded with iterative projection with three Newton iterations. Weld connections in the finite element model of knots are modeled with rigid elements (RBODY).

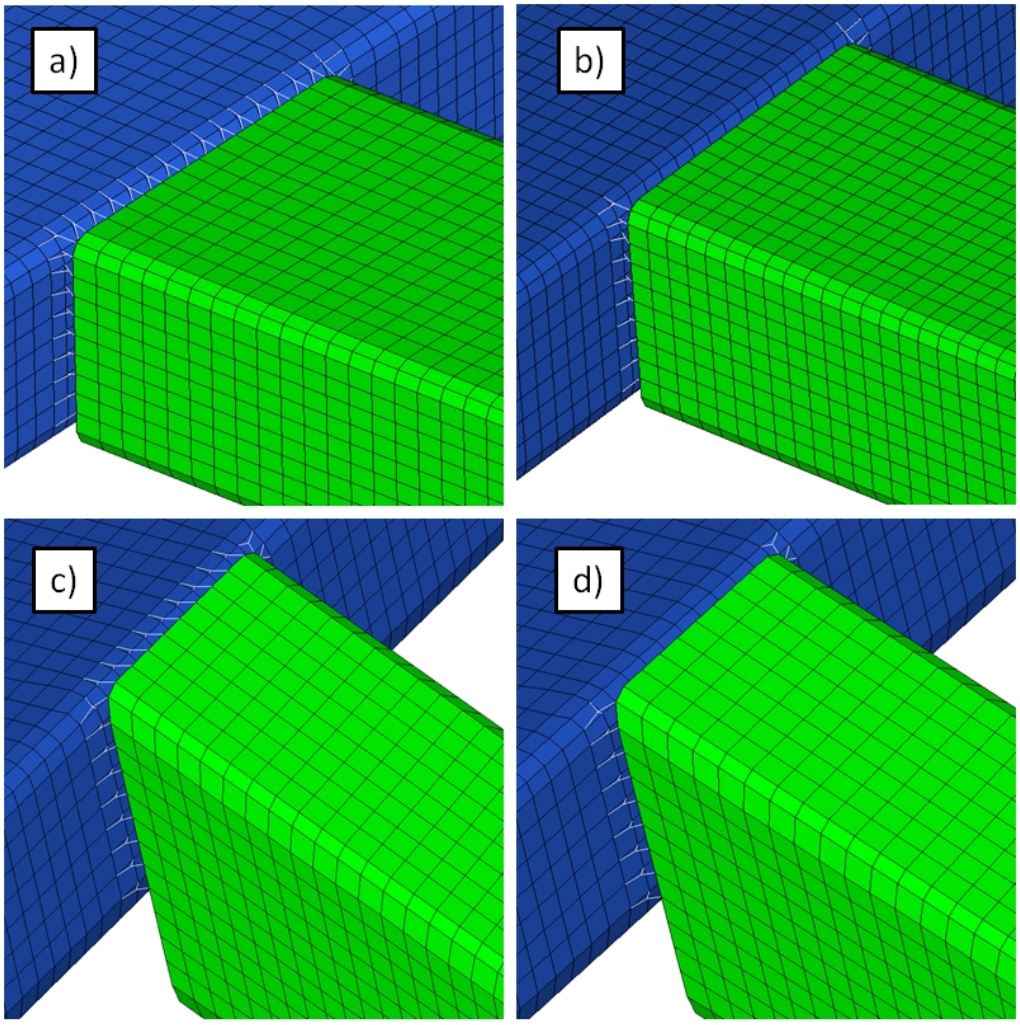


Figure 5.15 : Weld connection modeling with rigid elements (RBODY): (a)Breast knot (full welding). (b)Breast knot (half welding). (c)Roof edge knot (full welding). (d)Roof edge knot (half welding).

All contacts in simulations were defined as sliding contact with Interface Type 7. Interface Type 7 is a general purpose interface and can simulate all types of impact between a set of nodes and a master surface, especially buckling during a high speed crash. The search for the closest segment is done via a direct search algorithm; therefore, there are no search limitations and all possible contacts are found. The energy jumps induced by a node impacting from the shell edges are removed by the use of a cylindrical gap around the edges. The main advantage of interface type 7 is that the stiffness is not constant and increases with the penetration preventing the node from going through the shell mid-surface. This solves many bad contact treatments. Cloumb friction law was used as a friction formulation. This formulation provides accurate results in crash analysis. The friction coefficient between all parts was set to 0.2.

5.6.5 Results

The computational mathematical models of knots are provided comparable results to experimental tests measurements and can thus be used for computational evaluation of all type buses in order to avoid numerous expensive full scale crash tests. Test and simulation results are compared with deformation characteristics, load – displacement curves and relative errors with respect to maximum loads. Relative error;

$$Relative\ Error\ = \frac{|Test\ Load - Simulation\ Load|}{Test\ Load} \quad \textbf{(5.1)}$$

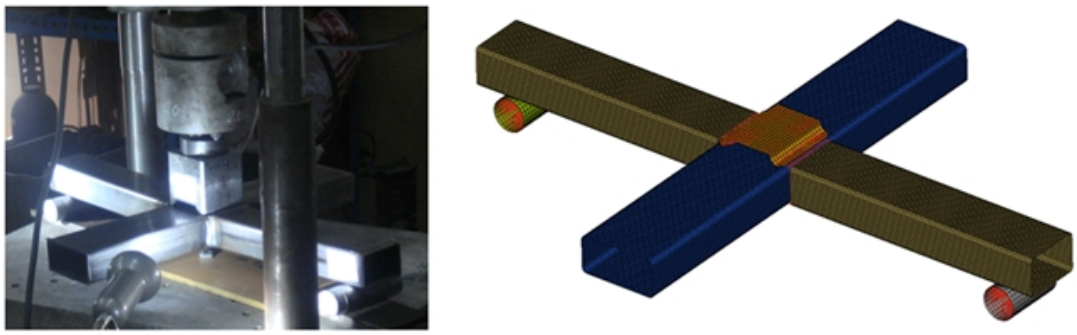


Figure 5.16 : Similarity between test setup and finite element model of breast knot.

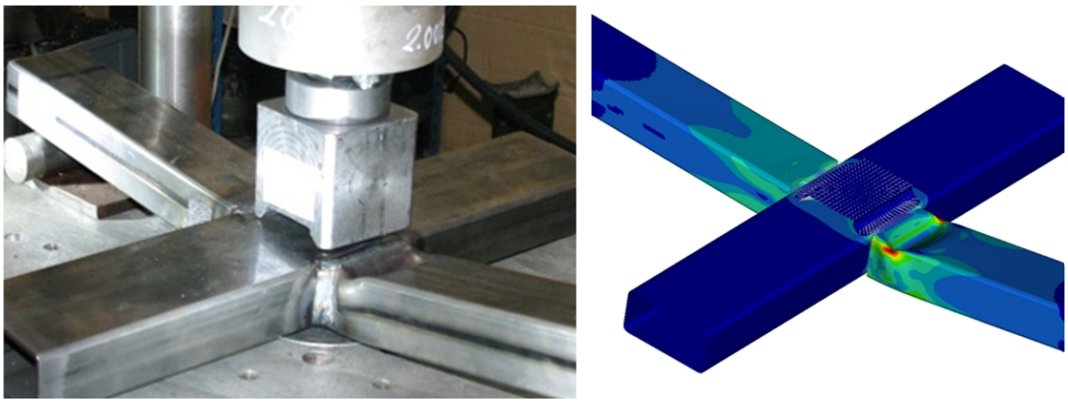


Figure 5.17 : Similarity between test result and finite element analysis result visuals of breast knot.

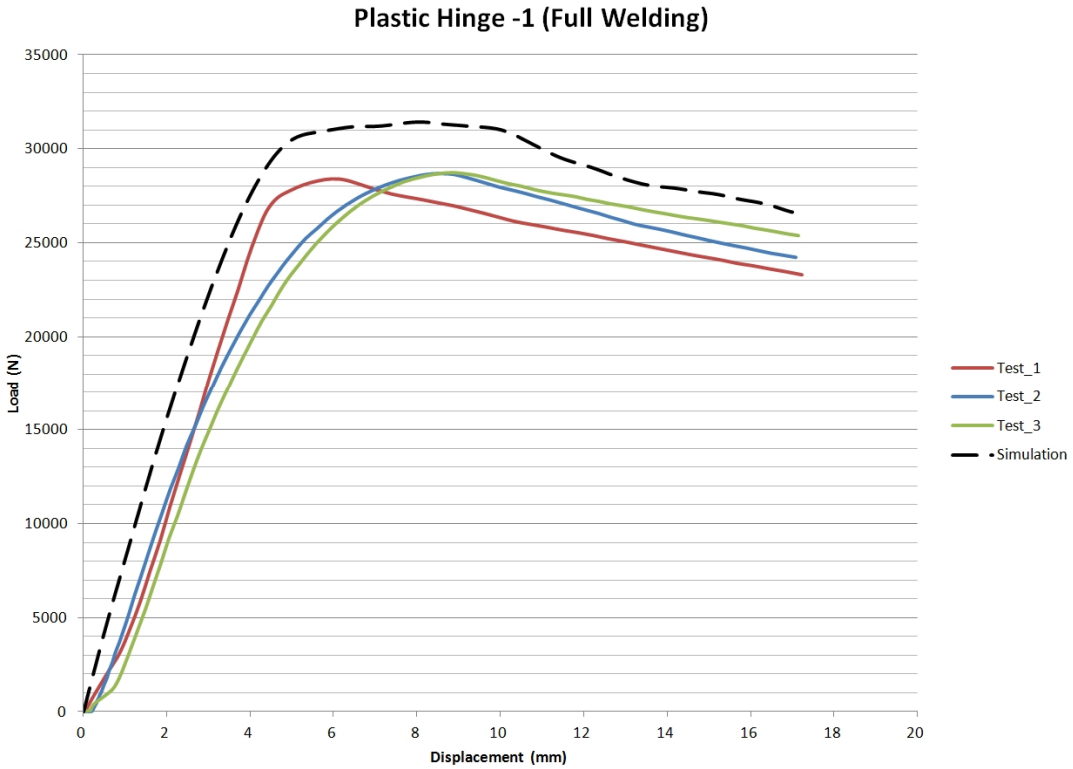


Figure 5.18 : Load – displacement curves of breast knot's test and finite element simulation results (full welding).

Table 5.1 : Relative error between breast knot's tests and finite element simulation results with respect to maximum loads (full welding).

	Load (Max.)	Relative Error (Max.)
Simulation	31429.41 N	-
Test_1	28377.52 N	10.75 %
Test_2	28683.37 N	9.57 %
Test_3	28726.88 N	9.41 %

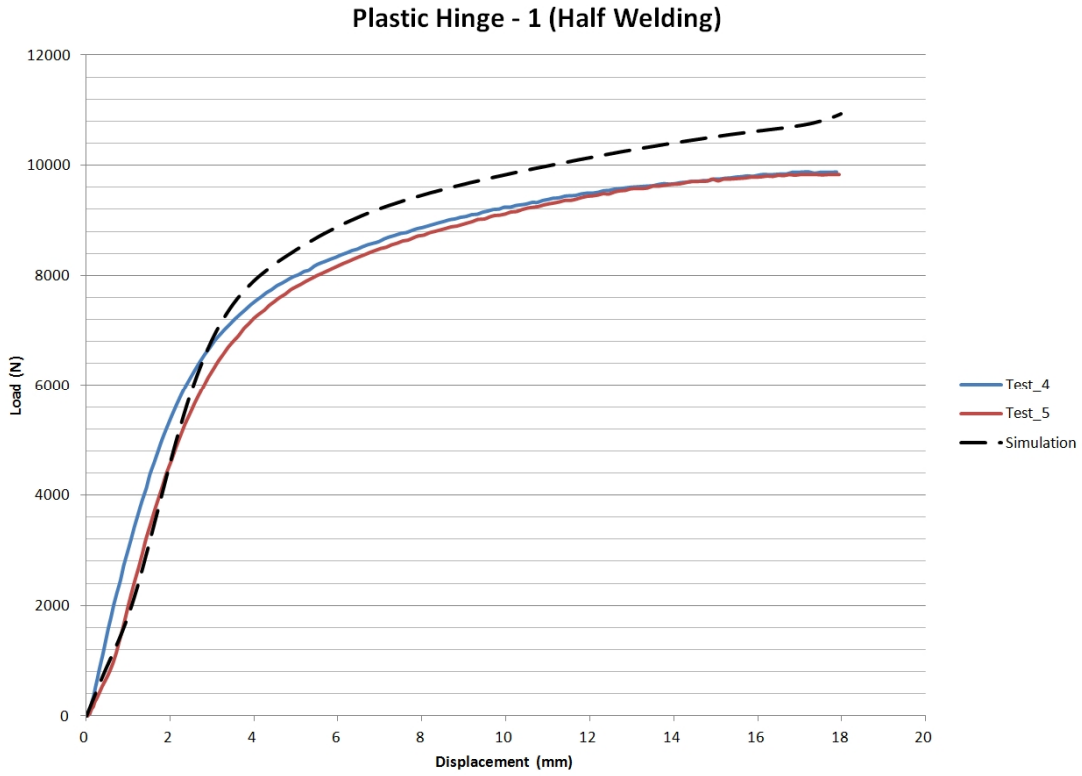


Figure 5.19 : Load – displacement curves of breast knot's test and finite element simulation results (half welding).

Table 5.2 : Relative error between breast knot's tests and finite element simulation results with respect to maximum loads (half welding).

	Load (Max.)	Relative Error (Max.)
Simulation	10928.76 N	-
Test_4	9872.78 N	10.70 %
Test_5	9822.46 N	11.26 %

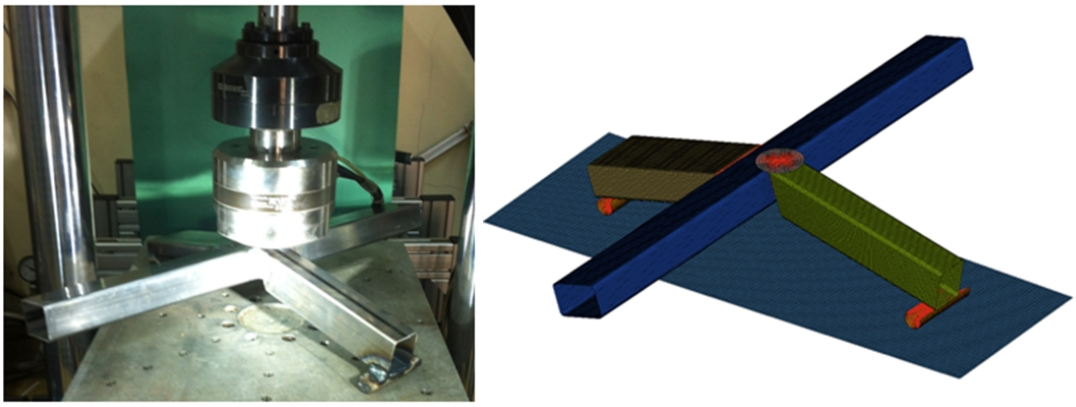


Figure 5.20 : Similarity between test setup and finite element model of roof edge knot.

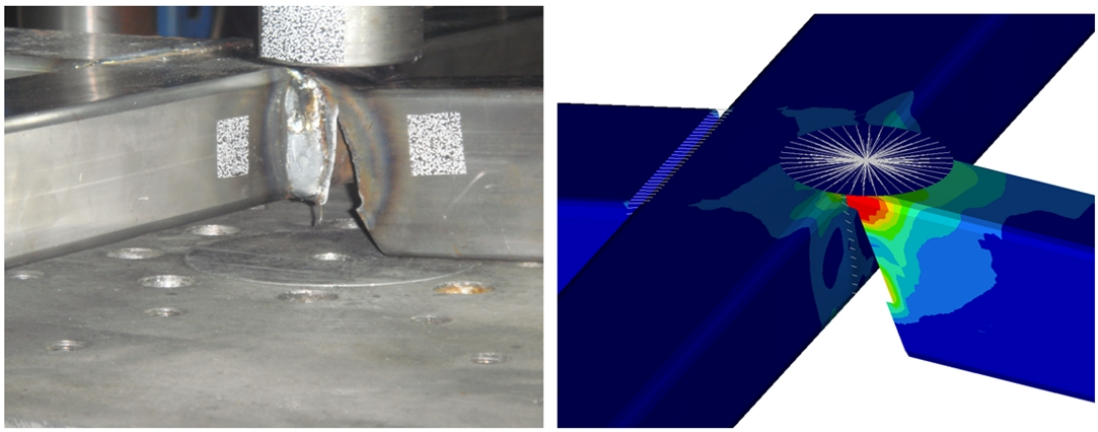


Figure 5.21 : Similarity between test result and finite element analysis result visuals of roof edge knot.

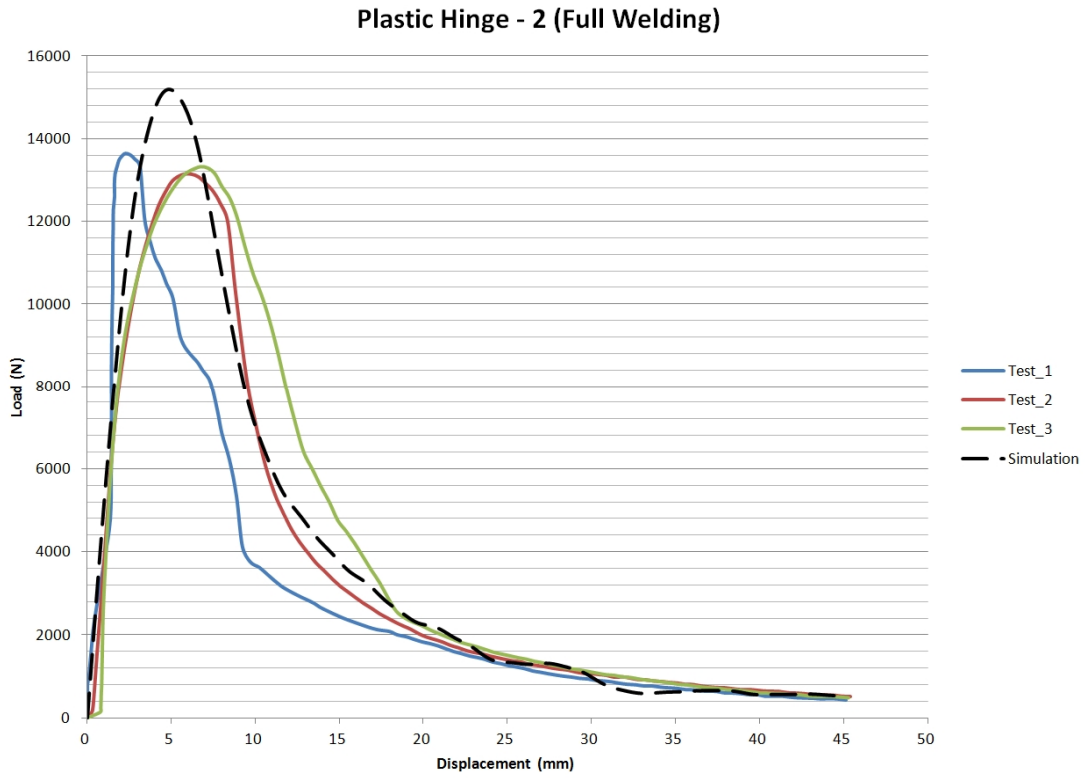


Figure 5.22 : Load – displacement curves of roof edge knot's test and finite element simulation results (full welding).

Table 5.3 : Relative error between roof edge knot's tests and finite element simulation results with respect to maximum loads (full welding).

	Load (Max.)	Relative Error (Max.)
Simulation	15199.16 N	-
Test_1	13638.96 N	10.27 %
Test_2	13151.10 N	13.47 %
Test_3	13334.06 N	13.99 %

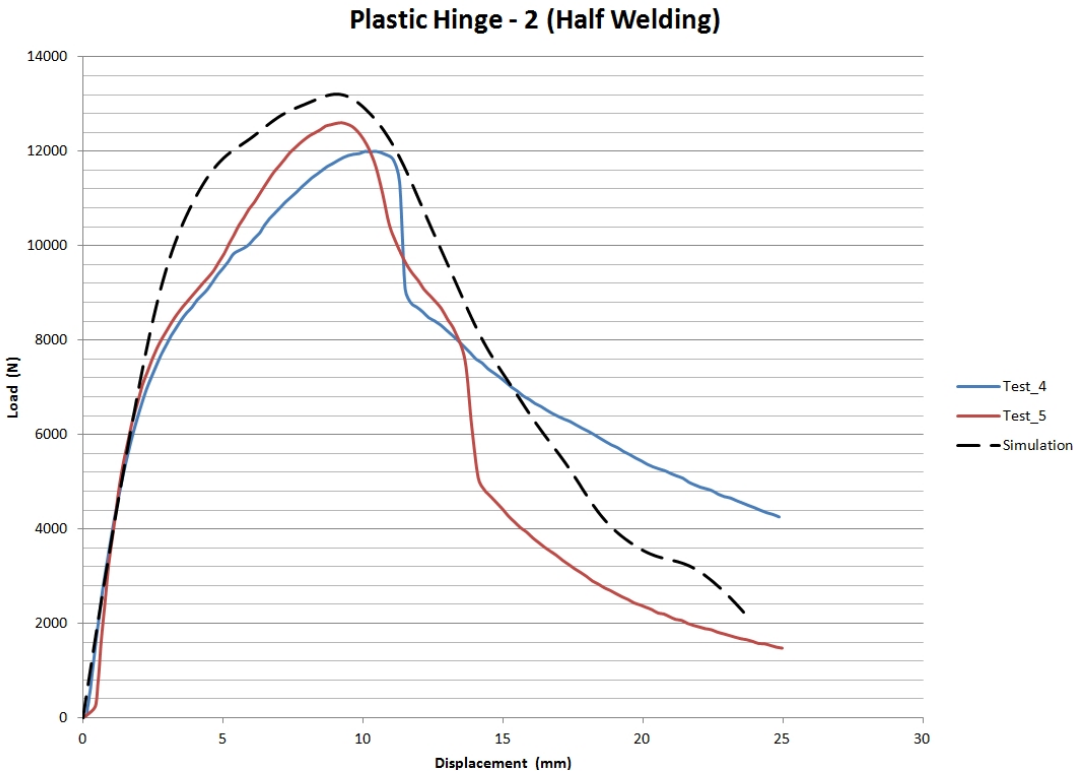


Figure 5.23 : Load – displacement curves of roof edge knot's test and finite element simulation results (half welding).

Table 5.4 : Relative between roof edge knot's tests and finite element simulation results with respect to maximum loads (half welding).

	Load (Max.)	Relative Error (Max.)
Simulation	13216.78 N	-
Test_4	12001.23 N	10.13 %
Test_5	12596.55 N	4.92 %

5.6.6 Convergence between test and simulation results

5.6.6.1 Mesh convergence

Mesh convergence refers to the smallness of the elements required in a model to ensure that the results of an analysis are minor affected by changing the size of the mesh.

Whenever, the finite element method is used, it is important that the accuracy of solution is dependent on mesh size. As mesh size decreases towards zero (leading to a model of infinite size), simulation moves toward the exact solution for the equations. However, since finite computational resources and time are limited, simulation relies on an approximation of the real solution.

The goal of simulation, therefore, is to minimize the difference (error) between the exact and the approximated solution, and to ensure that the error is below some accepted tolerance level that will vary from case to case based on geometry and analysis goals. The aim of this study is to identify the influence of different mesh sizes on the mesh convergence behavior.

5.6.6.2 Solution accuracy

A better mesh quality guarantees a more accurate solution. For improving the mesh quality for accurate solution, one may need to refine the mesh at certain areas of the geometry where the gradients of the field whose solution is sought. Moreover, this means that, if a mesh is not sufficiently refined, the accuracy of the solution is more limited. Thus, the required accuracy in turn dictates the mesh quality.

Element convergence studies can determine the mesh refinement requirements necessary to achieve accurate results for a variety of different element sizes in regions of high plastic strain. These convergence studies can also evaluate the quality of a finite element model and the apparent accuracy of its results. Of all the considerations that go into constructing an accurate finite element model, the choice of element type and level of refinement of the element mesh are the most fundamental.

5.6.6.3 CPU time requirement

CPU time is a necessary yet an undesirable factor. For a highly refined mesh, where the number of cells per unit area is maximum, the CPU time required will be relatively large. In general, if the CPU time taken is more it indicates that the solution that is being generated will be of good accuracy. However, for the solution of given accuracy and rate of convergence, greater CPU time required indicates an inferior mesh quality.

Finer meshes come with a cost however: more computational time and large memory requirements. It is desired to find the minimum number of elements that give you a converged solution.

In general however, it is necessary to conduct convergence tests on your finite element model to confirm that a fine enough element discretization has been used. In a solid mechanics problem, this would be done by creating several models with different mesh sizes and comparing the resulting deflections.

5.6.6.4 Convergence study

In this study, the results of a convergence study for an impulsively loaded knots constructed of RADIOSS thin shell elements using both reduced and full integration. Four loading levels are considered; the first maintains strains within the elastic range, the second induces moderate plastic strains, the third produces large deformations and large plastic strains, and fourth generates cracks and material failures.

In a test problem with a accurate result, it is straightforward to assess convergence of a FEA. With a first coarse mesh and a second refined mesh, direct comparison with the test result for the displacement of interest reveals whether the error is reducing with mesh refinement; that is, whether the FEA is converging. Then comparison of the result for this displacement from the refined mesh reveals whether the error is sufficiently low; that is, whether the FEA has converged.

In an application, however, the true answer for the stress of interest is sought, but, of course, not known a priori. Under these circumstances, checking for converging requires at least two successively-refined meshes for a total of three meshes: a coarse (C), a medium (M), and a fine (F). Furthermore, the medium and fine meshes should

not be the outcome of minor refinements if a reasonably stern test of converging is to result. To avoid this shortcoming, at the outset it systematically refined meshes throughout by scaling element lengths. For each successive level of mesh refinement in the convergence study, all shell elements in the model is split in all directions.

Three cases of mesh size were used in the study to provide information about the mesh convergence results:

- Coarse mesh : Element size of 16 mm
- Medium mesh : Element size of 8 mm
- Fine mesh : Element size of 4 mm

Figures below show the obtained load-displacement curves from the experiments and the simulations for all models. The coarse mesh models are not able to capture local buckling of the tube and thus the post-buckling range of the load-displacement curve was substantially divergent from experimental curve. The medium mesh models showed close shape in the pre-buckling range. However, in the post-buckling range it showed much of the stiffness. In the post-buckling range, the fine mesh models obtained the closest shape with experimental results.

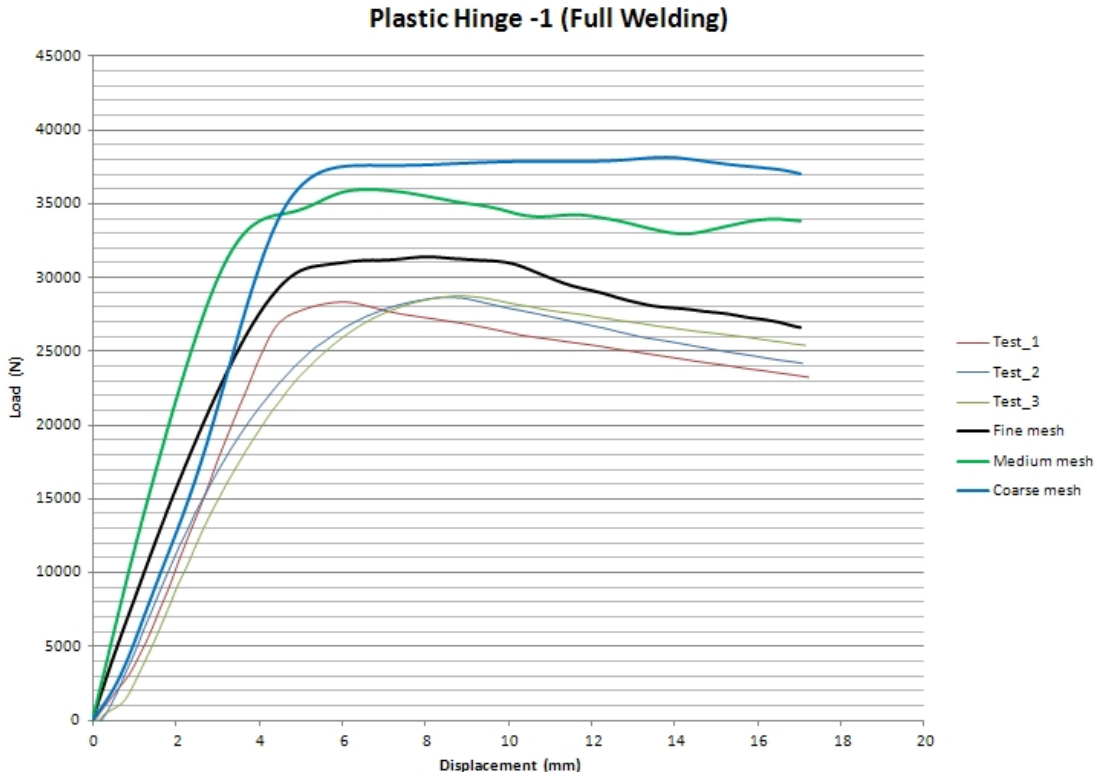


Figure 5.24 : Mesh convergence study according to load – displacement curves of breast knot's test and finite element simulation results (full welding).

Table 5.5 : Relative error between breast knot's test and mesh convergence results with respect to maximum loads (full welding).

	Number of Shell Elements	Load (Max.)	Relative Error (Max.)
Fine mesh	13360	31429.41 N	9.41 %
Medium mesh	3366	35930.72 N	25.08 %
Coarse mesh	880	38192.38 N	32.95 %
Experiment	-	28726.88 N	-

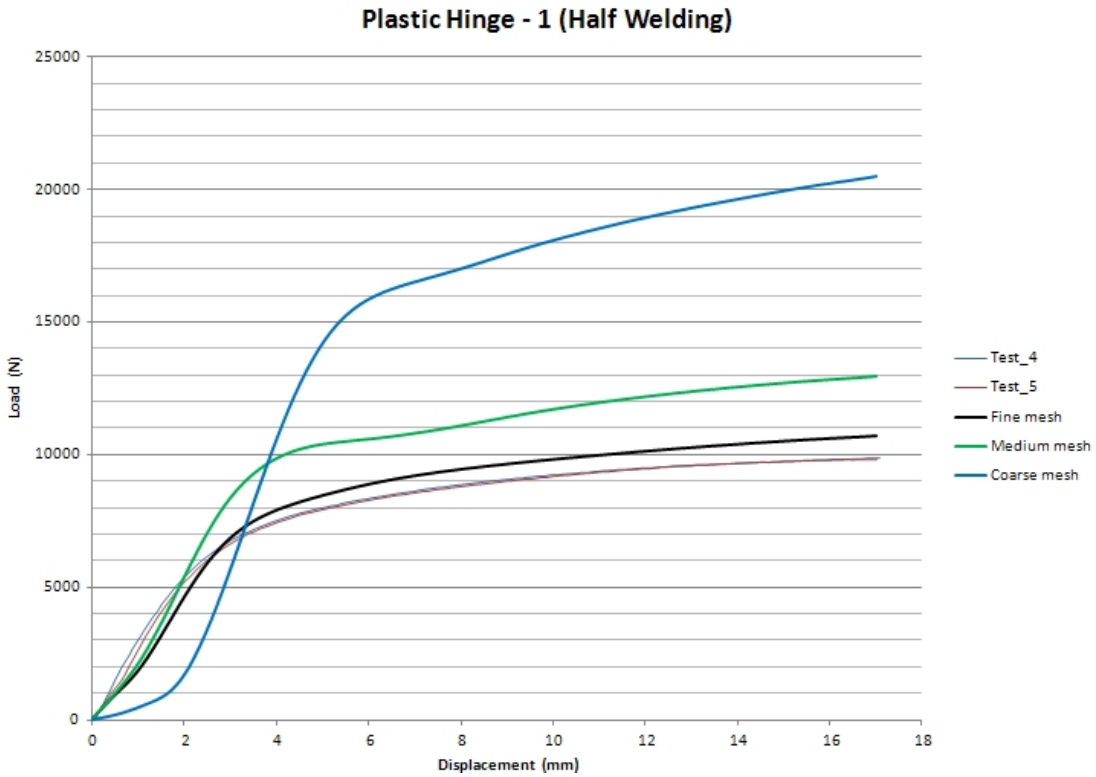


Figure 5.25 : Mesh convergence study according to load – displacement curves of breast knot's test and finite element simulation results (half welding).

Table 5.6 : Relative error between breast knot's test and mesh convergence results with respect to maximum loads (half welding).

	Number of Shell Elements	Load (Max.)	Relative Error (Max.)
Fine mesh	13360	10928.76 N	10.70 %
Medium mesh	3366	13624.68 N	38.00 %
Coarse mesh	880	21749.78 N	120.30 %
Experiment	-	9872.78 N	-

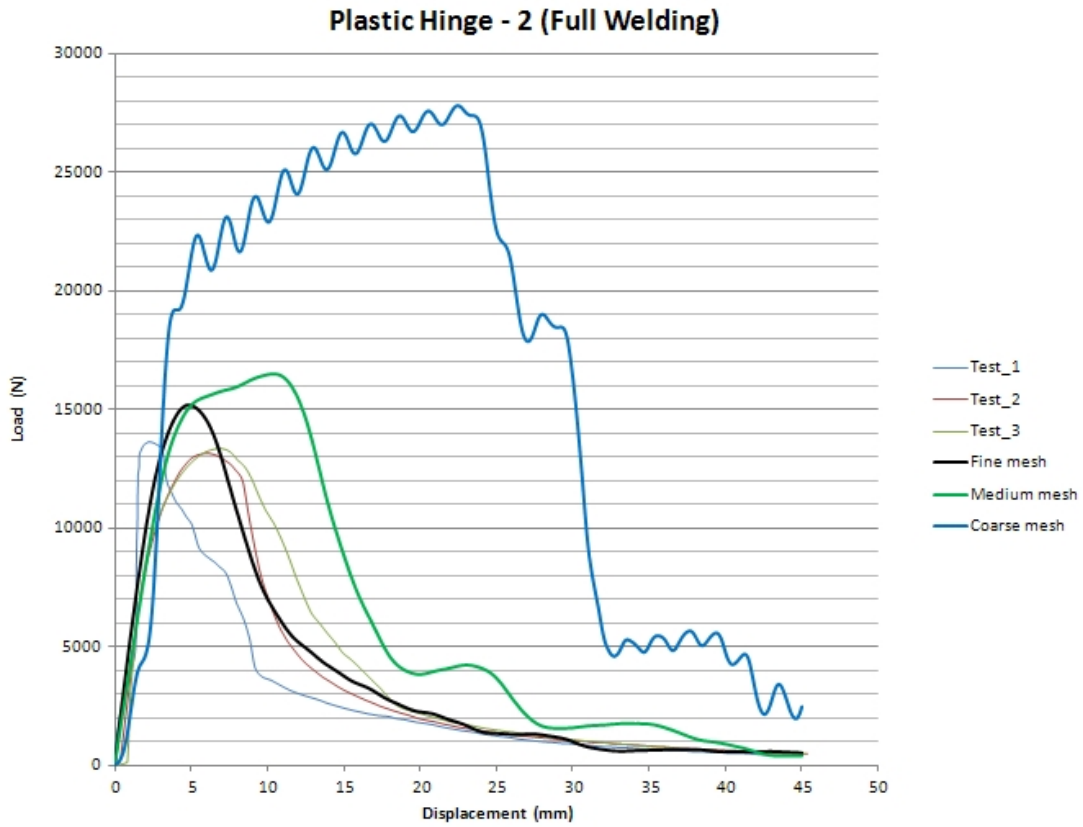


Figure 5.26 : Mesh convergence study according to load – displacement curves of roof edge knot's test and finite element simulation results (full welding).

Table 5.7 : Relative error between roof edge knot's tests and mesh convergence results with respect to maximum loads (full welding).

	Number of Shell Elements	Load (Max.)	Relative Error (Max.)
Fine mesh	12127	15199.16 N	11.44 %
Medium mesh	2970	16525.26 N	21.16 %
Coarse mesh	890	27774.78 N	92.20 %
Experiment	-	13638.96 N	-

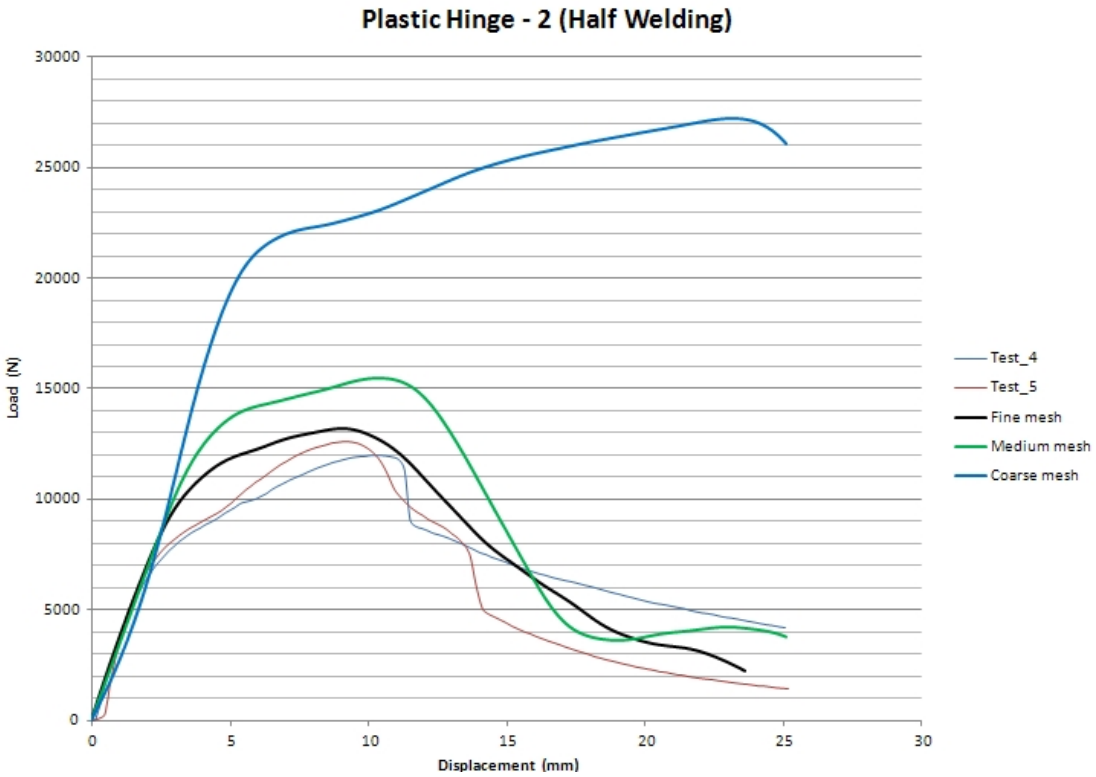


Figure 5.27 : Mesh convergence study according to load – displacement curves of roof edge knot's test and finite element simulation results (half welding).

Table 5.8 : Relative between roof edge knot's tests and mesh convergence results with respect to maximum loads (half welding).

	Number of Shell Elements	Load (Max.)	Relative Error (Max.)
Fine mesh	12127	13216.78 N	4.92%
Medium mesh	2970	15474.09 N	22.84%
Coarse mesh	890	27237.44 N	116.23%
Experiment	-	12596.55 N	-

The breast knots in the experiments and the simulations buckled locally what lead to extensive deformations in the result. The roof edge knots in the experiments and the simulations did not buckled locally, showed crack propagation and material failure in the results.

Figure 5.28 shows a comparison of deformations in the real sample and FE models. The coarse mesh model is not able to capture the local deformation under the support and only global deformations of the tube. The medium mesh model captured the local buckling effect but still the number of elements was not enough to obtain a smooth deformation pattern. The fine mesh model is sufficiently refined to fully replicate the deformation shape of the tube.

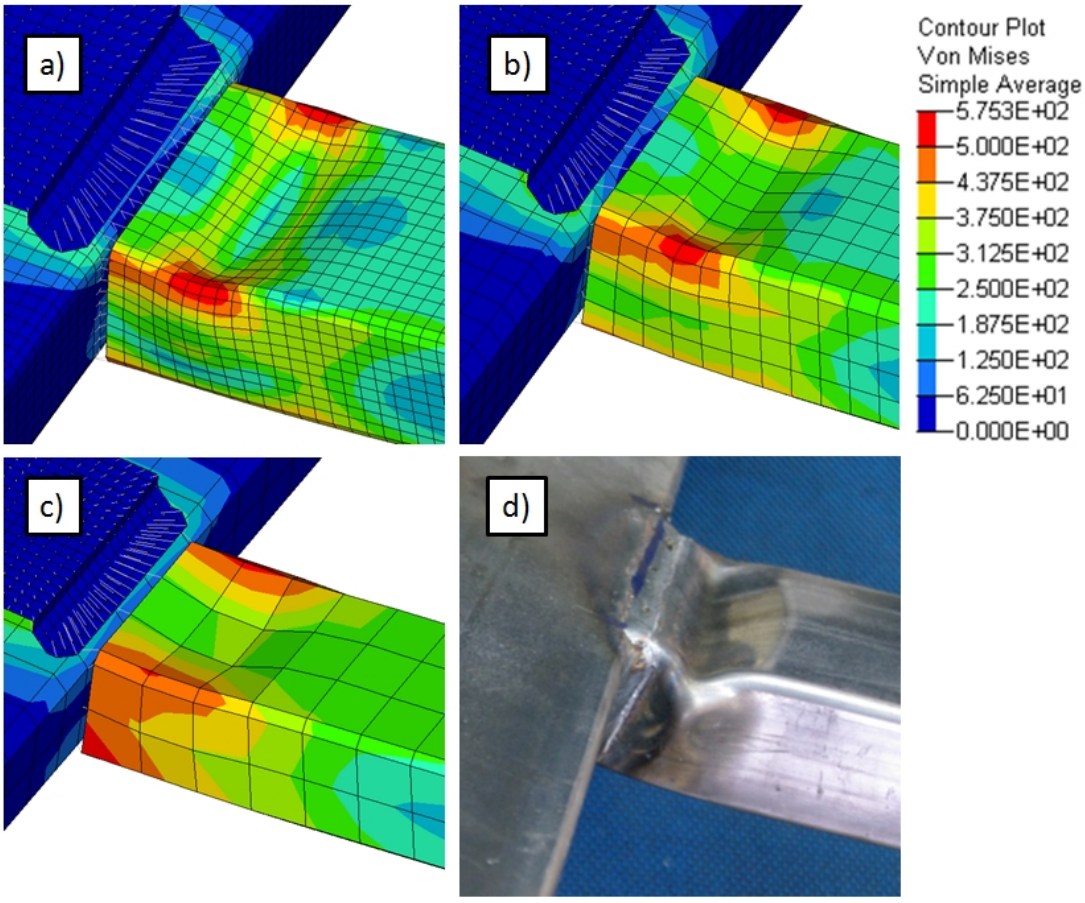


Figure 5.28 : Local buckling deformation of breast knot in the FE models: (a)Fine mesh. (b)Medium mesh. (c)Coarse mesh. (d)Experiment.

The idea of using only local mesh refinement for a convergence study can be extended. If a model is required to produce accurate stresses only at certain regions of interest, the role of all elements away from these regions is one of only

representing geometry and transmitting load. This demands a much lower level of mesh refinement than for accurate stress prediction. Thus, these elements can be considerably larger, subject to the constraints of permitting both reasonable quality transitions and geometry representation.

Using larger elements away from regions of interest in a model is common practice but a more subtle point is, providing they don't misrepresent the geometry and suitable mesh transitions can be carried out; these elements can be considerably larger than those in regions of interest, without loss of accuracy.

Due to limitations in computer power, only high deformed regions of the bus are modeled with fine mesh. Low deformed regions of the bus are modeled with medium sized mesh. The medium sized mesh was assumed a good tradeoff between accuracy and computational cost for the rollover simulation of the bus.

The issue of mesh size is important in all analyses; there are other issues that affect the selection of an appropriate element size in more advanced analyses. The practically important issue of the implementation of numerical schemes and, in particular, the plasticity algorithms that are employed in such schemes. The plasticity algorithms considered here are of predictor-corrector type. The plasticity algorithms of interest are all of predictor-corrector type. Investigations of convergence have been carried out in the figures below. The aim of this study was to identify the influence of different parameters on the plasticity behavior. The mentioned plasticity and nonlinearity algorithms:

- 4 node shell element integration (QEPH)
- 3 node shell element integration (DTK18)
- Geometric nonlinearities
- Strain calculation
- Thickness change
- Shell plane stress plasticity

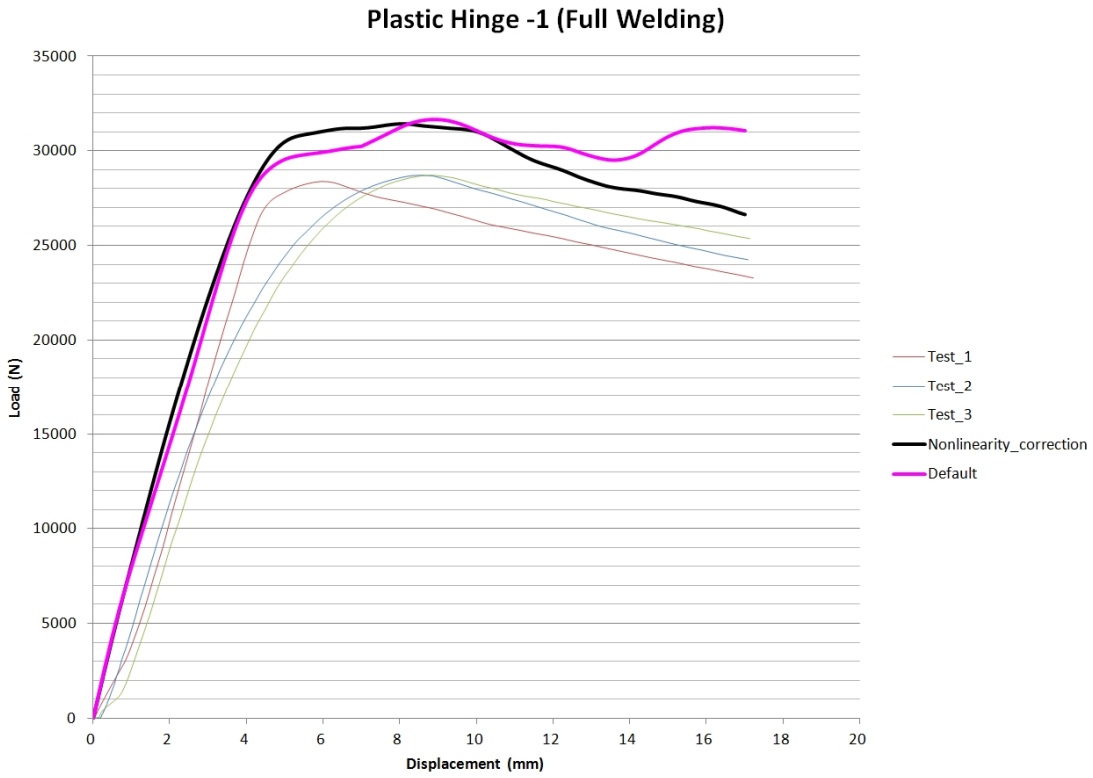


Figure 5.29 : Nonlinearity convergence study according to load – displacement curves of breast knot's test and finite element simulation results (full welding).

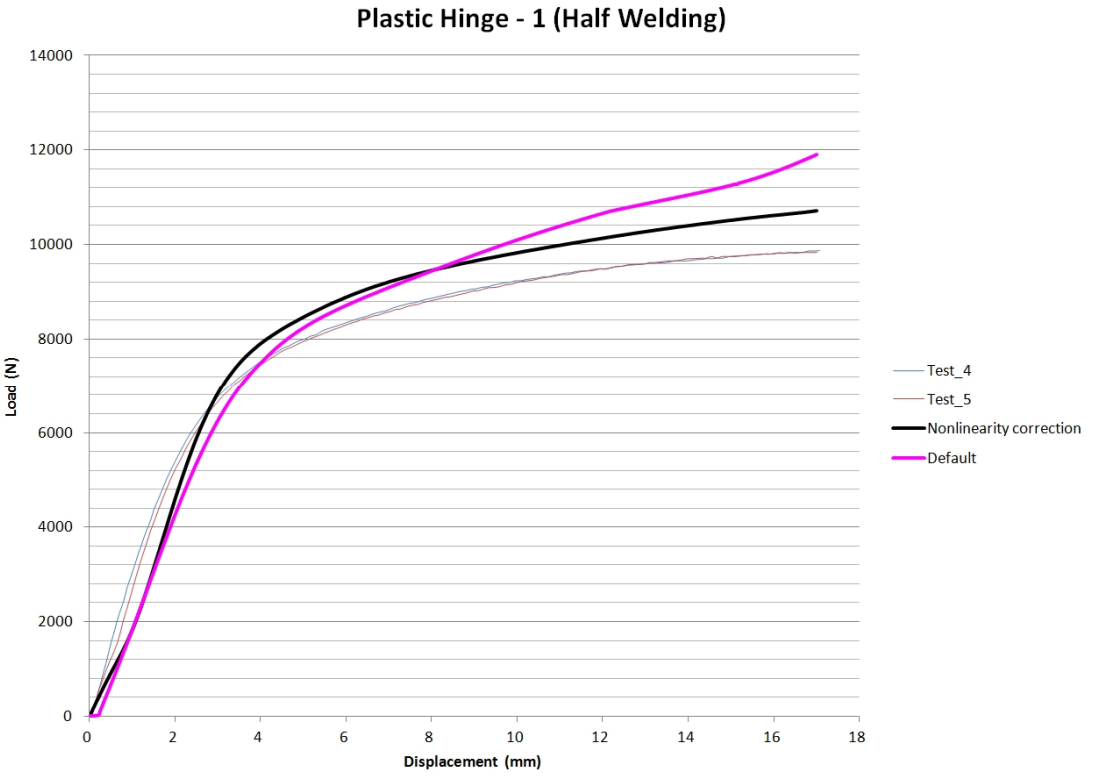


Figure 5.30 : Nonlinearity convergence study according to load – displacement curves of breast knot's test and finite element simulation results (half welding).

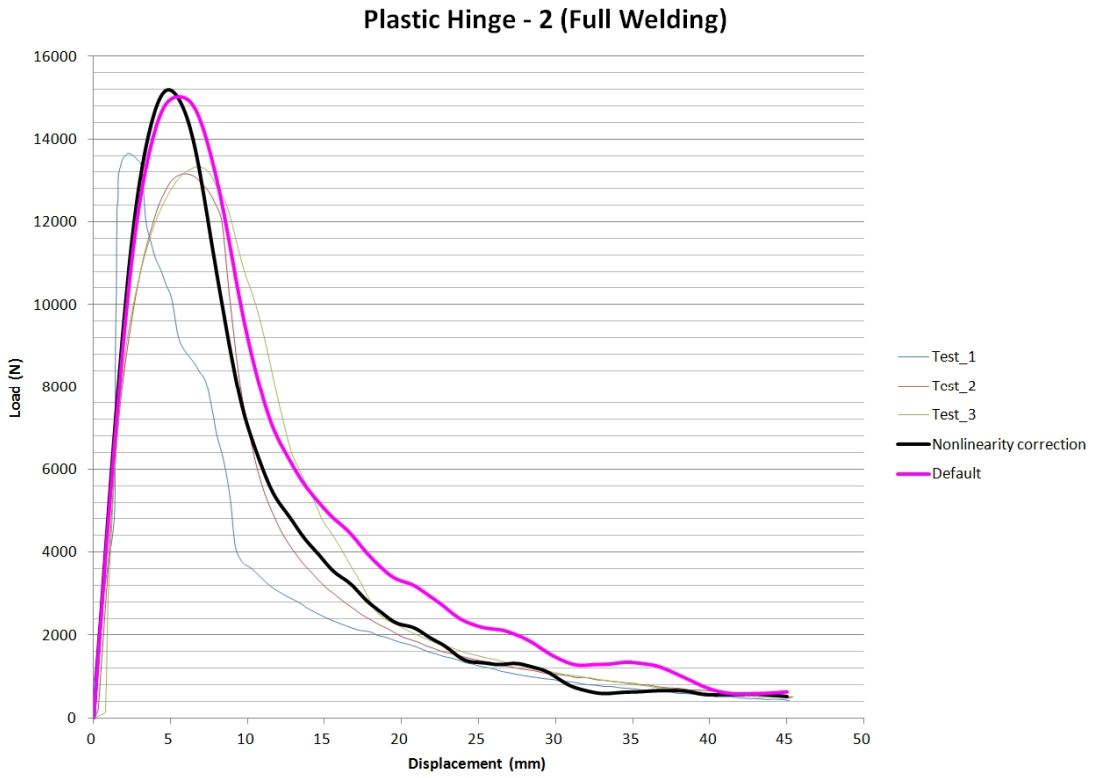


Figure 5.31 : Nonlinearity convergence study according to load – displacement curves of roof edge knot's test and finite element simulation results (full welding).

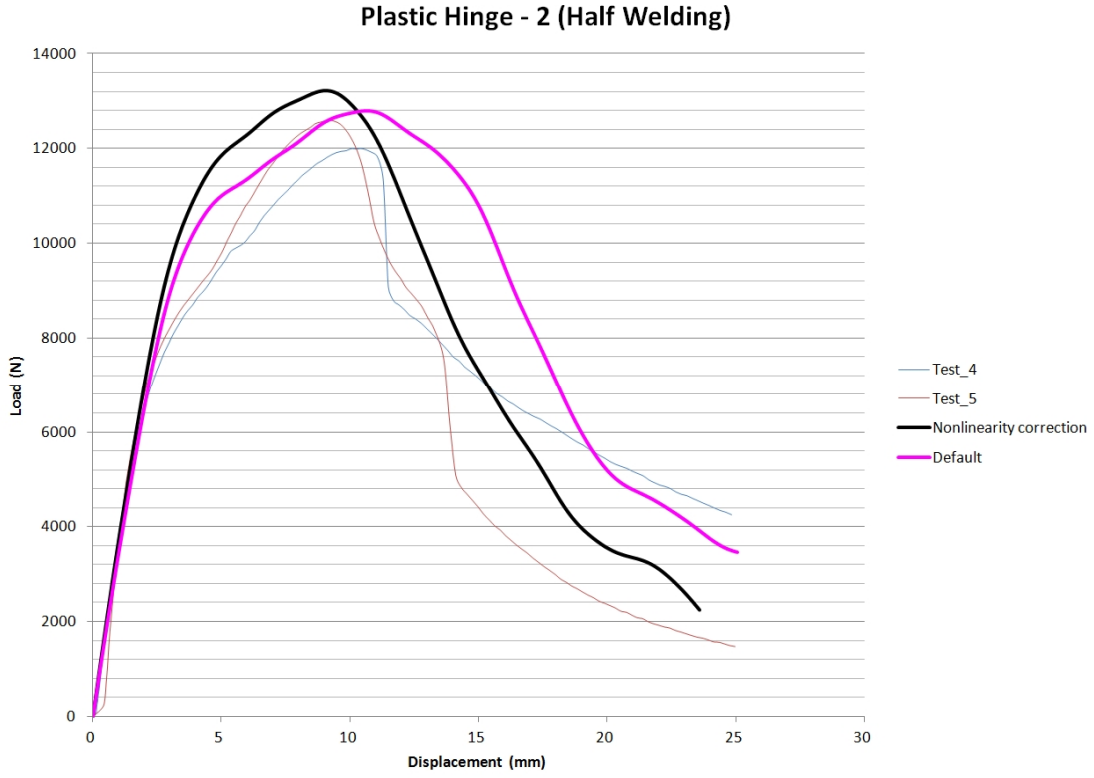


Figure 5.32 : Nonlinearity convergence study according to load – displacement curves of roof edge knot's test and finite element simulation results (half welding).

Results show that plasticity and geometric nonlinearity algorithms provide the most accurate results and the more the mesh is fine, the more accurate the results will be. To pass this test, a good curvature representation of element formulation is needed; the default formulation does not satisfy this condition.

The same plasticity and geometric nonlinearity algorithms in the full body rollover analysis are used for the all validation analyses. The plasticity and geometric nonlinearity algorithms will be discussed with details in next chapter. However, summary of the plasticity and geometric nonlinearity algorithms in validation analysis are mentioned below as simplified.

5.6.7 Conclusion

Load - displacement curves both for the experiments and the simulations were compared and it was seen that there are similar characterized curves and consistent correlation between the experiments and the simulations results. Relative error between the experiments and the simulations is in round numbers 10%, maximum 13.99% with respect to maximum loads. Similarity between test result and finite element analysis result visuals of knots are presented at Figure 5.17 and 5.21.

Using CAE tools like RADIOSS reduces number of physical tests and thereby saving cost and lots of time. This also enhances multiple choices of design variation and verification. Having got consistent correlation in component and vehicle level, confidence levels are increased to optimize the product design and this will even help in avoiding physical tests.

Based on that validation study, factor of correlation should be taken minimum 1.15 or more than that value in the computational simulation’s results evaluation. Final design could be confidently implemented with taking into consideration factor of correlation.

6. NUMERICAL MODEL FOR COACH ROLLOVER ANALYSIS

6.1 Actual Structure of the Vehicle

The coach chosen for the analysis in this thesis has an all-metal monocoque body. The engine and gearbox are situated in the rear and the luggage area is under the passenger area middle of the front and the rear axle. The chassis side members stop in front of the boot, but two square sections are extended further back to support a part of the engine load. The door is in the front of the near side wall, while the second door is between the axles near the rear axle. Windows are mounted on rubber seal mounts onto the framework.

The body framework is composed of carbon steel rectangular and square section tubes. The rings are assembled of four continuous beams: two pillars, roof and floor members. No significant section weakening or stress concentration was apparent in rings, apart from some possible effects due to welding. The main structural rings start at the rear door pillar and the structure in the very front is less substantial employing primarily open section beams. The pillars of the front two rings are connected to the continuous floor members via adjacent. Additional floor members and stump pillars are arranged between the rings. The waistrail and two more longitudinal rails run along the side with three diagonals behind the rear axle to strengthen the side of the luggage compartment. The frameworks of the front and rear bulkheads are made of relatively light open section members.

Four longitudinal roof rails and cantrails run along the roof, but they are all interrupted by the roof cross members and welded together. Most joints in the main load carrying structure are continuously welded, and brackets with bolts are used to connect axle members to the floor members.

The roof and sides are clad with aluminum and FRP (fiber-reinforced plastic) skins. Steel sheets are also attached to the inner side structure between the waistrail and the middle rail running above the wheel arches. The aluminum segments are pop riveted

to the roof framework and only to the horizontal beams in the side, while spot welding is employed to fix the interior steel sheets to the side skeleton. Hardboard panels are used to build the luggage compartment.



Figure 6.1 : The coach chosen for rollover simulation (KARSAN STAR).

6.2 Center of Gravity Measurement of the Vehicle

Distribution of mass and center of gravity (CG) location in the FE model influences its behavior during impact simulations. It determines an unstable position of the bus during a rollover test, thus directly influencing the kinetic energy absorbed by the bus body.

The reference and the total energy to be absorbed in the rollover test depend directly on the position of the vehicle's centre of gravity position. Therefore, its determination should be as accurate as practicable. The method of measurement of dimensions, angles and load values, and the accuracy of measurement shall be recorded for assessment by the technical service.

The position of the centre of gravity is defined by three parameters:

- Longitudinal distance (l_1) from the centre line of front axle.
- Transverse distance (t) from the vertical longitudinal central plane of the vehicle.
- Vertical height (h_0) above the flat horizontal ground level when the tires are inflated as specified for the vehicle.

The position of the vehicle's centre of gravity shall be determined in the unladen kerb mass condition or the total effective vehicle mass condition. For the determination of the position of the centre of gravity in the total effective vehicle mass condition, the individual occupant mass (factored by the constant, k = 0.5) shall be positioned and rigidly held 100 mm above and 100 mm forward of the R point of the seat.

Unladen kerb mass (M_k) means the mass of the vehicle in running order, unoccupied and unladen but with the addition of 75 kg for the mass of the driver, the mass of fuel corresponding to 90% of the capacity of the fuel tank specified by the manufacturer, and the masses of coolant, lubricant, tools and spare wheel, if any.

Total occupant mass (M_m) means the combined mass of any passengers, crew who occupy seats fitted with occupant restraints.

Total effective vehicle mass (M_t) means the unladen kerb mass of the vehicle (M_k) combined with the portion (k = 0.5), of the total occupant mass (M_m), considered to be rigidly attached to the vehicle.

The longitudinal (l_1) and transverse (t) coordinates of centre of gravity shall be determined on a common horizontal ground (see Figure 6.2) where each wheel or twinned wheel of the vehicle is standing on an individual load cell. Each steered wheel shall be set to its straight-ahead position. The individual loadcell readings shall be noted simultaneously and shall be used to calculate the total vehicle mass and centre of gravity position.

The longitudinal position of the centre of gravity relative to the centre of the contact point of the front wheels (see Figure 6.2) is given by:

$$l_1 = \frac{(P_3+P_4)L_1+(P_5+P_6)L_2}{(P_{total})} \quad \textbf{(6.1)}$$

where:

P_1 = reaction load on the load cell under the left-hand wheel of the first axle
P_2 = reaction load on the load cell under the right-hand wheel of the first axle
P_3 = reaction load on the load cell under the left-hand wheel(s) of the second axle
P_4 = reaction load on the load cell under the right-hand wheel(s) of the second axle

P_5 = reaction load on the load cell under the left-hand wheel(s) of the third axle

P_6 = reaction load on the load cell under the right-hand wheel(s) of the third axle

P_{total} = (P_1+P_2+P_3+P_4+P_5+P_6) = M_k unladen kerb mass; or,

= Mt total effective vehicle mass, as appropriate

L_1 = the distance from centre of wheel on 1st axle to centre of wheel on second axle

L_2 = the distance from centre of wheel on 1st axle to centre of wheel on third axle, if fitted

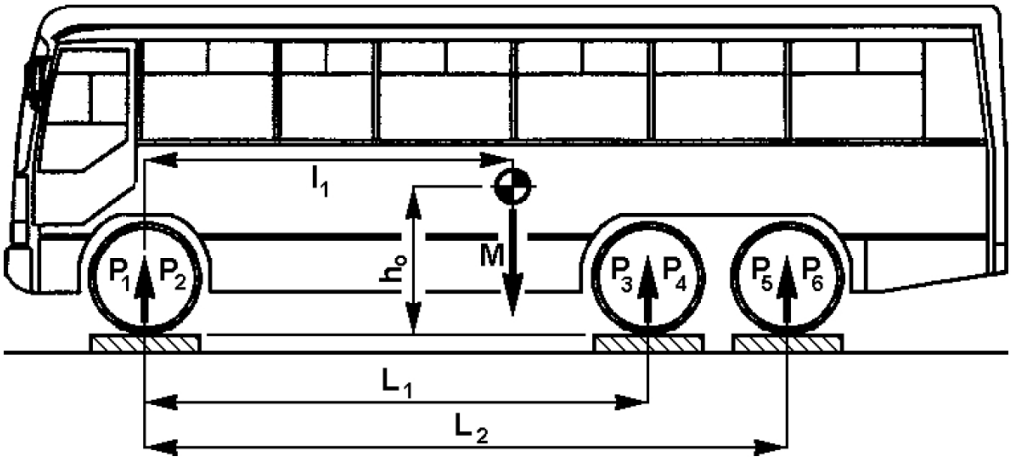


Figure 6.2 : Longitudinal position of the centre of gravity [1].

The transverse position (t) of the vehicle's centre of gravity relative to its longitudinal vertical centre plane (see Figure 6.3) is given by,

$$t = \left((P_1 - P_2)\frac{T_1}{2} + (P_3 - P_4)\frac{T_2}{2} + (P_5 - P_6)\frac{T_3}{2}\right)\frac{1}{P_{total}} \qquad \textbf{(6.2)}$$

where:

T_1 = distance between the centers of the footprint of the wheel(s) at each end of the first axle

T_2 = distance between the centers of the footprint of the wheel(s) at each end of the second axle

T_3 = distance between the centers of the footprint of the wheel(s) at each end of the third axle

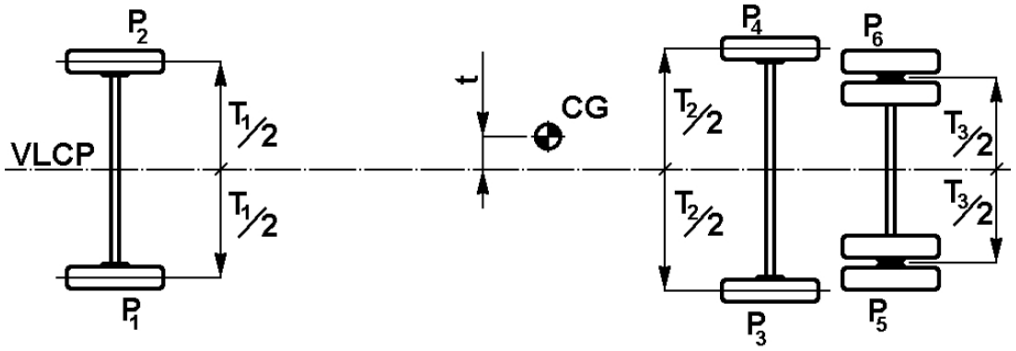


Figure 6.3 : Transverse position of centre of gravity [1].

The height of the centre of gravity (h_0) shall be determined by tilting the vehicle longitudinally and using individual load-cells at the wheels of two axles. Two loadcells shall be positioned on a common horizontal plane, to receive the front wheels. The horizontal plane shall be at sufficient height above the surrounding surfaces that the vehicle can be tilted forward to the required angle without its nose touching that surface.

The inclination of the tilting test shell be determined by the equation (see Figure 6.4):

$$\alpha = \arcsin\left(\frac{H}{L_1}\right) \quad \textbf{(6.3)}$$

where:

H = height difference between the footprints of the wheels of the first and second axles

L_1 = the distance from centre of wheel's first and second axles

The unladen kerb mass of the vehicle shall be checked as follows:

$$F_{total} = F_1 + F_2 + F_3 + F_4 = P_{total} = M_k \quad \textbf{(6.4)}$$

where:

F_1 = reaction load on the load cell under the left hand wheel of the first axle

F_2 = reaction load on the load cell under the right hand wheel of the first axle

F_3 = reaction load on the load cell under the left hand wheel of the second axle

F_4 = reaction load on the load cell under the right hand wheel of the second axle

The height (h_0) of the vehicle centre of gravity is given by:

$$h_0 = r + \left(\frac{1}{tg\ \alpha}\right)\left(l_1 - L_1 \frac{F_3 + F_4}{P_{total}}\right) \quad \textbf{(6.5)}$$

where:

r = height of wheel centre (on first axle) above the load cell top surface

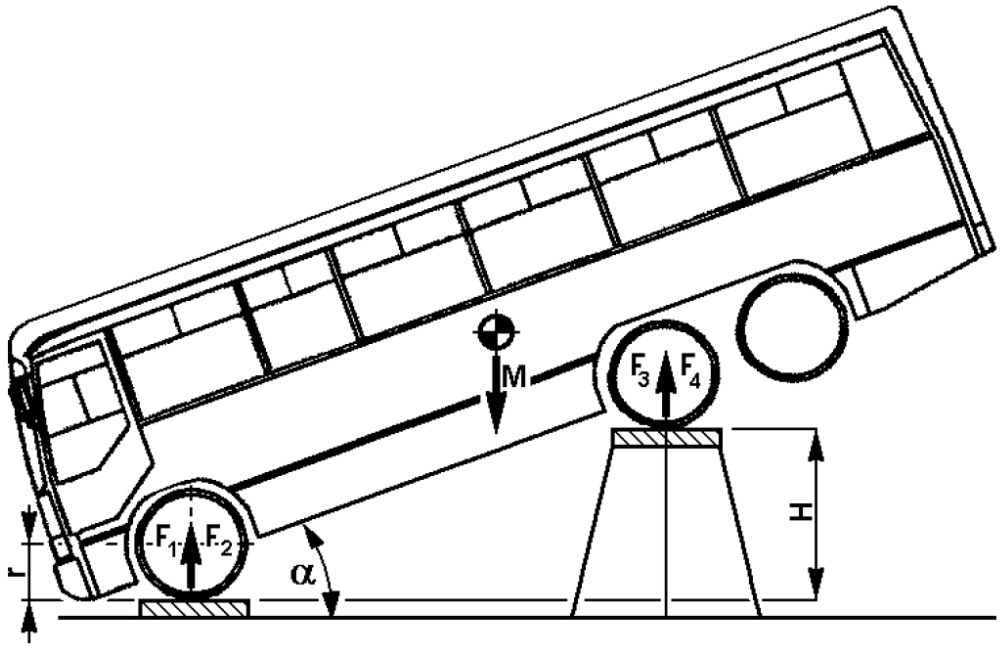


Figure 6.4 : Determination of height of centre of gravity [1].

The center of gravity (CG) of the vehicle was measured in Hexagon Studio using portal crane on the test platform (see Figure 6.5). Table 6.1 provides the information about CG location of the coach at unladen kerb mass.



Figure 6.5 : The center of gravity measurement test of the coach.

Table 6.1 : Location of the CG of the coach at unladen kerb mass.

Specification	Description	Measurement
l_1	Longitudinal distance from the centre line of front axle	2827 mm
t	Transverse distance from the vertical longitudinal central plane of the vehicle	-30 mm
h_0	Vertical height above the flat horizontal ground level when the tires are inflated as specified for the vehicle	1010 mm

6.3 FE Modeling of the Components of the Vehicle

6.3.1 General definition

The finite element model of the vehicle was performed by the specialized pre-processor software HyperMesh and HyperCrash. The vehicle was modeled with the quad QEPH (formulation with physical hourglass stabilization for general use) elements with five integration points through the shell thickness and the model contains triad elements less than 5% of the vehicle model. The QEPH formulation provides a good precision/cost ratio. QEPH elements do not have hourglass energy. QEPH shells will give better results if the mesh is fine enough. QEPH formulation is recommended for isotropic materials because the stabilization forces are computed based on isotropic assumptions. During the simulation, geometric nonlinearities and thickness change at the shell elements was taken into account for membrane strain calculation. Plasticity calculation was proceeded with iterative projection with three Newton iterations. Weld connections in the finite element model of knots are modeled with rigid elements (RBODY).

All structural members of the skeleton and some of metallic panels have been modeled. Floor, windows and all moving parts of the body (doors, skylights, covers, etc.) have been modeled with RBE3 elements. Properties of the floor to side connection may vary a lot on the collapse mode in actual accidents was not always evident. Windows may increase significantly the strength of the roof, particularly in the fore and aft and vertical direction. However, their effect on lateral strength is less pronounced, and, what is more important, their contribution is very unreliable because most of them break during the accident. The effect of the moving parts is

also either negligible or very unreliable. The prime interest of the analysis is to consider the effects on the structural behavior.

All joints between shell elements are assumed as rigid. This is a reasonable assumption for the welded joints between rectangular tubes. Satisfaction of the joint strength requirements brings them very close to the theoretical assumption. Brackets to chassis or powertrain members bolted joints can also provide reasonable rigidity.

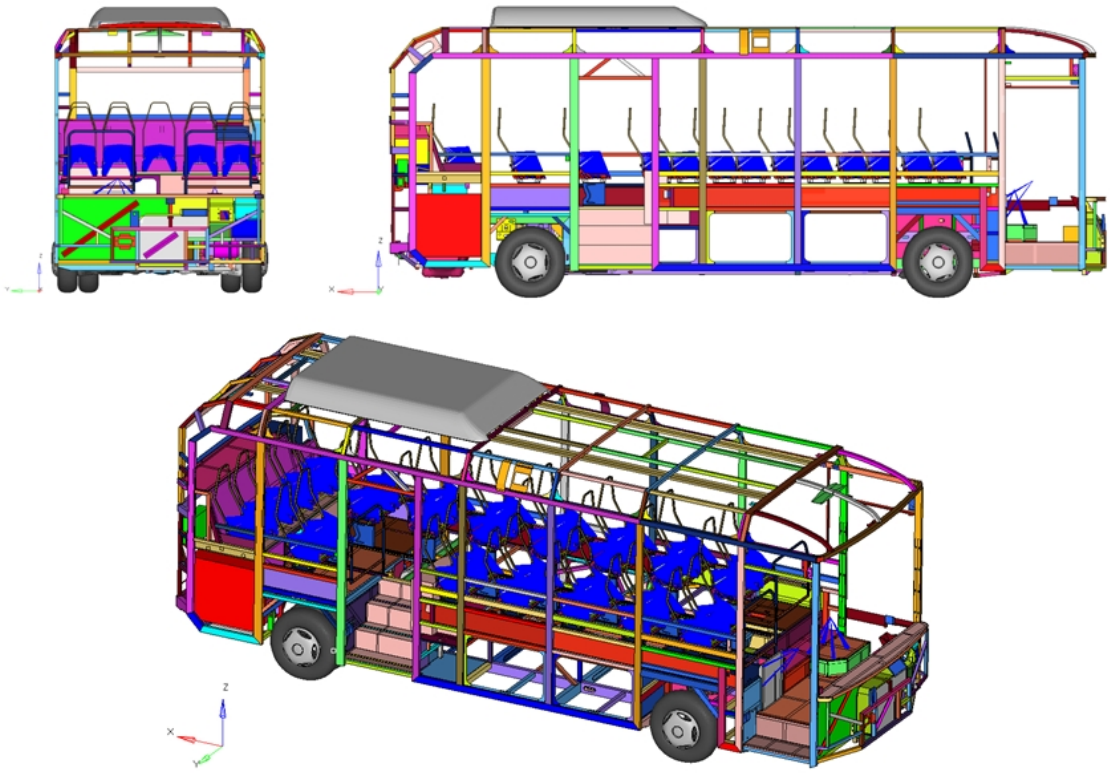


Figure 6.6 : Finite element model of the vehicle.

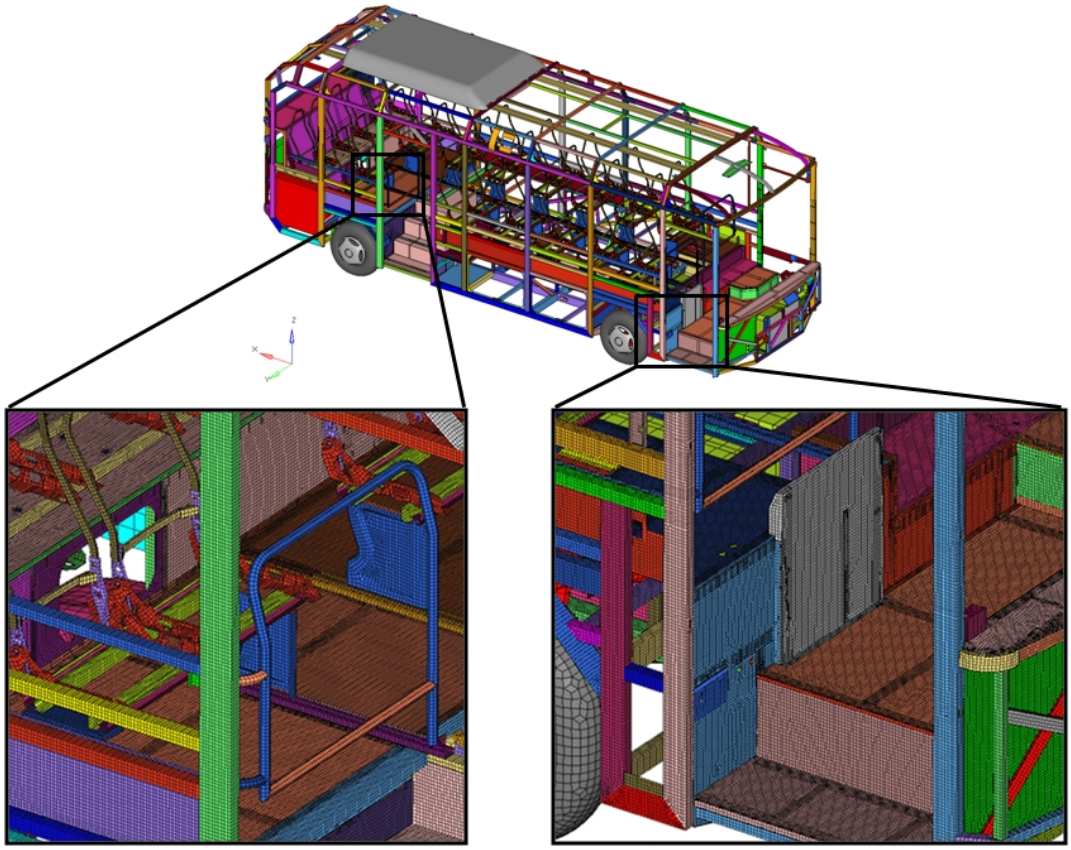


Figure 6.7 : Mesh details of the finite element model.

It is important to not only to have compliance of the total mass in the FE model with the real bus but also to have good correlation of overall moments of inertia. For that reason majority of bus interior elements should be reflected in the FE model as well. Figure 6.8 shows relevant nonstructural parts of the interior included in the FE model of the bus.

Non-structural components of the finite element model for mass and inertia compliance:

- Engine
- Gearbox
- Angle Drive
- Radiator
- Expansion Tank
- Exhaust
- Supply Module

- Fuel Tank
- Front Axle Components
- Rear Axle Components
- Air Tanks
- Battery
- Air conditioner
- Heater
- Refrigerator

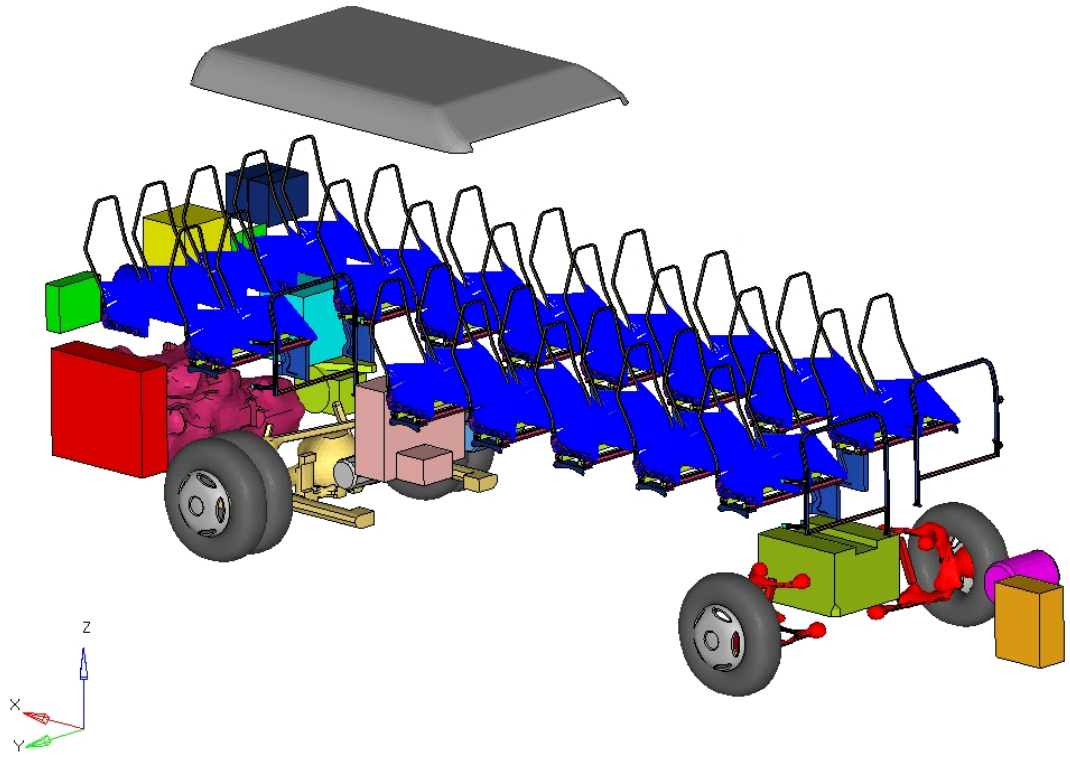


Figure 6.8 : Non-structural components of the finite element model for mass and inertia compliance.

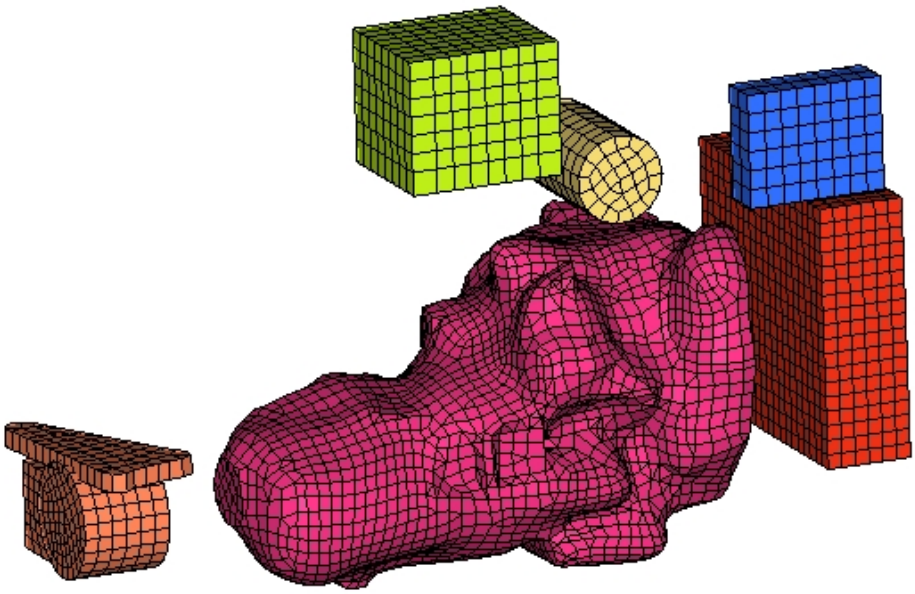


Figure 6.9 : Simplified finite element model of powertrain components.

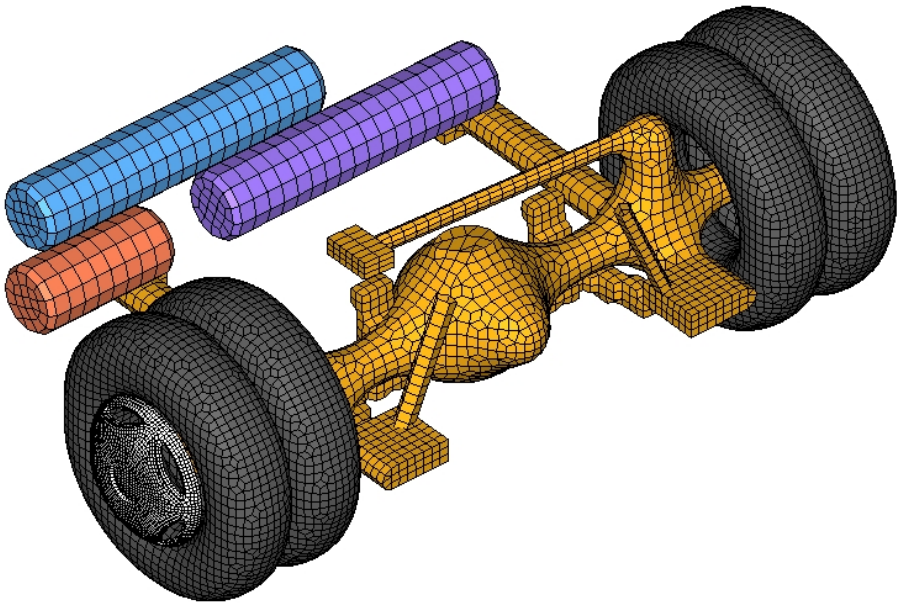


Figure 6.10 : Simplified finite element model of rear axle components.

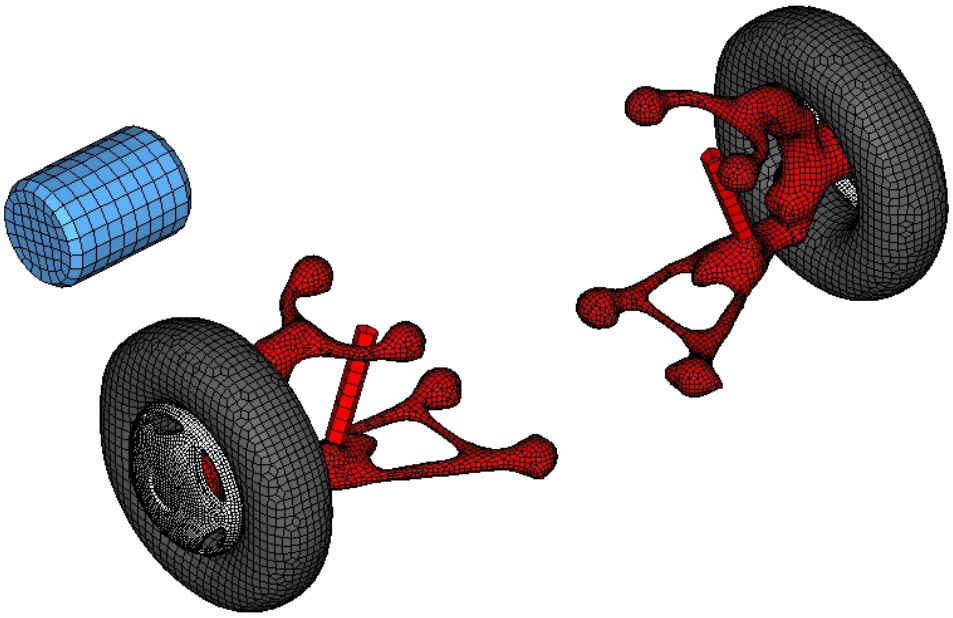


Figure 6.11 : Simplified finite element model of front axle components.

It is also necessary to increase the mass of the bus with the mass of its passengers when the bus is equipped with the seat belts. A different percentage of the total occupant mass contributes to the kinetic energy depending on which restraint system (RS) is used in the bus. The conservative assumption is made in ECE 66-02 [1] that the amount of mass to be added is 68 kg for each seat. The passenger mass was added to the model using 0D lumped masses in nodes as ADMAS feature. Nodes with masses were located in the dummy's center of gravity, which is defined in ECE 66-02 [1] (see Figure 6.13). Moreover, glass and trim components are modeled with RBE3 elements for only mass compliance.

Non-structural components are modeled with RBE3 elements for mass compliance:

- Laminated and Tempered Glasses
- Exterior Trim Components
- Human Masses
- Driver and Crew Seats

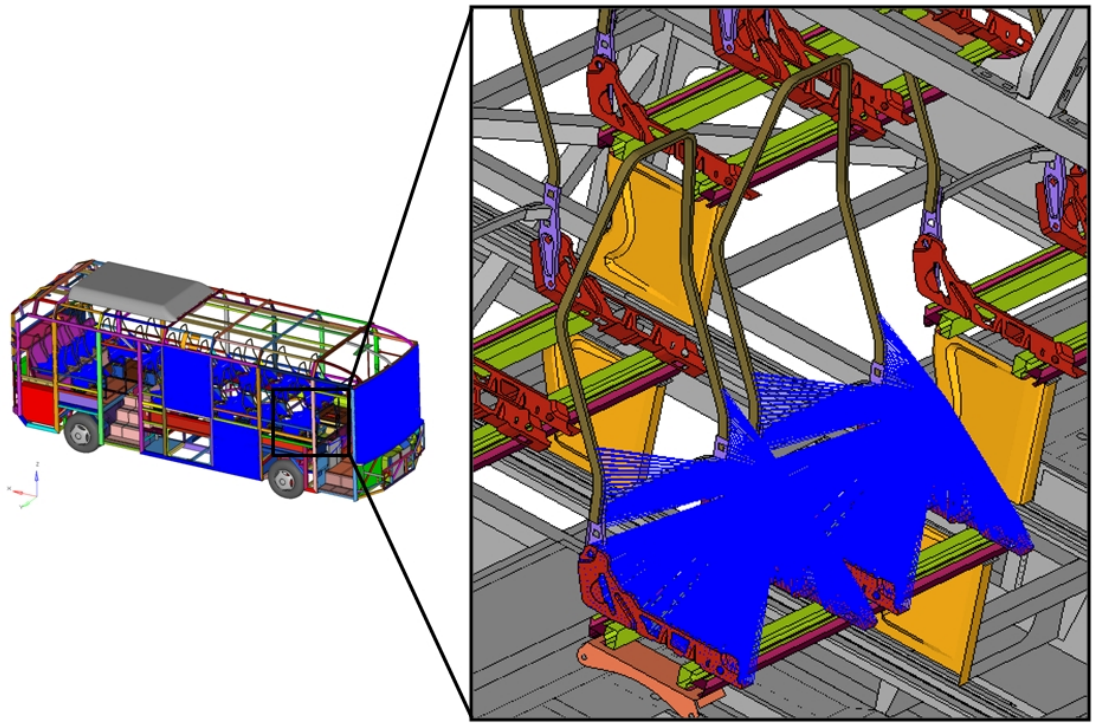


Figure 6.12 : Simplified finite element model of human masses.

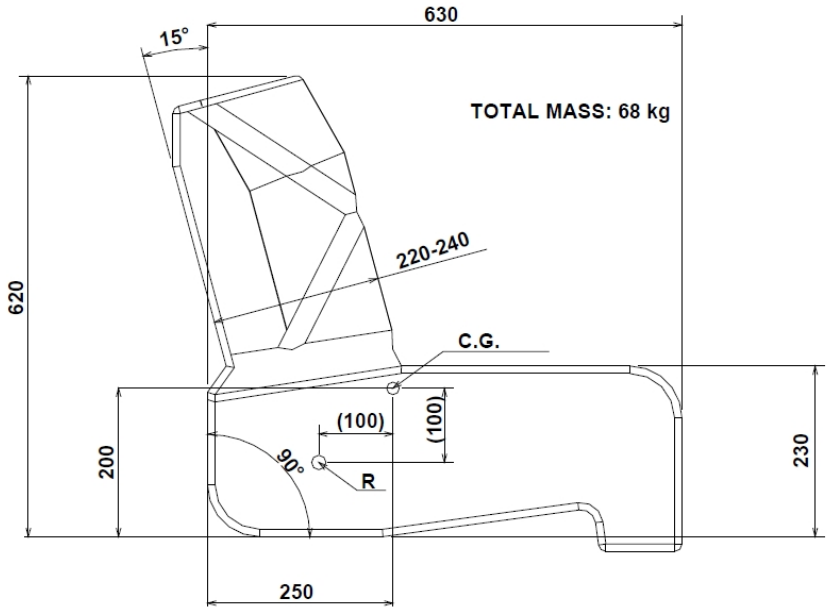


Figure 6.13 : Dimensions for anthropomorphic ballast [1].

The center of gravity of the vehicle was measured in Hexagon Studio. After the measurement of CG value, mass balancing was made with ADMAS elements in finite element model as possible. Total occupant mass distribution can be seen at

Table 6.2. Table 6.3 provides the information about calculated CG location of the vehicle from FE model at total effective mass.

Table 6.2 : Total occupant mass distribution.

	Number of People	Unit Weight
Passengers	31	68 kg
Crew	1	75 kg
Total Occupant Mass x k = [(31 x 68 kg) + 75 kg] x 0.5 = 1091.5 kg		

Table 6.3 : Location of the CG of the coach at total effective mass.

Specification	Description	Measurement
$\mathbf{l_1}$	Longitudinal distance from the centre line of front axle	2792 mm
t	Transverse distance from the vertical longitudinal central plane of the vehicle	-29 mm
$\mathbf{h_0}$	Vertical height above the flat horizontal ground level when the tires are inflated as specified for the vehicle	1089 mm

The complete model had 1617572 nodes, 10534 brick elements (HEX8N), 6854 triangular membrane elements (SHELL3N), 1516467 quadrilateral membrane elements (SHELL4N), 31658 rigid elements (RBODY), 73 RBE3 constraint elements and 91 added nodal mass elements (M-ADV0).

6.3.2 0D elements

ADMAS (added mass) assigns additional non-structural mass to nodes or a group of nodes. The total additional non-structural mass of a part or a group of parts can be defined (applied to shells and solids only) or a surface mass can be assigned to a surface and RADIOSS would then compute the added node based mass value using area (volume) - weighted distribution.

6.3.3 1D elements

The RBODY element specifies that the motion of a set of grid points (all having the same set of dependent degree of freedom numbers) are dependent on the six degrees of freedom at another grid point. When rigid elements are used, selected degrees of

freedom are eliminated from the solution set using equations (automatically generated in RADIOSS) that represent rigid body notion of the “dependent” degrees of freedom based on rigid motion of a selected set of “independent” degrees of freedom.

The RBODY element specifies that the motion of a set of grid points (all having the same set of dependent degree of freedom numbers) are dependent on the six degrees of freedom at another grid point. The formulations of dependent motion:

$$\dot{u}_s\ (slavetranslation) = [Tra]\left(\dot{u}_m + \dot{D}_{sm} \otimes \dot{\theta}_m\right) \quad \textbf{(6.6)}$$

$$\dot{\theta}_s\ (rotation) = [Rot]\ \dot{\theta}_m \quad \textbf{(6.7)}$$

$$[Tra], [Rot] = \begin{bmatrix} i & 0 & 0 \\ 0 & j & 0 \\ 0 & 0 & k \end{bmatrix} (i, j, k = 0, 1) \quad \textbf{(6.8)}$$

In explicit finite element computation, inertia computation of rigid bodies should be computed as spherical. If a rigid body has the same order of size or is smaller than the elements to which it is connected, using Ispher = 1 is recommended in order to ensure the stability of the connected elements.

The RBE3 element is not a rigid element but is used to distribute loads and mass from some central grid point to other grids in the model. It is defined by a dependent, central point at which the load or mass is defined along with grids to which the load or mass are to be distributed along with weighting factors at these distributed grids. The dependent point on the RBE3 should never be connected to other elastic elements in the model to avoid stiffening of the structure by the RBE3 element.

In general, the equations for one RBE3 can be represented in matrix notation as:

$$R_{dd} U_d + R_{dN} U_N = 0 \quad \textbf{(6.9)}$$

R_{dd} is the square, *d x d* matrix of coefficients for the dependent (or reference) grid of the RBE3 entry. It can have up to d = 6 dependent components. For all six components, R_{dd} and U_r are:

$$R_{dd} = \begin{bmatrix} 1 & 0 & 0 & 0 & \overline{d}_z & -\overline{d}_y \\ 0 & 1 & 0 & -\overline{d}_z & 0 & -\overline{d}_x \\ 0 & 0 & 1 & \overline{d}_y & -\overline{d}_x & 0 \\ 0 & -\overline{d}_z & \overline{d}_y & \overline{e}_{yz} & 0 & 0 \\ \overline{d}_z & 0 & -\overline{d}_x & 0 & \overline{e}_{zx} & 0 \\ -\overline{d}_y & \overline{d}_x & 0 & 0 & 0 & \overline{e}_{xy} \end{bmatrix}, \quad U_d = \begin{Bmatrix} u_x^a \\ u_y^a \\ u_z^a \\ \theta_x^a \\ \theta_y^a \\ \theta_z^a \end{Bmatrix} \quad \textbf{(6.10)}$$

R_{dN} is a rectangular, *d x N*, matrix of coefficients for the *N* independent grids on the RBE3:

$$R_{dN} = \frac{1}{w_T}[R_{d1} \quad R_{d2} \quad . \quad . \quad . \quad R_{dN}] \quad , \quad U_N = \begin{Bmatrix} U_1 \\ U_2 \\ . \\ . \\ . \\ U_N \end{Bmatrix} \quad \textbf{(6.11)}$$

A typical sub-matrix in R_{ai} is of size *d* by 3 with R_{ai} and U_i. For *d* = 6:

$$R_{di} = \frac{1}{W_T}\begin{bmatrix} \omega' & 0 & 0 \\ 0 & \omega' & 0 \\ 0 & 0 & \omega' \\ 0 & \omega' d'_z & -\omega' d'_y \\ -\omega' d'_z & 0 & \omega' d'_x \\ \omega' d'_y & -\omega' d'_x & 0 \end{bmatrix} \quad , \quad U_i = \begin{Bmatrix} u'_x \\ u'_y \\ u'_z \end{Bmatrix} \quad \textbf{(6.12)}$$

A RBE3 is processed by solving Eq. 6.9 for the dependent degrees of freedom, U_d, in terms of the independent degrees of freedom, U_N **(6.9)**.

6.3.4 2D elements

6.3.5 Element integration

The shell element in RADIOSS is a simple bilinear Mindlin plate element coupled with a reduced integration scheme using one integration point. It is applicable in a reliable manner to both thin and moderately thick shells. This element is very efficient if the spurious singular modes, called “hourglass modes”, which result from the reduced integration are stabilized.

The reduced integration scheme, especially with one-point quadrature (in the mid-surface), is widely used in programs with explicit time integration such as RADIOSS and other programs applied essentially in crashworthiness studies. These elements dramatically decrease the computation time, and are very competitive if the hourglass modes (which result from the reduced integration scheme) are “well” stabilized.

For full integration, the number of integration points is sufficient for the exact integration of the virtual work expression. The full integration scheme is often used in programs for static or dynamic problems with implicit time integration. It presents no problem for stability, but sometimes involves "locking" and the computation is often expensive.

For reduced integration, the number of integration points is sufficient for the exact integration of the contributions of the strain field that are one order less than the order of the shape functions. The incomplete higher order contributions to the strain field present in these elements are not integrated.

The reduced integration scheme, especially with one-point quadrature is widely used in programs with explicit time integration to compute the force vectors. It drastically decreases the computation time, and is very competitive if the spurious singular modes (often called “hourglass modes” which result from the reduced integration scheme) are properly stabilized. In two dimensions, a one point integration scheme will be almost four times less expensive than a four point integration scheme. The savings are even greater in three dimensions. The use of one integration point is recommended to save CPU time, but also to avoid "locking" problems, for example shear locking or volume locking.

Shear locking is related to bending behavior. In the stress analysis of relatively thin members subjected to bending, the strain variation through the thickness must be at least linear, so constant strain first order elements are not well suited to represent this variation, leading to shear locking. Fully integrated first-order isoparametric elements (tetrahedron) also suffer from shear locking in the geometries where they cannot provide the pure bending solution because they must shear at the numerical

integration points to represent the bending kinematic behavior. This shearing then locks the element, the response is far too stiff.

However, as mentioned above, the disadvantage of reduced integration is that the element can admit deformation modes that are not causing stresses at the integration points. These zero-energy modes make the element rank deficient and cause a phenomenon called hourglassing: the zero-energy modes start propagating through the mesh, leading to inaccurate solutions. This problem is particularly severe in first-order quadrilaterals and hexahedra.

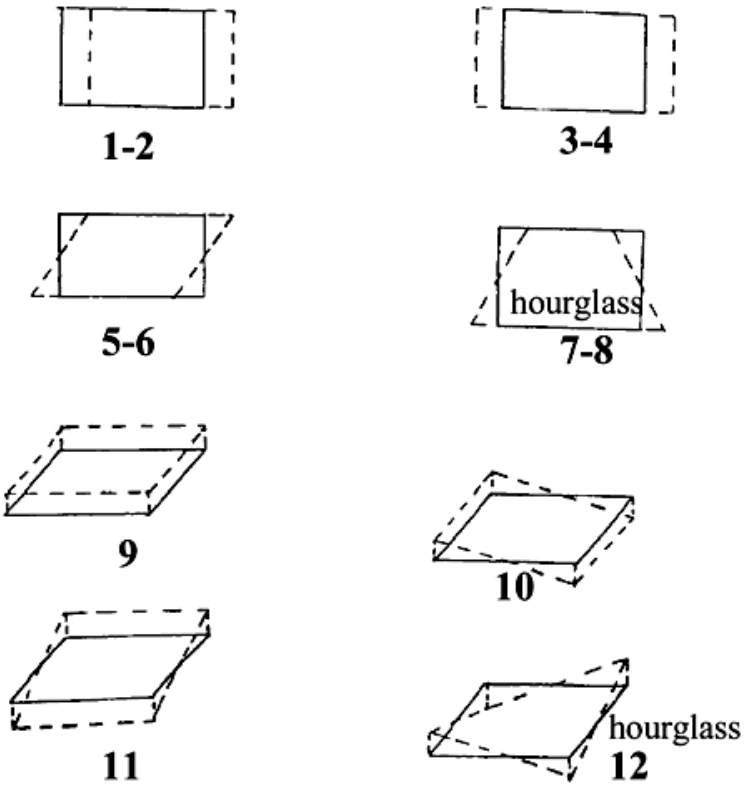


Figure 6.14 : Hourglass modes at translational modes of shell [60].

To prevent these excessive deformations, a small artificial stiffness or viscosity associated with the zero-energy deformation modes is added, leading in anti-hourglass force and moment vectors:

$$M\frac{dv}{dt} = f^{ext} - f^{int} + f^{hgr} \quad \textbf{(6.13)}$$

$$I\frac{d\omega}{dt} = M^{ext} - M^{int} + M^{hgr} \quad \textbf{(6.14)}$$

Zero energy or hourglass modes are controlled using a perturbation stabilization as described by Flanagan - Belytschko [61], or physical stabilization as described in below [62].

The shell element formulation used at simulations in this thesis is QEPH (Quadrilateral Elasto Plastic Physical Hourglass Control) element formulation. With one-point integration formulation, if the non-constant part follows exactly the state of constant part for the case of elasto-plastic calculation, the plasticity will be under-estimated due to the fact that the constant equivalent stress is often the smallest one in the element and element will be stiffer. Therefore, defining a yield criterion for the non-constant part seems to be a good ideal to overcome this drawback.

The rate of stresses of non-constant part:

$$\{\dot{\sigma}_i\}^H = [C]\{\dot{\varepsilon}\}^H = [C]\begin{Bmatrix} \phi_{,x}\dot{q}_x{}^a \\ \phi_{,y}\dot{q}_y{}^a \\ 0 \end{Bmatrix} = \eta\begin{Bmatrix} \dot{\sigma}^a{}_{x\eta} \\ \dot{\sigma}^a{}_{y\eta} \\ 0 \end{Bmatrix} + \xi\begin{Bmatrix} \dot{\sigma}^a{}_{x\xi} \\ \dot{\sigma}^a{}_{y\xi} \\ 0 \end{Bmatrix} \qquad \textbf{(6.15)}$$

where $\alpha = m, b$ corresponds to the membrane and bending terms respectively. Note that the shear terms are eliminated to avoid shear locking. The transverse shear terms can also be written as the same way:

$$\{\dot{\tau}_i\}^H = \eta\begin{Bmatrix} \dot{\tau}_{x\eta} \\ \dot{\tau}_{y\eta} \end{Bmatrix} + \xi\begin{Bmatrix} \dot{\tau}_{x\xi} \\ \dot{\tau}_{y\xi} \end{Bmatrix} \qquad \textbf{(6.16)}$$

We can now redefine 12 generalized hourglass stresses by integrating their rate ones, and the stress field can be expressed by:

Membrane, bending: $\{\sigma^a{}_i\} = \{\sigma^a{}_i\}^0 + \{\sigma^a{}_i\}^H = \{\sigma^a{}_i\}^0 + \eta\begin{Bmatrix} \sigma^a{}_{x\eta} \\ \sigma^a{}_{y\eta} \\ 0 \end{Bmatrix} + \xi\begin{Bmatrix} \sigma^a{}_x \\ \sigma^a{}_{y\xi} \\ 0 \end{Bmatrix}$

Shear: $\{\tau_i\} = \{\tau_i\}^0 + \{\tau_i\}^H = \{\tau_i\}^0 + \eta\begin{Bmatrix} \dot{\tau}_{x\eta} \\ \dot{\tau}_{y\eta} \end{Bmatrix} + \xi\begin{Bmatrix} \dot{\tau}_x \\ \dot{\tau}_{y\xi} \end{Bmatrix}$

Even the redefinition for shear is not necessary as it is not included in the plastic yield criterion, but the same stress calculation as the constant part with the updated Lagrangian formulation is always useful when large strain is involved.

a) Plastic yield criterion:

The von Mises type of criterion is written by:

$$f = {\sigma^2}_{eq}(\xi, \eta, \zeta) - {\sigma^2}_y = 0 \quad \textbf{(6.17)}$$

for any point in the solid element, where σ_y is evaluated at the quadrature point.

As only one criteria is used for the non-constant part, two choices are possible:

I. taking the mean value, i.e.: $f = f(\bar{\sigma}_{eq})$; $\bar{\sigma}_{eq} = \frac{1}{\Omega}\int_\Omega \sigma_{eq} d\Omega$

II. taking the value by some representative points, e.g. eight Gauss points

The second choice has been used in elements at simulations in this thesis.

b) Elasto-plastic hourglass stress calculation:

The incremental hourglass stress is computed by:

- Elastic increment: $(\sigma_i)_{n+1}^{trH} = (\sigma_i)_n^H + [C]\{\dot{\varepsilon}\}^H \Delta t$
- Check the yield criterion
- If $f \geq 0$, the hourglass stress correction will be done by unradial return ; $(\sigma_i)_{n+1}^H = P((\sigma_i)_{n+1}^{trH}, f)$

6.3.6 Computation of thickness change

The necking of the shells undergoing large strains in hardening phase can be taken into account by computing normal strain ε_{zz} in an incremental process. The incompressibility hypothesis in plasticity gives:

$$d\varepsilon_{zz}^p = -\left(d\varepsilon_{xx}^p + d\varepsilon_{zz}^p\right) \quad \textbf{(6.18)}$$

where the components of membrane strains $d\varepsilon_{xx}^p$, $d\varepsilon_{yy}^p$ are computed as:

$$\begin{Bmatrix} d\varepsilon_{xx}^p \\ d\varepsilon_{yy}^p \end{Bmatrix} = \frac{d\varepsilon^p}{\sigma_y}[A]_{2x2}\begin{Bmatrix} \sigma_{xx} \\ \sigma_{yy} \end{Bmatrix} \quad \textbf{(6.19)}$$

The plan stress condition $d\sigma_{zz} = 0$ allows to resolve for $d\varepsilon_{zz}$:

$$d\varepsilon_{zz} = -\frac{v}{1-v}\left(d\varepsilon_{xx} + d\varepsilon_{yy}\right) + \frac{1-2v}{1-v} d\varepsilon_{zz}^{p} \qquad \textbf{(6.20)}$$

6.3.7 Elastic-plastic stress calculation

To determine the elastic-plastic state of a shell element, a number of steps have to be performed to check for yielding and defining a plasticity relationship. Stress - strain and force - displacement curves for a particular ductile material are shown in Figure 6.15.

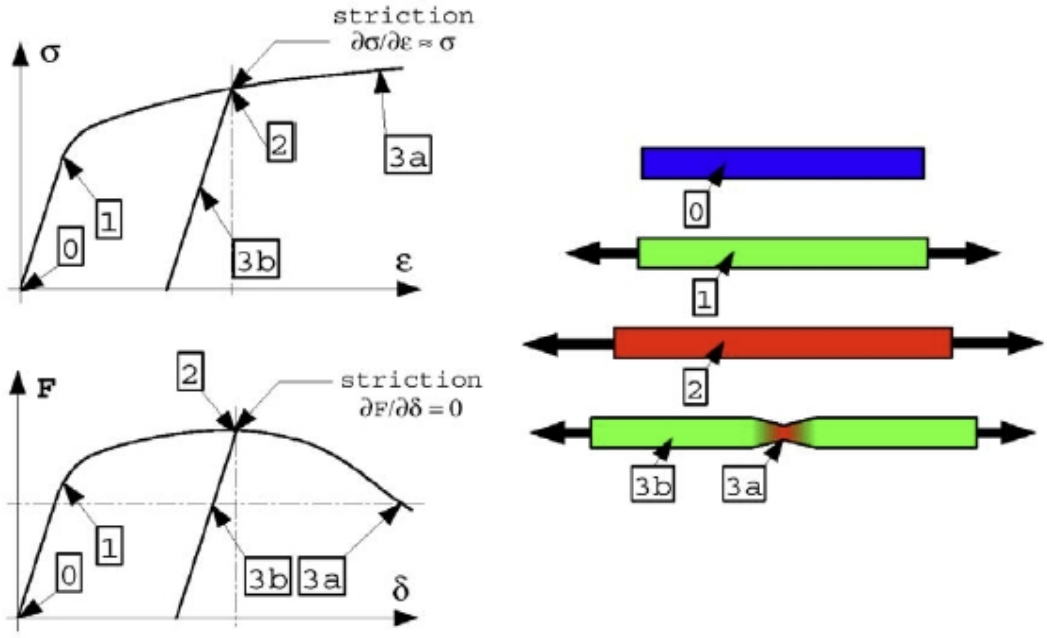


Figure 6.15 : Material curves for plastic stress calculation [60].

The elastic-plastic stress calculation used at simulations in this thesis is an iterative algorithm as Newton-Raphson method. It has been extended to plane stress situations. This method is more computationally expensive, but provides high accuracy on stress distribution, especially when one is interested in residual stress or elastic return. This method is also recommended when variable thickness is being used. After some calculations, the plastic stresses are defined as:

$$\sigma_x^{pa} = \frac{\sigma_x^{el} + \sigma_y^{el}}{2\left(1+\frac{\Delta r}{1-v}\right)} + \frac{\sigma_x^{el} - \sigma_x^{el}}{2\left(1+\frac{3\Delta r}{1+v}\right)} \qquad \textbf{(6.21)}$$

$$\sigma_y^{pa} = \frac{\sigma_x^{el} + \sigma_y^{el}}{2\left(1+\frac{\Delta r}{1-v}\right)} - \frac{\sigma_x^{el} - \sigma_x^{el}}{2\left(1+\frac{3\Delta r}{1+v}\right)} \quad \textbf{(6.22)}$$

$$\sigma_{xy}^{pa} = \frac{\sigma_{xy}^{el}}{1+\frac{3\Delta r}{1+v}} \quad \textbf{(6.23)}$$

where $\Delta r = \frac{E\Delta\varepsilon^p}{2\sigma_{yield}(t+\Delta t)}$ **(6.24)**

The value of $\Delta\varepsilon^P$ must be computed to determine the state of plastic stress. This is done by an iterative method. To calculate the value of $\Delta\varepsilon^P$, the von Mises yield criterion for the case of plane stress is introduced:

$$\sigma^2{}_x + \sigma^2{}_y - \sigma_x\sigma_y + 3\sigma^2{}_{xy} = \sigma^2{}_{yield}\,(t+\Delta t) \quad \textbf{(6.25)}$$

and the values of σ_x, σ_y, σ_{xy} and σ_{yield} are replaced by their expression as a function of $\Delta\varepsilon^P$ Eq. 6.23, with, for example **(6.23)**:

$$\sigma_{yield}(t+\Delta t) = a + b\varepsilon^{p^n}(t+\Delta t) \quad \textbf{(6.26)}$$

and:

$$\varepsilon^p(t+\Delta t) = \varepsilon^p(t) + \Delta\varepsilon^p \quad \textbf{(6.27)}$$

The nonlinear equation Eq. 6.25 is solved iteratively for $\Delta\varepsilon^P$ by Newton's method using three iterations. This is sufficient to obtain $\Delta\varepsilon^P$ accurately.

Nonlinear material calculations in shells are based on plane stress theory, using the membrane and bending strains to define the strain on the surface parallel to the shell's reference surface at each integration point through the shell's thickness. In this thesis, 5 number of integration points through the thickness is used in properties of shell elements.

6.4 Residual Space Modeling

Residual space means a space to be preserved in the passengers', crew and driver's compartment to provide better survival possibility for passengers, driver and crew in case of a rollover accident.

The definition of survival space is the statement in the regulation ECE 66-02 [1] was used to form the basis of the survival space model. It was introduced 500 mm above the floor, under the passengers' feet, 150 mm away from the inside surface of the side of the vehicle, throughout the entire vehicle (trim lengths were also considered and added to these values).

The rearmost position of the residual space is a vertical plane 200 mm behind the S_R point of the rearmost outer seat, or the inner face of the rear wall of the vehicle if this is less than 200 mm behind that S_R point. The foremost position of the residual space is a vertical plane 600 mm in front of the S_R point of the foremost seat (whether passenger, crew, or driver) in the vehicle set at its fully forward adjustment.

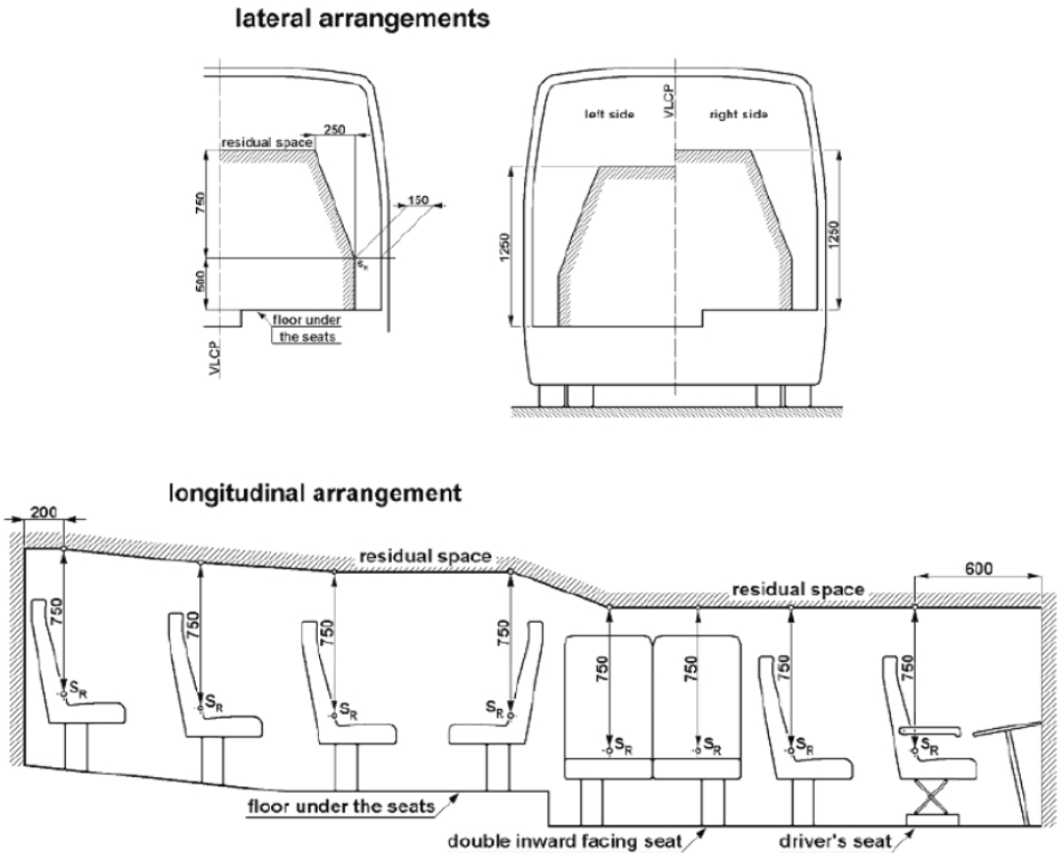


Figure 6.16 : Specification of residual space [1].

The residual space is continuous in the passenger, crew and driver compartment(s) between its rearmost and foremost plane and is defined by moving the defined vertical transverse plane through the length of the vehicle along straight lines through the S_R points on both sides of the vehicle. Behind the rearmost and in front of the foremost seat's S_R point the straight lines are horizontal.

There is no stiffness connection these between these rigid beam frames as shell elements are modeled using “void material” for visual purposes only. The envelope of the vehicle’s residual space is defined by creating a vertical transverse plane within the vehicle, which has the periphery described in Figure 6.16, and moving this plane through the length of the vehicle. The model of the survival space consists in rigid beam frames in each section, rigidly mounted in the hard region under the floor (see Figure 6.18).

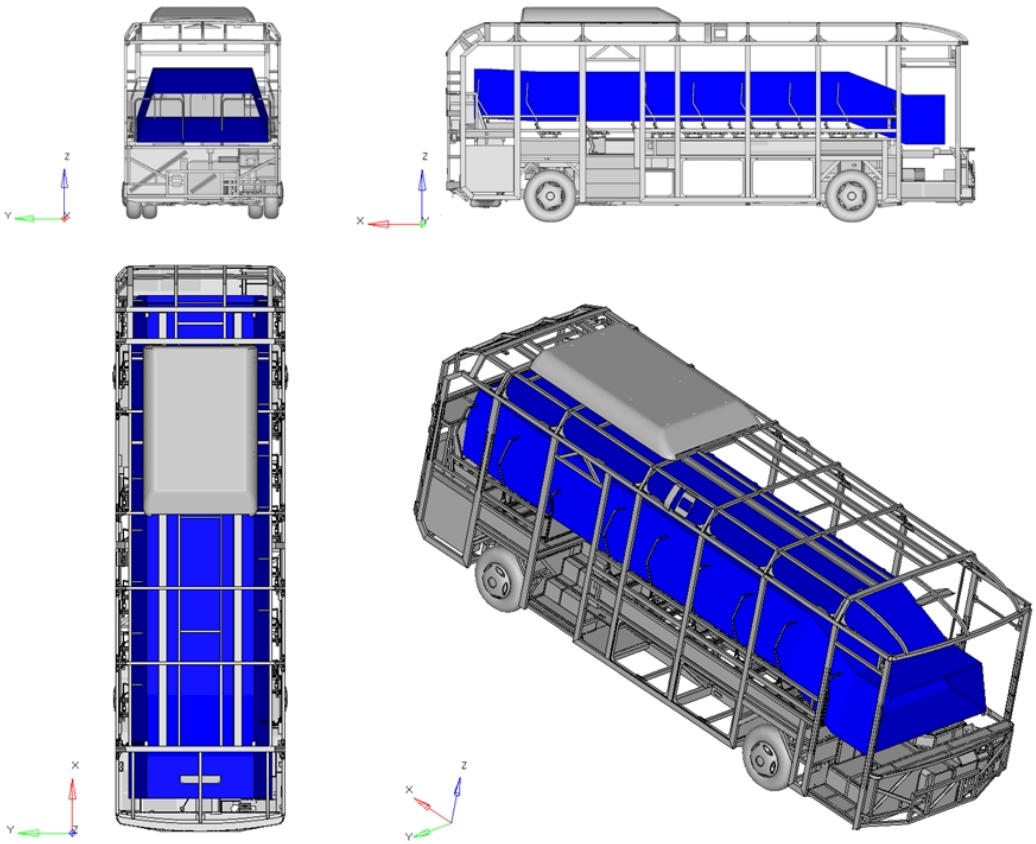


Figure 6.17 : Finite element model of the vehicle and residual space.

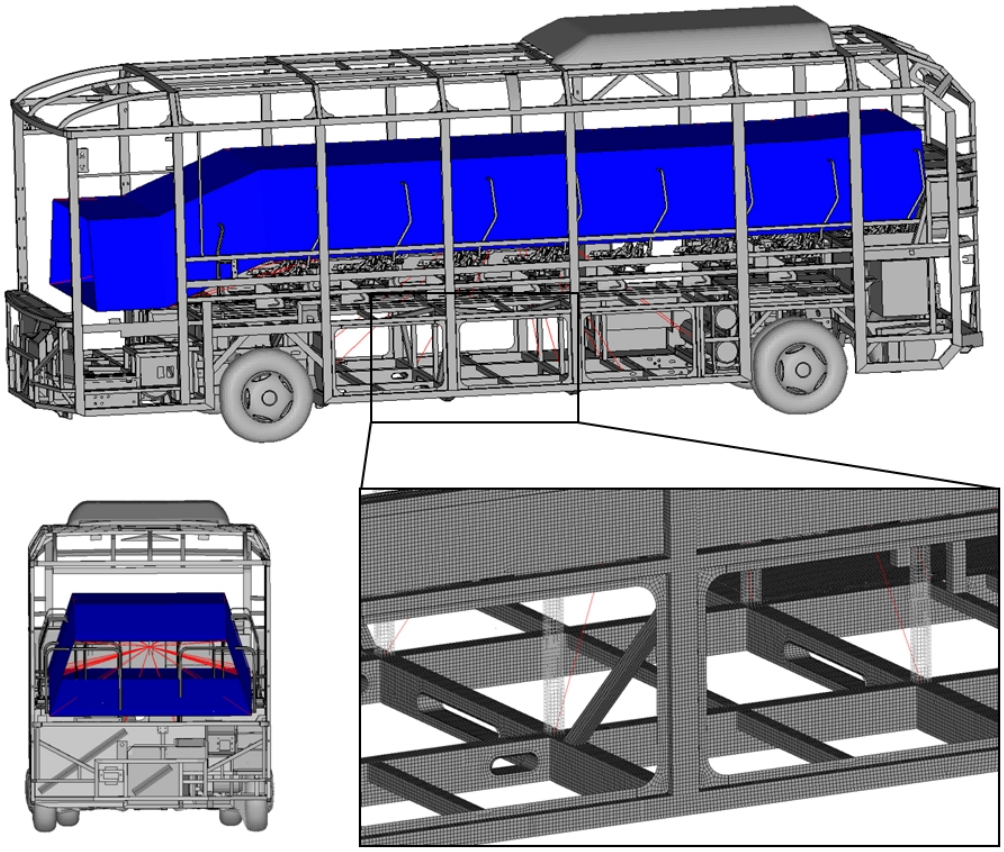


Figure 6.18 : Residual space connection to the base of the vehicle.

6.5 Material Modeling

6.5.1 Mechanical properties of materials used in the vehicle

In accordance with ECE 66-02 [1] regulation, S420MC and S355JR Steels, which are used on the actual vehicle structure, was performed tensile strength test at ITU Faculty of Mechanical Engineering; Laboratory of Strength of Materials and Biomechanics, in order to determine mechanical properties such as stress-strain curve, yield strength, ultimate tensile strength, Young's modulus, toughness and cross-sectional narrowing at specimens.

The specimens, which used in the tensile strength tests, are presented at Figure 6.19. Specimen head are used for clamping to applying force. Narrow region of the specimen is expected to deform and break when load is applied. As a result, Load - Displacement curve is obtained from tensile strength test.

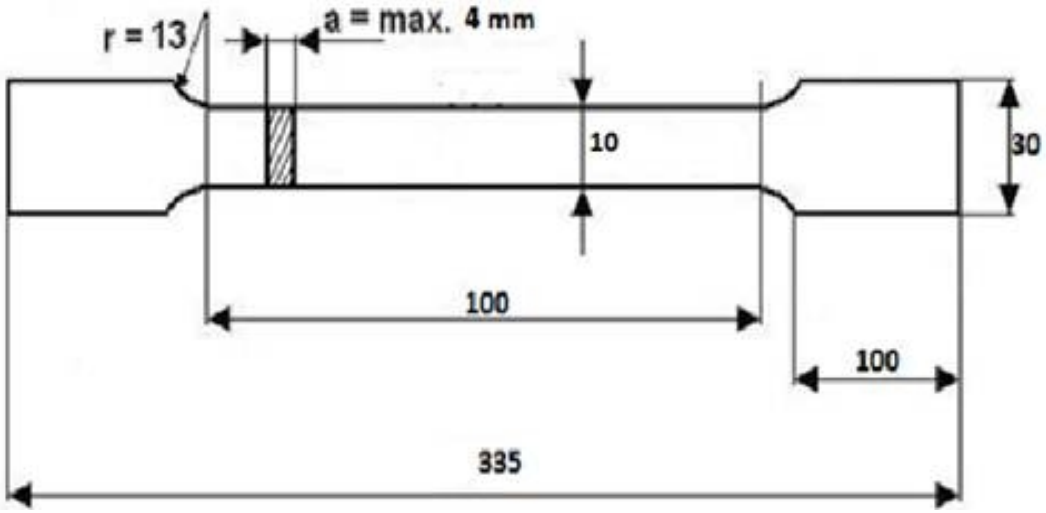


Figure 6.19 : Test specimen for tensile strength tests.

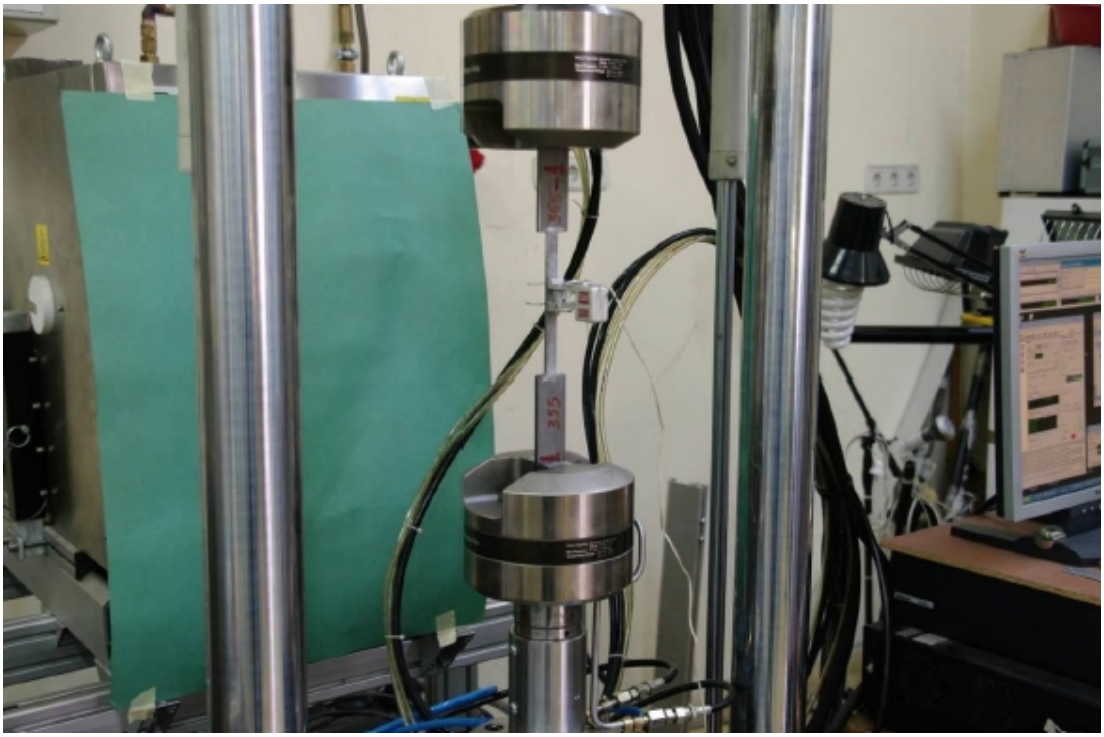


Figure 6.20 : Picture of tensile strength test system.

The tensile strength were tests made with MTS Minibionix Model 858-II Dynamic Universal Test Machine *(Model Number: 359.XX, Part Number: 100-146-714, Serial Number: 10189576, Manufacture Date: 07.20.2005, MTS System Corporation, 14000 Technology Drive, Eden Prairie, MN USA, 55344, Capacity: 25 kN Axial Load – 200 Nm Torsion)*. The tests were made in the laboratory environment. Pulling speed at the tests was set to 10 mm/minute. Visuals about the tests are presented at Figure 6.20 and Figure 6.21.

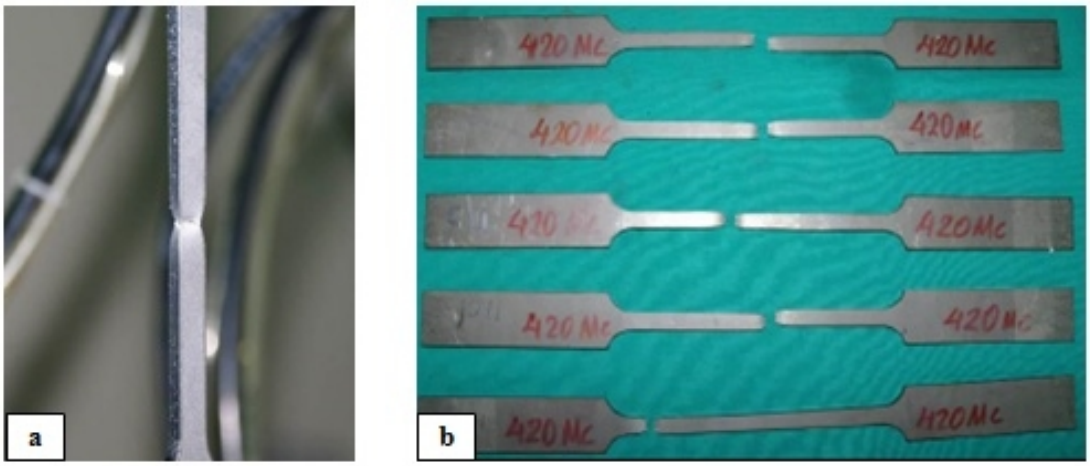


Figure 6.21 : The specimens for tensile strength tests. (a) During test. (b) After test.

Engineering stress - strain curve is proceeded from load - displacement curve with using formulas which given below. Engineering stress is obtained from the force divided by the specimen's first cross-sectional area **(6.28)**.

$$\sigma_e = F \ / \ A_0 \qquad \textbf{(6.28)}$$

Engineering strain is obtained from elongation of specimen divided by initial length of the specimen **(6.29)**.

$$\varepsilon_e = \Delta L \ / \ L_0 \qquad \textbf{(6.29)}$$

During the tensile strength test, specimen is undergone plastic deformation until failure occurs. Engineering stress - strain curve is obtained by both load and elongation is dividing a constant value. However, cross-section is narrowing continuously during the tensile strength test. True stress is obtained from the force divided by the specimen's current real cross-sectional area **(6.30)**. True stress - strain curve and true stress - plastic strain curve are proceeded from engineering stress - strain curve with using formulas which given below **(6.31) (6.32)**.

$$\sigma_T = \sigma_e \ (1 + \ \varepsilon_e) \qquad \textbf{(6.30)}$$

$$\varepsilon_T = In \ (1 + \ \varepsilon_e) \qquad \textbf{(6.31)}$$

$$\varepsilon_{plas} = \varepsilon_{true} - \sigma_{true} \ / \ E \qquad \textbf{(6.32)}$$

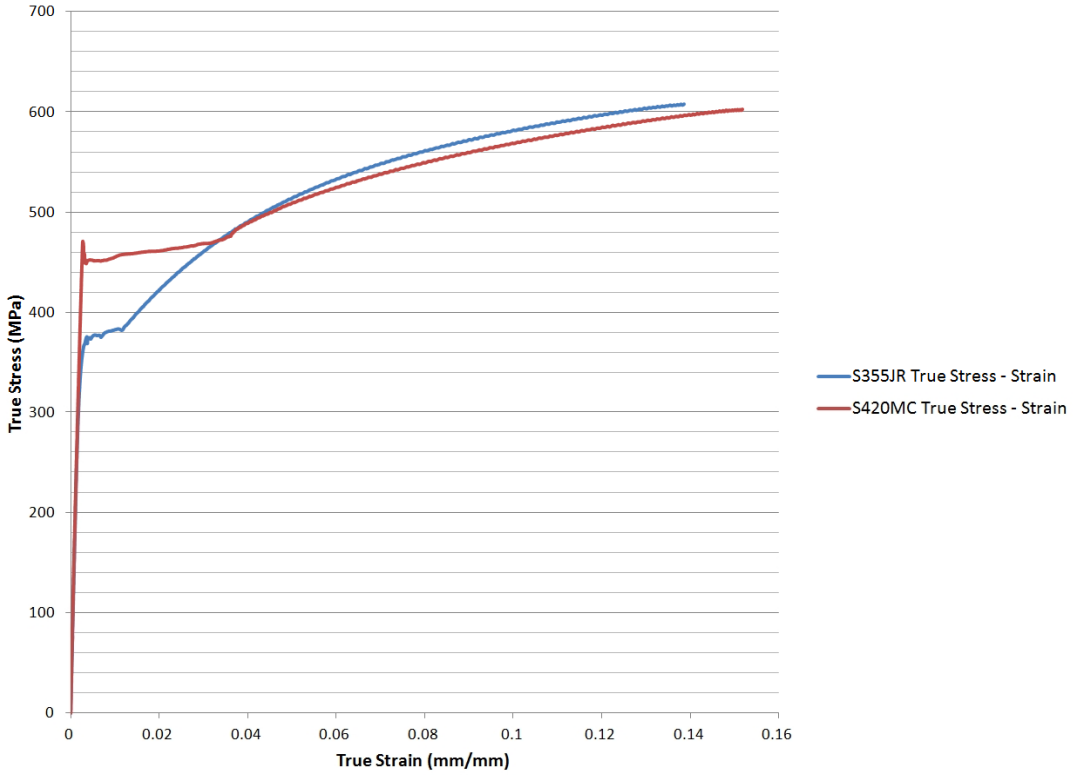


Figure 6.22 : True stress - strain curves of S420MC and S355JR steels.

For obtaining the material data, tensile strength tests were applied on several specimens at ITU Faculty of Mechanical Engineering; Laboratory of Strength of Materials and Biomechanics. The true stress – plastic strain curve was imposed in RADIOSS accordingly. The material model for the deformable structure in RADIOSS is called “Elastic Plastic Piecewise Linear Material (Law 36)”. This is an elasto-plastic material model, which uses the Young’s modulus if stresses are below the yield strength and the measured stress-strain curve if the stresses are above the yield strength. Moreover, failure criteria was defined at material model based on the tensile strength tests. Thus, elements were deleted if stresses are above the ultimate tensile strength.

6.5.2 Plastic tabulated piecewise linear material model

The material model used at simulations in this thesis is “Plastic Tabulated Piecewise Linear Material Model (Law 36)”. The elastic-plastic behavior of isotropic material is modeled with user defined functions for work hardening curve. The elastic portion of the material stress-strain curve is modeled using the elastic modulus, E, and Poisson's ratio, ν. The curves are extrapolated if the plastic deformation is larger than

the maximum plastic strain. The hardening model may be isotropic, kinematic or a combination of the two models. The isotropic hardening model used at simulations in this thesis.

The strain hardening behavior of materials is a major factor in structural response as metal working processes or plastic instability problems. A proper description of strain hardening at large plastic strains is generally imperative. For many plasticity problems, the hardening behavior of the material is simply characterized by the strain-stress curve of the material. Isotropic elastic-plastic material laws in RADIOSS use von Mises yield criteria. The models involve damage for ductile or brittle failures with or without dislocation. The cumulative damage law is used to access failure.

For some kinds of steels, the yield stress dependence to pressure has to be incorporated especially for massive structures. The yield stress variation is then given by:

$$\sigma_y = \sigma_y^0(\varepsilon_p) * f(p) \quad \textbf{(6.33)}$$

where *p* is the pressure. Drucker – Preger [63] model gives a nonlinear function *f(p)*. However, for steel type materials where the dependence to pressure is low, a simple linear function considerer:

$$\sigma_y = \sigma_y^0(\varepsilon_p) * C * p(\varepsilon_p) \quad \textbf{(6.34)}$$

where *C* is user defined constant and *p* the computed pressure for a given deformed configuration.

6.5.3 Failure model

Failure models can be simulated using several material laws in RADIOSS. A method is set up to correspond to the material parameters in the cumulative damage law. This law use a global notion of cumulative damage to compute failure. The rupture phase is very sensitive and the simulation results strongly depend upon the starting point for necking. The point-by-point definition of the hardening curve in law 36 enables to bypass the adaptation difficulties when using the Johnson-Cook model. However,

the results following the necking point are very sensitive to the position of points defining the hardening curve.

This model also contains a failure criterion based on the total accumulated effective plastic strain, ε_p. When the effective plastic strain exceeds the specified value for the effective plastic strain at failure, ε_p^f, failure is detected. For shell elements, failure is assumed to occur when the effective plastic strain at any through-thickness integration point reaches ε_p^f. Once any integration point in a shell element fails, the effective plastic strain is set to the failure value ε_p^f for all through-thickness integration points in that element and all stresses in that element are set to zero. The element remains failed throughout the rest of the calculation. Deleted elements do not carry any load, and are deleted from all applicable slide surface definitions. Clearly, this option must be judiciously used to obtain accurate results at a minimum cost.

Nonlinear material calculations in shells are based on plane stress theory, using the membrane and bending strains to define the strain on the surface parallel to the shell's reference surface at each integration point through the shell's thickness. In this thesis, 5 number of integration points through the thickness is used in properties of shell elements.

The elastic-plastic behavior of the material is defined by "Plastic Tabulated Piecewise Linear Material Model (Law 36)" model. However, the stress-strain curve for the material incorporates a last part related to damage phase as shown in Figure 6.23. The damage parameters are:

- Tensile rupture strain (ε_{t1}): damage starts if the highest principal strain reaches this tension value.
- Maximum strain (ε_{m1}): the element is damaged if the highest principal strain is above the tension value. The element is not deleted.
- Maximum damage factors (σ_{max}): this value should be kept at its default value (0.999).
- Failure strain (ε_{f1}): the element is deleted if the highest principal strain reaches the tension value.

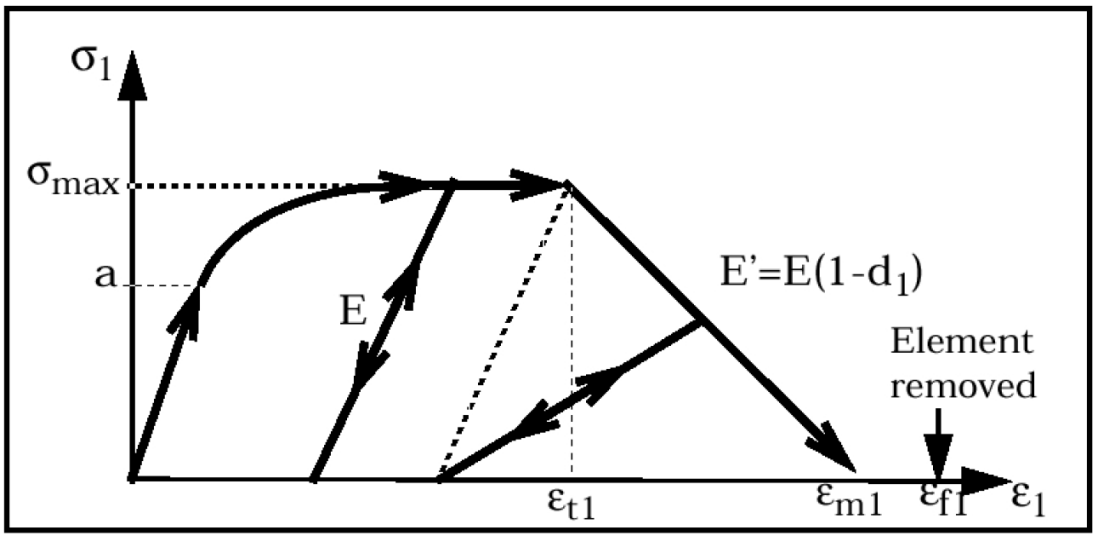


Figure 6.23 : Stress - strain curve for damage affected material [60].

The element is removed if one layer of element reaches the failure tensile strain, (ε_{f1}). The nominal and effective stresses developed in an element are related by:

$$\sigma_n = \sigma_{eff}\,(1-d) \qquad \textbf{(6. 35)}$$

where 0 < d < 1 is the damage factor.

The strains and the stresses in each direction are given by:

$$\varepsilon_1 = \frac{\sigma_1}{(1-d_1)E} - \frac{\nu\sigma_2}{E} \qquad \textbf{(6. 36)}$$

$$\varepsilon_2 = \frac{\sigma_2}{E} - \frac{\nu\sigma_2}{E} \qquad \textbf{(6.37)}$$

$$\gamma_{12} = \frac{\sigma_{12}}{(1-d_1)G} \qquad \textbf{(6. 38)}$$

$$\sigma_1 = \frac{E(1-d_1)}{[1-(1-d_1)\upsilon^2]}(\varepsilon_1 + \nu\varepsilon_2) \qquad \textbf{(6. 39)}$$

$$\sigma_2 = \frac{E}{[1-(1-d_1)\upsilon^2]}(\varepsilon_2 + (1-d_1)\nu\varepsilon_1) \qquad \textbf{(6.40)}$$

The conditions for these equations are:

0 < d < 1;

$\varepsilon = \varepsilon_t$; d = 0,

$\varepsilon = \varepsilon_m$; d = 1,

A linear damage model is used to compute the damage factor in function of material strain.

$$d = \frac{\varepsilon - \varepsilon_t}{\varepsilon_m - \varepsilon_t} \quad \textbf{(6.41)}$$

The stress-strain curve is then modified to take into account the damage by Eq. 6. 35. Therefore:

$$\sigma = E \frac{\varepsilon_m - \varepsilon}{\varepsilon_m - \varepsilon_t} \left(\varepsilon - \varepsilon_t^p\right) \quad \textbf{(6.42)}$$

The softening condition is given by:

$$\varepsilon_m - \varepsilon_t \leq \varepsilon_t - \varepsilon_t^p \quad \textbf{(6.43)}$$

6.6 Contact Modeling

6.6.1 Introduction

Interfaces solve the contact and impact conditions between two parts of a model. Contact-impact problems are among the most difficult nonlinear problems to solve as they introduce discontinuities in the velocity time histories. Prior to the contact, the normal velocities of the two bodies which come into contact are not equal, while after impact the normal velocities must be consistent with the impenetrability condition. In the same way, the tangential velocities along interfaces are discontinuous when stick-slip behavior occurs in friction models. These discontinuities in time complicate the integration of governing equations and influence performance of numerical methods.

Central to the contact-impact problem is the condition of impenetrability. This condition states that bodies in contact cannot overlap or that their intersection remains empty. The difficulty with the impenetrability condition is that it cannot be

expressed in terms of displacements, as it is not possible to anticipate which parts of the bodies will come into contact.

In structural crash or vehicle crash simulations, the majority of the contacts result from the buckling of tubular structures and metal sheets. Modeling the structure using shell and plate finite elements, the physics of the contact cannot be described in a precise way. The reflection of the waves in the thickness is not captured and the distribution of contact pressures in the thickness is not taken into account. The peculiarity of the contacts occurring during the crash of a structure lies more in the complexity of the structural folding and the important number of contact zones than in the description of the impact or the contact itself.

6.6.2 Equations of equilibrium

Let Ω be a volume occupied by a part of the body in the current configuration, and Γ the boundary of the body. In the Lagrangian formulation, Ω is the volume of space occupied by the material at the current time, which is different from the Eulerian approach where we examine a volume of space through which the material passes. τ is the traction surface on Γ and *b* are the body forces.

Force equilibrium for the volume is then:

$$\int_{\Gamma} \tau_i d\Gamma + \int_{\Omega} \rho b_i d\Omega = \int_{\Omega} \rho \frac{\partial v_i}{\partial t} d\Omega \qquad \textbf{(6.44)}$$

with ρ the material density.

The Cauchy true stress matrix at a point of Γ is defined by:

$$\tau_i = n_j \sigma_{ji} \qquad \textbf{(6.45)}$$

where *n* is the outward normal to Γ at that point. Using this definition, Eq. 6.44 is written **(6.35)**:

$$\int_{\Gamma} n_j \sigma_{ji} d\Gamma + \int_{\Omega} \rho b_i d\Omega = \int_{\Omega} \rho \frac{\partial v_i}{\partial t} d\Omega \qquad \textbf{(6.46)}$$

Gauss theorem allows the rewrite of the surface integral as a volume integral so that:

$$\int_{\Gamma} n_j \sigma_{ji} d\Gamma = \int_{\Omega} \frac{\partial \sigma_{ij}}{\partial x_j} d\Omega \quad \textbf{(6.47)}$$

As the volume is arbitrary, the expression can be applied at any point in the body providing the differential equation of translation equilibrium:

$$\frac{\partial \sigma_{ij}}{\partial x_j} + \rho b = \rho \frac{\partial v_i}{\partial t} \quad \textbf{(6.48)}$$

Use of Gauss theorem with this equation leads to the result that the true Cauchy stress matrix must be symmetric:

$$\sigma = \sigma^T \quad \textbf{(6.49)}$$

so that at each point there are only six independent components of stress. As a result, moment equilibrium equations are automatically satisfied, thus only the translational equations of equilibrium need to be considered.

6.6.3 Principle of virtual power

The basis for the development of a displacement finite element model is the introduction of some locally based spatial approximation to parts of the solution. The first step to develop such an approximation is to replace the equilibrium equations by an equivalent weak form. This is obtained by multiplying the local differential equation by an arbitrary vector valued test function defined with suitable continuity over the entire volume and integrating over the current configuration:

$$\int_{\Omega} \left(\delta v_i \left(\frac{\partial \sigma_{ji}}{\partial x_j} + \rho b_i - \rho \dot{v}_i \right) \right) d\Omega = 0 \quad \textbf{(6.50)}$$

The first term in Eq. 6.41 is then expanded:

$$\int_{\Omega} \left(\delta v_i \frac{\partial \sigma_{ji}}{\partial x_j} \right) d\Omega = \int_{\Omega} \left[\frac{\partial}{\partial x_j} \left((\partial v_i) \sigma_{ji} \right) - \frac{\partial (\delta v_i)}{\partial x_j} \sigma_{ji} \right] d\Omega \quad \textbf{(6.51)}$$

Using Gauss theorem gives:

$$\int_{\Omega} \left(\frac{\partial}{\partial x_j} \left((\partial v_i) \sigma_{ji} \right) \right) d\Omega = \int_{\Gamma_\sigma} \left[(\partial v_i) n_j \sigma_{ji} \right] d\Gamma \quad \textbf{(6.52)}$$

taking into account that stresses vanish on the complement of the traction boundaries.

Replacing Eq. 6.43 in Eq. 6.42 gives:

$$\int_{\Omega}\left(\delta v_i \frac{\partial \sigma_{ji}}{\partial x_j}\right) d\Omega = \int_{\Omega}(\partial v_i)\tau_i d\Gamma - \int_{\Omega}\frac{\partial(\delta v_i)}{\partial x_j}\sigma_{ji}\, d\Omega \qquad \textbf{(6.53)}$$

If this last equation is then substituted in Eq. 6.50, one obtains:

$$\int_{\Omega}\left(\frac{\partial(\delta v_i)}{\partial x_j}\right)\sigma_{ji} d\Omega - \int_{\Gamma}\partial v_i \rho b_i d\Omega - \int_{\Gamma}(\delta v_i)\tau_i d\Gamma + \int_{\Omega}\delta v_i \rho \dot{v}_i d\Omega = 0 \qquad \textbf{(6.54)}$$

The preceding expression is the weak form for the equilibrium equations, traction boundary conditions and interior continuity conditions. It is known as the principle of virtual power.

6.6.4 Penalty method

The contact formulation used in RADIOSS is a penalty type formulation. The choice of the penalty factor is a major aspect of this method. The first advantage to this formulation is its natural integration in an explicit code. Each contact is treated like an element and integrates itself perfectly into the code architecture, even if the programming is vectorial and parallel. Contrary to the kinematic formulations, the penalty method ensures the conservation of momentum and kinetic energy during impact.

In order to respect kinematic continuity, the penalty spring must be as rigid as possible. If the impedance of the interface becomes higher than those of the structures in contact, some numerical rebounds (high frequency) can occur. To ensure the stability of the integration diagram, without having additional constraints, this rigidity must be low. With a too low penalty, the penetration of the nodes becomes too strong and the geometrical continuity is no longer ensured.

The compromise selected consists in using a stiffness of the same order of magnitude than the stiffness of the elements in contact. This stiffness is nonlinear and increases with the penetration, so that a node is not allowed to cross the surface.

These choices provide a clear representation of physics, without numerical generation of noise, but require the contact stiffness in the calculation of the criteria of stability of the explicit scheme to be taken into account.

In the solution of constrained optimization problems, penalty methods consist in replacing the constrained optimization problem with a sequence of unconstrained optimization problems. The virtual power continues to be minimized so as to find the stationary condition, but a penalty term is added to Eq. 6.54 so as to impose the impenetrability condition:

$$\delta Q = \int_{\Gamma^c} \rho \phi (\gamma_N) d\Gamma \quad \textbf{(6.55)}$$

where;

$\phi(\gamma_N) = 0$ if $\gamma_N = 0$

$\phi(\gamma_N) > 0$ if $\gamma_N < 0$

ρ is an arbitrary parameter known as the penalty parameter. The penalty function φ is an arbitrary function of the interpenetration and its rate. It is emphasized that the weak form including the virtual power and the penalty term Eq. 6.55 is not an inequality form.

6.6.5 Contact interface

The contact interface used at simulations in this thesis is “General Purpose Contact Interface (Type 7)”. It is a fast search algorithm without limitations. With this interface, each node can impact one or more segments, on both sides, on the edges or on the corners of the segments. The only limitation to this interface concerns high impact speed and/or small gap. There is no limitation to the size of the spring stiffness factor. This is to avoid node penetrations larger than the gap size, removing problems that were associated with the other interfaces.

For these situations, the interface will continue to work properly, but the time step can decrease dramatically. That is why, this is recommended to have a good aspect ratio elements or a regular mesh to obtain reasonable results; however, it is not an obligation.

Type 7 interface allows sliding between contact surfaces. Coulomb friction between the surfaces is modeled. In type 7 interface a critical viscous damping coefficient is defined, allowing viscous damped sliding.

The friction on a surface may be calculated by two methods. The first method suitable for contact tangential velocity greater that 1 m/s consist in computing a viscous tangential growth by:

$$\Delta\vec{F}_t = C_t V_t \tag{6.56}$$

In the second method an artificial stiffness K_s is input. The change of tangent force F_t is obtained the following equation:

$$\Delta F_t = K_s \delta_t \tag{6.57}$$

where δ_t is the tangent displacement.

The normal force computation is given by:

$$F_n = K_s P + C \frac{dP}{dt} \tag{6.58}$$

where;

$$K_s = K_0 \left(\frac{Gap}{Gap - P}\right)$$

$$C = VIS_s \sqrt{2K_s M}$$

K_0 = Initial interface spring stiffness

VIS_s = Critical damping coefficient on interface stiffness

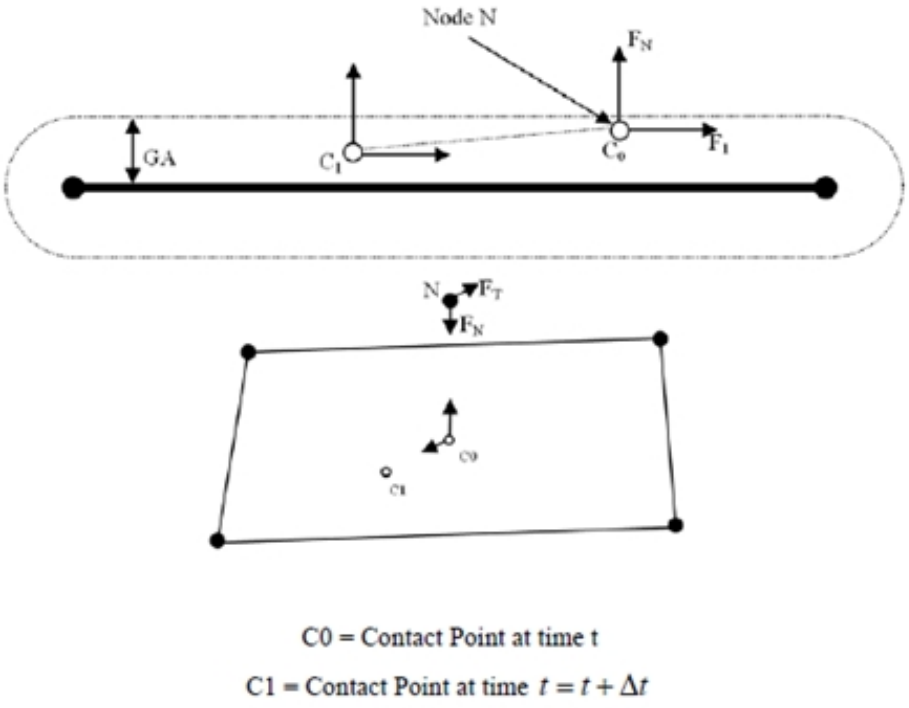


Figure 6.24 : Cloumb friction [60].

The tangential force computation is given by:

$$F_t = min(FRIC * F_n, F_{ad}) \quad \textbf{(6.59)}$$

where;

$F_{ad} = C_t V_t$

$C = VIS_s \sqrt{2K_s M}$

F_{ad} = adhesion force

VIS_F = Critical damping coefficient on interface friction

If the friction force is greater than the limiting situation, $|F_t| > \mu |F_n|$, the frictional force is reduced to equal the limit, $|F_t| = \mu |F_n|$, and sliding will occur. If the friction is less than the limiting condition, $F_t \leq \mu F_n$, the force is unchanged and sticking will occur.

Time integration of the frictional forces is performed by:

$$\vec{F}_t^{\,new} = \vec{F}_t^{\,old} + \Delta\vec{F}_t \quad \textbf{(6.60)}$$

where $\Delta\vec{F}_t$ is obtained from from Eq. 6.56 or Eq. 6.57.

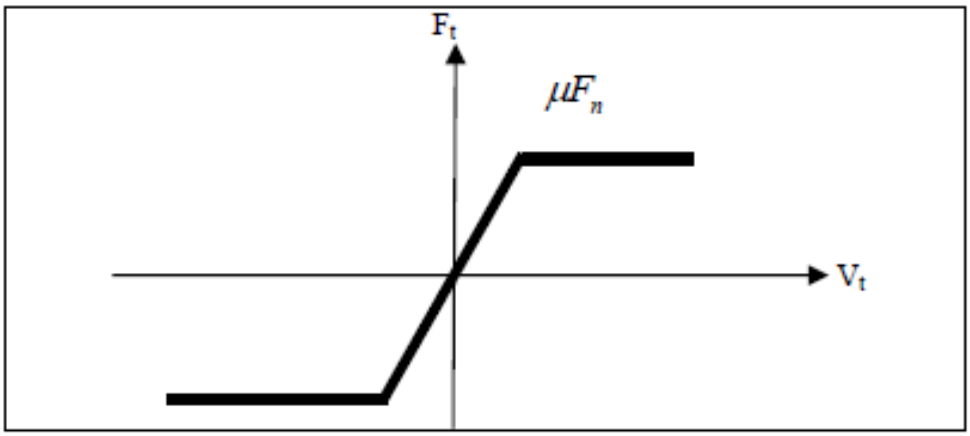


Figure 6.25 : Friction on type 7 interface [60].

All contacts at simulations in this thesis were defined as sliding contact with Interface Type 7. Interface Type 7 is a general purpose interface and can simulate all types of impact between a set of nodes and a master surface, especially buckling during a high speed crash. The search for the closest segment is done via a direct search algorithm; therefore, there are no search limitations and all possible contacts are found. The energy jumps induced by a node impacting from the shell edges are removed by the use of a cylindrical gap around the edges. The main advantage of interface type 7 is that the stiffness is not constant and increases with the penetration preventing the node from going through the shell mid-surface. This solves many bad contact treatments. Cloumb friction law was used as a friction formulation. This formulation provides accurate results in crash analysis. The friction coefficient between all parts was set to 0.2.

Contact interactions for contact pairs are defined as self-contact surfaces in FE model of the vehicle (see Figure 6.26). Contact interactions typically are defined by specifying self-contact for the default surface, which allows an easy, yet powerful, definition of contact. Self-contact for a surface that spans multiple bodies implies self-contact for each body as well as contact between the bodies. All surfaces can span multiple unattached bodies, so self-contact in this algorithm is not limited to contact of a single body with itself.

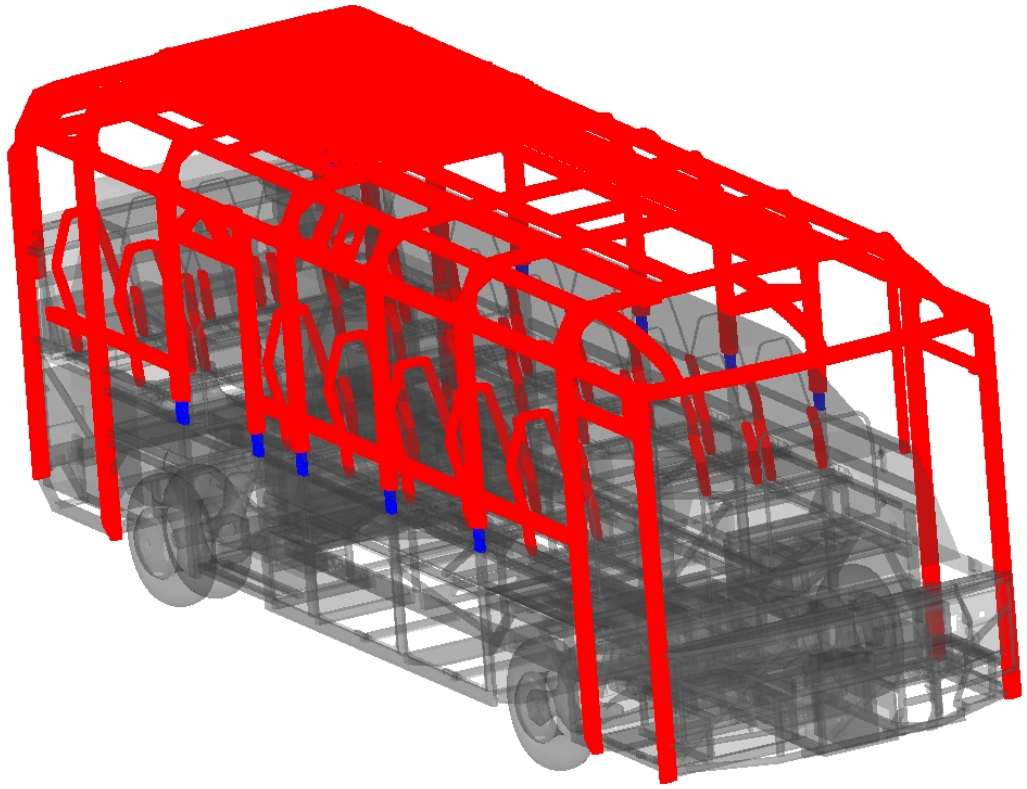


Figure 6.26 : Self-contact surfaces in FE model of the vehicle.

6.7 Kinematic Conditions of the Rollover Event

6.7.1 Boundary condition

6.7.1.1 Fixed rigid wall

A rigid wall is a flat surface defined by a normal vector, *n*. It may be of infinite extent in each direction, or may be finite in either or both in-plane directions. The rigid wall may be fixed in space, or may have a defined mass and initial velocity in the direction of the normal vector *n*.

Rigid walls are an inexpensive method for modeling unilateral contact (for example, contact between a deforming body and a rigid body) when the target surface is planar. Moving rigid walls can be useful in modeling pendulum impact tests.

A kinematic condition is applied on each impacted slave node. Therefore, a slave node cannot have another kinematic condition unless these conditions are applied in orthogonal directions. A fixed wall is a pure kinematic option on all impacted slave

nodes. It is defined using two points, M and M1. These define the normal, as shown in Figure 6.27.

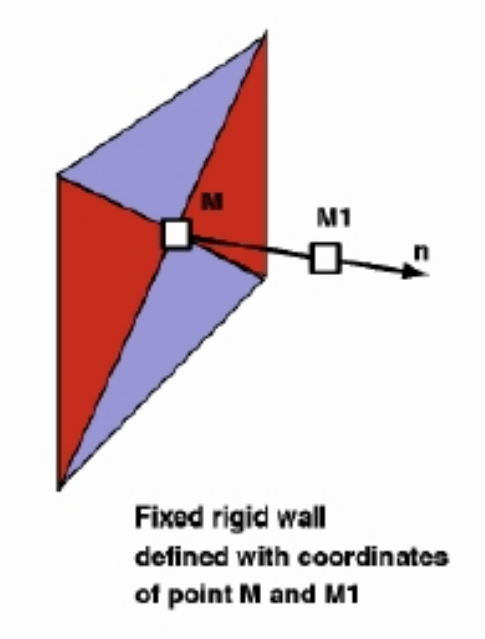


Figure 6.27 : Fixed rigid wall definition [60].

6.7.1.2 Slave node penetration

Slave node penetration is checked by software every time step. Figure 6.28 shows how penetration is checked. If penetration occurs, a new velocity must be computed. This new velocity is computed using one of three possible situations. These are:

- Sliding
- Sliding with friction
- Tied

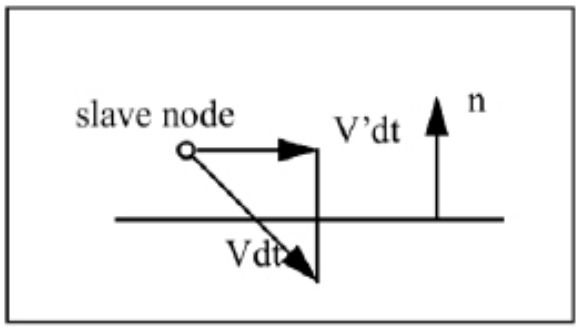


Figure 6.28 : Slave node penetration [60].

For a node which is allowed to slide along the face of the rigid wall, the new velocity $\overrightarrow{V'}$ is given by:

$$\overrightarrow{V'} = \vec{V} - (\vec{V}.\vec{n})\vec{n} \quad \textbf{(6.61)}$$

6.7.1.3 Rigid wall impact force

The force exerted by nodes impacting onto a rigid wall is found by calculating the impulse by:

$$\vec{I} = \sum_{i=I}^{N} \vec{F}_i \Delta t = \sum_{i=I}^{N} \Delta m_i \left(\vec{V}_i - \overrightarrow{W}\right) \quad \textbf{(6.62)}$$

where;

N is the number of penetrated slave nodes

$\overrightarrow{W}$ is the wall velocity

The force can then be calculated by the rate of change in the impulse:

$$\vec{F} = \frac{d\vec{I}}{dt} \quad \textbf{(6.63)}$$

6.7.1.4 Rigid wall modeling according to the ECE 66-02 regulation

The full-scale vehicle is standing stationary and is tilted slowly to its unstable equilibrium position. The rollover test starts in this unstable vehicle position with zero angular velocity and the axis of rotation runs through the wheel-ground contact points. At this moment, the vehicle is characterized by the reference energy. The vehicle tips over into ditch, having a horizontal, dry and smooth concrete ground surface with a nominal depth of 800 mm.

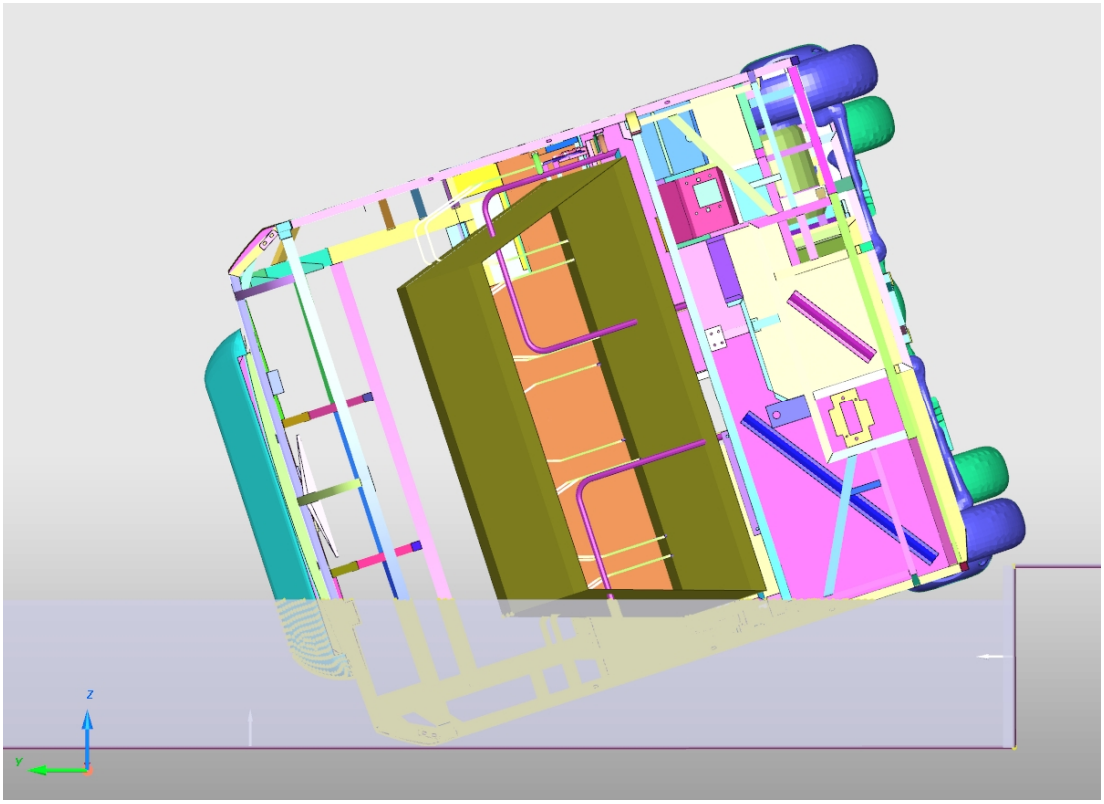


Figure 6.29 : Rigid wall modeling according to the ECE 66-02 regulation - 1.

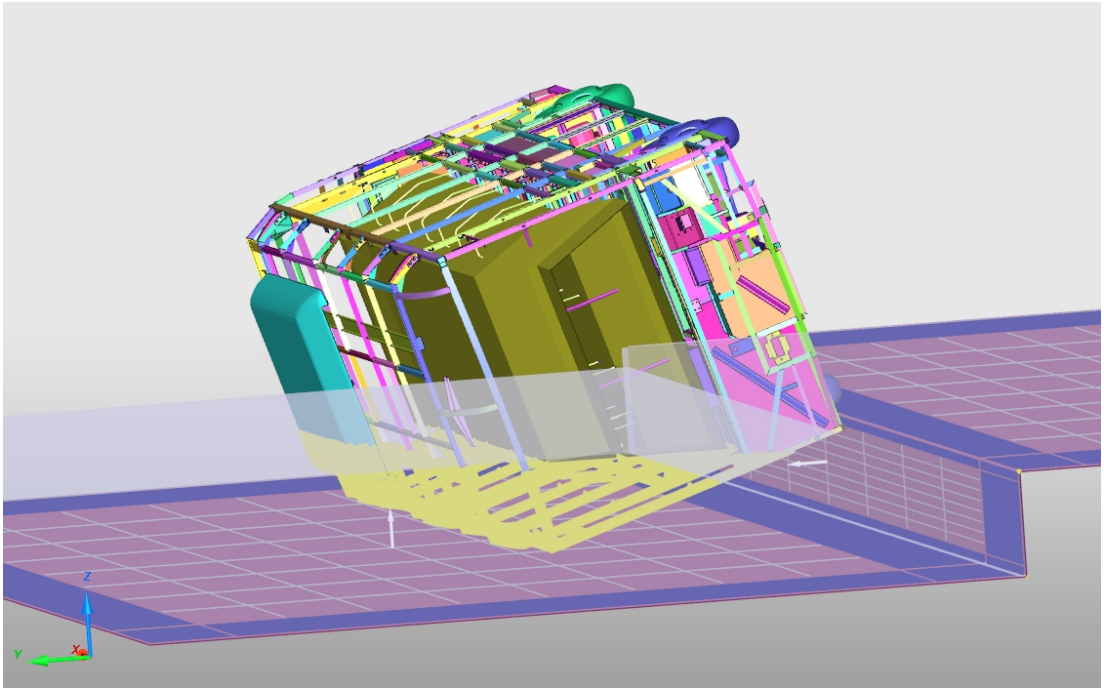


Figure 6.30 : Rigid wall modeling according to the ECE 66-02 regulation - 2.

6.7.2 Initial conditions

A transient dynamic problem requires the specification of initial conditions in order to be completely defined. In this simulation, initial conditions are specified as initial velocities and accelerations. All initial velocities and accelerations may be set to zero by setting a flag in the input, or the initial velocity and acceleration of every node or a subset of nodes may be explicitly defined.

The time variation of quantities in RADIOSS is specified by "load curves." An arbitrary number of load curves may be defined, and any number of boundary conditions or loads may reference one load curve. Each load curve may have an arbitrary number of points.

Nodes can be given prescribed velocities as a function of time in any global coordinate direction, or in an arbitrary direction specified by a given vector in RADIOSS. In cases where prescribed velocities at $t = 0$ are not equal to defined initial velocities, significant dynamic loads are induced in the model due to the incompatibility of boundary and initial conditions.

6.7.2.1 Gravity load

Density vs. depth curves are often used to initialize hydrostatic stresses arising in an element due to gravity acting on an overburden material. The hydrostatic pressure acting on a material point at a depth d_0 is given by;

$$p = -\int_{d_0}^{d_{top}} \rho\,(z) g\, dz \qquad \textbf{(6.64)}$$

where p is pressure, drop is depth at the top of the material to be initialized, $\rho\,(z)$ is the mass density at depth z, and g is the acceleration of gravity. This integral is evaluated numerically for each material to be initialized.

6.7.2.2 Initial angular velocity

The transient dynamic analysis of rotating bodies often requires to initialize velocities for some part of the model to be consistent with rotation about an arbitrary axis. RADIOSS allows initial velocities to be computed for a subset of elements composing a model based on a given angular velocity vector through the origin. This feature is activated by specifying the number of elements to receive velocity

initialization, and then giving the angular velocity and list of rotating elements. If static initialization (via a stress initialization file or via a static dynamic relaxation solution) has been performed, then the initial velocities computed with this option are evaluated on the statically deformed geometry.

Elements are initialized for rotational motion by computing initial velocities from $v = w \, x \, r$ for all nodes of all elements using the listed materials. If static initialization is used (via either input from a stress initialization file or dynamic relaxation in RADIOSS), r is evaluated using the post-initialization geometry.

Body force loads due to the angular velocity are always calculated with respect to the deformed configuration, and act radially outward from the axis of rotation. Torsional effects arising from changes in angular velocity are not included. Angular velocity is assumed to have the units of radians per unit time.

The body force density b at a point P in the body is calculated from;

$$b = \rho \, (\omega \, x \, \omega \, x \, r) \qquad \textbf{(6.65)}$$

where p is the mass density, ω the angular velocity, and r is a position vector from the origin to point P. Although the angular velocity may vary with time, the effects of angular acceleration are not included in this formulation.

This feature is useful for studying transient deformations of three-dimensional objects which are rotating about any axis of rotation through the global origin. Typical applications of this feature could include modeling the deformations of a tire spinning about an axle, or the impact of a foreign object on a rotating object rapidly about its own axis.

The position of the vehicle in unstable equilibrium at point of rollover, and the position at first contact with the ground is specified at Figure 6.31 and Figure 6.33. The simulation is started at the point of first contact with the ground. The initial conditions at the point of first contact with the ground are defined using the change of potential energy from the unstable equilibrium position.

The total energy according to formula indicated in the ECE 66-02 regulation:

$$E^{*} = 0.75\ M\ g\ \Delta h \qquad \textbf{(6.66)}$$

where M is the unladen kerb mass of the vehicle structure and %50 of the total occupant mass, g is the gravitational acceleration and $\Delta h = h_{CG\ I} - h_{CG\ II}$ [1]. The total energy is applied to the structure by an angular velocity to all the parts of the vehicle.

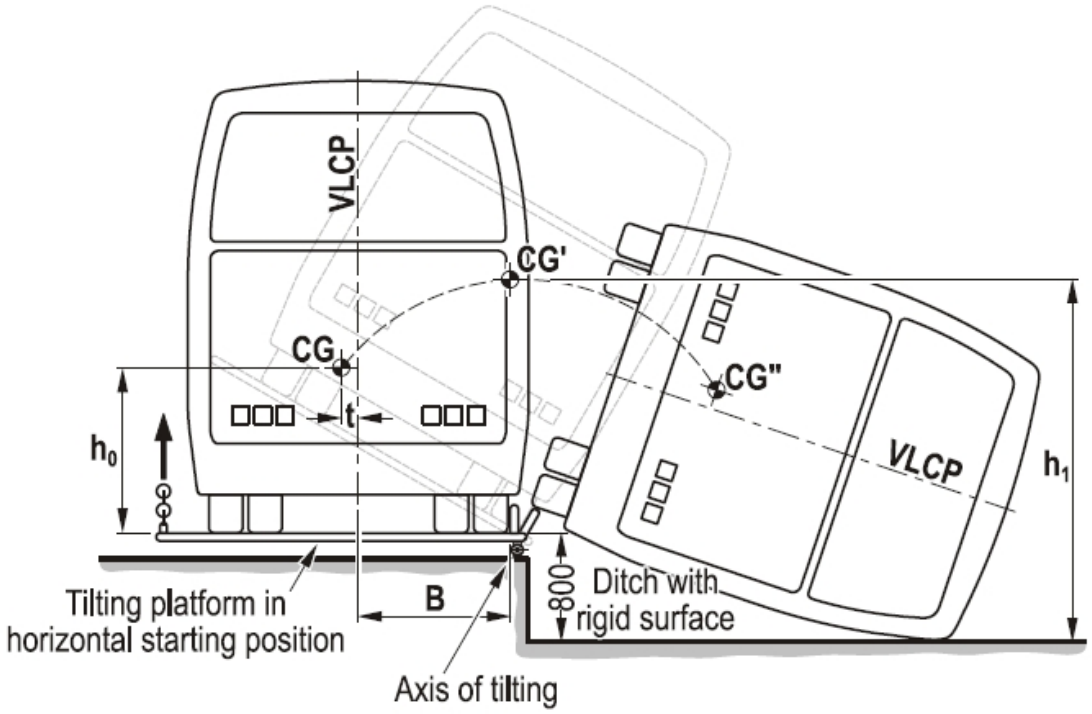


Figure 6.31 : Rotation of the vehicle to the point of first contact with the ground - 1 [1].

The height difference between the horizontal lower plane of the ditch and the plane of the tilting platform on which the bus is standing, shall be 800 mm. The tilting platform, related to the ditch, shall be placed as follows (see Figure 6.32):

- The axis of its rotation is 100 mm from the vertical wall of the ditch;
- The axis of the rotation is 100 mm below the plane of the horizontal tilting platform.

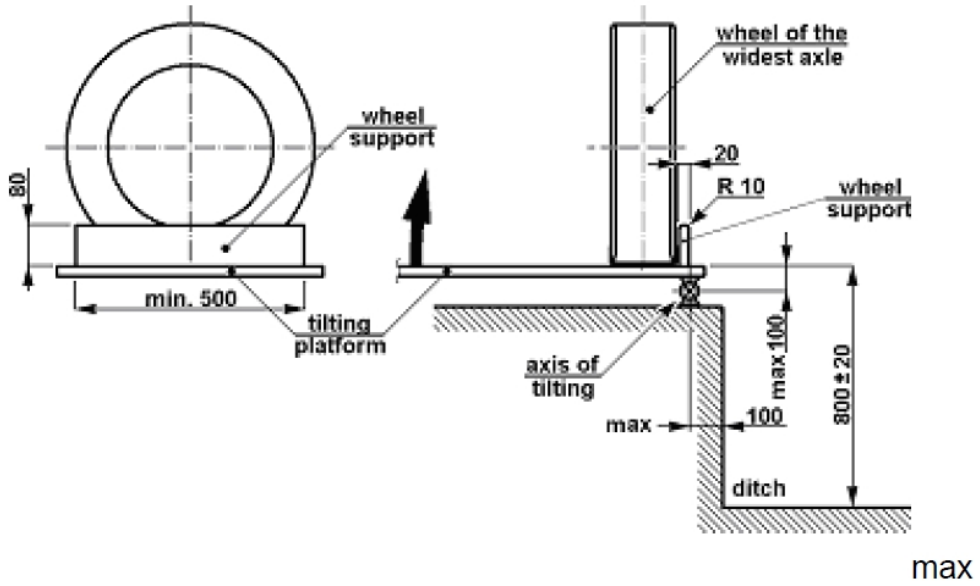


Figure 6.32 : Geometry of the tilting bench [1].

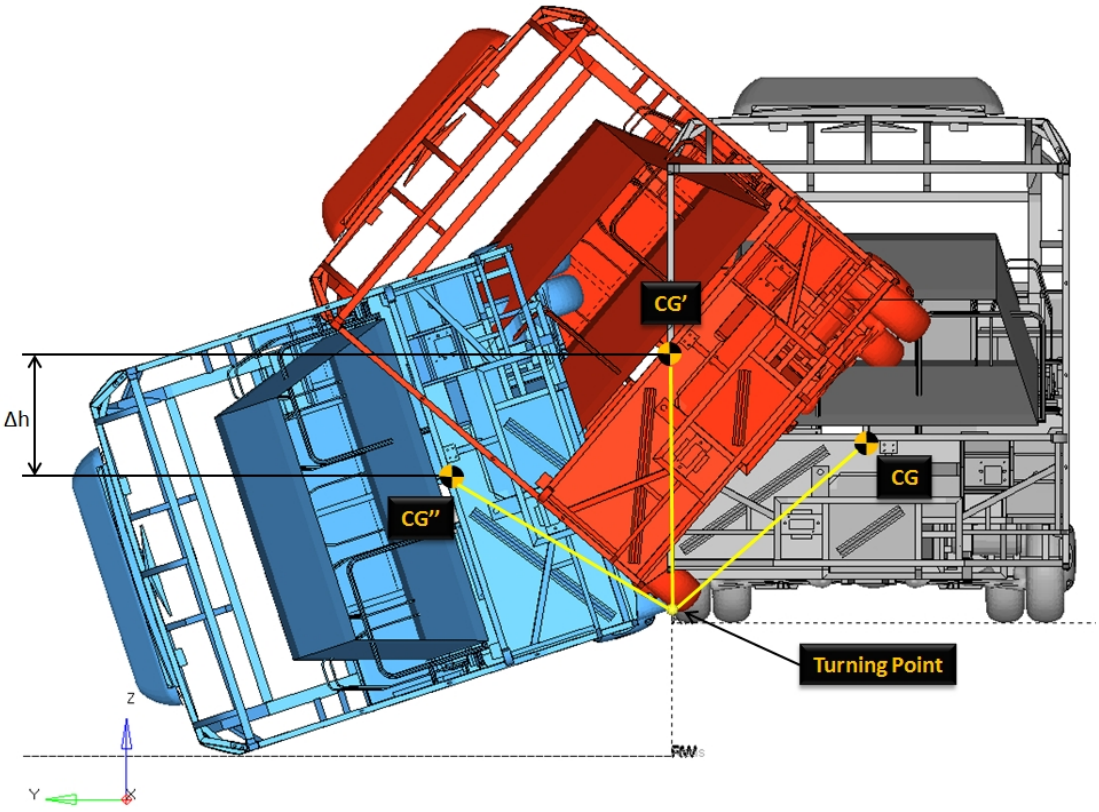


Figure 6.33 : Rotation of the vehicle to the point of first contact with the ground - 2.

6.8 Time Step

Many of the time step control options influence the solution results. The solution of the nonlinear dynamic response of a finite element system accurate is the numerical model represents correctly the physical model. The critical time step given for finite element system is determined by a theoretical approach in which the highest frequency of the discretized system controls this value. Therefore, the time step limitations are related to the model and cannot be changed without incidence on the quality of results.

Generally, in the study of the nonlinear dynamic response of a system, three physical laws have to be respected:

- Conservation of mass,
- Conservation of energy,
- Conservation of momentum dynamic equilibrium.

The last one is generally respected as the equation of motion is resolved at each resolution cycle. However, in the case of adding masses especially when using /DT/NODA/CST option, it is useful to verify the momentum variation. The two other conservation laws are not explicitly satisfied. They should be checked a posteriori after computation to insure the validity of the numerical model with respect to the physical problem.

The time incrementation in RADIOSS is fully automatic and *a priori* requires no user intervention. The step used for time integration (or moving forward in time) can be calculated using two different methods. The method used depends on the type of simulation being performed.

The two time step methods are:

- The element time step
- The nodal time step

The time step used by the solver is the largest possible time step, as determined by the Courant condition that will maintain stability. If the default large strain formulation is used, the time step is computed at each cycle. Large element

deformation can give a large time step decrease. If the deformation is too large, negative volumes can result, which make it impossible to invert the Jacobian matrix and to integrate the stress over the volume. If the small strain formulation is used, assuming a constant Jacobian matrix during time and also a constant volume, all spatial variables are defined at $t = 0$. This is either the beginning of the analysis or the time at which the small strain formulation is initiated. If the sound speed is constant, the time step thus becomes constant. Using this formulation, the time step has no effect on the computation since the initial volume is used.

6.8.1 Element time step control

The element time step is computed at the same time as the internal forces. The characteristic length and the sound speed are computed for each element in every cycle. The computed time step is compared to a minimum time step value and a scale factor is applied to insure a conservative bound. Different minimum time step values can be given to different element types.

The stable element time step:

$$\Delta t = min_{Elements} \left(\frac{l}{c}\right) \quad \textbf{(6.67)}$$

where;

l is the element characteristic length,
c is the speed of sound in the material.

If deformation is large enough for the time step to reach the minimum defined value, three options are possible under the user's control:

- Stop the analysis when the minimum time step value is reached. This is the default for brick and quadrilateral elements.
- Delete the element(s) defining the time step. This is the default for shell elements.
- Implement small strain formulation using a constant time step. This only works for shell and brick elements.

6.8.2 Nodal time step control

The nodal time step is calculated after the computation of all the internal forces at each node using the following equation:

$$\Delta t = min_{Nodes} \sqrt{\frac{2m}{k}} \quad \textbf{(6.68)}$$

where *m* is the nodal mass and *k* an equivalent nodal stiffness.

The nodal stiffness is one half of eigenvalue from element stiffness matrix; for a truss element this value is equal to the diagonal term of the stiffness matrix. It is computed from the accumulation of element and interface stiffnesses. These stiffnesses are obtained during internal force computation.

As for the element time step, minimum time step and scale factors are required. The default value is for the scale factor is 0.9, however, the scale factor is used as 0.67 at simulations in this thesis for better stabilization, which is recommended in literature, too.

If the minimum time step is reached, either the analysis can be stopped or a mass scaling formulation can be applied. In this latter case, mass is added to the affected nodes so that the time step remains constant at the minimum value. This option can be enabled using the same third keyword as used in the element time step control. It must be checked that added masses do not affect the accuracy of results.

6.9 Parallel Computation

The rollover and validation simulations were performed with SMP parallel processing algorithm of RADIOSS. The simulations were run at Dell 64-bit workstation with Intel Xeon CPU E5-2650 0 @ 2.00 GHz 2 processors and 32 GB RAM. The processors have 8 number of cores and 16 number of threads. The rollover simulation time interval was set to 0.25 second. The simulation was run approximately 66 hours of clock time. The vehicle was showed the maximum deformation before the simulation time interval. It can be admissible for enough amount of information at simulation results.

Analysis of systems with high number of d.o.f., the use of shared memory parallel machine architectures is common. At simulation in this thesis with RADIOSS, SMP (Shared Memory Processors) model of parallel programming is used. SMP makes possible the exploration of shared memory on processors.

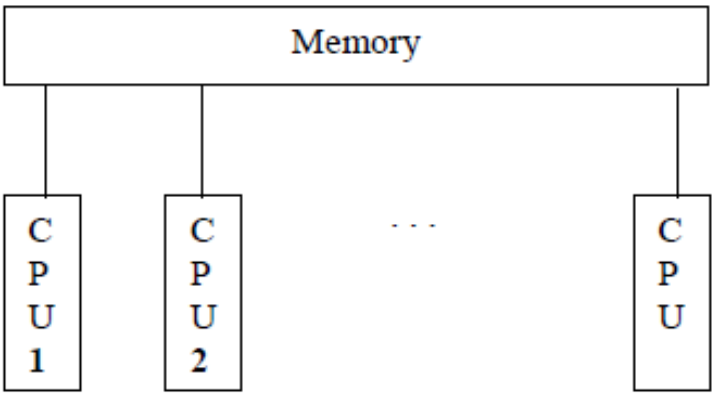


Figure 6.34 : Architecture of shared memory [60].

In this case, all processors can access to a common memory space. From programming point of view, each process called parallel task, reach to the entire memory space allocated by the program. It is necessary to manage properly the access to this shared memory by introducing barriers and locking mechanisms. The SMP model programming has the advantage to be managed easily. However, the performance of the method depends on the ratio between the memory access speed and the CPU speed.

The parallelism approach used in RADIOSS SMP is a multi-task programming type. The tasks are explicitly managed by the programmer. The computation tasks are attributed to the processors by a dynamic procedure as they are available. This approach is especially adapted to the super-computers used as computation server where the load of a given processor varies with respect to others. The SMP version is developed for computers with shared memory architecture and cannot be used efficiently on the super-computers with distributed memory or cluster structures.

7. RESULTS

The first contact with the ground took place along the cantrail like other severe rollover accidents. Assuming the most frequent case of a pure lateral roll on reasonably even ground the load would be distributed along the whole cantrail. The time interval between the first contact with the ground and start of collapse (period of elastic-plastic deformations) is very short. Uneven distribution of the roof lateral stiffness may cause uneven ground reaction forces along the cantrail. However, it is very unlikely that these uneven and transient forces could disturb the rolling axis of the heavy vehicle rolling with maximum momentum. The inertia resisting this action is particularly great because it refers to rotation about lateral axes of greatest moments of inertia. It is argued therefore that under the assumed conditions the whole cantrail should start moving laterally by the same amount. Of course, during roll and particularly after the coach finishes on its roof these deflections may become different depending on the strength distribution. The previous experience indicates also that the collapse mode is not altered if the increase of all external loads is not exactly proportional.

In Figure 7.1, sequential pictures from the simulation results for selected time steps are illustrated. Firstly, the vehicle comes into contact with ground, then starts absorbing energy by elasto-plastic deformation, and bends at the plastic hinge zones. After sufficient deformation occurs, the vehicle starts sliding and springback occurs at pillars.

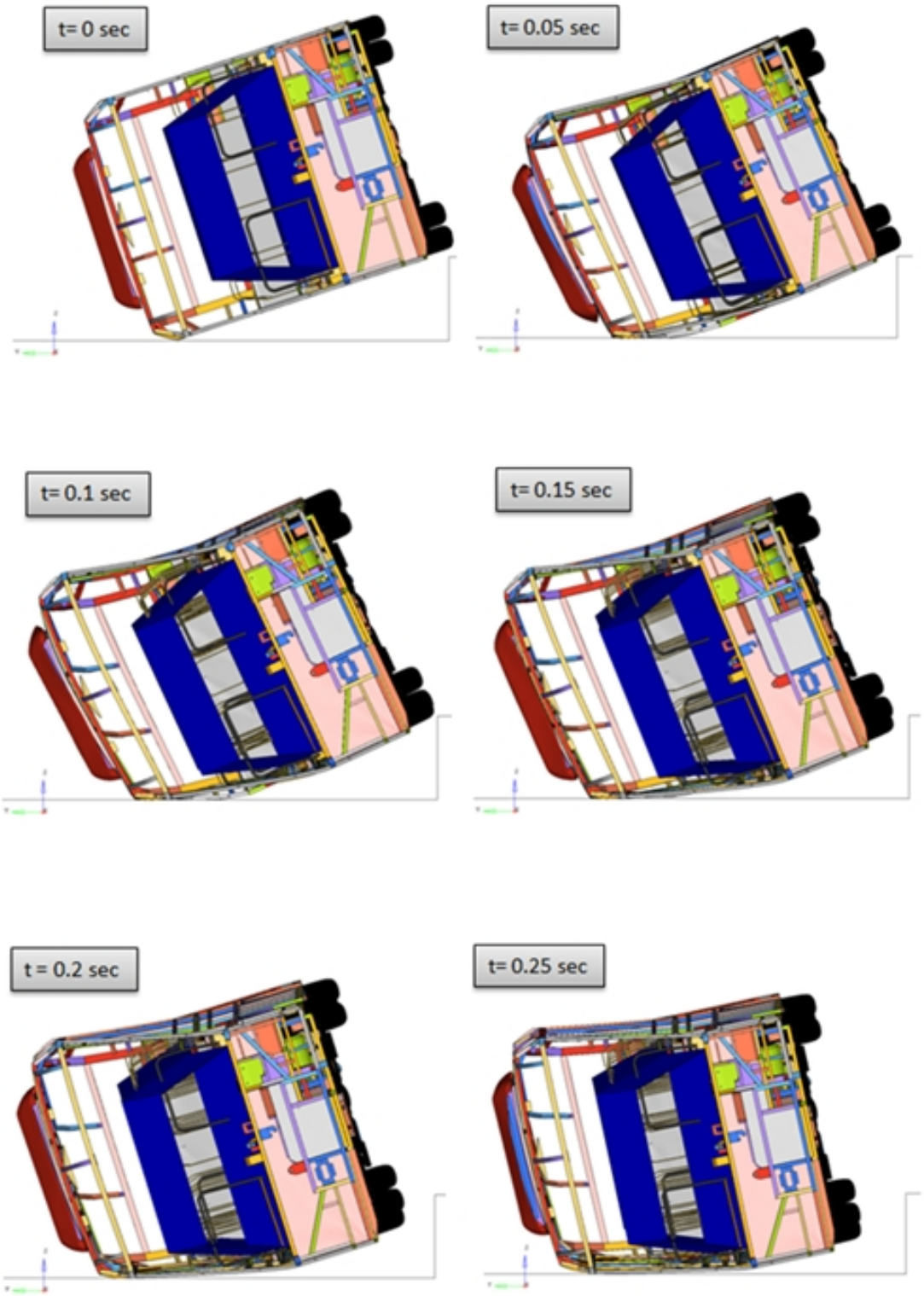


Figure 7.1 : Sequential pictures showing behavior of deformation of the vehicle through the time steps.

Figure 7.10 and 7.11 show the peaks dynamic deformed shape front and rear section of the vehicle structure. During the simulation, it was observed that the vehicle side structure does not intrude into residual space envelope. It was also observed that considerable amount of elastic energy is stored in elastic deformations of the structure and later released after sliding of the vehicle on the ground.

As seen in the graphics, the nearest pillars to the residual space are which are surrounding the doors. Deformation increases in the door area, which is because of no continuity of the cross connections between pillars. Bay sections of the coach structure are illustrated at Figure 7.2.

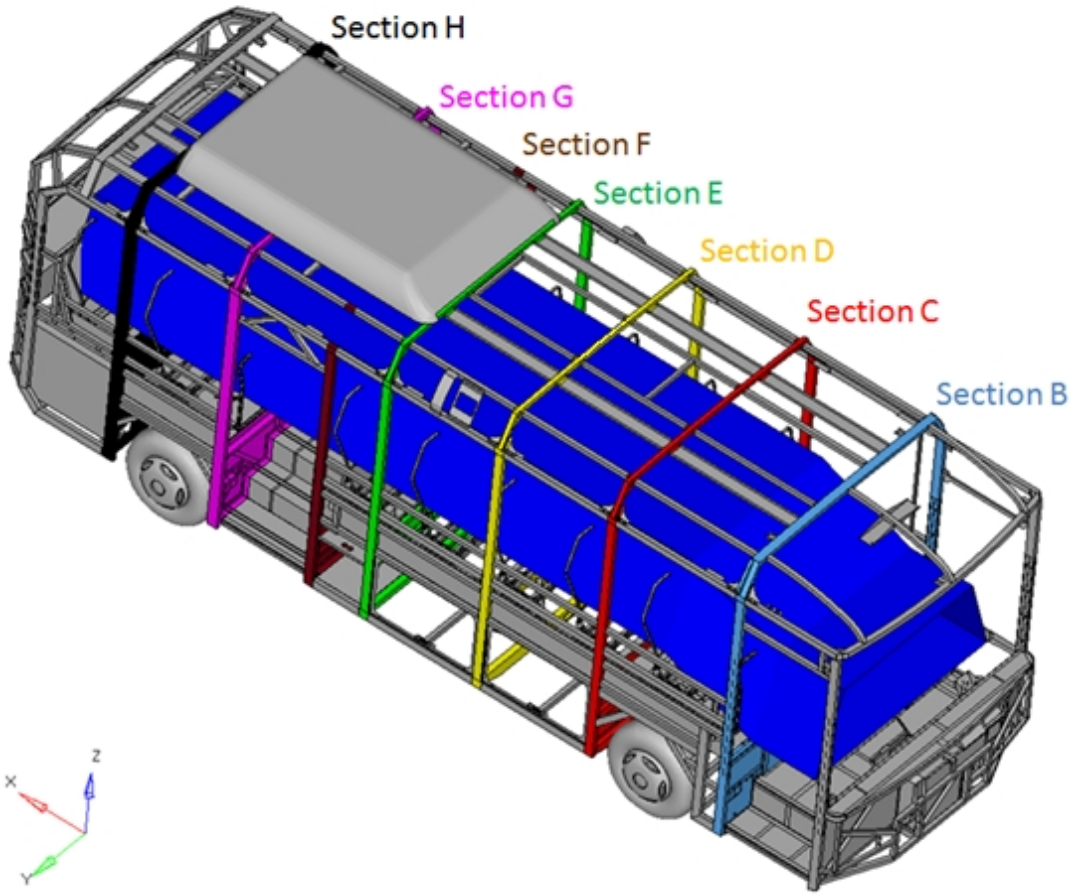


Figure 7.2 : Bay sections of the coach structure.

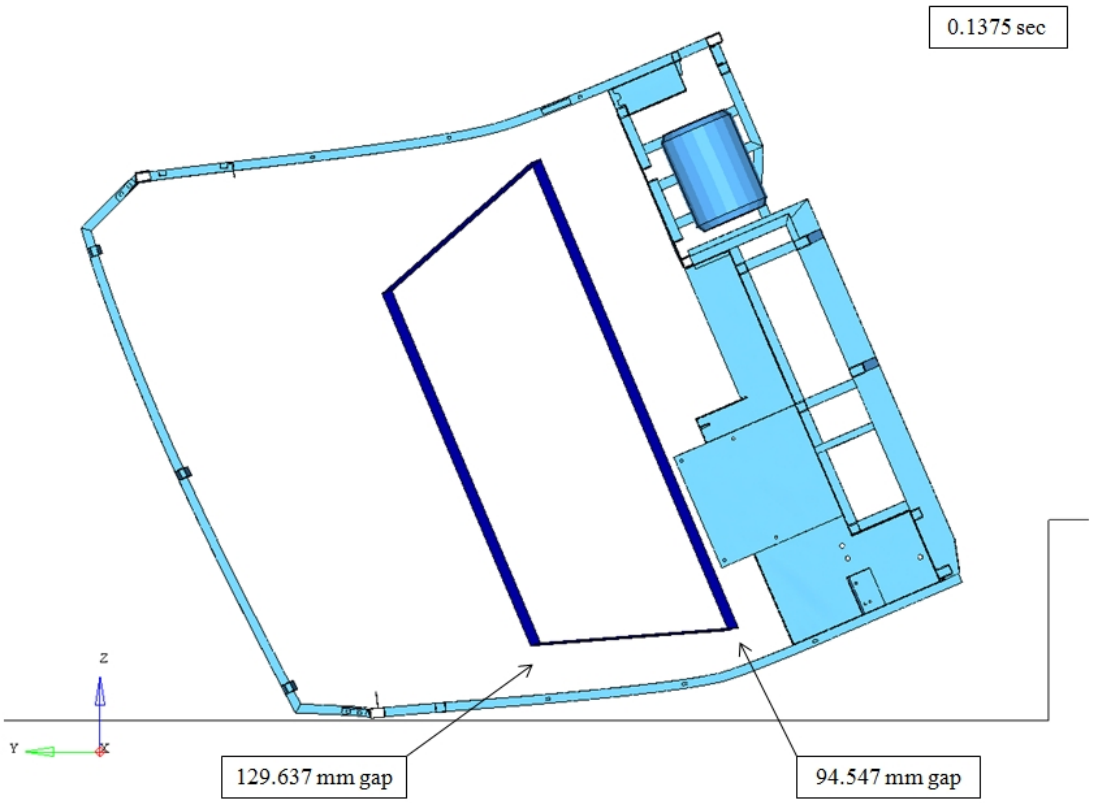


Figure 7.3 : Maximum deformation at Section B at 0.1375 second.

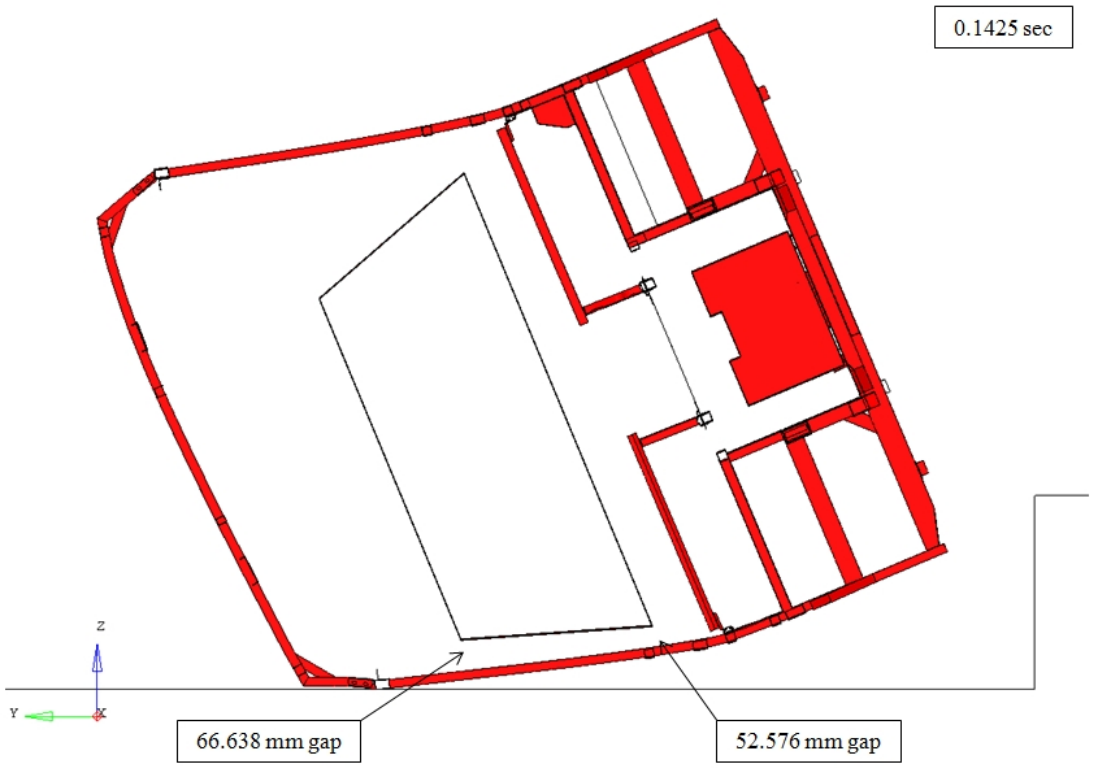


Figure 7.4 : Maximum deformation at Section C at 0.1425 second.

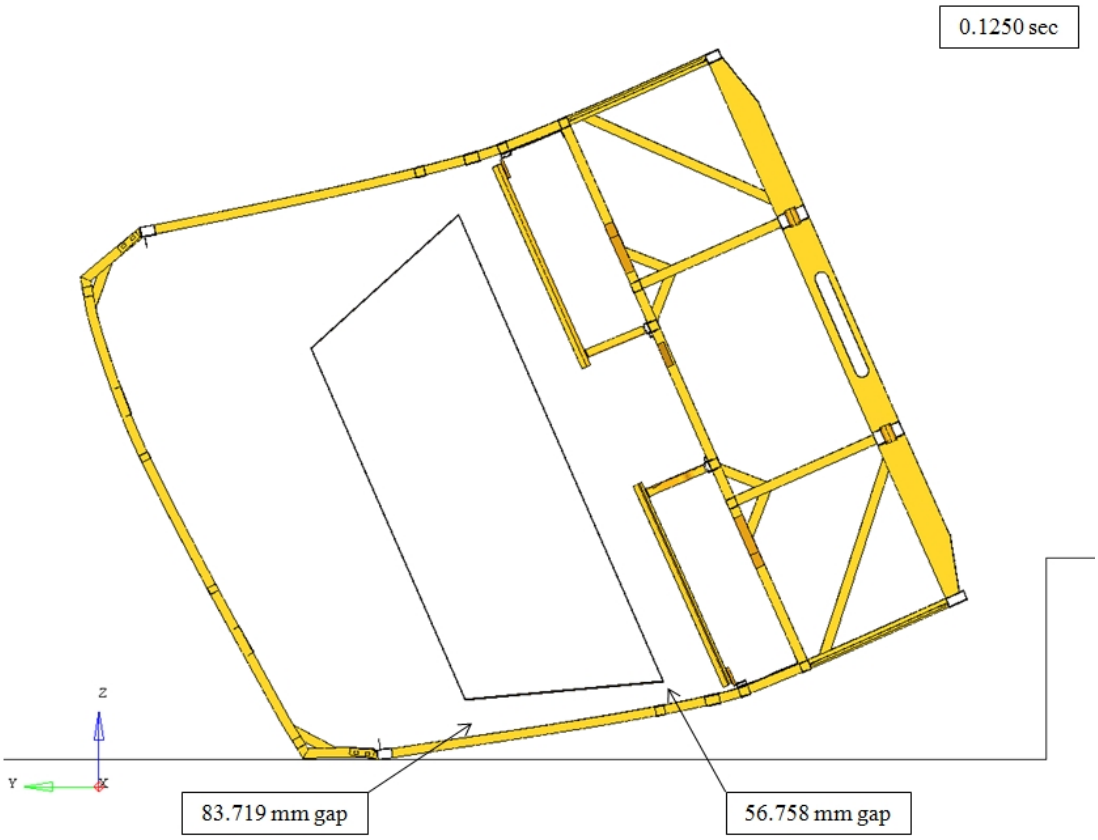


Figure 7.5 : Maximum deformation at Section D at 0.125 second.

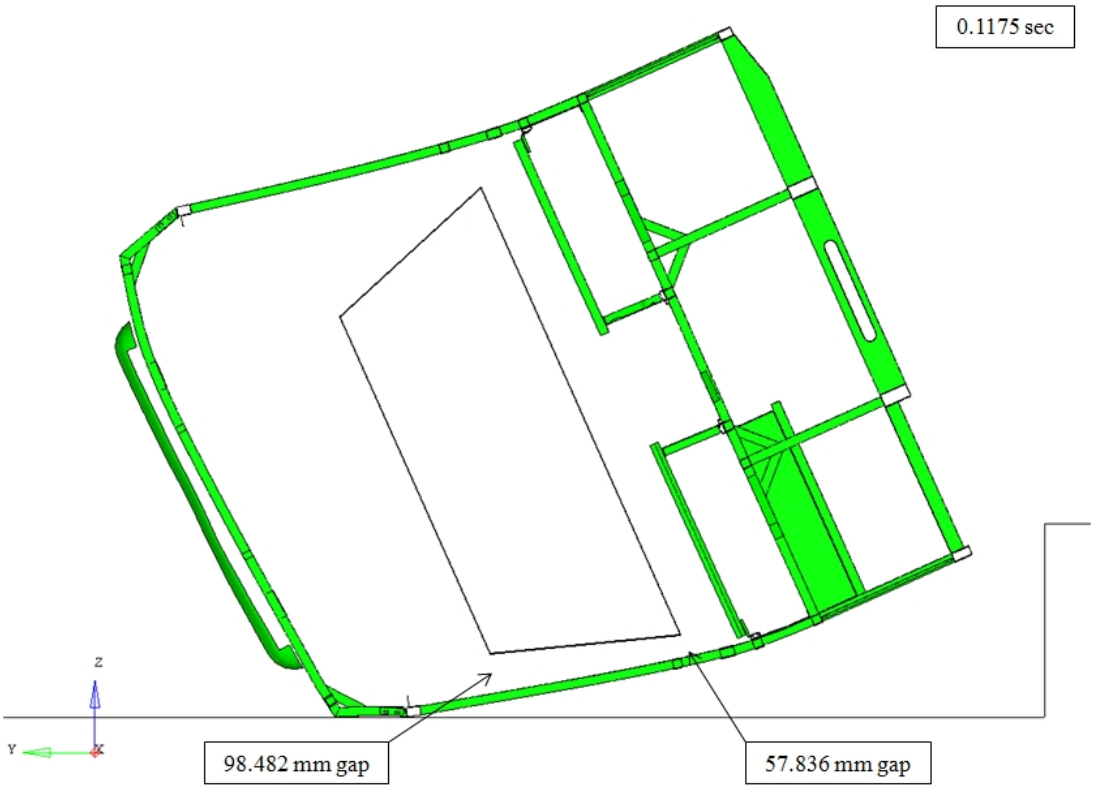


Figure 7.6 : Maximum deformation at Section E at 0.1175 second.

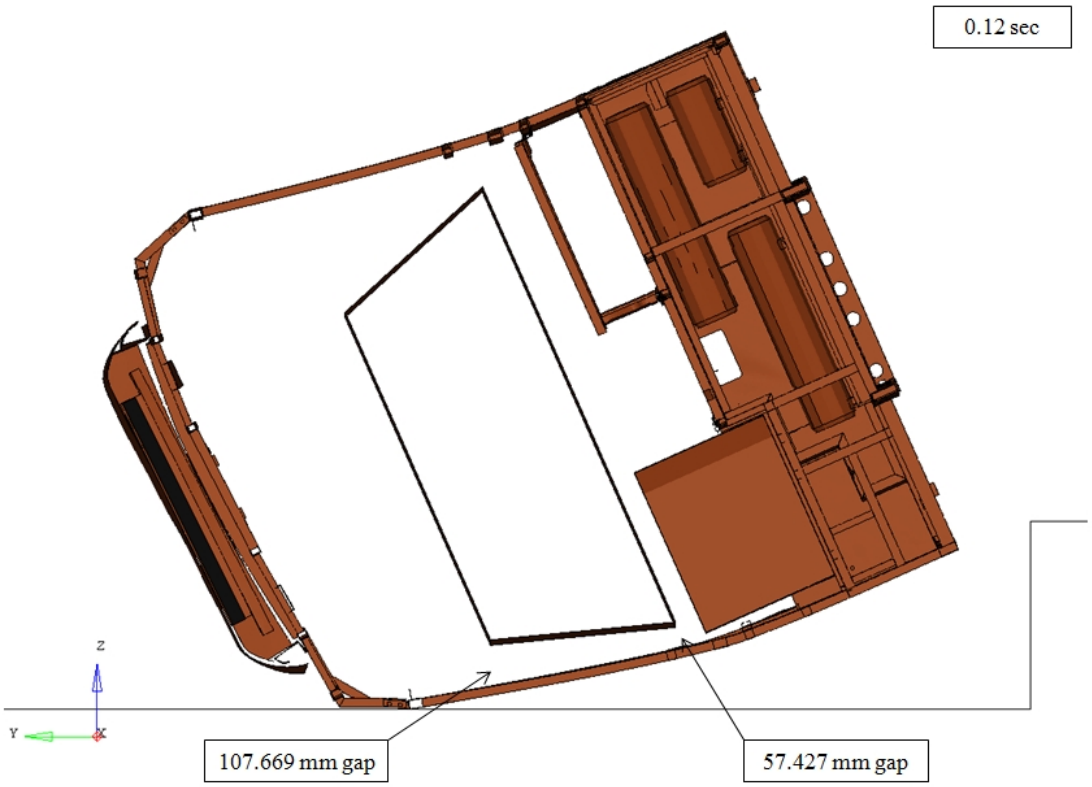


Figure 7.7 : Maximum deformation at Section F at 0.12 second.

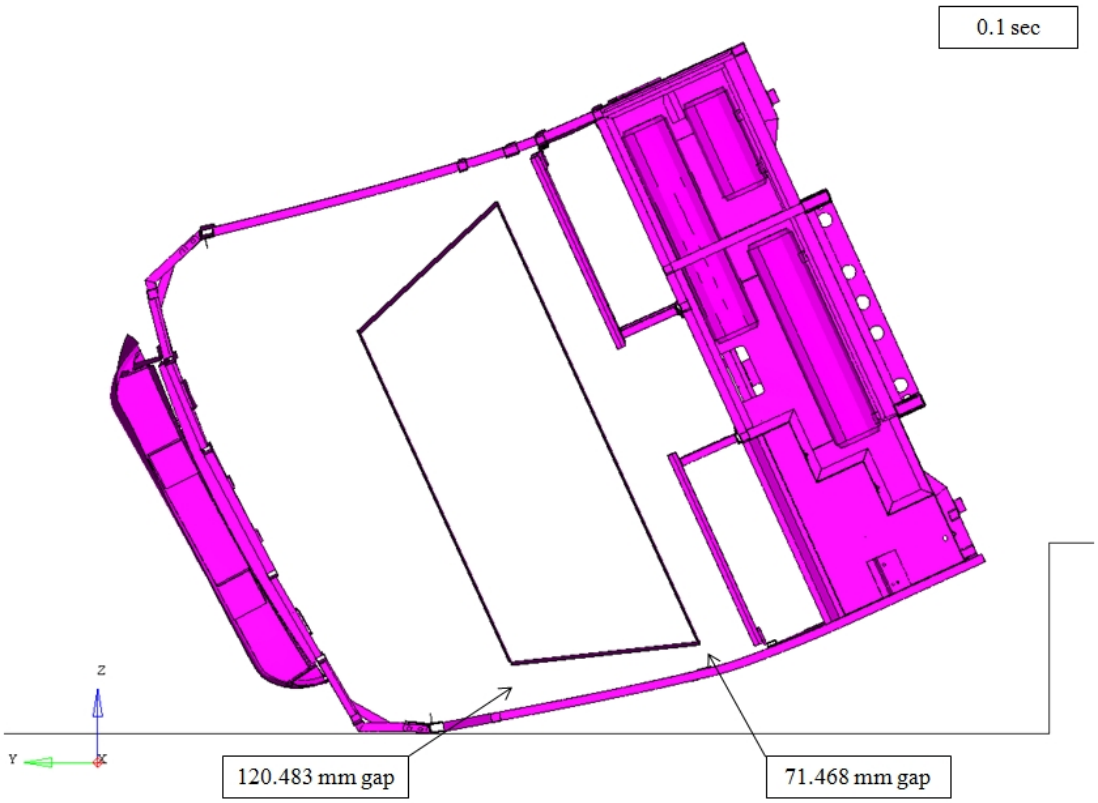


Figure 7.8 : Maximum deformation at Section G at 0.1 second.

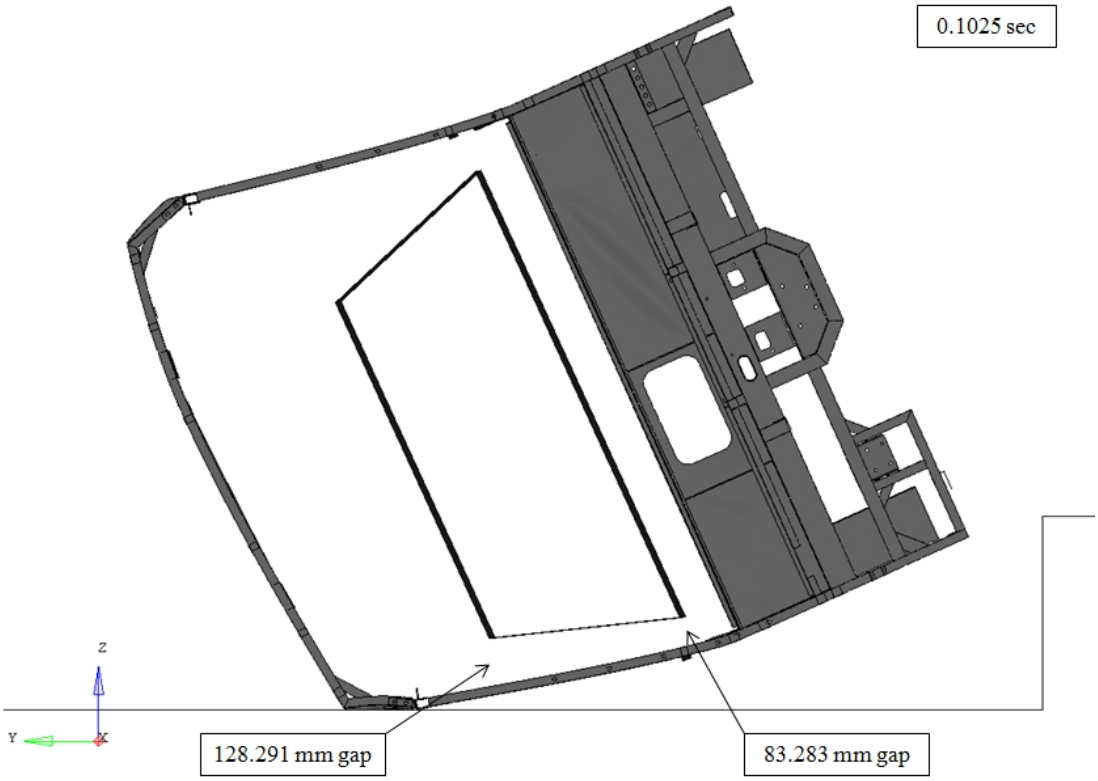


Figure 7.9 : Maximum deformation at Section H at 0.1025 second.

Table 7.1 : Maximum relative displacement between edge of residual space and pillars of the vehicle with respect to factor of correlation [mm].

Bay Section	B	C	D	E	F	G	H
Upper Edge	129.637	66.638	83.719	98.482	107.669	120.483	128.291
Lower Edge	94.547	52.576	56.758	57.836	57.427	71.468	83.283

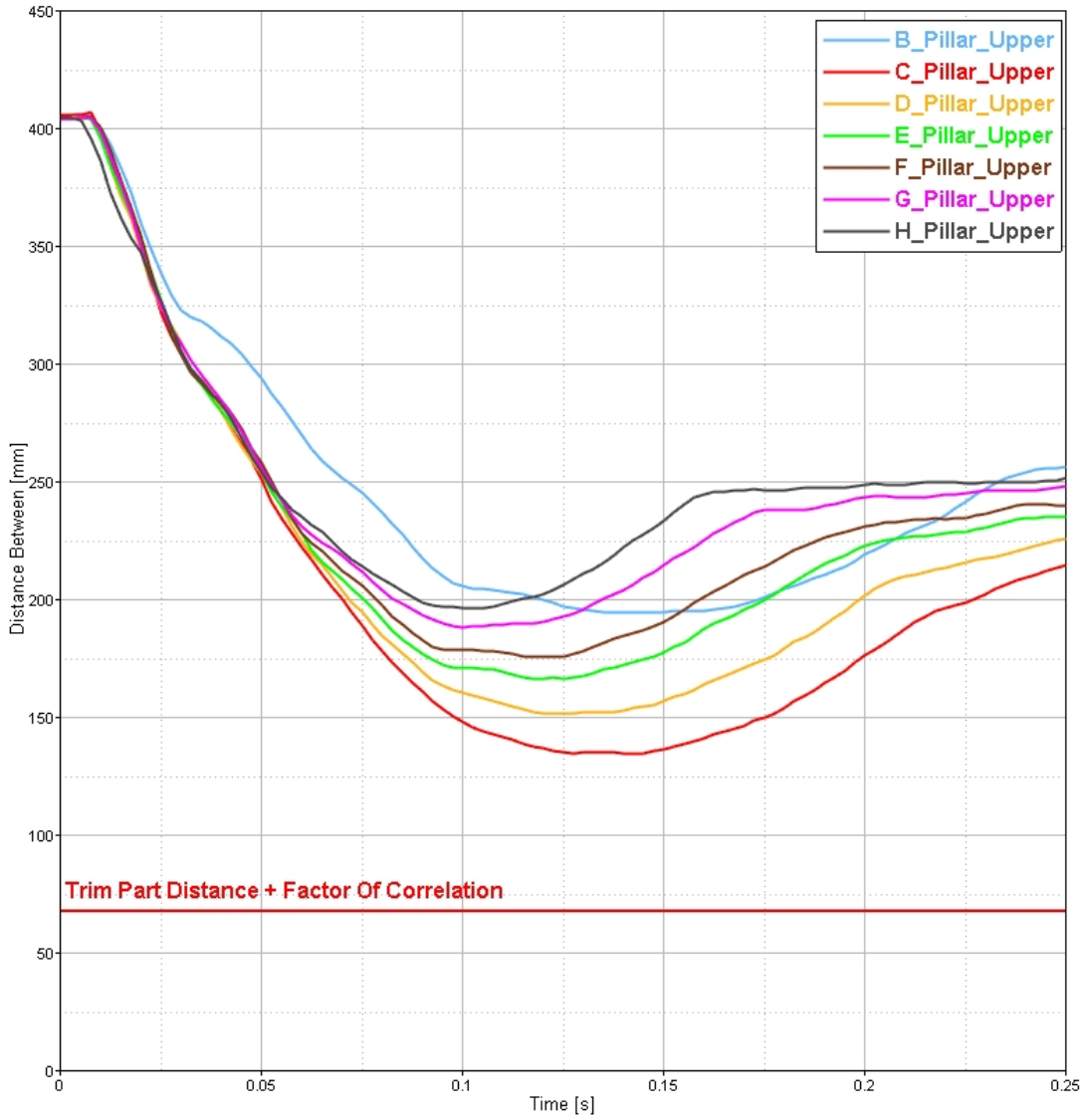


Figure 7.10 : Distance between upper edge of the residual space and pillars of the vehicle.

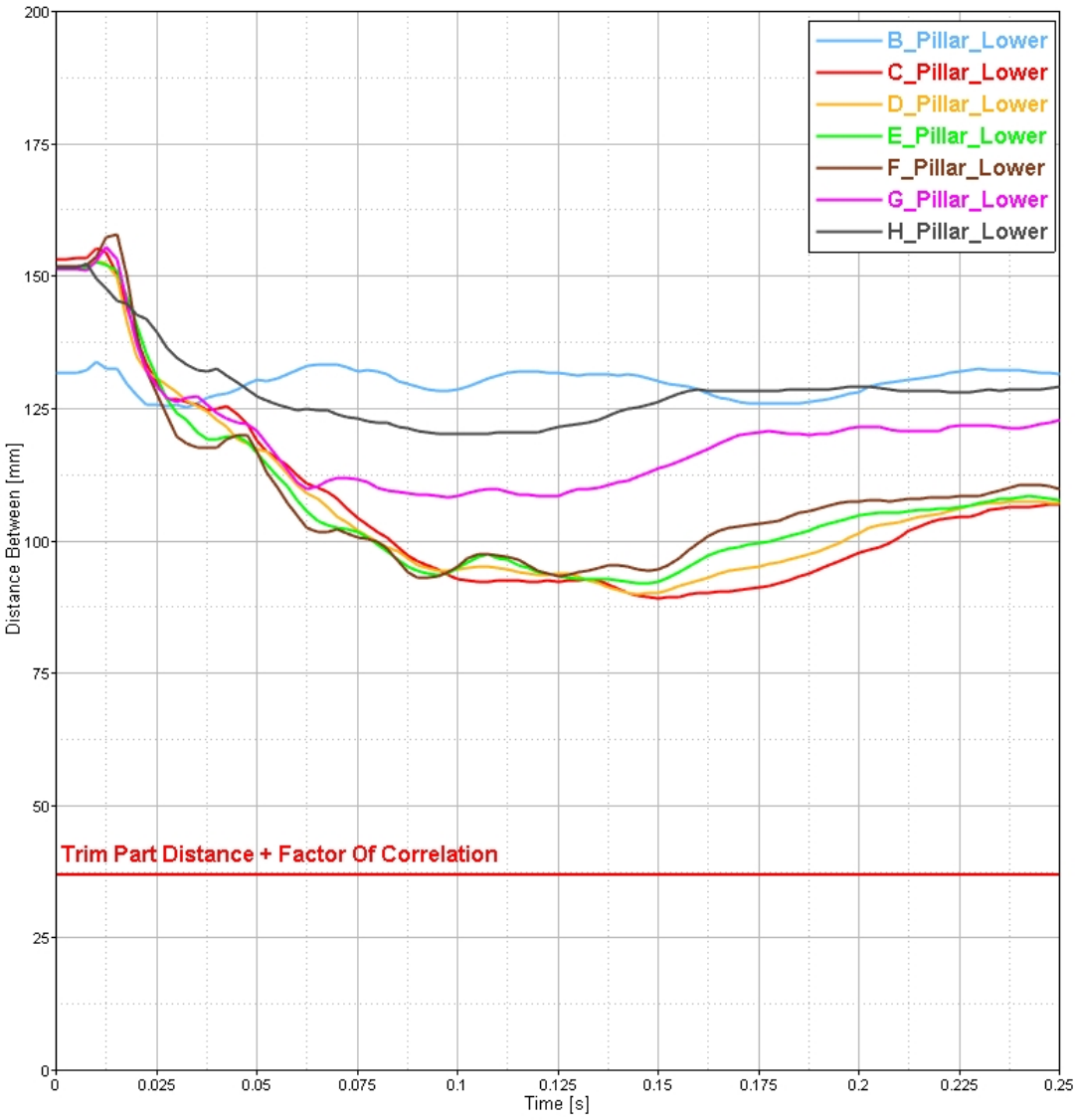


Figure 7.11 : Distance between lower edge of the residual space and pillars of the vehicle.

From the simulation, it has been possible to come to the following conclusions. First, the structure of coaches and body sections can be divided into two parts, the upper part (i.e. the passengers' compartment above the floor) and the lower part (below the floor). Only the upper part of the structure undergoes large deformations, whereas the lower part is practically not deformed. This happens owing to the presence of crossbars and other elements in the lower part of the structure, which make it much stiffer than the upper one. Second, these deformations develop only in some localized areas of the window and roof pillars that are bended in the transversal direction of the vehicle, whereas the other parts of the pillars remain substantially not deformed. Because of the rollover, two plastic hinges were developed in each window pillar during the bending process, one just above the floor plane and the other one just below the roof (see Figure 7.14).

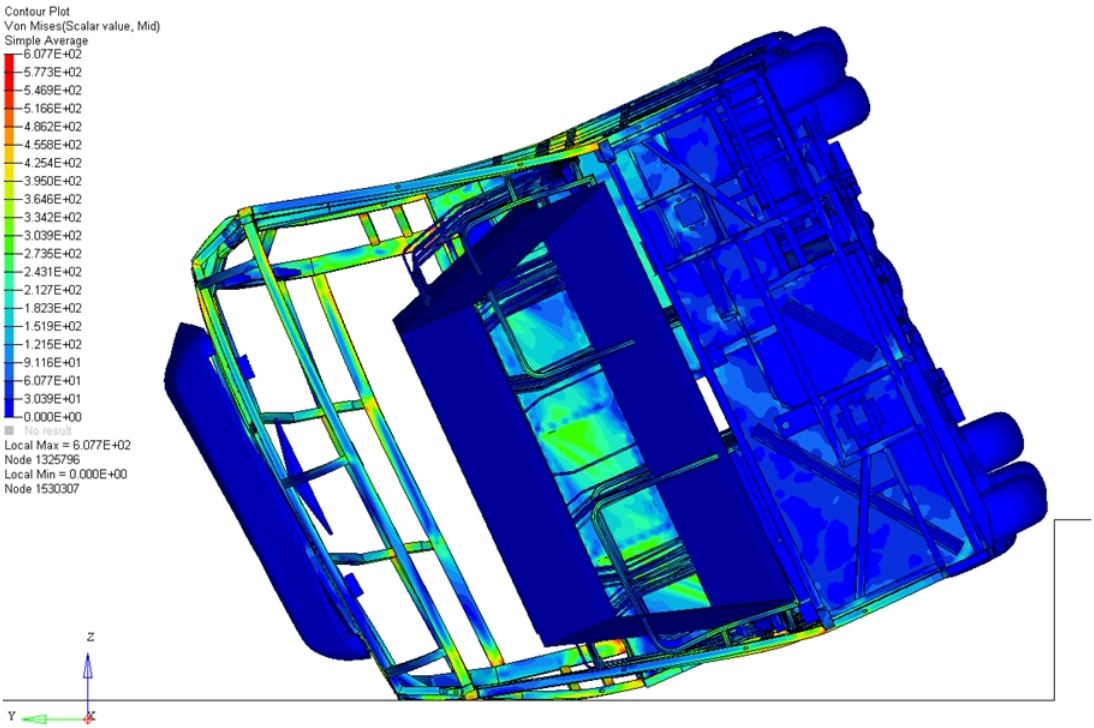


Figure 7.12 : Contours of von Mises stress distribution for maximum stress value from front view of the vehicle.

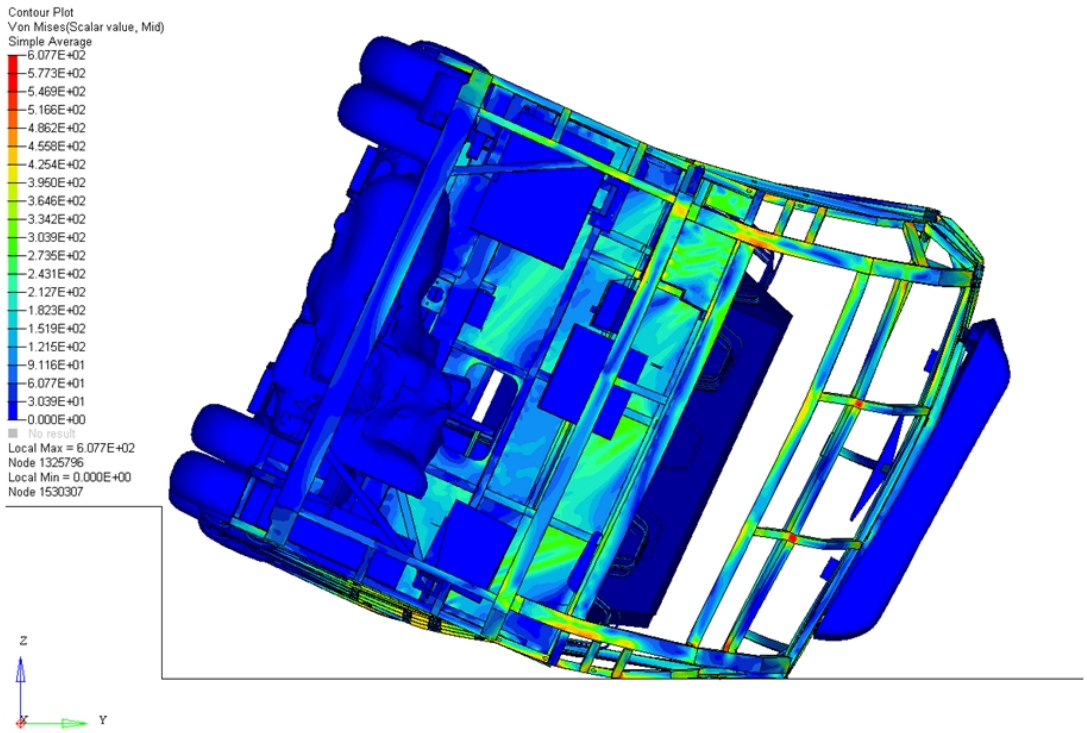


Figure 7.13 : Contours of von Mises stress distribution for maximum stress value from rear view of the vehicle.

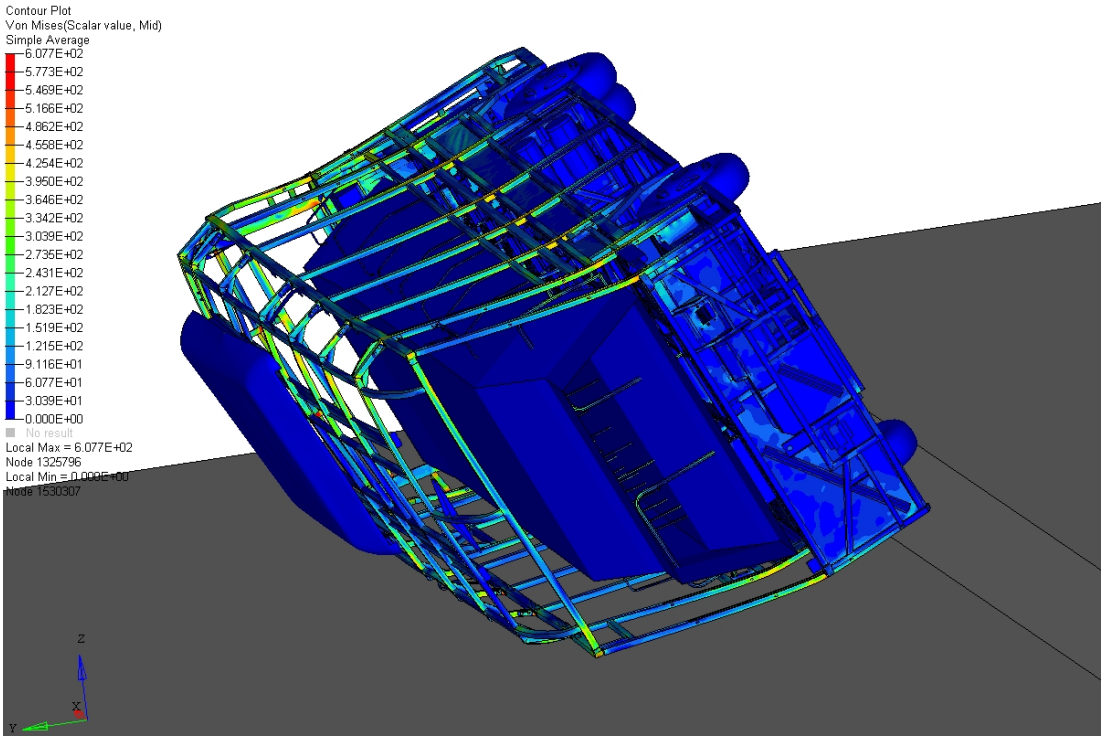


Figure 7.14 : Contours of von Mises stress distribution for maximum stress value from general view of the vehicle.

Large distortion occurs in the superstructure of the coach while the underbody does not have significant deformation. Plastic zones, due to local buckling are concentrated in the cantrail of the side wall, as illustrated in Figure 7.17. This deformation mechanism makes the impact loads from the ground cannot be transferred to the roof components smoothly, thus deteriorating the resistance of the superstructure against rollover impact.

The closed ring model is superior to the baseline model in terms of the residual space intrusion, which indicates that the closed ring configuration improves the resistance to residual space intrusion.

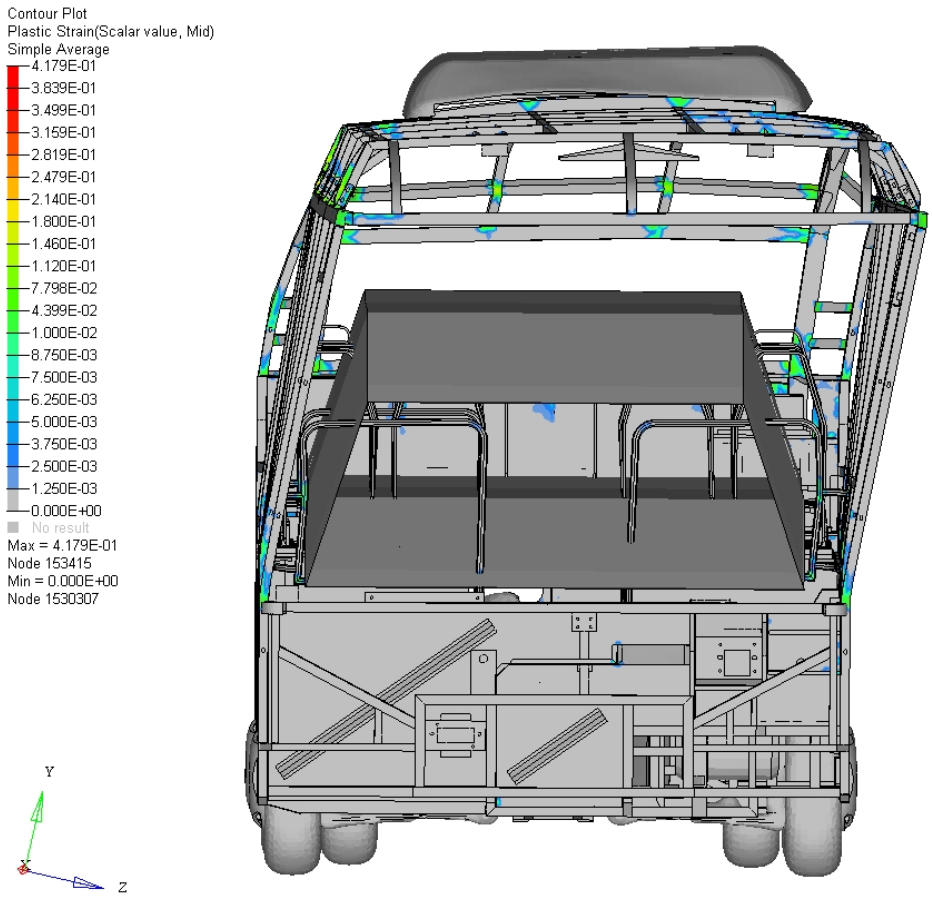


Figure 7.15 : Contours of effective plastic strain distribution at the end of the simulation from front view of the vehicle.

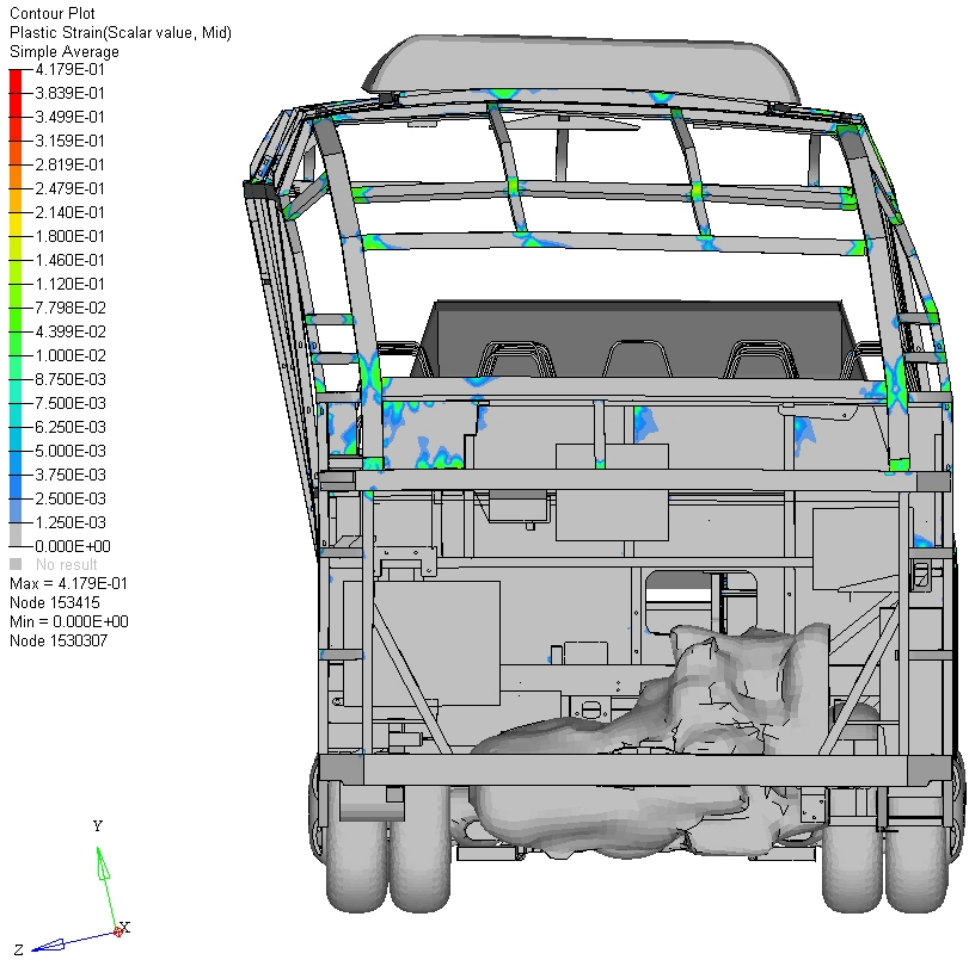


Figure 7.16 : Contours of effective plastic strain distribution at the end of the simulation from rear view of the vehicle.

Most of the deformation energy is then absorbed by the material concentrated in hinges. Structural design is produced vehicle bodies that collapse in a reasonably controllable manner. Structure of the vehicle is absorbed a sufficient amount of energy without intruding into the survival space and without developing fatal retardations. In the case of rollover, the deformed roof structure is also supported the vehicle weight without collapsing into the survival space.

Rollover simulation can be performed based on tracking the energy balance during the whole process. All components defining the total energy should satisfy the principle of energy conservation during the rollover. Obtained values of energy should be verified against hand calculations as a first check of the correctness of the simulation.

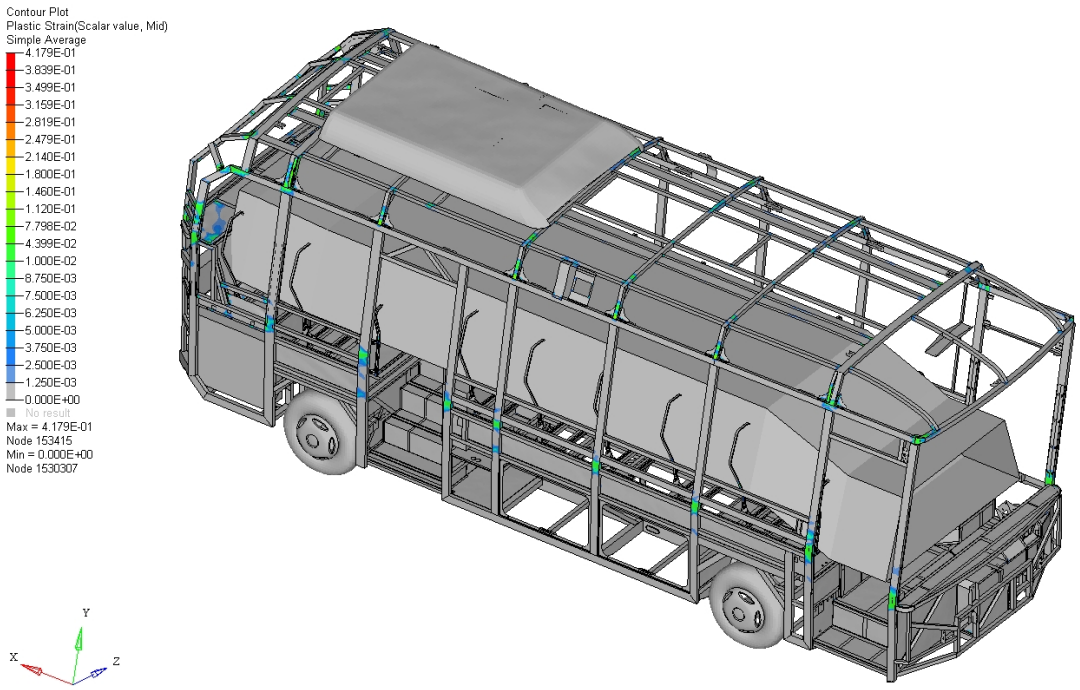


Figure 7.17 : Contours of effective plastic strain distribution at the end of the simulation from general view of the vehicle.

Potential energy, which is the only component of energy at the unstable position. At maximum deformation point, it has its local minimum before elastic springback. Kinetic energy, due to zero initial velocity at unstable point, it comes only from the potential energy. After the bus is hitting (touching) the ground the kinetic energy is transformed to the different types of mechanical work (mostly work done by elastic and plastic deformations). Plastic hinges are developed in the bus structure. During their operation portion of kinetic energy is absorbed through the deformation work. Local deformation work is the absorbed energy by the local structural deformations. Friction work produced during sliding of the bus on the concrete ditch surface. Energy transferred to the ground through the deformation, crushing and vibration. Energy dissipated in other ways like by sound, by oscillation of the parts and components of the bus, etc.

Figure 7.18 shows internal energy and kinetic energy from HyperGraph output. The initial value of total energy was found to be 67.907 kJ. The final value of total energy was found to be 86.5 kJ. The final value of internal energy was found to be 56.255 kJ. The final value of kinetic energy was found to be 30.245 kJ. The sum of the internal energy and kinetic energy values were found nearly the same with final total

energy value. Total energy minus global external work (DTE) curve was remained flat. In addition, hourglass curve was remained flat at zero energy.

Total energy minus global external work (DTE) curve should remain flat for the whole simulation as a consequence of energy conservation. This graph is a direct check of our simulation results against the analytical approximation. In the case of rollover simulation, the kinetic energy should be contributed by the change of the internal energy of rotating bus (see Figure 7.19). Thus, the curves should be symmetrical.

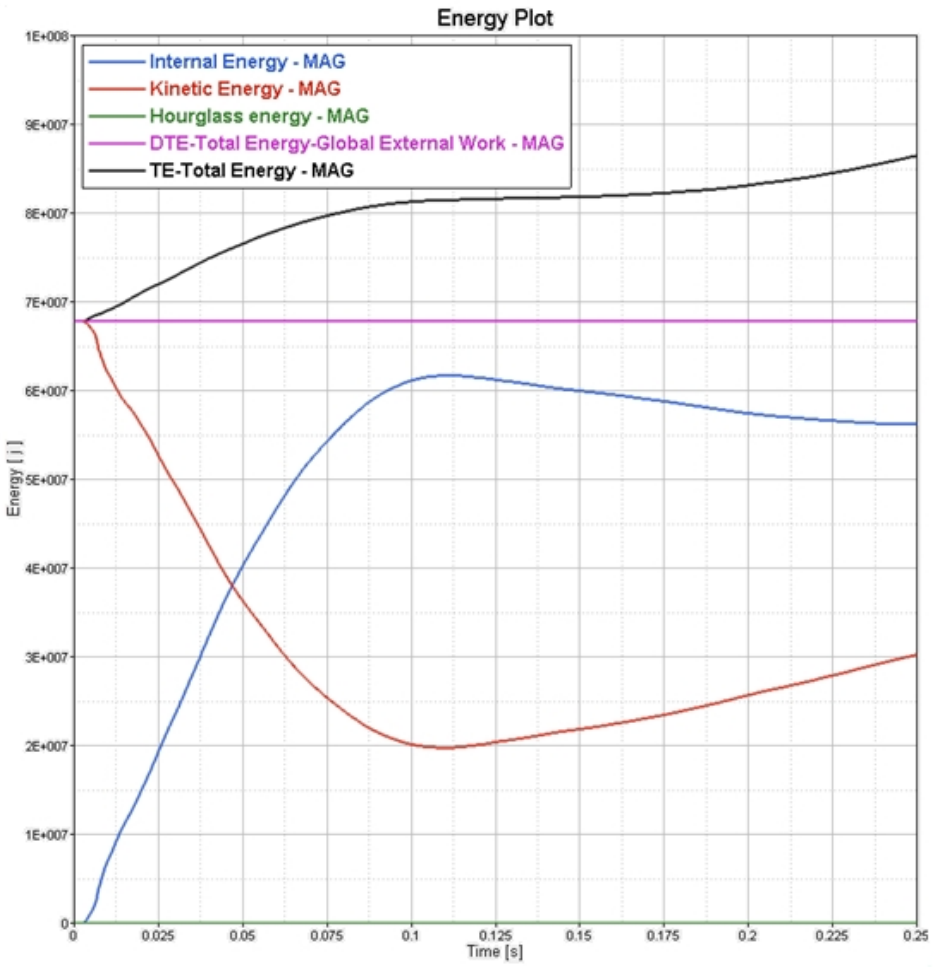


Figure 7.18 : Energy distribution of the simulation versus time.

In order to check the accuracy of simulation results, it was verified whether the total energy minus global external work (DTE) remained constant during the simulation time. A graph showing various energy distributions from the rollover simulation of the vehicle structure (see Figure 7.18). The figure shows that energy distribution did remain constant, indicating that analysis results were accurate. It could be observed

that kinetic energy drops and transforms into internal energy (strain energy + sliding energy) over time and hourglass energy remains negligible.

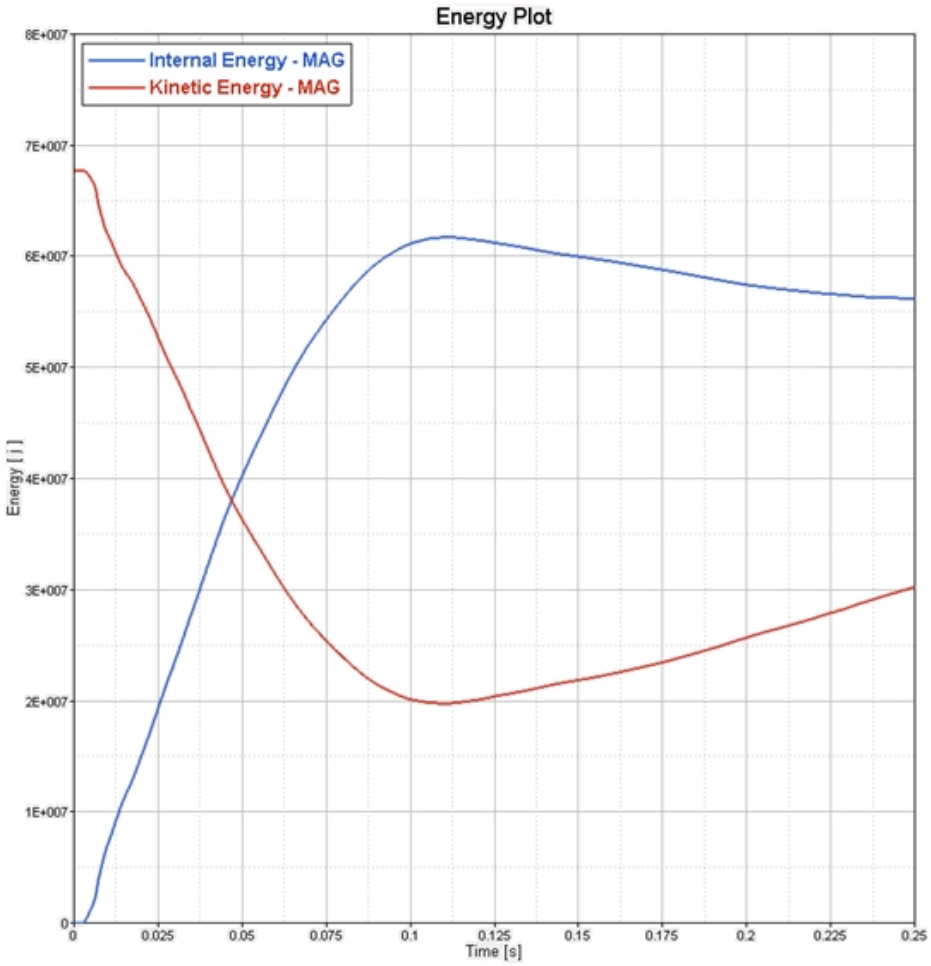


Figure 7.19 : Comparison of the internal and kinetic energy distribution of the simulation versus time.

8. CONCLUSION

A rollover event is one of the most crucial hazards for the safety of passengers and bus drivers. In past years, it was observed that the deforming body structure seriously threatened passengers' lives. Today, European regulation ECE 66-02 [1] is in force to prevent the catastrophic consequences of such rollover accidents from occurring and thereby ensuring passenger safety for buses and coaches. According to said regulations, certification can be obtained by numerical simulation. The bending deformation enables engineers to investigate whether there is any intrusion in the passenger residual space along the entire vehicle.

The structural configurations of side window pillars have significant effects on the residual space intrusion amount and impact load distribution. By extending the window pillar into the roof assembly, the intrusion values at each pillar are dramatically reduced and the ratio of residual kinetic energy to the internal energy drops remarkably from the closed ring model. Deformation mode of superstructure during the rollover process is changed, and plastic zones are found in some regions where the window pillars are connected with the cantrail, as well as the joints between the roof knots and the roof rails. This configuration allows more side window pillars to bear impact loads so that the rollover resistance of the whole superstructure is improved. Moreover, the side pillars shall be connected to the floor and roof cross members, is the most important resistant part. The whole structure should have sufficient rings to absorb the energy.

The evaluation and verification of analytical techniques, based on a well defined series of component testing, can be used in the early design stages to improve rollover structural integrity and crashworthiness of a coach superstructure for ECE 66-02 type approval, and hence avoid an expensive and time consuming full scale test program. The reason for joint testing as used in the quasi-static approach also

helps to avoid both the weld and material failure modeling at an early design cycle. This is not possible in the full scale testing approach.

The developed simulation technique was validated before applying it on complete buses. This validation consisted on carrying out a rollover test on a multipurpose coach module and the simulation of such test. The obtained numeric results showed a good correlation with the experimental ones.

Verification and validation methodology for the finite element simulations of standardized rollover test are introduced. Computational mechanics analyses were verified by the energy balance tracking. The numerical results were compared to the results from the experiments on different levels of the validation hierarchy. Consistent correlation of results was obtained for each case. Based on that validation study, factor of correlation was taken as “1.15” in computational simulation’s results evaluation. Final design was confidently implemented with taking into consideration factor of correlation.

It was observed that the vehicle side structure does not intrude into residual space envelope. For the baseline vehicle, it can be seen that the shortest distance between the residual space and pillar at front section is found to be 55.252 mm at the lower corner at time 0.15 sec at C Pillar and 66.638 mm at the upper corner at time 0.1425 sec at C Pillar, which comfortably satisfies the requirements of ECE 66-02.

REFERENCES

[1] **ECE 66-02** (2010). *Uniform provisions concerning the approval of large passenger vehicles with regard to the strength of their superstructure,* Revision 1, Addendum65, Revision 1, Amendment 2, United Nations Economic Commission for Europe, Geneva, Switzerland.

[2] **Directive 70/156/EEC** (1970). *The approximation of the laws of the member states relating to the type-approval of motor vehicles and their trailers*, Off. J. Eur. Commun. L 42, 1–15, European Parliament and of the Council.

[3] **European Commission** (2001). White Paper European Transport Policy for 2010: Time to Decide. Office for Official Publications of the European Communities, Luxembourg.

[4] **European Commission** (2002). The Route to Road Safety, European Commission,adress:http://europa.eu.int/comm/research/growth/gcc/projects/inaction-roadsafety.html. , Date retrieved: 22.08.2013.

[5] **ECBOS** (2001). Task 1.1 statistical collection. Concept report (Annex, No. 1:1), Technical University Graz, Graz, Austria.

[6] **Evans, L.** (2002). Traffic crashes. American Scientist Online, Vol. **90**, pp. 244–253.

[7] **Directive 2001/85/EC** (2001). Special provisions for vehicles used for the carriage of passengers comprising more than eight seats in addition to the driver's seat and amending Directives 70/156/EEC and 97/27/EC, 2002, Off. J. Eur. Commun. L 42, 1–102 (report), European Parliament and of the Council.

[8] **Botto, P., Caillieret, M., Tarrier, C., Got, C. and Patel, A.** (1994). Evaluation of restraint system for coach passengers. In: Paper Presented at the 14th International Technical Conference on Enhanced Safety of Vehicles, Munich, Germany.

[9] **Botto, P., and Got, C.** (1996). Vehicle rollover and occupant retention. In: Paper Presented at the 15th International Technical Conference on the Enhanced Safety of Vehicles, Melbourne, Australia.

[10] **Martinez, L., Aparicio, F., Garcia, A., Paez, J. and Ferichola, G.** (2003). Improving occupant safety in coach rollover. Int. J. Crashworthiness 8 (2), 121–132.

[11] **Rasenack, W., Appel, H., Rau, H. and Rietz, C.** (1996). Belt systems in passenger coaches. In: Paper Presented at the 15th International Technical Conference on the Enhanced Safety of Vehicles, Melbourne, Australia.

[12] **Matolcsy, M.** (2001). Standard accident as the basis of vehicle approval test. Intern. EAEC Congress 2001, Section BO1, Safety, pp.9, Bratislava, Slovakia.

[13] **Matolcsy, M.** (1977). Bus research and development at AUTÓKUT Research Institute, Hungary Conf. On Design, Construction and Operation of PSV's., ImechE, Paper No. C145/77, pp.113-138, Cranfield, UK.

[14] **Cranfield** (1977). *The investigation of 8 bus rollover accidents in Great Britain 1976-77*. Report of School of Automotive Studies, manuscript, pp.46, Cranfield, UK.

[15] **Matolcsy, M. and Batiz, Z.** (1987). Constructional analysis of accidents and accident statistics. Proc. of XVIII. Meeting of Bus and Coach Experts, GTE, Vol. **1**, pp. 251-258, Budapest, Hungary.

[16] **AUTÓKUT Report** (1980). *Technical analysis of real bus accidents*. Reference No. JA-243/80, Hungary.

[17] **AUTÓKUT Report** (1988). *Accidents happened to IKARUS buses*. Reference No. 88.547, Hungary.

[18] **Transport Canada** (2002). *Evaluation of occupant protection in buses*. Road Safety and Motor Vehicle Regulation (ASFBE), Ottawa, Canada.

[19] **Url** <http://www.haber7.com/trafik-kazalari/haber/1031300-ogrencileri-tasiyan-otobus-devrildi-1-olu-45-yarali>, Date retrieved: 27.05.2013.

[20] **Matolcsy, M.** (2003). A grave bus rollover accident and its lessons. IAT03, Conference on Innovative Automotive Technology, Koper, Slovenia.

[21] **Apparicio, F. and Garcia, A.** (1990). Coaches in traffic accidents. A study of the Spanish situation during the years 1984-88. Proc. of XXI. Meeting of Bus and Coach Experts, GTE, Vol. **2**, pp.3-14, Budapest, Hungary.

[22] **Krüger, J.** (1993). Entwicklungsmöglichkeiten der Bussicherheit auf der Basis Ausgewahlter schwerer Busunfalle in Deutschland. Proc. pf XXIV. Meeting of Bus and Coach Experts, GTE, Vol. **2**, pp. 303-313, Budapest, Hungary.

[23] **Matolcsy, M.** (2007). The severity of bus rollover accidents, Scientific Society of Mechanical Engineers, Paper Number: 07 0989, Hungary.

[24] **Matolcsy, M.** (2003). Lessons And Conclusions- Learned From The Analysis Of Bus Rollover Accidents, The International Conf. Of Science And Motor Vehicles 2003, 84th GRSG, 5-9 May 2003, agenda item 4, Belgrade, Serbia.

[25] **Subic A. and He J.** (1996). Optimization of the Omnibus Roll Cage Structure, In Road Safety Research Grant, School of Engineering: Ballarat, Australia.

[26] **Borkowski, W. and Hryciow, Z.** (2006). Modeling of the Bus Superstructure in Order to Confirm Requirements of 66 ECE Regulation. Journal of KONES Powertrain and Transport.

[27] **Belingardi, G., Martella, P and Peroni, L.** (2005). Coach Passenger Injury Risk During Rollover: Influence of the Seat and the Restraint System, 19th International Technical Conference on the Enhanced Safety of Vehicles. National Highway Traffic Safety Administration, Washington, DC, USA.

[28] **Elitok, K., Güler, M. A., Bayram, B. and Stelzmann, U.** (2006). An Investigation on the Rollover Crashworthiness of an Intercity Coach, Influence of Seat Structure and Passenger Weight, in 9th International LS-DYNA Users Conference. 2006, Dearborn, MI, USA.

[29] **Deshmukh P. S.** (2006). Rollover and Roof Crush Analysis of Low-Floor Mass Transit Bus, in Mechanical Engineering. Wichita State University, KS, USA.

[30] **A.P.T.** (1997). *Standard Bus Procurement Guidelines*, American Public Transit Association , Editor. 1997.

[31] **Castejon L., Miravete, A. and Cuartero J.** (2006). Composite Bus Rollover Simulation and Testing, International Journal of Heavy Vehicle Systems, pp. 281 - 297.

[32] **Castejon L., Miravete A. and Larrode E.** (2001). Intercity Bus Rollover Simulation. International Journal of Vehicle Design, Vol. **26**, pp. 204-217.

[33] **Gadekar, G. B., Kshirsagar, S. and Anilkumar, C.** (2005). Rollover strength prediction of bus structure using LS-DYNA 3D, Altair CAE Users Conference 2005, Bangalore, India.

[34] **Cranfield Impact Centre** (2008). *CIC Cranfield Impact Centre*, cited 14.12.2008; Available from: Cranfield Impact Centre.

[35] **Walton, A. C., H. S. M. R. and Anderson J. C.** (2006). Preventing passenger ejection from buses, coaches and minibuses, Louise Turner, TTS, DIT.

[36] **Pavlata P., Martinu, M. and Petrok T.** (2005). Virtual Simulations of Bus Approval Tests according to European Standards, Virtual Product Development Conference & MSC Software User Meeting 2005. Munich, Germany.

[37] **National Science Foundation** (2006). *Simulation-Based Engineering Science*, Blue Ribbon Panel, National Science Foundation.

[38] **Schwer L.E.** (2006). An Overview of the ASME Guide for Verification and Validation in Computational Solid Mechanics, in LS-DYNA Anwenderforum. 2006: Ulm.

[39] **FMVSS 220** (1991). School Bus Rollover Protection, U.S. Department of Transportation National Highway Traffic Safety Administration, TP-220-02, Washington, DC, USA, 16.07.1991.

[40] **Matolcsy, M.** (1993). Some basic questions of roof strength calculation related to the international regulation Proc. of 24th Meeting of Bus and Coach Experts, Vol. **2**, pp. 339-347, Budapest, Hungary.

[41] **Dias, J. M. and Pereira, M. S.** (1995). Dynamics of Flexible Mechanical Systems With Contact-Impact and Plastic Deformations, Journal of Nonlinear Dynamics, Vol. **8**, pp. 491-512.

[42] **Anceau, J. H., Drazetic, P. and Ravalard, I.** (1992). Plastic Hinges Behaviour in the Multibody Systems, Mecanique Materiaux Electricite, No 444, France.

[43] **Kecman, D.** (1983). Bending Collapse of Rectangular and Square section Tubes, Int. J. of Mech. Sci., Vol. **25**, pp. 623-636.

[44] **Matolcsy, M.** (1997). Crashwortiness of bus structures and rollover protection, Kluwer Academic Publishers, Series E: Applied Sciences, Vol. **332**, pp. 321-360.

[45] **Molnar, C. S.** (1977). Loss of stability in case of axially compressed thin-walled rectangular tubes and their energy absorping capability, Technical University of Miskoic, Hungary.

[46] **Matolcsy, M.** (1987). Plastic hinge theory to analyse the structural strength and energy absorption of bus frames, Proc. of Int. Conf. on Science and Vehicle, Belgrade, Hungary.

[47] **Tidbury, G.** (1975). The strength of the superstructure of buses. Proc. of 6th Meeting of Bus and Coach Experts, pp. 216-224, Budapest, Hungary.

[48] **Voith, A.** (1976). The safety of passengers in the case of bus rollover accidents, Budapest Technical University, Budapest, Hungary.

[49] **Newmark, N. M.** (1959). A Method of Computation for Structural Dynamics, J. Engineering Mechanics Division, ASCE, Vol. **67**, pp. 67-94.

[50] **Farhoornand, I.** (1972). Nonlinear Dynamic Stress Analysis of Two-dimensional Solids, Ph.D. Thesis, University of California, Berkeley, Graduate Division.

[51] **Belytschko, T. B. and Hsieh, B. J.** (1974). Nonlinear Transient Analysis of Shells and Solids of Revolution by Convected Elements, AIAA Journal, Vol. **12**, pp. 1031-1039.

[52] **Hughes, T. J. R., Pister, K. S. and Taylor, R. L.** (1979). Implicit-Explicit Finite Elements in Nonlinear Transient Analysis, Computer Methods in Applied Mechanics and Engineering, 17/18, 159.

[55] **Hughes, T. J. R.** (1983). "Analysis of Transient Algorithms with Particular Reference to Stability Behavior" Computational Methods for Transient Analysis, eds. T. Belytschko and T. J. R Hughes, 67-155, North Holland.

[54] **AIAA (1998)**. Guide for the Verification and Validation of Computational Fluid Dynamics Simulations, American Institute of Aeronautics and Astronautics, AIAA-G-077-1998, Reston, VA.

[55] **Trucano, T. G., Pilch, M. and Oberkampf, W. L.** (2002). General concepts for experimental validation of ASCI code applications, Sandia National Laboratories, SAND2002-0341, Albuquerque, NM, USA.

[56] **Oberkampf, W. L., Trucano, T. G. and Hirsch, C.** (2002). Verification, Validation, and Predictive Capability in Computational Engineering and Physics, Applied Mechanics Reviews. Vol. **57**, pp. 345–384.

[57] **Belytschko, T. and Mish, K.** (2001). Computability in non-linear solid mechanics. International Journal for Numerical Methods in Engineering, Vol. **52**, pp. 3-21.

[58] **Oberkampf, W. L.** (2004). Verification and Validation in Computational Simulation, Transport Task Force Meeting, Salt Lake City, Utah, USA, 29.05.2004. Data retrieved: 29.08.2013, address: http://www.psfc.mit.edu/ttf/2004/talks/oberkampf.pdf

[59] **Du Bois P.** (2004). Vehicle Crashworthiness and Occupant Protection, J.E.B. P. Prasad, Editor, American Iron and Steel Institute.

[60] **Radioss** (2009). Large Displacement Finite Element Analysis, Radioss Theory Manual, 10.0 version, Troy, MI, USA.

[61] **Flanagan D. and Belytschko T.** (1981). A Uniform Strain Hexahedron and Quadrilateral with Orthogonal Hourglass Control, Int. Journal Numerical Methods in Engineering, Vol. **17**, pp. 679-706.

[62] **Zeng Q. and Combescure A.** (1998). A New One-point Quadrature, General Nonlinear Quadrilateral Shell Element with Physical Stabilization. Int. J. Numer. Meth. Engng. Vol. **42**, pp. 1307-1338.

[63] **Drucker, D. C. and Prager, W.** (1952). Soil mechanics and plastic analysis for limit design. Quarterly of Applied Mathematics, Vol. **10**, pp. 157–165.

APPENDICES

APPENDIX A: Bus rollover accidents statistics.

APPENDIX B: Technical drawing of test knots.

APPENDIX C: Technical drawings of KARSAN STAR.

APPENDIX A

Table A.1 : Bus rollover accidents statistics.

	Date City (district) Country	Bus type Category Operator	Circumstances of rollover	Fatalities and injuries	Damage of superstructure
1.	07.08.2002 Tampico Mexico	Local Operator	Because of the high speed the bus could not take the curve, rolled over.	8 fatalities 13 injuries	-
2.	10.08.2002 Haragaulsk Georgia	Local Operator	In a hilly district two buses – a small and a large one – collided and the large bus with 15passengers on board rolled down into a precipice.	7 fatalities 9 injuries	-
3.	15.08.2002 Poland	Minibus Local Operator	Minibus collided with a truck on a slippery road and after that rolled over. All the passengers and the driver died.	9 fatalities	-
4.	27.08.2002 Budapest Hungary	Mercedes Minibus Local Operator	The ambulance car (minibus) was hit by a car and turned on its side. 3 person on board, only the driver was injured.	1 injury	The windscreen and the driver seat out, but no serious damage, the survival space was unharmed.
5.	13.08.2001 Kagenfurt Austria	High Decker Tourist Coach Italian Operator	30 Italian pilgrims on board, the bus crashed the part of a tunnel and rolled over.	10 serious injuries 20 light injuries	The superstructure damaged, the survival space probably harmed. The seats torn up.
6.	05.09.2002 Eger Hungary	IKARUS Classic Category III (12m) VOLÁN-AGRIA	The bus was passing a truck, which pushed it down from the road. The bus rolled down into a 0,5 m deep ditch and laid on its side.	3 serious injuries 6 light injuries	No serious damage on the superstructure.
7.	11.09.2002 Belényes Romanian	Ford Transit Minibus Local Operator	17 people on board. The bus drifted out from the road in an “S” curve, hit a pole and rolled into a 90 m deep precipice. Those passengers survived who were ejected after the first collisions.	8 fatalities 9 serious injuries	The superstructure completely damaged.
8	13.09.2002 Main USA	Minibus	15 people on the board. The minibus hit the guard of a wooden bridge (100 km/h) and rolled down into a river. One person survived, breaking out rear window and climbing out.	14 fatalities	-

9.	13.09.2002 Szolnok Hungary	VW Transporter Minibus Local Operator	The empty minibus had a frontal collision with a truck, after that rolled down into a 0,8-1 m deep ditch, stopping on its roof.	1 light injury	The front wall and the roof seriously damaged.
10.	11.09.2002 Sárvár Hungary	Ford Transit Minibus	5 passengers on board. The minibus was hit by a car, after that it turned on its side and slipped into a 1 m deep ditch.	No injury	Only slight structural damage.
11.	11.09.2002 South Africa	Local Operator	The bus left the road in a hilly district and rolled down into a precipice. Many people were ejected from the bus and compressed.	21 fatalities 52 injuries	The superstructure collapsed, the bus was totally damaged.
12.	28.07.1998 Napoli Italy	Category III High Decker Hungarian Operator	46 passengers on board. The bus left the line of the highway, the driver made a quick steering correction, the bus turned on its side and slide away around 35 m.	38 injuries, many of them seriously	The survival space was not damaged, slight deformations on the superstructure.
13.	31.10.2002 Johannesburg South Africa	Category III (11 M) Local Operator	The bus slipped on the wet road rolled over, stopped on its roof, on flat ground. 44 German, Canadian and English tourists on board.	10 fatalities 12 seriously injured	The superstructure collapsed no residual space. Seats were deformed and broken by the roof 4 PH deformation mechanism.
14	16.11.2002 London U.K.	Plaxton- Volvo B10-H Category III High Decker UK Operator	43 passengers and 2 drivers on the board. The bust left the highway and veered off onto hard-shoulder and down the inclined embankment and rolled to its left side and slid down, 3 persons were ejected and killed by the bodywork.	6 fatalities 5 serious injuries	No major deformation of the superstructure.
15.	05.12.2002 Sárkeresztes Hungary	Kässbohrer Category III (12 m) German Operator	Speeding (120 km/h) on wet road, the bus slipped, hit a truck and rolled into a ditch (1 m deep) and stopped on its side. The driver died.	2 fatalities 5 serious injuries 2 light injuries	Drivers compartment disappeared, the superstructure slightly deformed, survival space was not harmed.
16.	06.12.2002 Szentendre Hungary	Minibus Local Operator	The minibus (ambulance car) hit a car, spun around and turned on its side.	2 serious injuries	Large scale deformation on the front wall, no significant deformation on the superstructure.
17.	20.12.2002 Cairo Egypt	Small Bus Local Operator	The bus slipped on the wet road and rolled down from an overbridge.	17 fatalities 17 injuries	The superstructure collapsed.

18.	02.06.2002 Brisbane Australia	Category III High Decker Local Operator	On a wet road, the bus slipped on the road, the wheels were blocked by the deep, muddy soil, the bus rolled down from the road on a slope and slopped on its roof (44 persons on board).	2 fatalities 1serious injury 17 light injuries	The superstructure got severe deformation the survival space was harmed.
19.	19.08.1992 Torreblance Spain	Category III (12 m) High Decker	The bus turned on its side on the road, slid away, collided with the metal safety rail and rolled down on a slope. After ½ rotation it stopped on its roof.	46 fatalities 9 serious injuries 1 light injury	The superstructure completely collapsed the roof came to the waistrail.
20.	06.09.1992	Kässbohrer Category III (12 m) High Decker German Operator	The bus (53 passengers on board) having a speed 60 km/h collided with a car, on an overbridge, turned on its left side, slipped away and hit the breast rail by its rear part.	20 fatalities 30 injuries	The rear left side of the superstructure was cut and pressed by the breast rail.

APPENDIX B

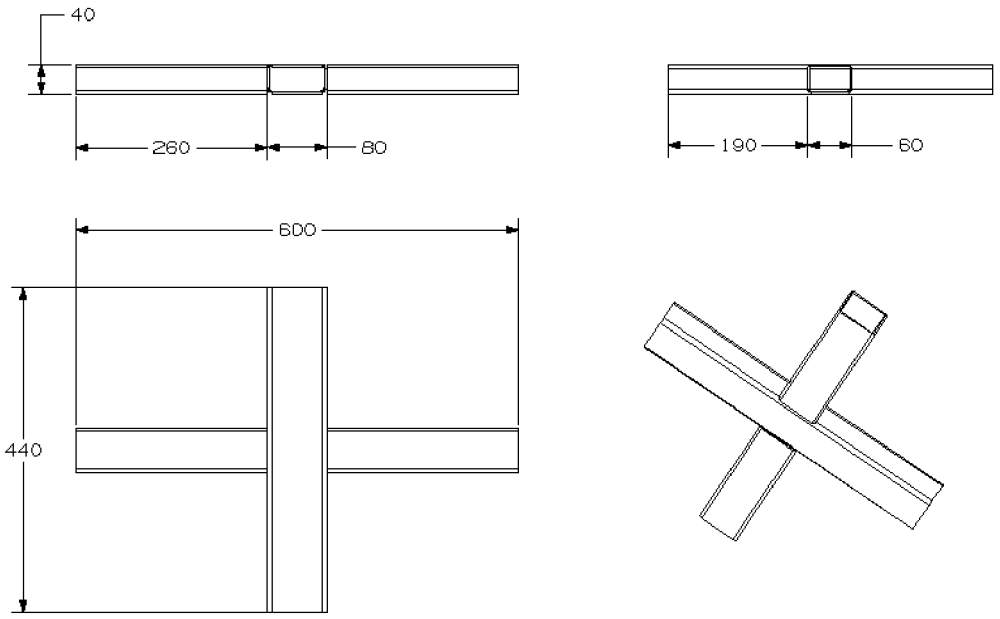


Figure A.1 : Technical drawing of breast knot.

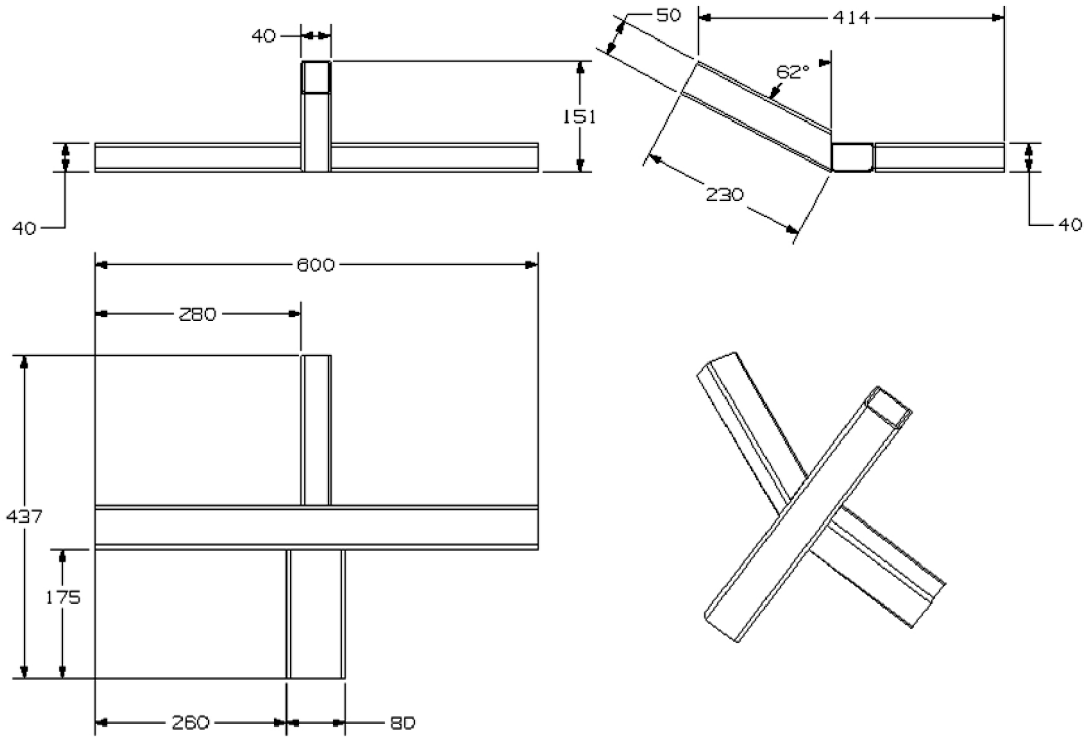


Figure A.2 : Technical drawing of roof edge knot.

APPENDIX C

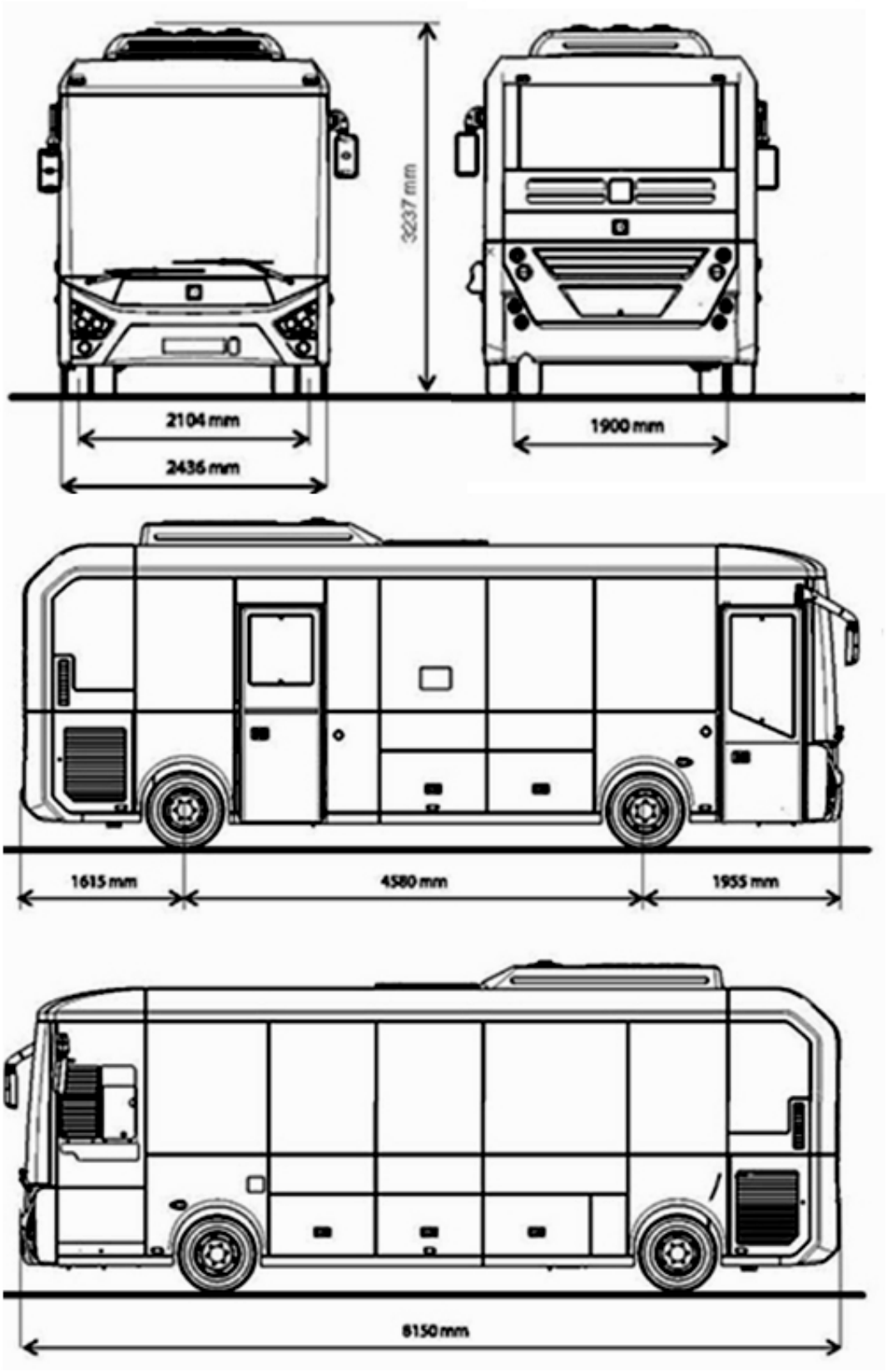


Figure A.3 : Geometrical sketch of KARSAN STAR.

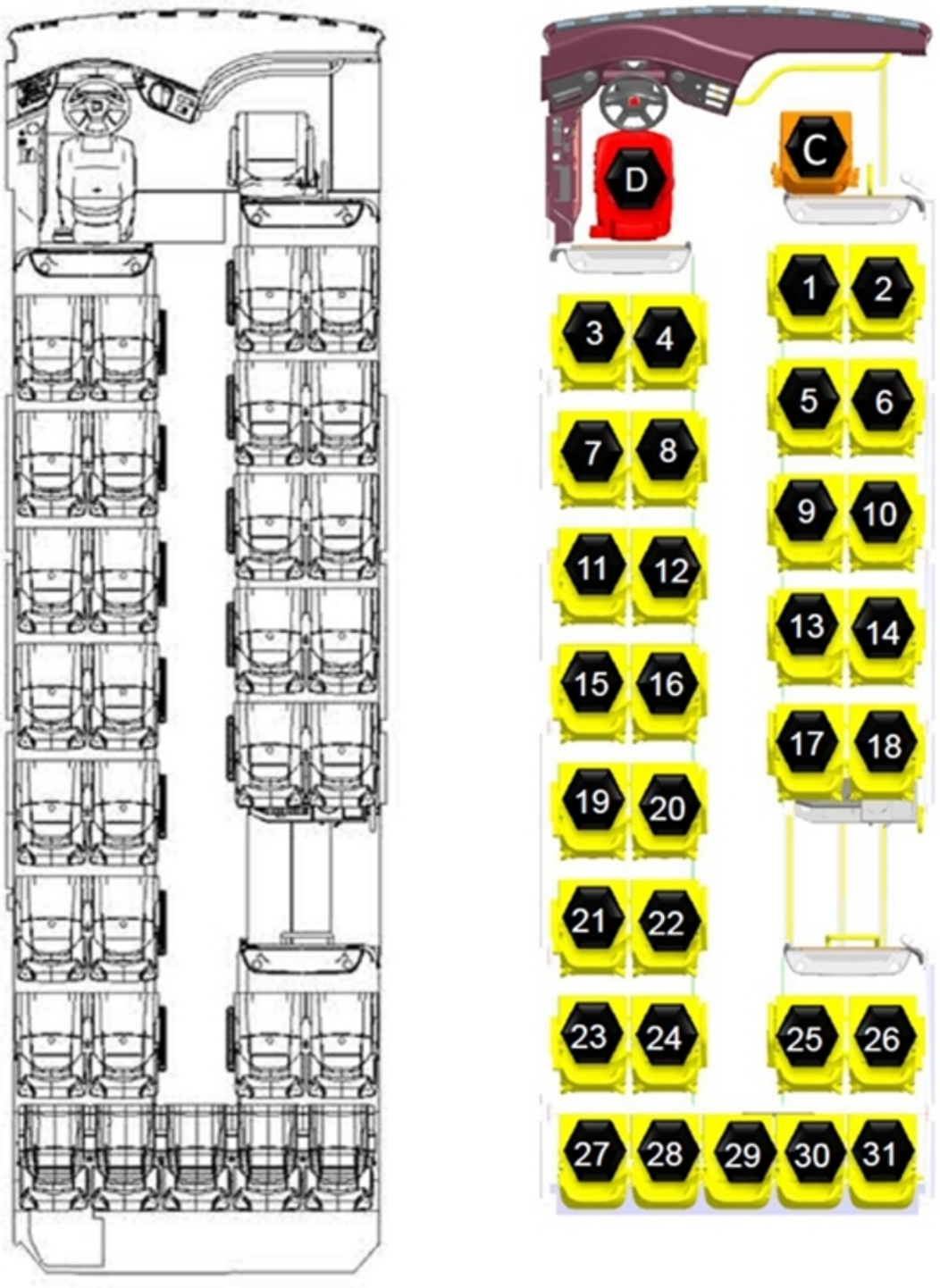


Figure A.4 : Seat layout of the KARSAN STAR.

CURRICULUM VITAE



Name Surname : ÖZGÜN KÜÇÜK

Place and Date of Birth : EDİRNE / 30.11.1988

E-Mail : ozgun_kucuk@hotmail.com

ozgun.kucuk@hexagonstudio.com.tr

EDUCATION:

B.Sc. : YILDIZ TECHNICAL UNIVERSITY / Mechanical Engineering (2011)

PROFESSIONAL EXPERIENCE AND REWARDS:

- HEXAGON STUDIO / Durability and Safety Engineer (January 2013 - …)
- ARÇELİK / Structural Analysis Engineer (October 2011 - January 2013)